Contributions to the study of the availability of metal ions in aquatic systems

Sandrine Mongin

Contributions to the study of the availability of metal ions in aquatic systems

Memoria presentatada por Sandrine Mongin para optar al grado de Doctora por la Universidad de Lleida

Trabajo realizado en el Departamento de Quimica de la Universidad de Lleida bajo la dirección del Dr. Jaume Puy i Llorens

Lleida, julio del 2012

A toutes les personnes qui ont été a mes côtés,

La véritable culture, celle qui est utile, est toujours une synthèse entre le savoir accumulé et l'inlassable observation de la vie.

Extrait de *Vie publique et vie privée* de *Francesco Alberoni*

Remerciements - Agradecimientos

Je voudrais tout d'abord remercier les personnes qui m'ont portée et supportée jusqu'à maintenant pour mener à bien ce travail de longue haleine. Je sais bien que cela n'a forcément été facile tous les jours!!! Je vous dédie donc un grand merci à vous toutes et tous sans qui ce travail n'aurait pas pu s'accomplir.

Je voudrais tout d'abord remercier mon directeur de thèse, Jaume Puy, pour m'avoir accueillie au sein de son laboratoire et m'avoir permis de mener à bien ce projet compliqué. Je lui adresse toute ma gratitude pour la confiance qu'il m'a témoignée.

Je remercie toutes les personnes du groupe de chimie-physique de l'Université de Lleida pour leur aide et leur discussion en tout genre, en particulier un grand merci à Encarna Companys, Josep Lluis Garcés y Josep Monné, ainsi que mes collègues de laboratoire, et pour cela, je commencerais par César, Maria, Silvia, Mireira, David, Sara, Diana. Un merci particulier à Josep Galceran, Pepe Salvador et Calin David qui ont été d'une aide indispensable à la réalisation de ce travail et sans qui tout cela n'aurait pas été possible. De plus je voudrais dire un merci particulier à Ramiro Uribe sans qui ce travail n'aurait pas été aussi complet, je te remercie pour nos longues discussions qui ont été d'un réel enrichissement.

Merci à vous tous pour ce que j'ai pu appendre à vos côtés, que ce soit sur le plan professionnel ou personnel.

Je remercie Hao Zhang et Bill Davison pour m'avoir reçue durant presque 3 mois au sein de leur laboratoire et de m'avoir enseigné la fabrication des DGTs. Je les remercie pour leur grande gentillesse et leur hospitalité. Je remercie également les personnes que j'ai côtoyées lors de ce stage: Jacquie, Chen, Jung, Mohamed, Stéphanie ainsi que Nick.

Je remercie également Isabelle Le Hecho et Ryszard Lobinsky qui m'ont accueillie au sein du LCABIE durant 4 mois, ainsi que Corinne Parat qui a eu la gentillesse de m'encadrer lors de ce stage.

Quiero dar las gracias a la gente que he conocido aquí y con la que poco a poco he desarrollado una gran amistad. Pienso especialmente en vosotros los compañeros de comida (acordaos del bar antiguo…): gracias a Emi, Lindon, Marc, a la Rebequiña y también a Roger, que llego más tarde y tuvo la suerte de haber conocido sólo el nuevo bar. Quiero dar también las gracias a la pareja colombianita, Sol y Harry. Me gustaría también agradecer a los compañeros de química orgánica por haber

Summary

Availability of metals for soil and water organisms does not depend only on the total metal concentration but also on speciation, as well as on the transport properties of these species. In general, the availability of metal species in natural media and the corresponding nutritional or toxic properties towards microorganisms, biofilms, algae and plants are determined by a set of chained events whose equilibrium approach only represents a simplified limiting case of the general dynamic situation.

Poorly defined species such as humic and fulvic acids, poly-saccharides, gels, (nano) particles and other colloids act as metal ligands and play a key role in the circulation and determination of the ecotoxicological properties of metal species in the natural media. Thermodynamic and statistical mechanics methods are here applied to describe the heterogeneity and polyfunctionality of humic and fulvic acids. An extension of the conditional affinity spectrum of NICA isotherm allows to study the competition effects arising in the metal binding to fulvic acids in a typical composition of a natural water.

An analytical dynamic technique, the Diffusive Gradients in Thin Films (DGT) has been used to measure the available metal flux in a synthetic system that contains metal complexes. A physicochemical framework for the interpretation of availability measurements under these conditions is reported. A main conclusion of this study is that the chelating resin disc of the DGT devices plays a key role in determining the lability degree of a complex measured with DGT. Moreover, at relatively low pH, or in presence of high affinity ligands, the equilibrium with the bulk metal concentration can be approached in the DGT sensor, disturbing linear accumulations at relatively short deployment times. Analysis of these phenomena and theoretical explanations are reported.

Resumen

La disponibilidad de metales por parte de los organismos del suelo y del agua no depende únicamente de la concentración total de dichos metales, sino también de la especiación y de las propiedades de transporte de estas subtancias. En general, la disponibilidad de las especies metálicas en medios naturales y sus correspondientes propiedades nutricionales o tóxicas hacia microorganismos, biofilms, algas y plantas están determinadas por un conjunto de eventos encadenados cuyo equilibrio representa sólo un caso particular de la situación dinámica general.

Especies poco definidas químicamente, tales como ácidos húmicos y fúlvicos, polisacáridos, geles, (nano) partículas y otros coloides actúan como ligandos de metales y juegan un papel clave en la circulación y la determinación de las propiedades ecotoxicológicas de las especies metálicas en los medios naturales. La heterogeneidad y la polifuncionalidad de los ácidos húmicos y fúlvicos son descrita en este estudio usando métodos termodinámicos y mecano-estadísticos. Una extensión del espectro de afinidad condicional de la isoterma NICA permite estudiar los efectos de competición que tienen lugar en la complejación entre los metales y los ácidos fúlvicos en un agua dulce representativa.

La técnica analítica dinámica denominada *Diffusive Gradients in Thin films* (DGT) se ha utilizado para medir el flujo disponible de metal en un sistema sintético que contiene complejos metálicos. Se ha desarrollado un marco físico-químico para la interpretación de las medidas de disponibilidad en estas condiciones. La principal conclusión de este estudio es que el disco de resina quelatante de los sensores DGT juega un papel clave en la determinación del grado de labilidad de un complejo medido esta técnica. Por otra parte, y como se demuestra experimentalmente, a un pH bajo, o a concentración alta de ligando, puede ser alcanzado el equilibrio entre la resina del sensor y el metal en el seno de la disolución, perturbando la acumulación lineal a tiempos de contacto relativamente cortos. Se presenta un análisis de estos fenómenos, así como su justificación mediante modelos teóricos.

Resum

La disponibilitat de metalls per part dels organismes del sòl i de l'aigua no depèn únicament de la concentració total d'aquests metalls, sinó també de l'especiació i de les propietats de transport d'aquestes subtàncies. En general, la disponibilitat de les espècies metàl·liques en medis naturals i les seves corresponents propietats nutricionals o tòxiques per a microorganismes, biofilms, algues i plantes estan determinades per un conjunt d'esdeveniments encadenats on el equilibri representa només un cas particular de la situació dinàmica general.

Espècies poc definides químicament, com ara àcids húmics i fúlvics, polisacàrids, gels, (nano) partícules i altres col·loides actuen com a lligands de metalls i juguen un paper clau en la circulació i la determinació de les propietats ecotoxicològiques de les espècies metàl·liques en els mitjans naturals. L'heterogeneïtat i la polifuncionalitat dels àcids húmics i fúlvics és descrita en aquest estudi utilitzant mètodes termodinàmics i mecano-estadístics. Una extensió de l'espectre d'afinitat condicional de la isoterma NICA permet estudiar els efectes de competició que tenen lloc en la complexació entre els metalls i els àcids fúlvics en una aigua dolça representativa.

La tècnica analítica dinàmica anomenada *Diffusive Gradients in Thin films* (DGT) s'ha utilitzat per a mesurar el flux disponible de metall en un sistema sintètic que conté complexos metàl·lics. S'ha desenvolupat un marc fisicoquímic per a la interpretació de les mesures de (bio)disponibilitat en aquestes condicions. La principal conclusió d'aquest estudi és que el disc de resina quelant dels sensors DGT juga un paper clau en la determinació del grau de labilitat d'un complex mesurat amb la tècnica DGT. D'altra banda, i com es demostra experimentalment, a un pH baix, o una concentració alta de lligand, es pot aconseguir l'equilibri entre la resina del sensor i el metall en el si de la dissolució, pertorbant l'acumulació lineal a temps de contacte relativament curts. Es presenta una anàlisi d'aquests fenòmens, així com la seva justificació mitjançant models teòrics.

<u>Résumé</u>

La quantité de métaux disponible pour les organismes terrestres et aquatiques ne dépend pas uniquement de leur concentration totale, mais aussi de la spéciation et des propriétés de transport de ces espèces. En général, la disponibilité des espèces métalliques dans les milieux naturels et leurs propriétés qu'elles soient nutritionnelles ou bien toxiques envers les microorganismes, les biofilms, les algues et les plantes sont déterminées par un enchaînement d'événements. L'équilibre ne représente qu'un cas particulier de la situation générale qui elle est dynamique.

Chimiquement mal définies, les espèces comme les acides humiques et fulviques, les polysaccharides, les (nano) particules et d'autres colloïdes, agissent comme des ligands métalliques qui vont jouer un rôle clé dans la circulation et la détermination des propriétés écotoxicologiques des espèces métalliques dans les milieux naturels. L'hétérogénéité et la multi-fonctionnalité des acides humiques et fulviques sont décrites dans cette étude par le biais de méthodes thermodynamiques et statistiques. Les effets de compétitions dans la complexation metal – acide fulvique, engendrés par la présence d'autres cations ont été étudiés dans une eau de rivière représentative, grâce à une extension du spectre d'affinité conditionnelle de l'isotherme NICA.

Dans ce travail, la technique d'analyse dynamique connue sous le nom de *Diffusive Gradients in Thin films* (DGT) a été utilisée pour mesurer le flux de métal disponible dans des solutions synthétiques contenant des complexes métalliques. Un model physico-chimique a été développé afin d'interpréter les résultats. La principale conclusion de cette étude est que le disque de résine chélatante des échantillonneurs DGT joue un rôle clé dans la détermination du degré de labilité d'un complexe mesuré par cette technique. Par ailleurs, il a été démontré, en accord avec les résultats expérimentaux, qu'en présence d'une concentration de protons relativement élevée, ou en présence de ligands ayant une forte affinité, l'équilibre entre la résine chélatante du DGT et le métal présent en solution peut être atteint. Ceci perturbe l'accumulation linéaire pour des temps d'échantillonnage relativement courts. L'analyse de ces phénomènes ainsi que leurs explications théoriques sont présentés dans ce rapport.

OBJECTIVES AND WORK PRESENTATION

The aim of the present thesis is to deepen the study of binding between metal ions and ligands (simple or macromolecular) by equilibrium (potentiometry) and dynamic (Diffusive Gradients in Thin films, DGT) techniques. We aim to understand the (bio)availability of metals cations in natural media. (Bio)availability is an important property since its determines the nutritive capacity or the ecotoxicity of these media.

As (bio)availability depends on the speciation, we firstly study the equilibrium complexation properties of humic substances (macromolecular ligands present in natural waters) with metal ions. Humic substances play an important role due to their ability in buffering the free metal concentration. The binding of metals ions by humic substances can prevent hydrolysis and precipitation and by this way, the circulation of metals in the natural media. Our study is also focussed on competitions effects. Notice that natural media are complex mixtures, where competition effects are always present. From an experimental point of view, the competitive effect of lead and cadmium on the proton binding is studied through proton titrations at varying fixed total metal concentrations. From a theoretical perspective, the competition effects are analysed by developing the formalisms of conditional affinity spectra at constant concentration of free ions (CAS) and constant total metal concentration (CAScTM).

Afterwards, the kinetic properties of the Cd-NTA dissociation are studied using the DGT technique, with this work, we now focus our attention to the measurement of metal fluxes which determine, in the general cases the (bio)availability. Ligands act buffering the metal flux at a limiting metal consuming surface (the membrane of a micro-organism, for instance) by complex dissociation. The nitrilotriacetic acid (NTA) is chosen, as it is a simple and well characterized ligand. The interpretation of the experimental data obtained through DGT allowed a further insight into the lability measurements by DGT.

The thesis is organised in three different parts. The first one, chapters 2 to 5, corresponds to the speciation studies of the metal ions in presence of macromolecular ligands.

Chapter 2, presents a theoretical background for describing the role of the organic matter present in natural systems on the availability of metals and how these interactions can be modelled.

Chapter 3 is devoted to description of the experimental method used in the study of the competition effects in humic acid binding at fixed total metal

concentration. The experimental work consisted of potentiometric titrations of humic acid with commercial combined glass electrodes, calibrated in terms of proton concentration at constant ionic strength. This technique allows the direct measurement of the free proton concentrations in the aqueous phase. The simple acid-base titration in presence of different amounts of other competing metals yields indirect information on the binding with these metals. Other ion selective electrodes were used, such as Cd^{2+}-ISE and Pb^{2+}-ISE, in order to validate the information on metal binding.

Chapter 4 is aimed to the analysis of the experimental work and to the development of the conditional affinity spectra of proton binding at fixed total metal concentration (CAScTM), which allows the interpretation of the binding results in terms of the effective distributions of binding energies in each condition.

Chapter 5 is devoted to a theoretical study of the distribution of occupied sites (and their corresponding affinities) of fulvic acid by 14 different cations in presence of major inorganic ions and trace metals at pH and concentration values representative of river water.

The second part of this thesis, chapter 6 to 9, corresponds to the study of the theoretical background of the DGT technique and the kinetic properties of metal-complexes.

Chapter 6, presents a theoretical background of the concept of complex lability and the dynamical techniques able to measure the labile metal fraction present in the medium. It is also shown the relevance of this fraction to the toxicological studies. Finally, the fundamentals of the DGT technique are reviewed.

Chapter 7 is devoted to the DGT experimental section. Different experiments were carried out to determine in the most accurate way possible, some operational parameters of the DGT sensors.

Chapter 8 shows the importance of the penetration of complexes into the resin layer of the DGT sensor and its influence in the lability measurement. This chapter is divided into two works. The first one describes the numerical model used to assess the impact of the resin layer on the lability of complexes. The second one, provides approximate analytical expressions for the calculation of the metal flux, lability degree and concentration profiles in a DGT experiment considering the species penetration into the resin layer.

Chapter 9 presents a rigorous analysis of the conditions were the consideration of the DGT resin layer acting as a perfect sink is valid. Different experimental conditions are explored: the effects of pH (proton competition), deployment time and dissolved ligand concentration.

The third part contains the general discussion and the conclusions.

The work presented in this thesis led to the publication of the following articles:

(1*)* *Competition effects in cation binding to humic acid: Conditional affinity spectra for fixed total metal concentration conditions.*

C. David, S. Mongin, C. Rey-Castro, J. Galceran, E. Companys, J. L. Garcès, J. Salvador, J. Puy, J. Cecilia, P. Lodeiro, F. Mas.

Geochimica Et Cosmochimica Acta 2010, 74, (18), 5216-5227.

(2) *Effective Affinity Distribution for the Binding of Metal Ions to a Generic Fulvic Acid in Natural Waters.*

C. Rey-Castro, S. Mongin, C. Huidobro, C. David, J. Salvador, J. L. Garcès, J. Galceran, F. Mas, J. Puy.

Environmental Science & Technology 2009, 43, (19), 7184-7191.

(3) *Key Role of the Resin Layer Thickness in the Lability of Complexes Measured by DGT.*

S. Mongin, R. Uribe, J. Puy, J. Cecilia, J. Galceran, H. Zhang, W. Davison

Environmental Science & Technology 2011, 45, (11), 4869-4875.

(4) *Contribution of Partially Labile Complexes to the DGT Metal.*

R. Uribe, S. Mongin, J. Puy, J. Cecilia, J. Galceran, H. Zhang, W. Davison

Environmental Science & Technology 2011, 45, (12), 5317-5322.

(5*)* *Two modes of operation of the DGT sensor: kinetic and equilibrium regimes*

S. Mongin, R. Uribe, C. Rey-Castro, J. Cecilia, J. Galceran, J. Puy.

In preparation for submission.

CHAPTER 4. *Competition effects in cation binding to humic acid*   **57**

Competition effects in cation binding to humic acid: Conditional affinity spectra for fixed total metal concentration conditions

CHAPTER 5. *Binding of metal ions to a generic fulvic acid in natural waters*   **65**

Effective Affinity Distribution for the Binding of Metal Ions to a Generic Fulvic Acid in Natural Waters.

CHAPTER 9. *Two modes of operation of the DGT*   **191**
sensor: kinetic and equilibrium regimes

CHAPTER 1

INTRODUCTION

1.1 Metals in the environment

Metals are defined chemically as "elements which conduct electricity, have a metallic luster, are malleable and ductile, form cations, and have basic oxides".[1]

Metals are found throughout the earth, in rocks, soils and sediments, primarily trapped in some stable form. Through natural processes such as weathering and erosion, small amounts of metals are removed from bedrock and are allowed to circulate in water and air. This is essential because many biochemical processes require a given amount of many of these metals. So, even if a trace metal is toxic at high concentrations, it may be needed in small quantities to maintain life. Therefore, the existing biogeochemical cycles ensure that the distribution of any given metal within an ecosystem be held relatively constant over time.

Humans have used various means to extract metals from the earth's crust. Despite the benefits that these activities infer, society has had to embrace the harsh consequences of metal pollution. Early on, metal pollution only affected that small portion of the population who were in the local region surrounding the source. During this period, mining, smelting and manufacturing took place in small, isolated facilities.

However, with the increase in the standard of living and in the number of technological advances, as seen in the 20th century, large quantities of various metals have been required to meet the demands imposed. Inevitably, as the usage of metals increased, so did the pollution associated with it. Pollutants were no longer restricted to local areas, but instead, were distributed over a wide area, by means of air and water. This has caused visible detrimental effects to the ecosystem and consequences to human health. The demand has been so extreme that quantities of most trace metals introduced into the environment by anthropogenic sources now far outweigh natural sources. This has produced a situation in which the natural biogeochemical cycle has been overwhelmed.

Metal pollutants are primarily distributed in the atmosphere, water, soil and sediments. Atmospheric metal pollution arises mainly from the mining, smelting and refining of metallic ores, the manufacturing and use of metallic products, and the burning of fossil fuels. Atmospheric pollutants are often the largest source of waterborne metals. For example, it is estimated that 70% of lead in water and over 50% of many of the other trace metals in the Great Lakes are derived from atmospheric transfer. However, in the case of mercury,

atmospheric pollutants account for only 30% of the total waterborne amount. Similarly, cadmium is delivered to water via direct industrial discharge into waterbodies. In general, freshwater ecosystems have low natural background metal levels and therefore tend to be sensitive to even small additions of most trace metals. Soils and sediments are the ultimate sink for many pollutants.

Arable soils receive metals from pesticides, fertilizers and animal waste. Metals tend to accumulate in the soil, where they can be taken up by crops. For example, high metal concentrations have rendered 9.5% of Japanese rice paddies incapable of producing consumable products. Accumulation of metals in sediments may enter the foodchain through benthic invertebrates or by fish feeding on the sediments. This deposition in the sediments may result in persistent metal concentrations within the aquatic ecosystem.

The global consumption of metals is increasing since the Middle Age. In the last two decades, in the developed countries, the awareness of the dangers of the toxicity was taken into account and the emissions of some metals have decreased (**figure 1.1**). To achieve this, a number of regulation related to its uses substitutes have been implemented, for example: the ban on leaded fuel and restrictions on the marketing of several measuring devices containing mercury.[2] Regarding natural waters, Directives of the European Parliament fixed quality standards of 41 contaminants including metals for natural and ground water. They impose the reduction or suppression of 13 substances in wastes before 2021.[3] Application of these quality standards would allow reaching the good status of natural water request by the Water Framework Directive before 2015.[4]
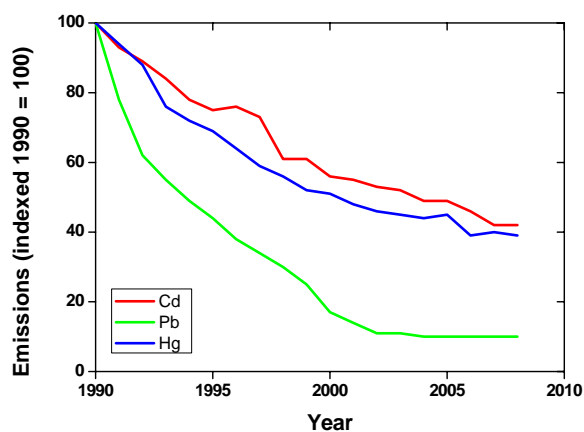
Figure 1.1. Emission trends of selected heavy metals (EEA member countries - indexed 1990 = 100)[5]

1.2 Importance of speciation

As mentioned in the previous section, some metals are essential for the complete life cycle of an organism, and their absence produces specific deficiency symptoms (e.g. cobalt, sodium, copper, magnesium, iron, potassium, zinc…). The term "toxic metal" is imprecise. The fundamental rule of toxicology is that all substances, including carbon and all other elements and their derivatives, are toxic given a high enough dose. The degree of toxicity of metals varies greatly from metal to metal and organism to organism. Toxicity should be defined by reference to dose-response curve for the species under consideration.

Moreover, the term "toxic metal" implies that pure metal and all its compounds have the same physico-chemical, biological, and toxicity properties. For example, there is no similarity in proprieties between pure tin, which has low toxicity, and tributyltin oxide, which is highly toxic to oysters and dogwhelks. Nor is there any similarity in properties between chromium in stainless steel, which is essentially non-toxic, and in the chromate ion, which has been associated with lung cancer.

Consequently, the knowledge of the physico-chemical forms of metals is of great importance. Speciation is the term used for the determination of species over theses different forms, and for the distribution itself.

In aquatic systems, the main forms of metals are: the free hydrated ion; complexes with simple inorganic ligands (such us chloride, nitrate, and carbonate), complexes with macromolecular ligands (like humic and fulvic acids), metal ions adsorbed on a variety of colloidal particles (for example clay and iron or manganese oxides), and precipitated metal compounds (e.g. metal sulphides). All these species can co-exist and, hence, the prediction of the metal ion distribution in these systems may be quite complicated.

1.3 Bioavailability, speciation and lability

Bioavailability is related to the flux that contributes to metal uptake, either directly (by direct passage through the membrane) or indirectly (after complex dissociation). This depends on the mass transport of the various metal species and the kinetics of the chemical reactions regulating the biouptake processes, both outside and within the biological membrane. [6-10]

Introduction

The uptake of contaminants by living organisms mostly occurs by exposure to dissolved species. Plants are exposed to pollutants in the soil by their roots and animals mainly by drinking contaminated water or indirectly by eating contaminating plants or other animals. Thus the concentration of contaminants in the aqueous phase is of great importance. Suspended particles such as colloids or dissolved organic matter can immobilize toxic elements by complexation, precipitation, adsorption and biotransformation; so the particles act as a sort of buffer for these elements. The buffer capacity of the natural environment strongly influences the impact of toxic chemicals.

It has been generally recognised that it is not the overall concentration of a pollutant which controls the toxicity in a contaminated site, but rather the concentration of the different speciation forms of this pollutant and, thus, the bioavailability of each different species has to be considered.

A major issue in the ongoing debate on the subject is the distinction between the total metal activity and the free-ion activity as the determinant bioavailability parameter. One of the key assumptions of the so called Free-Ion Activity Model (FIAM) is that the transport of the metal in solution is fast compared to the actual uptake by the organism (so that the latter is rate-determining). Then it is justified to reason that the complex association/dissociation reactions are practically at equilibrium, so that for all species the bulk and the surface activities are approximately the same. Thus for systems with bioinactive complexes, which obey the above assumption concerning the rate-limiting step, the FIAM may be accepted to apply. In these cases, the free-ion activity controls the reactions of the metal with surface sites of the organisms and consequently governs the "bioavailability" of the metal in the complex medium.[11]

As mentioned above, applicability of the FIAM requires sufficiently fast transport in solution. For a metal complex system, this means that the limiting flux of free ions (unsupported by coupled transport of labile complex species) should be much larger than the real biouptake flux. For systems with a high degree of complexation, this condition might be rather severe. We may then ask the obvious question of whether an organism will be satisfied with a very small offer of free metal ions or if its uptake rate will provoke dissociation of complex species so as to increase the supply of free metal? The answer to this question is not trivial since the relation between the biouptake rate and the bulk metal concentration is not linear in a wide range of concentrations (whereas the transport rate is).

Lability criteria have been developed to predict which process controls the metal flux when a ligand is present in the system:[9,10,12] either the dissociation process (in which case the system is called partially labile or nonlabile), or the transport process to the surface (in which case the system is called labile). Recently, a quantitative parameter called the degree of lability has been introduced to measure the percentage of the complex contribution to the uptake flux with respect to its maximum contribution obtained when the kinetics of the complexation processes is fast enough to reach equilibrium conditions at any time and relevant spatial position.[8-10,13-15] Among others, lability is influenced by the kinetics of the complexation processes, the transport phenomena present in the system, the size of the sensor, and the processes at the surface leading to the internalization.

1.4 References

(1)   Atkins, P.; Jones, L., *Chemistry - Molecules, Matter and Change*. Freeman, W. H.: New York, **1997**.

(2)   Directive 2007/51/EC of the European Parliament and of the Council of 25 September 2007 amending Council Directive 76/769/EEC relating to restrictions on the marketing of certain measuring devices containing mercury (Text with EEA relevance). In.

(3)   Directive 2008/105/EC of the European Parliament and of the Council of 16 December 2008 on environmental quality standards in the field of water policy, amending and subsequently repealing Council Directives 82/176/EEC, 83/513/EEC, 84/156/EEC, 84/491/EEC, 86/280/EEC and amending Directive 2000/60/EC of the European Parliament and of the Council. In.

(4)   Directive 2000/60/EC of the European Parliament and of the Council of 23 October 2000 establishing a framework for Community action in the field of water policy. In.

(5)   Göttlicher, S.; Gager, M.; Tista, M., *European Union emission inventory report 1990-2009 under the UNECE Convention on Long-range ransboundary Air Pollution (LRTAP)*. European Environmental Agency: Copenhagen, **2011**; p 93. http://www.eionet.europa.eu/events/EIONET/Technical%20report_1.

(6)   Buffle, J., *Complexation Reactions in Aquatic Systems. An Analytical Approach*. Ellis Horwood Limited ed.; Chichester, UK, **1988**.

(7)   Buffle, J.; Horvai, G., *In situ Monitoring of Aquatic Systems; Chemistry of Environmental Systems*. John Wiley & Sons: Chichester, UK, **2000**; Vol. 6.

(8)   Galceran, J.; Van Leeuwen, H. P., Dynamic of Biouptake Processes: the Role of Transport, Adsorption and Internalization. In *Physicochemical kinetics and transport at chemical-biological surface*, Van Leeuwen, H. P.; Köster, W., Eds. Wiley: Chichester, UK, Chapter 4, 2004.

(9)   Salvador, J.; Puy, J.; Cecilia, J.; Galceran, J., Lability of complexes in steady-state finite planar diffusion. *Journal of Electroanalytical Chemistry* **2006,** *588*, (2), 303-313.

(10)   Salvador, J.; Puy, J.; Galceran, J.; Cecilia, J.; Town, R. M.; van Leeuwen, H. P., Lability criteria for successive metal complexes in steady-state planar diffusion. *Journal of Physical Chemistry B* **2006,** *110*, (2), 891-899.

(11)   Campbell, P. G. C., Interactions between Trace Metal and Aquatic Organisms : A Critique of the Free-ion Activity Model. In *Metals Speciation and Bioavailability in Aquatic Systems*, Tessier, A.; Turner, D. R., Eds. John Wiley & Sons: Chichester, 1995.

(12)   van Leeuwen, H. P., Revisited: The conception of lability of metal complexes. *Electroanalysis* **2001,** *13*, (10), 826-830.

(13)   Galceran, J.; Puy, J.; Salvador, J.; Cecilia, J.; Mas, F.; Garces, J. L., Lability and mobility effects on mixtures of ligands under steady-state conditions. *Physical chemistry chemical physics* **2003,** *5*, (22), 5091-5100.

(14)   Galceran, J.; Puy, J.; Salvador, J.; Cecilia, J.; van Leeuwen, H. P., Voltammetric lability of metal complexes at spherical microelectrodes with various radii. *Journal of Electroanalytical Chemistry* **2001,** *505*, (1-2), 85-94.

(15)   Pinheiro, J. P.; Galceran, J.; Van Leeuwen, H. P., Metal speciation dynamics and bioavailability: Bulk depletion effects. *Environmental Science & Technology* **2004,** *38*, (8), 2397-2405.

Part I

CHAPTER 2

THEORETICAL BACKGROUND

BINDING OF CATIONS BY NATURAL MATTER

2.1 The role of organic matter on the bioavailability of metals

The term Organic Matter (OM) is used to define the set of natural and anthropogenic organic compounds of an ecosystem. Generally the boundary between Dissolved Organic Matter (DOM) and particle OM is a size of 0.45 μm.

Natural DOM found in aquatic systems has two principal sources: terrestrial and aquatic. Naturally occurring organic compounds in soils have been object of scientific research for more than 200 years, because agricultural scientists early recognized the importance of natural organic matter in enhancing soil fertility and water-holding capacity.[1] Principal sources of terrestrial DOM are higher plants and micro-organisms.[2,3] The aquatic DOM is mainly due to the degradation of micro-organisms and phytoplankton.

The anthropogenic DOM observed in aquatic systems comes mainly from surface runoff (landfill leachate, urban runoff, etc), urban (domestic and industrial) and agricultural wastewater.[3,4]

Soil organic matter denotes all organic material in the soil, including undecayed plant and animal tissues, their partial decomposition products, and the soil biomass. Thus, this term includes:

- Identifiable, high molecular weight organic material such as polysaccharides and proteins

- Simple substances such as sugars, amino acids, and other small molecules

- Humic Subtances (HS)

Distribution of the soil organic matter is shown in **figure 2.1**.

Aiken *et al.*[5] state that HS are a general category of naturally occurring, biogenic, heterogeneous organic substances that can generally be characterized as being yellow to black colour, of high molecular weight, and refractory.[2,6] This definition is still broadly relevant but as discussed in a special issue of the Soil Science Journal, 1999[7-9], the classical interpretations suggesting that HS have high molecular weight values may not be as acceptable now.[10]
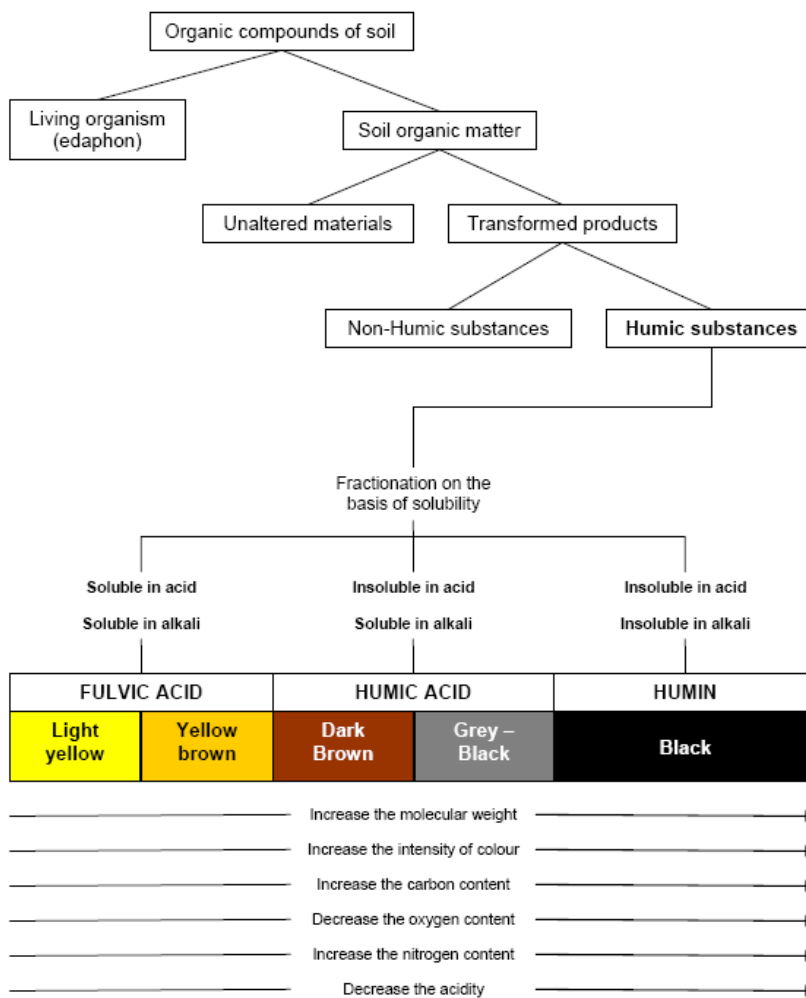
Figure 2.1.Distribution of the soil organic compounds and fractionation of soil organic matter and humic substances showing some chemical properties[11,12]

There is still debate as to the exact mode of formation of HS, but there are two major pathways that have wide support[8]. One of these pathways involves the biochemical modification, transformation, and degradation of pre-existing plant components by micro-organisms. In the second pathway, the HS are microbiologically synthesized, in part or in entirety, from a range of molecules derived from plant precursors (e.g., phenols, saccharides and peptides) and

thereby constitute a new, separate class of compounds. The essential difference between the two pathways is that the first is based on the progressive oxidation and degradation of existing plant polymers and the second involves the formation of new macromolecules that are themselves oxidatively degraded over time.

In aqueous systems, such as rivers, about 50 % of DOM is HS; they are three major fractions of HS (Fulvic Acid (FA), Humic Acid (HA) and humin), whose definitions are operational and based on aqueous solubility properties. The boundary between these fractions are, however, not clear: HA and FA can be considered as a continuum.[10] **Figure 2.1** shows a flow diagram outlining the interrelationship of these three fractions:[12]

- HA, as defined by Aiken et al.[5], are the fraction of HS that is insoluble at pH below 2 in aqueous solution but is soluble at higher values. They can be extracted from soil with various basic reagents but they are insoluble in dilute acid. They are dark brown to black in colour.

- FA are defined[5] as the fraction of humic substances that is soluble in water under all pH conditions. They remain in solution after removal of HA by acidification. FA are light yellow to yellow-brown in colour.

- Humin is defined[5] as the fraction of humic substances that is not soluble in water at any pH value. Humin is black in colour.

In recent years, HS are isolated from water by non-ionic macro-porous resins (XAD-8).

An important characteristic that defines a humic substance is the type and content of functional groups.[6,11,13,14] **Table 2.1** shows some of the functional groups encountered in humic acids, being the carboxylic and phenolic the major ones. Some models of humics often simplify the system to two different functional groups (carboxyl and phenolic). Due to the abundance of this type of groups able to lose protons, these macromolecules are predominantly charged negatively and they can affect the speciation, the cycles, and the bioavailability of chemical elements. Indeed, HS have a great interaction capacity with metals or organic contaminants[6] that can change their bioavailability.[15]
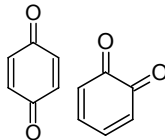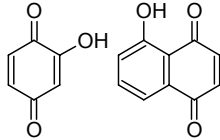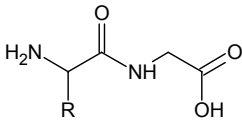
Amino	$-NH_2$	Anydride	$R-COO-COR'$
Amide	$R-CO-NH_2$	Imino	$=NH$
Alcohol	$R-CH_2OH$	Ether	$R-CH_2-O-CH_2-R'$
Aldehide	$R-CHO$	Ester	$R-COOR'$
Carboxyl	$R-COOH$	Quinone	
Carboxylate ion	$R-COO^-$		
Enol	$R-CH=CH-OH$	Hydroxi-quinone	
Ketone	$R-CO-R'$		
Keto acid	$R-CO-COOH$	Peptide	
Unsatured carbonyl	$-CH=CH-CH=C$		

Table 2.1. Some of important structural groups of humic substances adapted from Stevenson (1982).[16]

The total acidic functional groups of FA (1000 - 1200 meq / 100 g)[17] are considerably higher than for HA (500 – 600 meq / 100 g)[17]. Other important differences in composition between FA and HA are depicted in **figure 2.1**, in which it can be seen that the carbon, nitrogen and oxygen contents as well as acidity change systematically with the increasing molecular weight. The oxygen in FA can be accounted for largely by functional groups (COOH, OH and C = O) whereas in HA a high proportion of oxygen seems to occur as a structural component of the nucleus.

HS are macromolecules that not have a single and defined structure. Although precise formulas for HS cannot be made, different type structures have been recorded in the literature. The scope of these structures has been recently questioned[18,19] ; nevertheless as a matter of example, one is presented here

(**figure 2.2**). Schulten and Schnitzer[20] suggested a complicated carbon – based structural network for soil HA, as shown in **figure 2.2**. This model was constructed in accordance with author's analytical data obtained by pyrolysis – gas chromatography / mass spectrometry (Py – GC / MS), pyrolysis – field ionisation mass spectrometry (Py – FIMS), ^{13}C nuclear magnetic resonance (^{13}C NMR), electron microscopy and also by chemical oxidative and reductive degradation of several HA preparations. It consists of numereous chemically coupled aromatic structures with long alkyl chains as to form a flexible network containing voids that trap and bind other organic components. Both carboxyl (COOH) and phenol (OH) groups are present in abundance and they occupy positions on both aromatic rings and aliphatic chains.
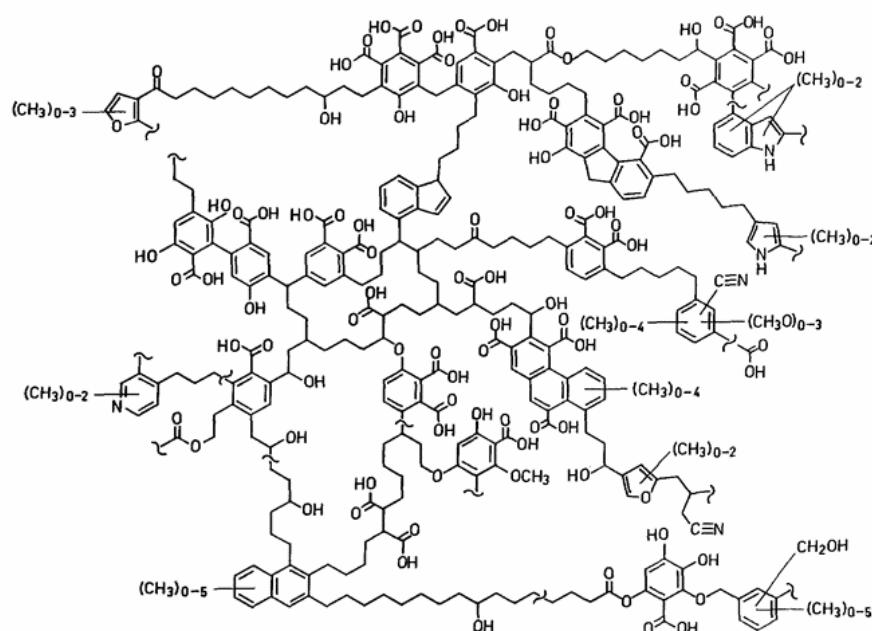
Figure 2.2. Hypothetical structure of humic acid according to Schulten and Schnitzer.[20]

The direct impact of DOM on the environment quality and on the food chain is today well known (deoxygenation, eutrophication …) but its indirect impact, as a factor of influence on the contaminant bioavailability is fundamental and poorly known. The binding between HS and metals present in environment has special importance[21], since it affects the free metal concentration and mobility in

natural waters, soils and groundwater. This binding depends on the pH value and ionic compounds present in the medium due to the competition between metal ions and protons and to the fact that the pH affects the charge of the molecule by regulating the dissociation of the functional groups. All these effects will be developed in the following section.

2.2 Model of chemical elements complexation by organic matter

The study of macromolecular complexation shows significant differences with the study of the equilibria of simple ligands due to the relatively high number of complexing sites and to several "secondary" effects that may influence the overall complexation process in greater o lesser extent.[6]

First, the complexation of cations by simple ligands will be discussed and, later on, the specific characteristics of the binding in macromolecular systems will be reviewed.

2.2.1 Complexation by simple ligands

The study of metal complexation by both inorganic and simple organic ligands has focused on the construction of a data base of stability constants for simple reactions in solution at selected temperatures and ionic strengths.

The dependence of the stability constant on the ionic strength is a function of the activity coefficients of the species involved (ions and neutral molecules). The simplest formulation is the equation for a 1:1 stoichiometry between an organic ligand (L) and a cation (M):

$$nL^{y^-} + M^{z^+} \rightleftharpoons LM^{(z-ny)} \qquad (2.1)$$

Where K^T is the thermodynamic equilibrium constant, defined by the law of mass action as:

$$K^T = \frac{a_{LM}}{a_L \, a_M} = \frac{c_{LM}}{c_L \, c_M} \cdot \frac{\gamma_{LM}}{\gamma_L \, \gamma_M} = K^* \cdot Q(\gamma_i) \qquad (2.2)$$

Where c represents the concentrations of species, a is the activity and γ the activity coefficient of each compound. K^* is the stoichimetric constant, and $Q(\gamma_i)$ the ratio of activity coefficients of the species associated to the equilibrium. The

goal of most of the studies regarding the ionic strength effect on the stoichiometric constant is to model the $Q(\gamma_i)$ term.

In dilute conditions and in the presence of a constant electrolyte background, K^* is independent of c_M, which is characteristic of the binding to simple ligands.

In general, it is assumed that the mean activity coefficient of an electrolyte consists of two contributions, namely: long-range (coulombian) interactions and short-range (specific) interactions. The first term is dependent of the nature of the salt concerned, whereas the second is associated to the specific differences. As concentration approaches infinite dilution, the second factor becomes negligible, and it is the electrostatic force among charges the only effect that determines the deviation from the ideal state. The limiting behaviour of the electrolyte solutions is described by the well-known Debye-Hückel equation.[22] Application of this equation is limited because it gives satisfactory agreement with experimental measurements only for low electrolyte concentrations, typically less than 10^{-3} mol L^{-1}. Therefore, several empirical extensions of the Debye-Hückel theory have been developed. They usually allow the Debye–Hückel equation to be followed at low concentration and add further terms in some power of the ionic strength to fit experimental observations. One example is the Davies equation[23], which is relatively simply and valid for a range of ionic strength between 0.01 and 0.1 mol.L^{-1}:

$$\log\gamma_i = \frac{-A\,z_i^2\,I^{1/2}}{\left(1+BI^{1/2}\right)} + CI \qquad \textbf{(2.3)}$$

where A, B, C are constants that depend on the solvent dielectric constant and temperature, z is the ionic charge and I is the ionic strength, calculated according to:

$$I = 0.5\sum_i c_i z_i^2 \qquad \textbf{(2.4)}$$

In the case of solutions with ionic strengths higher than the range valid for the Davies equation (sea water, synthetic concentrated solutions…), other empirical extensions of the Debye-Hückel theory can be used, such as the Specific ion Interaction Theory (SIT)[24] for ionic strength between 0.5 and 3 mol.L^{-1} or the Pitzer's equation.[25]

The molecular weight of a simple ligand is usually lower than 500, therefore the application of this type of model to the aquatic environment, mixtures of

colloids, polyelectrolytes and the polyfuncional ligands is quite limited. However the simple ligand model is very useful to understand the complexation reactions in aqueous solution and provides solid basis for speciation studies.

2.2.2 Complexation in macromolecular systems

Due to the complexity of humic substances (heterogeneous and undefined composition), it is not possible to treat these molecules as a simple ligand, and must be considered as a macromolecular system.

A macromolecular species refers to a species that cannot be fully isolated, but can be separated into groups of homologous compounds possessing operationally similar properties. These species are polidisperse, showing more or less broad range of molecular weights and molecular compositions. Examples of this category are HS, natural polysaccharides (e.g. alginic acid), colloidal particles, etc.

The study of macromolecular complexation shows significant differences with the study of the equilibria of simple ligands, due to the following reasons:

(a) The electrostatic interaction due to the presence of a high number of functional charged groups in the macromolecule.[6,26-28] Macromolecules carry a high local charge density, which influences the stability of the complexes. We can consider, for instance, the particular case of proton dissociation from an initially uncharged macromolecule acid. As the dissociation proceeds, the net charge become progressively more negative, and therefore each proton experiences a larger net attractive Coulombic force than the previous one, which means that the apparent dissociation constants decreases, i.e. the acid becomes weaker.

(b) The intrinsic interactions, due to the different functional groups in the macromolecules.[6,11,29,30] This heterogeneity usually derives from chemically different functional groups, but it can also arise from identical groups with different chemical environment. In some treatment it is convenient to assign an intrinsic binding constant to each set of sites and a relative abundance to describe the distribution of the different affinities.[27,31]

(c) The steric conformation[6,7,32] (i.e. changes in the spacial distribution) of the macromolecules can vary with the chemical conditions of the medium, such as pH, ionic strength, or amount of complexed cations.

(d) Competition effects. An additional problem in the study of cation binding to macromolecules is the competition among different cations.[6,33-35] In general, a variety of different inorganic ionic species co-exist in natural systems. Therefore, two or more species compete with each other for the same complexing site of the macromolecule. Even in the simplest case of the complexation of only one metal ion, the competition with protons is always present. This problem is easily affordable in simple ligands, whereas in macromolecular systems is not so straightforward due to the different binding stoichiometries (which are often ill – defined) among the competing ions.

In general, the previous physicochemical effects are coupled, that is, they occur simultaneously. In the **figure 2.3** shown below, the intrinsic and electrostatic bindings formed between HS and metal (M^{2+}) are schematized.
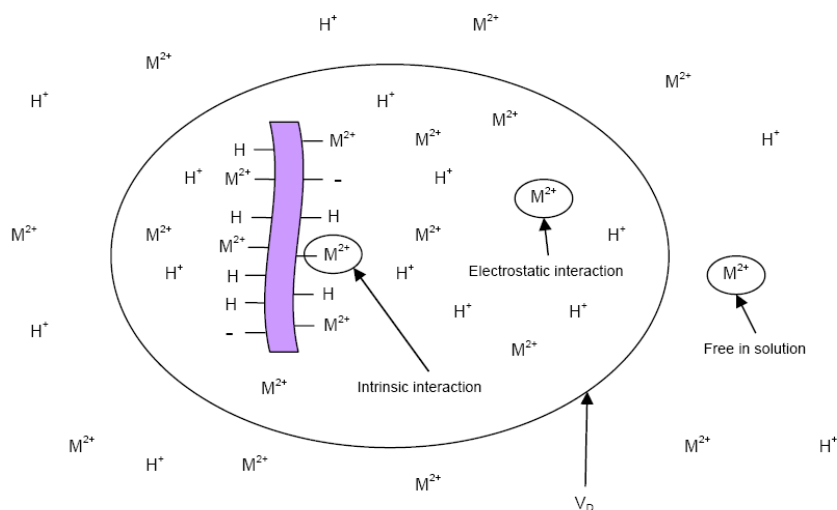
Figure 2.3. Scheme of the intrinsic and electrostatic interactions in a humic substance molecule.

2.2.2.1 Proton binding: discrimination between intrinsic and electrostatic interactions

The usual starting point for the understanding of ion binding to natural organic matter is the proton binding as a function of pH in a simple 1:1 electrolyte. In this case there is no interference of metal ions and the magnitude of the particle

charge solely depends on the pH and the electrolyte concentration. By analysis of proton binding curves measured at different ionic strengths, the intrinsic chemical affinity and the electrostatic contribution to proton binding can be determinated separately using an electrostatic model.

The major ion binding sites in humic and fulvic acids are attributed to the carboxylic and phenolic groups. Therefore, the chemical heterogeneity can be accounted for in a binding model by a series of "intrinsic proton affinity constants", as known as the affinity spectrum (see section 2.2.2.3).

However, as the dissociation of acidic groups proceeds, the net charge of the macromolecule becomes more negative leading to an increase of the electrostatic interactions that affects the proton binding behavior. This "electrostatic affinity" must be taken into account into the model. Higher is the electrolyte concentration, smaller is the electrostatic effect. Morever, the medium ionic strength also plays a role. Due to screening of charges by the background ions, the electrostatic effect usually becomes weaker as the ionic strength increases.

The discrimination between intrinsic and electrostatic effects can only be done after making simplifying assumptions. The central assumption is that at a given pH and electrolyte concentration the local electrostatic potential near the binding sites can be characterized by only one characteristic average value of the potential. This implies that (i) the charge is assumed to be smeared-out over the macromolecule and that (ii) effects of particle size, shape and site density and the distribution of potentials inside the particle or on the particle surface are largely neglected. Schematically, the situation is illustrated in **figure 2.4**, which emphasizes that different HS from a certain source are all represented in the electrostatic model by one type of average monodisperse spheres that can be either impenetrable or penetrable for ions.

Once that suitable electrostatic model is chosen for the calculation of the characteristic electrostatic potential of the macromolecule as a function of the electrostatic charge (C/kg) at a given pH and ionic strength, then the ion activity (or concentration) in the bulk solution can be converted into the ion activity (or concentration) in the solution adjacent to the binding sites. From the estimated potential on the surface of the macromolecule it is possible to redraw the experimental charge versus pH curves measured at different salt concentration as charge versus pH adjacent to the binding site (pH_0). In this way, the electrostatic interaction are taken into account explicitly in pH_0, which means

that the effect of the salt concentration on the proton binding isotherm should vanish. Therefore, when an appropriate electrostatic model is used, the charge versus pH_0 curves should merge into one "Master Curve" (MC). The MC reflects only the effects of the intrinsic affinities on the proton binding. The method originates from De Wit et al.[27,29] (see section 2.2.2.3)

impenetrable   penetrable
sphere   sphere
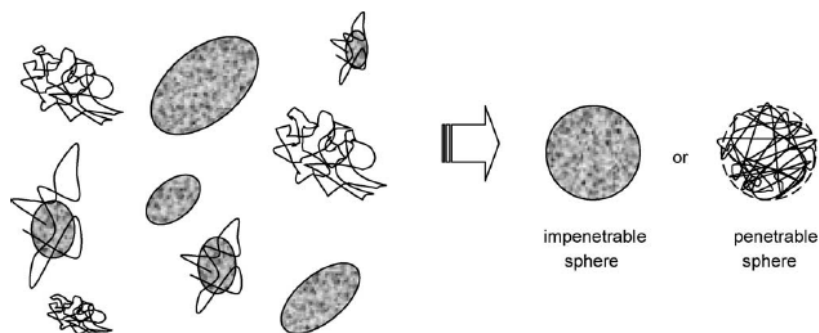
Figure 2.4. Schematic picture of the simplified description of the electrostatic interactions represented by one characteristic potential.[36]

2.2.2.2 Electrostatic models – Donnan model

A model of electrostatic interactions can provide a description of three aspects of ion binding: (i) the ionic strength dependency of proton and metal binding through their effect on the local electrostatic potential at the binding sites, (ii) the extent of non-specific ion binding in response to the residual (usually negative) charge on the humic substances; and (iii) second order effects due to long range interactions, e.g. binding on high affinity type sites can affects the specific binding to all sites. Basically all three aspects are reflected in the ion accumulation around molecules governed by a Botzmann factor that includes the local electrostatic potential and that has been used in the master curve construction.

Due to the electrostatic effects, the effective value of the apparent binding constant might be changed by up to four orders of magnitude compared to the intrinsic constant. Furthermore, the electrostatic effect contributes to apparent heterogeneity in binding at constant ionic strength, since as cation binding to the humic molecules increases, the net charge decreases and the electrostatic effect diminishes. Therefore, to achieve a reasonable description of the chemical

heterogeneity of humic substances, the electrostatic interactions need to be recognized.

In general, the molecule charge and the distribution of counter ions that compensates the charge can be described by the Poisson-Botzmann (PB) equation.[37] In order to apply the PB equation to humic substances, the structure, the shape and the size of the molecule must be known. Wit et al.[27,29], Milne et al.[38,39] Saito et al.[40] assumed the molecules to be homogeneous with respect to size (whereas HS are known to be heterogeneous and represented by non-permeable spheres). These authors suggested, as the optimum radius, the value that yields better convergence of the mastercurve. However, the optimized values found are, in general, relatively small compared to the experimentally estimated molecular sizes.

An alternative picture is the Donnan model which represents the extreme case of a macromolecule being permeable to solvent and small ions, where the charge is uniformly distributed within the molecular domain, and the net charge is zero. This is called the Donnan model because it is formally the same as the "Donnan effect", which accounts for the unequal distribution of charge in a macroscopic system where two solutions are separated by a membrane that is permeable to small (mobile) ions but not to macroions (**figure 2.5**).
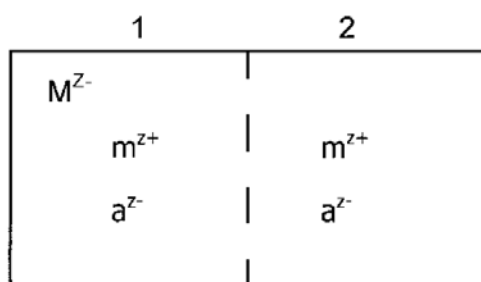
Figure 2.5. Schematic diagram of Donnan equilibrium. M represents the (anionic) macroion, wich cannot pass through the membrane (dashed line). Electrolyte ions are denoted by m (cation) and a (anion). At the equilibrium $c_{m_1} > c_{m_2}$ and $c_{a_1} < c_{a_2}$.[41]

In a microscale version, the membrane is conceptual. It is assumed that the charged groups inside the macromolecule are compensated by the counter-ions within a "Donnan volume" that surrounds the macromolecule. Kinninburgh et al.[42] wrote the electroneutrality condition as:

$$q/V_{\mathrm{D}} + \sum z_j \left(c_{D,j} - c_j \right) = 0 \qquad \text{(2.5)}$$

where q is the net charge of humic substances (eq g^{-1} or eq mol^{-1}), V_{D} is the volume of the Donnan solution phase (L kg^{-1}, see **figure 2.3** for a schematic representation of V_{D}), $c_{\mathrm{D},j}$ are the molar concentrations of the various cations and anions present in the Donnan phase, c_j are the concentrations in the bulk solution and z_j are their charges, including the sign.

The concentrations in the two phases are related by a Boltzmann factor:

$$c_{D,j} = \chi^{z_j} c_j \qquad \text{(2.6)}$$

The Boltzmann factor is linked to the uniform Donnan potential (Ψ_{D}) by:

$$\chi = \exp\left(-\mathrm{e}\,\psi_{\mathrm{D}}/kT \right) \qquad \text{(2.7)}$$

where e is the charge of the electron, k is Boltzmann's constant and T is the absolute temperature.

Koopal et al[36] advice the use of the empirical Donnan volume relation suggested by Benedetti et al[43] for reason of convenience and because this model does not need information on the size of the macromolecule and/or the molar mass. A critical aspect of this model is how the Donnan volume depends on changes in solution chemistry. Benedetti et al[43] discussed this point in some detail and concluded that the most influential parameter is the ionic strength (i.e. the effect of the pH or the macromolecule charge on the volume is neglected). The variation of Donnan volume with ionic strength, I, for various humic substances is assumed to follow the empirical relation:

$$\log V_D = b\left(1 - \log I \right) - 1 \qquad \text{(2.8)}$$

where the coefficient b varies with the type of humic substance. In the case of humic acid, b$\approx$0.43, which gives the following V_{D}'s (in L.kg^{-1}): 1.95 (0.01M), 1.22 (0.03M) and 0.72 (0.1M).

Knowing (i) the Donnan volume (V_{D}); (ii) the bulk concentrations of all ions present (c_j), and (iii) the net charge of the humic substance (q) given by a model (for example NICA, see below, or WHAM), it is possible to solve **equations 2.6** to obtain the Boltzmann factor, and thereby the amount of binding of each ion.

These values lead to imposed charge values of the humic substances and iterative calculations proceed until convergence.

2.2.2.3 Intrinsic interaction. The affinity spectrum formalism

The intrinsic heterogeneity of a macromolecule derives from the presence of reactive groups which differ in their chemical affinities for a particular species (i. e., the proton or metal ion). As mentioned above, the differences in affinity may result from different type of reactive surface groups or from a variation in the chemical environment of a specific group. Due to these effects, natural organic matter appears to be chemically heterogeneous. One of the consequences is that the overall affinity of the macromolecular ligand decreases with progressive complexation since the higher affinity sites are mainly responsible for ion binding at low coverage and the lower affinity sites dominate the binding process at higher coverage.

Several methods have been developed to investigate the distribution of affinity constants on the basis of binding or adsorption isotherms. The main principle of these methods is that the heterogeneous set of binding sites is subdivided into subgroups of "equal binding energy". For each subgroup of equal-energy sites a binding equation for a homogenous substrate applies, the "local binding function". The "overall binding function",θ is interpreted as a superposition of a set of local isotherms $\theta_i = f(c_M, k)$, each corresponding to a local binding site, weighted by its probability of occurrence, the affinity spectrum $p(k)$.[44,45]

For a continuous distribution:

$$\theta(c_M) = \int_0^\infty p(k) f(c_M, k) \, dk \qquad \textbf{(2.9)}$$

where the affinity spectrum $p(k)$ is normalized to unity. It is not the most general relationship because it assumes that all binding sites have the same local isotherm and that they do not interact. Moreover, although the local equilibrium process could be assayed in terms of other isotherms, the simplest assumption is to postulate a Langmuirian isotherm. So, restricting the kernel of the integral to a Langmuir isotherm, the coverage can be written as:

$$\theta(c_M) = \int_0^\infty p(k) \frac{kc_M}{1 + kc_M} \, dk \qquad \textbf{(2.10)}$$

For a discrete distribution of affinities, this integral is reduced to a summation.

2.2.2.3.1 Determination of the distribution function

Given some experimental data, through semianalytical and numerical procedures, one can solve the integral **equation 2.10** and obtain the affinity spectrum p(k).

For the investigation of humic substances, the mostly used methods are based on approximations of the local binding function; the simplest method is called the Condensation Approximation (CA).[46] In this method, the local isotherm is approximated by a step function. The overall isotherm, plotted as bound amount vs. log activity, now represents the cumulative intrinsic affinity distribution function with bound amount = abundance and log (*a*) = -log *k*, where k is the affinity constant. Other methods, more involved than the CA, have also been proposed in literature[47,48]. One example of these numerical procedures will be shown in chapters 3 and 4, as has been tested for the present thesis.

Proton affinity distributions derived from acid-base titration of purified humic and fulvic acids[27,29,31,39,49-51] clearly show two broad peaks (bimodal distribution) The first one, has a maximum in the pH range 3-5 and is characteristic of carboxylic groups that weakly bind protons and that can be indicated as "low (proton) affinity" sites. A second broad peak is often found with a maximum at a much higher pH, which is characteristic of phenolic groups that strongly bind protons, and can be called "high (proton) affinity" sites. Other groups such as, for example alcohols, ethers, and bidentate sites are also likely to be included in these distribution.

2.2.2.3.2 Multidimensional affinity spectra

In going from single component binding to multicomponent binding several factors have to be considered. For humics substances, it is logical to assume that the active sites for protons also are involved in the binding of other cations. That is to say, all specifically bound cations, including the proton, compete for the same sites. Competition is taken into account in a binding model by considering that the reference sites can be occupied by different ions, and this will affect both the local and the overall binding equation.

Let us assume that the adsorption process can be viewed as binding to independent sites, each of which obeys the competitive Langmuir isotherm. In this case, the adsorption isotherms can be written as:[52-58]

$$\theta_i\left(c_1,c_2\right)=\int_0^\infty\int_0^\infty p\left(k_1,k_2\right)\frac{k_ic_i}{1+k_1c_1+k_2c_2}dk_1dk_2 \qquad \text{for i=1,2,} \tag{2.11}$$

where $p(k_1,k_2)$ is the affinity distribution, which in this case is a function of two affinity constants k_1 and k_2 and, therefore, can be regarded as a two dimensional spectrum. Generalization of **equation 2.10** to n competing species (a n-dimensional affinity spectrum) is straightforward. This affinity distribution is always normalized to unity. The fact that both isotherms $\theta_1(c_1,c_2)$ and $\theta_2(c_1,c_2)$ can be expressed in terms of a single affinity distribution $p(k_1,k_2)$ reflects that these isotherms are not two entirely independent functions and may be related. This affinity spectrum can be obtained from the experimental binding curve of the system and through numerical inversion techniques.

2.2.2.3.3 The NICA isotherm model

In order to describe the distribution function two options are possible: one can take a discrete or a continuous distribution. The most popular models are WHAM V/VI/VII[41,59-63] which use a discrete distribution of affinities and the Non-Ideal Competitive Adsorption isotherm (NICA)[29,33,35,41,42,49,61,64-68] which assumes a continuous distribution of affinities.

Some aspects of NICA model for multicomponent systems, will be considered with more detail here.

Proton and metal ion binding to a negatively charged site of type S are assumed to follow the reactions:

$$S^-+H^+ \rightleftharpoons SH$$
$$S^-+M^{z+} \rightleftharpoons SM^{(z-1)+} \tag{2.12}$$

where M^{z+} is a cation of charge z^+; S^-, $SM^{(z-1)+}$ and SH are surface species. These reactions imply monodental binding to all of the sites, i.e. one cation per site. For simplicity at this stage, we do not consider bidentate binding. Under the assumptions of congruency of the distribution function for H^+ and M^{2+} and within the NICA model, the total fractional surface coverage of component i, $\theta_{i,T}$, is then given by the following integral equation similar to the **equation 2.9**:

$$\theta_{i,T}=\int_{\Delta\log K_i}\theta_{i,L}\,p\left(\log k_i\right)\mathrm{d}\left(\log k_i\right) \tag{2.13}$$

where $f(\log k_i)$ is the distribution function of the affinity constant, k_i, $\theta_{i,L}$, is the local adsorption isotherm, i.e, the isotherm for binding of ion i to a group of identical sites, and $\Delta\log k_i$ is the range of $\log k_i$ considered. This equation can be solved analytically for certain distributions in combination with certain local isotherms. It has also been extended to multicomponent systems.[64,69-71] By separating the non-ideality into an intrinsic heterogeneity part applicable to all ions and an ion-specific part applicable to each individual ion, Koopal et al.[64] have derived the monomodal form of the NICA equation:

$$\theta_{i,T} = \frac{Q_i}{Q_{\max i}} = \frac{\left(\tilde{k}_i c_i\right)^{n_i}}{\sum_j \left(\tilde{k}_j c_j\right)^{n_j}} \frac{\left(\sum_j \left(\tilde{k}_j c_j\right)^{n_j}\right)^p}{1 + \left(\sum_j \left(\tilde{k}_j c_j\right)^{n_j}\right)^p} \qquad (2.14)$$

where Q_i is the total amount of the component i bound to the humic acid in mol kg^{-1}, $Q_{\max i}$ is the total number of sites able to bound the species i, in mol kg^{-1}, $\tilde{k}_j$ is related to the average affinity constant for the component j, and c$_j$ is the bulk concentration of j in mol L^{-1}. The various summations are over all j components (including i). This includes the proton and the metal ions present. Parameters $n_{i,j}$ ($0 < n_{i,j} \leq 1$) are related to binding non-ideality; the smaller the value of n, the greater the non-ideality. p ($0 < p \leq 1$) represents the intrinsic heterogeneity and is common to all components; the smaller value of p, the greater the heterogeneity. The value of p cannot be obtained from data for monocomponent binding alone since such data always reflect the combined effect of the both the non-ideality and the generic heterogeneity and so they can only give the product of $n_i \times p$. Therefore, a multicomponent set of binding data is needed to resolve n_i and p.

The NICA model can be easily extended to a bimodal distribution (carboxylic and phenolic sites):

$$Q_i = Q_{\max i,1} \frac{\left(\tilde{k}_{i,1}c_i\right)^{n_{i,1}}}{\sum_j \left(\tilde{k}_{j,1}c_j\right)^{n_{j,1}}} \frac{\left(\sum_j \left(\tilde{k}_{j,1}c_j\right)^{n_{j,1}}\right)^{p_1}}{1 + \left(\sum_j \left(\tilde{k}_{j,1}c_j\right)^{n_{j,1}}\right)^{p_1}} +$$

$$Q_{\max i,2} \frac{\left(\tilde{k}_{i,2}c_i\right)^{n_{i,2}}}{\sum_j \left(\tilde{k}_{j,2}c_j\right)^{n_{j,2}}} \frac{\left(\sum_j \left(\tilde{k}_{j,2}c_j\right)^{n_{j,2}}\right)^{p_2}}{1 + \left(\sum_j \left(\tilde{k}_{j,2}c_j\right)^{n_{j,2}}\right)^{p_2}}$$

(2.15)

where the subscripts 1 and 2 refers to the carboxylic and phenolic type of the distribution respectively. With a mixture of bound divalent cations M^{2+}, the total number of sites is given by the sum of the concentration of all the surface species:

$$Q_{\max H,1} = Q_{ref1} + Q_{H1} + 2\sum Q_{M_j 1}$$

$$Q_{\max H,2} = Q_{ref2} + Q_{H2} + 2\sum Q_{M_j 2}$$

(2.16)

Q_{ref} is the number of sites in the reference state, i.e. free of bound ion, Q_H is the number of protoned sites, $Q_{\max H,1}$, $Q_{\max H,2}$ are the total number of sites able to bound protons and $\sum Q_{M_j}$ is the number of sites occupied by divalent cations.

$Q_{\max H,1}$, $Q_{\max H,2}$, Q_{H1}, $Q_{H,2}$ can be estimated from an acid-base titration and $Q_{M_j 1}$, $Q_{M_j 2}$ can be estimated from the metal titration. The maximum amounts of metal and proton bound are related by:

$$\frac{Q_{\max H,1}}{Q_{\max i,1}} = \frac{n_{H,1}}{n_{i,1}} \quad \text{and} \quad \frac{Q_{\max H,2}}{Q_{\max i,2}} = \frac{n_{H,2}}{n_{i,2}}$$

(2.17)

Once the site occupancies have been established, the net charge of the humic substances (q) is given by the charge contribution from the various surfaces species of the two modes with:

$$q_1 = -Q_{\max H,1} + Q_{H1} + 2\sum Q_{M_j 1}$$

$$q_2 = -Q_{\max H,1} + Q_{H2} + 2\sum Q_{M_j 2}$$

(2.18)

$$q = q_1 + q_2 \qquad\qquad \textbf{(2.19)}$$

This net charge gives rise to a local electrostatic potential, which tends both to attract oppositely charged ions and to exclude coions.

2.2.2.4 The combined description of electrostatic interaction and specific binding: NICA-Donnan model

NICA model can be combined with electrostatic interactions by introducing the concentration of species at the localisation of binding site instead of using the bulk concentration c_j In order to calculate these concentrations, several assumptions have to be made and a certain electrostatic model has to be chosen. When the Donnan model for the electrostatics applies, we obtain the NICA-Donnan model (the Donnan concentrations c_{Dj} are introducing in the NICA model).

Therefore, the specific binding (intrinsic interactions) is described by the NICA model and the non-specific binding (electrostatic interactions) is described by the Donnan model.

The NICA-Donnan model has been extensively applied to heterogeneous complexation, thus yielding satisfactory results in modelling the binding and in predicting the effect of the ionic strength and the competition between several ions present in the medium, largely by potentiometric techniques[33,34,72,73] but also by voltammetry.[72,74]

2.2.2.5 The master curve approach

As mentioned in the preceding sections, the binding of ions to natural organic matter is simultaneously influenced by electrostatic and intrinsic interactions. As a result of the electrostatic effects, the experimental binding curve depends on the ionic strength. However, a suitable model allows taking into account such electrostatic interactions. Ideally, if an appropriate model is used, the dependence of the binding isotherm on ionic strength should vanish and corrected isotherms will merge into a *master curve*[27], which is independent of the salt level. The above mentioned descriptions of the intrinsic heterogeneity (e.g., the estimation of the proton affinity spectrum) can be applied to this master curve. The application of this formalism to experimental data of proton

binding is shown in **figure 2.6** The experimental proton titration data (a) is transformed (through a charge balance) into a binding curve (b) which can expressed as charge (Q), proton coverage (θ) etc. pH. The set of charge curves obtained over a range of ionic strengths (c) is used to optimize the parameters of the electrostatic model (e.g., the Donnan volume). If the electrostatic model is correct, the charge curves at different ionic strength plotted versus the pH adjacent to the binding site (pH_0) yield a single master curve (d), which can be used for the analysis of the intrinsic protonation parameters by means of an arbitrary isotherm and by solving **equation 2.10**, to obtain the affinity spectrum (e).

In general, electrostatic model parameters derived from proton binding data are assumed to apply also to cation binding equilibria.

If the NICA-Donnan model is used to fit the experimental values, two different strategies can be used:

Theoretical Background – Binding of Cations by Natural Matter
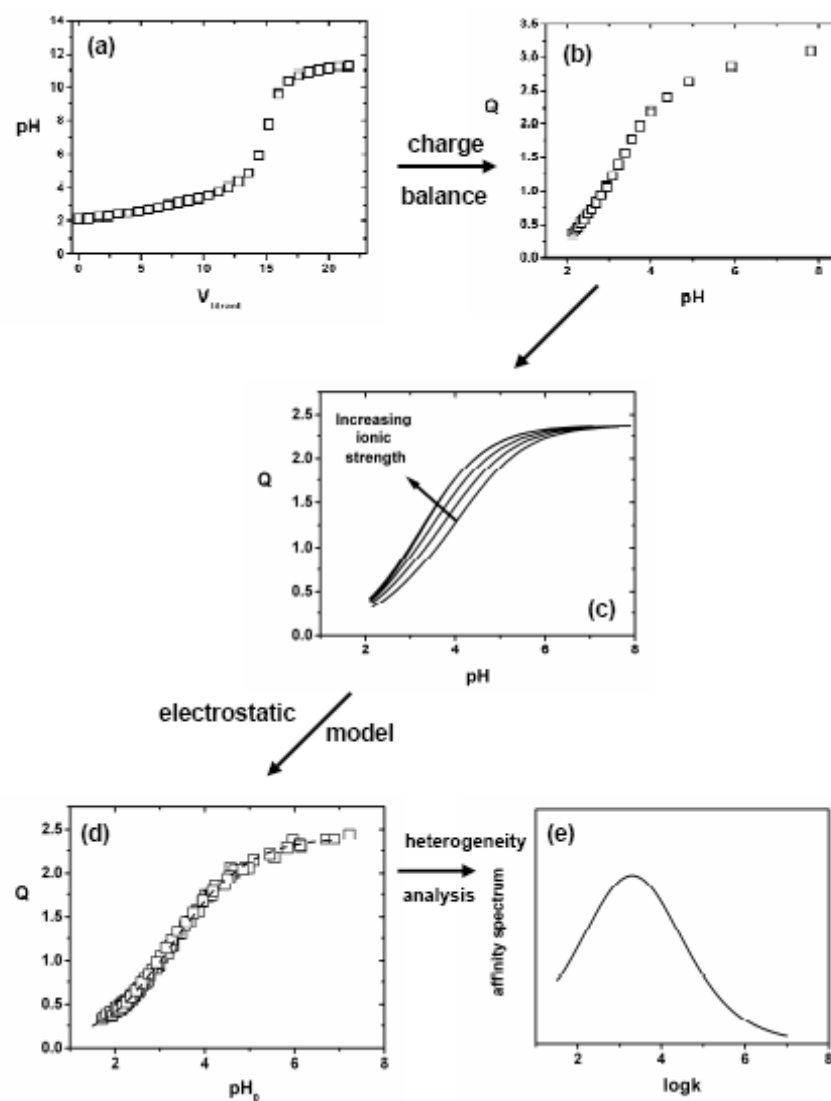
Figure 2.6. Schematic representation of the procedure for the analysis of proton titration data (adapted from de Wit et al.[27] , using experimental data from [75]).

2.3 Reference

(1)   Kononova, M. M., *Soil Organic Matter - Its Nature, Its Role in Soil*. Pergamon Press: New York, **1961**.

(2)   Kracht, O. Origin and genesis of dissolved organic matter. Max Planck Institut für biogeochimie, 2001.

(3)   Labanowski, J. Matière organique naturelle et anthropique: vers une meilleure compréhension de sa réactivité et de sa caractérisation. Université de Limoges, 2004.

(4)   Meybeck, M.; De Marsily, G.; Fustec, E., *La Seine en son bassin. Fonctionnement d'un système fluvial anthropisé*. Elsevier: Paris, **1998**; p 749.

(5)   Aiken, G.; McKnight, R.; Wershaw, R.; Maccarthy, P., In *Humic subtances in soil, sediment, and water*, Aiken, G.; McKnight, R.; Wershaw, R., Eds. Wiley Interscience: New York, Chapter 1, 1985.

(6)   Buffle, J., *Complexation Reactions in Aquatic Systems. An Analytical Approach*. Ellis Horwood Limited ed.; Chichester, UK, **1988**.

(7)   Clapp, C. E.; Hayes, M. H. B., Sizes and shapes of humic substances. *Soil Science* **1999,** *164*, (11), 777-789.

(8)   Swift, R. S., Macromolecular Properties of Soil Humic Substances: Fact, Fiction, and Opinion. *Soil Science* **1999,** *164*, (11), 790-802.

(9)   Wershaw, R. L., Molecular Aggregation of Humic Substances. *Soil Science* **1999,** *164*, (11), 803-813.

(10)   Hayes, M. H. B.; Graham, C. L., Procedures for the Isolation and Fractionation of Humic Substances. In *Humic Subtances: Versatils Components of Plants, Soil and Water*, Ghabbour, E. A.; Davies, G., Eds. The Royal Society of Chemistry: Cambridge, 2000.

(11)   Stevenson, F. J., *Humus Chemistry. Genesis, composition, Reactions*. New York, **1994**.

(12)   Hayes, M. H. B.; Swift, R. S., In *The Chemistry of Soil Constituents*, Greenland, D. J.; Hayes, M. H. B., Eds. Wiley-Interscience: New York, Chapter 3, 1978.

(13)   Wershaw, R., In *Humic subtances in soil, sediment, and water*, Aiken, G.; McKnight, R.; Wershaw, R., Eds. Wiley Interscience: New York, Chapter 22, 1985.

(14)   Hayes, M. H. B.; Maccarthy, P.; Malcolm, R. L.; Swift, R. S., Humic Subtances II. In *Search of Structure*, Wiley Interscience: New York, 1989.

(15)   Campbell, P. G. C., Interactions between Trace Metal and Aquatic Organisms : A Critique of the Free-ion Activity Model. In *Metals Speciation and Bioavailability in Aquatic Systems*, Tessier, A.; Turner, D. R., Eds. John Wiley & Sons: Chichester, 1995.

(16)   Stevenson, F. J., *Humus Chemsitry. Genesis, Composition, Reactions*. Wiley Interscience: New York, **1982**.

(17)   Tan, K. H., *Principles of soil chemistry Fourth Edition*. CRC Press: New York, **2011**.

(18)   Burdon, J., Are the Traditional Concepts of the Structures of Humic Substances Realistic? *Soil Science* **2001,** *166*, (11), 752-769.

(19)   MacCarthy, P., The Principles of Humic Substances. *Soil Science* **2001,** *166*, (11), 738-751.

(20)   Schulten, H. R.; Schnitzer, M., A state of the art structural concept for humic substances. *Naturwissenschaften* **1993,** *80*, (1), 29-30.

(21)   Companys, E. Speciation of heavy metals in macromolecular systems by electroanalytical techniques. Universitat de Lleida (Spain), 2003.

(22)   Bockris, J.; Reddy, A., *Modern electrochemistry*. 2 edn. ed.; New York, **1998**.

(23)   Dickson, A. G.; Whitfield, M., An ion-association model for estimating acidity constants (at 25ºC and 1 Atm total pressure) in electrolyte mixtures related to seawater (ionic strength less than 1mol / kg H2O). *Marine Chemistry* **1981,** *10*, (4), 315-333.

(24)   Guggenheim, E. A.; Turgeon, J. C., Specific interactions of ions. *Transactions of the Faraday Society* **1955,** *51*, (6), 747-761.

(25)   Pitzer, K. S., *Ion interaction approach: Theory and data correction*. Boca Raton, Florida, **1991**.

(26)   Bartschat, B. M.; Cabaniss, S. E.; Morel, F. M. M., Oligoelectrolyte model for cation binding by humic subtances. *Environmental Science & Technology* **1992,** *26*, (2), 284-294.

(27)   Dewit, J. C. M.; Vanriemsdijk, W. H.; Nederlof, M. M.; Kinniburgh, D. G.; Koopal, L. K., Analysis of ion binding on humic subtances and the determination of intrinsic affinity distributions. *Analytica Chimica Acta* **1990,** *232*, (1), 189-207.

(28)   Miyajima, T., In *Ion exchange and solvent extraction*, Marinsky, J. A. a. M., Y., Ed. Marcel Dekker: New Tork, Chapter 7, p 275, 1995.

(29)   Dewit, J. C. M.; Vanriemsdijk, W. H.; Koopal, L. K., Proton binding to humic subtances. 2. Chemical heterogeneity and adsorption models. *Environmental Science & Technology* **1993,** *27*, (10), 2015-2022.

(30)   Ritchie, J. D.; Perdue, E. M., Proton-binding study of standard and reference fulvic acids, humic acids, and natural organic matter. *Geochimica Et Cosmochimica Acta* **2003,** *67*, (1), 85-96.

(31)   Nederlof, M. M.; Dewit, J. C. M.; Vanriemsdijk, W. H.; Koopal, L. K., Determination of proton affinity distribution for humic subtances. *Environmental Science & Technology* **1993,** *27*, (5), 846-856.

(32)   Paoletti, S.; Benegas, J. C.; Pantano, S.; Vetere, A., Thermodynamics of the conformational transition of biopolyelectrolytes: The case of specific affinity of counterions. *Biopolymers* **1999,** *50*, (7), 705-719.

(33)   Kinniburgh, D. G.; van Riemsdijk, W. H.; Koopal, L. K.; Borkovec, M.; Benedetti, M. F.; Avena, M. J., Ion binding to natural organic matter: competition, heterogeneity, stoichiometry and thermodynamic consistency. *Colloids and Surfaces a-Physicochemical and Engineering Aspects* **1999,** *151*, (1-2), 147-166.

(34)   Pinheiro, J. P.; Mota, A. M.; Benedetti, M. F., Effect of aluminum competition on lead and cadmium binding to humic acids at variable ionic strength. *Environmental Science & Technology* **2000,** *34*, (24), 5137-5143.

(35)   Tipping, E., Modeling ion-binding by humic acids. *Colloids and Surfaces a-Physicochemical and Engineering Aspects* **1993,** *73*, 117-131.

(36)   Koopal, L. K.; Saito, T.; Pinheiro, J. P.; van Riemsdijk, W. H., Ion binding to natural organic matter: General considerations and the NICA-Donnan model. *Colloids and Surfaces a-Physicochemical and Engineering Aspects* **2005,** *265*, (1-3), 40-54.

(37)   Lyklema, J., *Fundamentals of interface and colloid science*. New York and London, **1995**; Vol. II.

(38)   Milne, C. J.; Kinniburgh, D. G.; Dewit, J. C. M.; Vanriemsdijk, W. H.; Koopal, L. K., Analysis of Metal-Ion Binding by a Peat Humic-Acid Using a Simple Electrostatic Model. *Journal of Colloid and Interface Science* **1995,** *175*, (2), 448-460.

(39)   Milne, C. J.; Kinniburgh, D. G.; Dewit, J. C. M.; Vanriemsdijk, W. H.; Koopal, L. K., Analysis of proton binding by a peat humic-acid using a simple electrostatic model. *Geochimica Et Cosmochimica Acta* **1995,** *59*, (6), 1101-1112.

(40)   Saito, T.; Nagasaki, S.; Tanaka, S.; Koopal, L. K., Electrostatic interaction models for ion binding to humic substances. *Colloids and Surfaces a-Physicochemical and Engineering Aspects* **2005,** *265*, (1-3), 104-113.

(41)   Tipping, E., *Cation blinding by humic substance*. Cambridge University Press ed.; Cambridge (UK), **2002**.

(42)   Kinniburgh, D. G.; Milne, C. J.; Benedetti, M. F.; Pinheiro, J. P.; Filius, J.; Koopal, L. K.; VanRiemsdijk, W. H., Metal ion binding by humic acid: Application of the NICA-Donnan model. *Environmental Science & Technology* **1996,** *30*, (5), 1687-1698.

(43)   Benedetti, M. F.; vanRiemsdik, W. H.; Koopal, L. K., Humic substances considered as a heterogeneous donnan gel phase. *Environmental Science & Technology* **1996,** *30*, (6), 1805-1813.

(44)   Garces, J. L.; Mas, F.; Puy, J.; Galceran, J.; Salvador, J., Use of activity coefficients for bound and free sites to describe metal-macromolecule complexation. *Journal of the Chemical Society-Faraday Transactions* **1998,** *94*, (18), 2783-2794.

(45)   Van Riemsdijk, W.; Koopal, L. K., Environmental particles. In Buffle, J.; van Leeuwen, H. P., Eds. Lewis: Boca Raton, 1992.

(46)   Roginsky, S. S., *Adsorption catalysis on heterogeneous surface*. Academy of Science U.S.S.R.: Moscow, **1948**.

(47)   Garces, J. L.; Mas, F.; Puy, J., Application of maximum entropy formalism in the determination of the affinity spectrum in macromolecular complexation. *Environmental Science & Technology* **1998,** *32*, (4), 539-548.

(48)   Koper, G. J. M.; Borkovec, M., Exact affinity distributions for linear polyampholytes and polyelectrolytes. *Journal of Chemical Physics* **1996,** *104*, (11), 4204-4213.

(49)   Milne, C. J.; Kinniburgh, D. G.; Tipping, E., Generic NICA-Donnan model parameters for proton binding by humic substances. *Environmental Science & Technology* **2001,** *35*, (10), 2049-2059.

(50)   Nederlof, M. M.; Vanriemsdijk, W. H.; Koopal, L. K., Heterogeneity analysis for binding data using an adapted smoothing spline technique. *Environmental Science & Technology* **1994,** *28*, (6), 1037-1047.

(51)   Avena, M. J.; Koopal, L. K.; van Riemsdijk, W. H., Proton binding to humic acids: Electrostatic and intrinsic interactions. *Journal of Colloid and Interface Science* **1999,** *217*, (1), 37-48.

(52)   Jaroniec, M.; Madey, R., *Physical Adsorption on Heterogeneous Solids*. Elsevier: Amsterdam, **1988**.

(53)   Rudzinski, W.; Nieszporek, K.; Moon, H.; Rhee, H. K., On the theoretical origin and applicability of the potential - theory approach to predict mixed - gas adsorption on solid - surfaces from single - gas adsorption - isotherms. *Chemical Engineering Science* **1995,** *50*, (16), 2641-2660.

(54)   Companys, E.; Garces, J. L.; Salvador, J.; Galceran, J.; Puy, J.; Mas, F., Electrostatic and specific binding to macromolecular ligands - A general analytical expression for the Donnan volume. *Colloids and Surfaces a-Physicochemical and Engineering Aspects* **2007,** *306*, (1-3), 2-13.

(55)   Garces, J. L.; Mas, F.; Puy, J., Affinity distribution functions in multicomponent heterogeneous adsorption. Analytical inversion of isotherms to obtain affinity spectra. *Journal of Chemical Physics* **2004,** *120*, (19), 9266-9276.

(56)   Garces, J. L.; Mas, F.; Puy, J., Conditional equilibrium constants in multicomponent heterogeneous adsorption: The conditional affinity spectrum. *Journal of Chemical Physics* **2006,** *124*, (4), 14.

(57)   Puy, J.; Galceran, J.; Huidobro, C.; Companys, E.; Samper, N.; Garces, J. L.; Mas, F., Conditional Affinity Spectra of Pb2+-Humic Acid Complexation from Data Obtained with AGNES. *Environmental Science & Technology* **2008,** *42*, (24), 9289-9295.

(58)   Puy, J.; Huidobro, C.; David, C.; Rey-Castro, C.; Salvador, J.; Companys, E.; Garces, J. L.; Galceran, J.; Cecilia, J.; Mas, F., Conditional affinity spectra

underlying NICA isotherm. *Colloids and Surfaces A: Physicochemical and Engineering Aspects* **2009,** *347*, (1-3), 156-166.

(59)   Tipping, E., Humic ion-binding model VI: An improved description of the interactions of protons and metal ions with humic substances. *Aquatic Geochemistry* **1998,** *4*, (1), 3-48.

(60)   Tipping, E.; Hurley, M. A., A Unifying Model of Cation Binding by Humic Substances. *Geochimica Et Cosmochimica Acta* **1992,** *56*, (10), 3627-3641.

(61)   Dudal, Y.; Gérard, F., Accounting for natural organic matter in aqueous chemical equilibrium models: a review of the theories and applications. *Earth-Science Reviews* **2004,** *66*, (3-4), 199-216.

(62)   Lofts, S.; Tipping, E., Assessing WHAM/Model VII against field measurements of free metal ion concentrations: model performance and the role of uncertainty in parameters and inputs. *Environmental Chemistry 8*, (5), 501-516.

(63)   Stockdale, A.; Bryan, N. D.; Lofts, S., Estimation of Model VII humic binding constants for Pd^{2+}, Sn^{2+}, U^{4+}, NpO_2^{2+}, Pu^{4+} and PuO_2^{2+}. *Journal of Environmental Monitoring* **2011,** *13*, (10), 2946-2950.

(64)   Koopal, L. K.; Vanriemsdijk, W. H.; Dewit, J. C. M.; Benedetti, M. F., Analytical isotherm equations for multicomponent adsorption to heterogeneous surfaces. *Journal of Colloid and Interface Science* **1994,** *166*, (1), 51-60.

(65)   Benedetti, M. F.; Milne, C. J.; Kinniburgh, D. G.; Vanriemsdijk, W. H.; Koopal, L. K., Metal-Ion Binding to Humic Substances - Application of the Nonideal Competitive Adsorption Model. *Environmental Science & Technology* **1995,** *29*, (2), 446-457.

(66)   Koopal, L. K.; van Riemsdijk, W. H.; Kinniburgh, D. G., Humic matter and contaminants. General aspects and modeling metal ion binding. *Pure and Applied Chemistry* **2001,** *73*, (12), 2005-2016.

(67)   Milne, C. J.; Kinniburgh, D. G.; Van Riemsdijk, W. H.; Tipping, E., Generic NICA-Donnan model parameters for metal-ion binding by humic substances. *Environmental Science & Technology* **2003,** *37*, (5), 958-971.

(68)   Dzombak, D. A.; Fish, W.; Morel, F. M. M., Metal humate interactions. 1.Discrete ligand and continuous distribution models. *Environmental Science & Technology* **1986,** *20*, (7), 669-675.

(69)   Rudzinski, W.; Charmas, R.; Partyka, S.; Bottero, J. Y., On the nature of the energetic surface heterogeneity in ion and adsorption at a water oxide interface - theoretical studies of some special features of ion adsorption at low ion concentrations. *Langmuir* **1993,** *9*, (10), 2641-2651.

(70)   Vanriemsdijk, W. H.; Bolt, G. H.; Koopal, L. K.; Blaakmeer, J., Electrolyte adsorption on heterogeneous surfaces - Adsorption models. *Journal of Colloid and Interface Science* **1986,** *109*, (1), 219-228.

(71)   Vanriemsdijk, W. H.; Dewit, J. C. M.; Koopal, L. K.; Bolt, G. H., Metal-ion adsorption on heterogeneous surfaces - Adsorption models. *Journal of Colloid and Interface Science* **1987,** *116*, (2), 511-522.

(72)   Pinheiro, J. P.; Mota, A. M.; Benedetti, M. F., Lead and calcium binding to fulvic acids: Salt effect and competition. *Environmental Science & Technology* **1999,** *33*, (19), 3398-3404.

(73)   Christl, I.; Kretzschmar, R., Relating ion binding by fulvic and humic acids to chemical composition and molecular size. 1. Proton binding. *Environmental Science & Technology* **2001,** *35*, (12), 2505-2511.

(74)   Berbel, F.; Diaz-Cruz, J. M.; Arino, C.; Esteban, M.; Mas, F.; Garces, J. L.; Puy, J., Voltammetric analysis of heterogeneity in metal ion binding by humics. *Environmental Science & Technology* **2001,** *35*, (6), 1097-1102.

(75)   Rey-Castro, C.; Lodeiro, P.; Herrero, R.; De Vicente, M. E. S., Acid-base properties of brown seaweed biomass considered as a Donnan gel. A model reflecting electrostatic effects and chemical heterogeneity. *Environmental Science & Technology* **2003,** *37*, (22), 5159-5167.

CHAPTER 3

EXPERIMENTAL SECTION

BINDING OF CATIONS BY NATURAL MATTER

3.1 Analytical techniques

3.1.1 Potentiometry

Potentiometry passively measures the potential of a solution between two electrodes, affecting very little the solution during the process. The potential is related to the activities of the ion under study. The potentiometric cell structure contains two electrodes: a working and a reference electrode, the electrodes are connected to a sensitive milli-volt meter (**figure 3.1**). Potentiometry usually uses electrodes made selectively sensitive to the ion of interest, Ion Selective Electrodes (ISE). The most common potentiometric electrode is the glass-membrane electrode used in a pH meter.
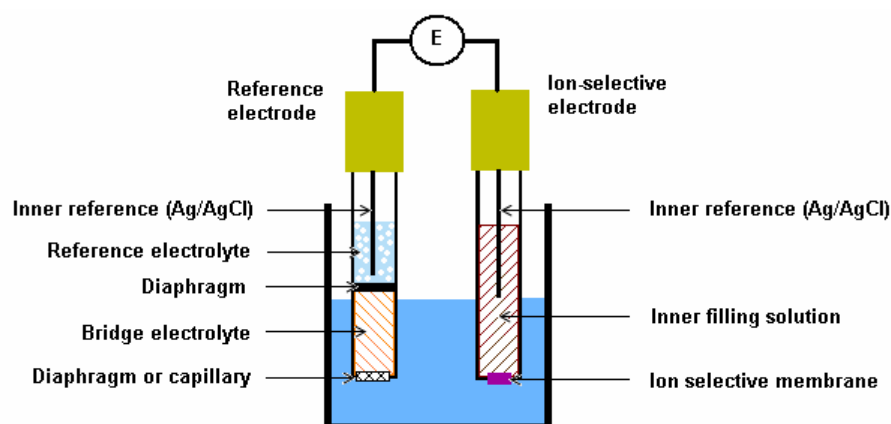
Figure 3.1. Schematic representation of a potentiometric cell with a working and a reference electrode.

3.1.2 Ion Selective Electrode (ISE)

An ISE (with its own internal reference) is immersed in an aqueous solution containing the ions to be measured, together with a separate and an external reference electrode (see **figure 3.1**). The target ions diffuse through the membrane from the high concentration side to the lower concentration side. Due to the difference in concentration between both sides, a difference of potential is developed across the membrane. In order to measure the value of this potential, metal-liquid interfaces on both side of the membrane are need. Theoretically, these could just be metal wires immersed in the solutions. But the electrical

potential on many simple metal-liquid junction is not stable; thus the need for a so-called reference system on both sides of the ISE membrane, with a particular metal-liquid interface which is know to have a stable potential.

In practice, the most common reference system is a silver wire coated with silver chloride and immersed in a concentrated solution of potassium chloride saturated with silver chloride.

The concentration of the target ion outside the solution can be related to the difference of potential, E, between the extern reference electrode, whose potential is considered constant during the measure, and the working electrode, whose potential is due to the activity of the ionic solutes in contact with the electrode surface. The relationship between E and the activity of the metal ion, a_i, is given by the Nikolsky-Eisenman equation[1] (a modified version of Nernst equation):

$$E = Q \pm \frac{RT}{z_i F} \ln\left(a_i + \sum_j k_{ij} a_j^{z_i/z_j} \right)$$
(3.1)

where R is the gas constant, T the temperature, z_i the ion charge, F the Faraday constant, k_{ij} the selectivity coefficient for the ion j with respect to the principal ion i and Q is a constant that includes all the measurement-circuit constants.

In a solution without interfering ions the last **expression 3.1** can be simplified to:

$$E = Q \pm S \ln\left(a_i \right)$$
(3.2)

where S refers to $RT/(z_i F)$.

Application of this equation requires the knowledge of how the activities are related to the concentrations. It is often preferable to fix the ionic strength, with the activity coefficients incorporated into the constant term Q.

The sensing part of the electrode usually consists of an ion-specific membrane, therefore, the ISE's are generally classified by the type of their membrane. There are four main types membranes: non-crystalline (include glass-membrane electrode), crystalline, compound or multi-membrane, and solid state electrodes.[1]

3.1.2.1 Glass-membrane electrode

A glass-membrane is an amorphous solid containing complex forms of silicates and other various ions, whose presence or absence affects the physical properties of the glass. It is permeable to H^+ and alkaline cations. By altering the composition of the glass, the membrane can be specifically sensitive to H^+, Na^+ and K^+. pH electrodes are made with a special composition in order to have very low selectivity coefficients for Group IA cations (to overcome the so-called "alkaline error" caused by the sensibility towards alkaline metals).

3.1.2.2 Crystalline ion selective electrode

These electrodes contain mobile ions of one sign and fixed sites of opposite sign. The membranes may be homogeneous or heterogeneous. The homogenous are prepared from either a single compound or a homogeneous mixture of compounds. The heterogeneous membrane is formed when an active substance (or a mixture of active substances) is mixed with an inert matrix, such as silicone rubber or PVC, or placed on hydrophobized graphite to form the sensing membrane.

In order to consider these layers at true equilibrium, it is necessary to use saturated solutions. In practice, these electrodes are applied in non-saturated solutions, so in this case the insoluble membrane slowly dissolves. Therefore the membrane must have a small solubility product in order to avoid the dissolution and ensure a response that is stable with time.

A series of electrodes are based on silver and metal sulphides, and are prepared by pressing the salt into a disk together with a polymeric support. The sensitivity to ions of these electrodes arises from the dissolution equilibria at the membrane surface. Examples of electrodes with their measuring ranges are given in **table 3.1**.

Cation	Material	Measuring range ($mol.L^{-1}$)
Pb^{2+}	PbS (Ag_2S)	10^{-1}-10^{-6}
Cd^{2+}	CdS (Ag_2S)	10^{-1}-10^{-7}
Cu^{2+}	CuS (Ag_2S)	10^{-1}-10^{-8}

Table 3.1. Examples of electrodes with solid state membranes[2]

3.1.3 Electrodes calibration

3.1.3.1 Glass-membrane electrode calibration

In this work, the calibration of the pH electrode has been conducted by a process based on the Gran's method[3] which allows a great accuracy.

To calibrate the electrode, a solution containing the same concentration of electrolyte as the sample plus some amount of acid is titrated with base.[4] The activity coefficients will then be constant and incorporated in the calibration parameters.

Expression 3.2 can be written for the pH electrode, in terms of proton concentration as:

$$E = E^{\circ} + g \log c_H \tag{3.3}$$

where E^o includes all the measurement-circuit constants and the activity coefficient, and g is $2.303\,RT/(z_i F)$ (59.17 mV at 25ºC).

As hydronium and hydroxide ions are in equilibrium with a constant that corresponds to the ionic product of water (in concentration, K_W), the **expression 3.3** can be also written in terms of concentration of hydroxide ions as:

$$E = E^{\circ\prime} - g \log\left(c_{OH}\right) \tag{3.4}$$

Equation 3.4 can be written in the following form:

$$E = E^{\circ\prime} - g \log\left(\frac{K_w}{c_H}\right) \tag{3.5}$$

If some amount of strong acid, V, is titrated with a volume v of strong base (whose concentration is c_B),

  ➤ before the equivalence point, the concentration of protons and the pH are:

$$c_H = \frac{c_B\left(v_e - v\right)}{V + v} \tag{3.6}$$

$$pH = -\log\left[\frac{c_B\left(v_e - v\right)}{V + v}\right] \tag{3.7}$$

where v_e is the volume corresponding to the equivalence point, which is obtained from the experimental representation of the potential versus the volume of strong base added (**figure 3.2**).

We can define a function:

$$\psi(E) = (V+v) \cdot 10^{E/g} \tag{3.8}$$

which, by means of 3.3 and 3.6, can be rewritten as:

$$\psi(E) = c_B (v_e - v) \cdot 10^{E^\circ/g} \tag{3.9}$$

➢ after the equivalence point, the concentration of protons and the pH are:

$$c_H = K_W \frac{V+v}{c_B(v-v_e)} \tag{3.10}$$

$$pH = -\log\left[K_W \frac{V+v}{c_B(v-v_e)} \right] \tag{3.11}$$

Another function can be defined:

$$\psi'(E) = (V+v) \cdot 10^{-E/g} \tag{3.12}$$

which, by means of **3.5** and **3.10**, becomes:

$$\psi'(E) = c_B (v-v_e) \cdot 10^{-E^{\circ\prime}/g} \tag{3.13}$$

$\Psi(E)$ and $\Psi'(E)$ can be rewritten in terms of v as:

$$\psi(E) = mv + n \tag{3.14}$$

and:

$$\psi'(E) = m'v + n' \tag{3.15}$$

From **equations 3.3 and 3.5**, pK_w may be calculated as:

$$pK_w = \frac{E^\circ - E^{\circ\prime}}{g} \tag{3.16}$$

Thus by linear fitting of $\Psi(E)$ and $\Psi'(E)$ versus v, K_w may be calculated by means of:

$$K_w = -\frac{c_B^2}{m \cdot m'} = -\frac{c_B^2 \cdot v_e^2}{n \cdot n'} \qquad (3.17)$$

Figure 3.2 illustrates the procedure: the potential is plotted versus the volume of base added **(a)**, the first derivate of this function **(b)** is calculated in order to determine with precision the equivalence point. From the Gran plots **(c)** $\Psi(E)$ (in green) and $\Psi'(E)$ (in pink), the ionic product of water is estimated. Thereby, the pH can be calculated before (with **equation 3.7**) and after (with **equation 3.11**) the equivalence point, and the calibration curve of the glass electrode can thus be plotted **(d)**.
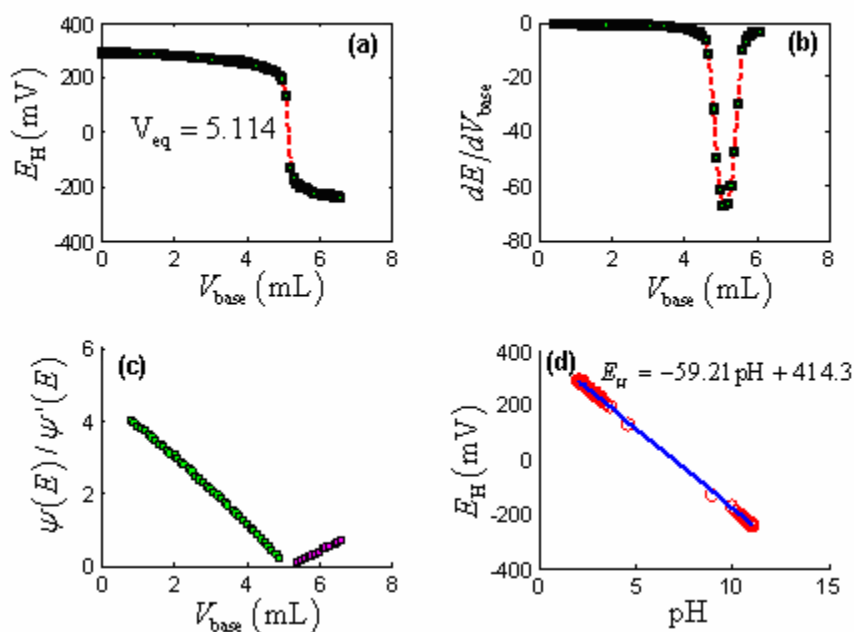
Figure 3.2. Glass electrode calibration, in KNO3 0.1 mol.L^{-1} at 25ºC, the procedure is described above.

3.1.3.2 Cadmium and lead selective electrode calibration

In the study shown in chapter 4, the free lead and cadmium concentrations were measured using a sulphide-based ISE. Both ISEs were calibrated by serial dilution of a standard stock solution of $Cd(NO_3)_2$ and $Pb(NO_3)_2$ (**figure 3.3**) at an adjusted ionic strength and pH≈4.

The nominal range of the Cd-ISE was 10^{-1} to 10^{-7} mol.L^{-1} (**table 3.1**) and of the Pb-ISE was 10^{-1} to 10^{-6} mol.L^{-1} (**table 3.1**) but as shown in **figure 3.3**, the calibration titration when metal is added to a KNO_3 reveals an accurate Nernstian response in the range ≈ 10^{-3} - 10^{-6} M. It was demonstrated that in metal buffer solution, the Nernstian range of the electrodes may be greatly extended depending on the total metal concentration. Serrano et al[5] show that in presence of ethylenediamine (as a complex ligand) with total cadmium concentration of 10^{-3} mol.L^{-1}, the Nerstian response of the electrode is within the range of free cadmium pCd 3 to pCd 10.3, but when the total metal concentration decreases, the response is deteriorated. For 10^{-5} mol.L^{-1}of total cadmium concentration, the Cd-ISE has a Nernstian behaviour until pCd ≈ 9 and for a total concentration of 10^{-6} mol.L^{-1} until pCd ≈ 7. Other authors found a good agreement between the calculated cadmium and lead activities values obtained from calibrations in buffered solutions and from extrapolations of unbufferd standards, and conclude that a linear calibration curve may be extended with confidence to lower concentrations in buffered solutions such as the humic solutions under study. [6-8]
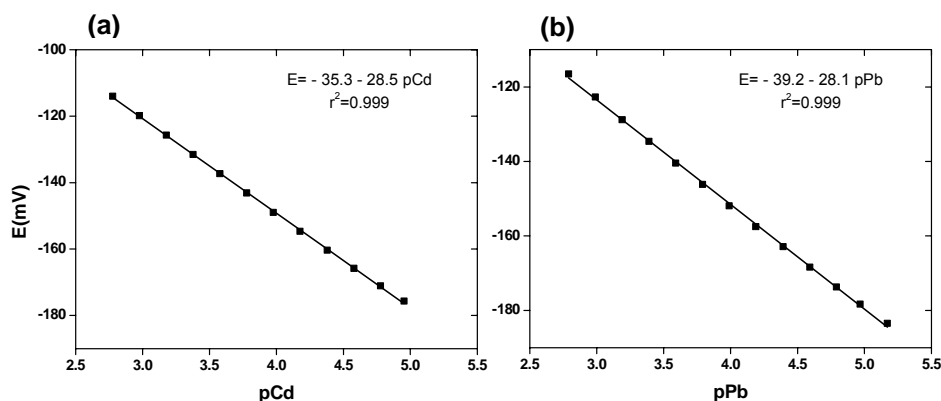
Figure 3.3. Examples of Cd^{2+} (a) and Pb^{2+} (b) ISE calibration in KNO3 0.1 mol.L^{-1} at 25ºC and pH ≈ 4

Therefore, in this work, an extension of the calibration will be assumed. As the smaller total metal concentration is 10^{-5} mol.L^{-1}, it was assumed that the Nerstian response of the lead and cadmium ISE is valid until 10^{-9} mol.L^{-1} of free metal.

3.2 Materials

3.2.1 Humic acid purification method

Because the mineral constituents disturb the measurements and influence the behaviour of the organic matter, it is essential to purify the OM extracted from the soil system in order to obtain an insight into the characteristics and properties of the organic matter itself. Many different processes have been used to fractionate and purify the OM and there are also many different kinds of HS owing to their origin, etc… The discrepancies in the results reported in the literature, while they are difficult to compare are, therefore, understandable.

To overcome this controversy, the International Humic Subtances Society (IHSS) has recently stimulated the standardisation of extraction procedures,[9] and standard and reference materials have been increasingly available to researches world-wide.

The extractions of HS from natural systems consume time. HS present in natural water are difficult to isolate, due to their low concentrations, as compared to the soils and sediments. To avoid the laborious work of extraction, isolation and purification, commercial HS are used. Sometimes, the quality of the commercial HA is criticised.[10-12] Many publications have compared commercial and natural HA[10,12-18], and one of the major limitations in working with commercial product is the lack of information on its origin and methods of extraction.

Vermeer[19] and Companys[20] have purified and characterised (through different analytical techniques) the commercial Aldrich HA (the same product that is used in this work). They concluded that this purified HA reflects many aspects found for natural HA, therefore it can be used as an analogue for soil type HA in speciation studies.

The purification procedure for the commercial HA is used in this work has sequentially followed these steps:

> ➢ 10 g of humic acid Aldrich (H1, 675-2) was added to 1 L of 0.1 M HCl / 0.3 M HF solution, stirred overnight and filtrated (Whatman Cellulose filter).

> ➢ The humic acid residue was washed several times with HCl 1 M, neutralised and dissolved in KOH solution to pH 9 under N_2 atmosphere during 24 hours.

> ➢ The remaining solution was then centrifuged at 12000 rpm to remove the suspended solids and then reprecipitated by adding HNO_3 1M to pH 1 with constant stirring.

> ➢ After 24 hours of stirring, the suspension was centrifuged during 50 min

> ➢ The precipitate was redissolved with KOH to pH 7 and exhaustively dialysed (molecular weight cut-off 12000) against purified water until the conductivity of the dialysate remained constant.

> ➢ The dialysed solution was then treated with a Dowex 50WX4 ion exchanger to transform the material completely into the acid form. The total organic carbon of the final stock was 2.175 $g.L^{-1}$.

> ➢ The purified humic acid was stored as a concentrated solution in the dark at 4ºC.

3.2.2 Other reagents

Potassium nitrate, analytical grade, was used as inert supporting electrolyte and prepared from solid KNO_3 (Fluka, Trace Select).

Lead and cadmium solutions were prepared from the nitrate salt (Merck, analytical grade).

0.1 M standard aqueous solution of KOH and HNO_3 (Ridel-de-Haën, Standard solution) were used in the titrations.

Ultrapure water (Milli-Q plus 185 System, Millipore) was employed in all the experiments. Purified water-saturated nitrogen was used for the deaeration and blanketing of solutions.

3.3 Procedure of potentiometric titrations

The metal (Pb, Cd) binding properties of the purified HA sample were studied through the effects of different metal concentrations on the acid-base titration data. In theory (see following chapter), the knowledge of proton binding and the total amount of metal are enough to infer the metal binding characteristics. However, to check the accuracy of the metal binding information obtained by acid-base titration, the free metal concentration was also monitored throughout the experiments using the corresponding ISEs. Potentiometric measurements were carried out with an 2-channel Orion Research Ionanalyzer 720A potentiometer attached to a Metrohm 655 Dosimat, for the automatic addition of solutions, and to a computer through a RS232 card by means of a data acquisition program. The titrations were performed in a glass jacked cell thermostated at 25ºC.

The total exclusion of carbon dioxide is an essential aspect concerning the exactness of proton titrations, therefore precautions have to be taken to ensure that the solutions to be titrated are free from carbon dioxide. For this purpose, high-purity N_2 ($\geq$99.999 %) is bubbled through the sample, and calcium chloride guard tubes were used throughout to prevent CO_2 contamination.

Electrolyte concentration gradients in the cell are undesirable, hence a good stirring system is required during the titration. A homogeneous solution is ensured using a stirring bar and a magnetic stirrer.

A home-made program controlled the function of both the Dosimat and the Ionanalyzer, simultaneously. It performs an automatic titration with several setup parameters: the volume of titrant solution to be added, the time interval between measurements and the maximum potential drift allowed for a measurement to be considered stable. The scheme of the experimental setup is given in **figure 3.4**.

In every proton titration (in absence or in presence of metal) a solution of 0.45 g.L^{-1} HA and 0.1 M KNO_3 was placed into the potentiometric cell, was extensively deaerated and allowed to equilibrate. In order to avoid hysteric effects the HA suspensions were cycled up to pH 7.0 to ensure full dispersion and then back to pH 3.5,[21] after which they were titrated to about pH 10. After each titrant addition, the reading was accepted when the drift in the potential measurement was less than 0.1 mV.min^{-1}.

Proton titrations in presence of metal were performed with lead and cadmium:

- ✓ In the study of the binding between HA and lead, the titrations are carried out after addition of different fixed total lead concentrations : 10^{-5} M, 10^{-4} M, 3.16×10^{-4} M, 5×10^{-4} M, 7.5×10^{-4} M and 10^{-3} M.

- ✓ In the study of the binding between HA and cadmium, the titrations are carried out after addition of different fixed total cadmium concentrations: 10^{-5} M, 10^{-4} M, 5×10^{-4} M, 10^{-3} M and 3×10^{-3} M.

The raw titration data consist of sets of E(mV) versus the volume of added base, which were converted into $-\log c_H$ or $-\log c_M$ versus v(KOH) data by means the glass and metal ISE electrode calibration (Nernst equation).

The calculation of the amounts of bound protons (Q_H) and non proton sites ($Q_{max,H}-Q_H$) in the HA during the titrations was carried out from the mass and charges balances (see equations 1 and 2 in Chapter 4) using the experimental data pH versus v(KOH).
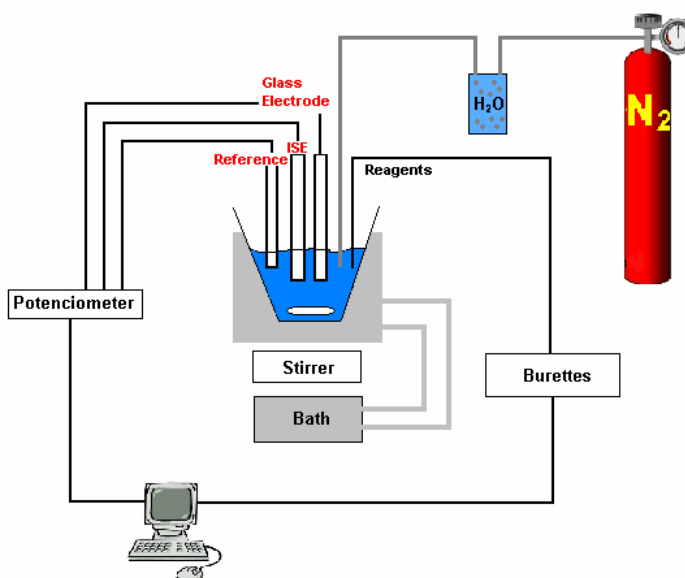
Figure 3.4. Experimental setup for a typical acid / base computer – controlled potentiometric titration.

3.4 References

(1)   Buck, R. P.; Lindner, E., Recommendations for nomenclature of Ion-Selective Electrodes - (IUPAC recommendations 1994). *Pure and Applied Chemistry* **1994,** *66*, (12), 2527-2536.

(2)   *Ion Selective Electrode Instruction for Use*. Metrohm Ion Analysis.

(3)   Gran, G., Determination of the Equivalence point in potentiometric titrations. Part II. *Analyst* **1952,** *77*, 661-671.

(4)   Rossotti, F. J. C.; Rossotti, H., Potentiometric titrations using gran plots. *journal of Chemical Education* **1965,** *47*, 375-378.

(5)   Serrano, N.; Díaz-Cruz, J. M.; Ariño, C.; Esteban, N.; Puy, J.; Companys, E.; Galceran, J.; Cecilia, J., Full-wave analysis of stripping chronopotentiograms at scanned potential (SSCP) as a tool for heavy metal speciation: Theorical development and application to Cd(II)-phthalate and Cd(II)-iodide systems. *Journal of Electroanalytical Chemistry* **2007,** *600*, (2), 275-284.

(6)   Milne, C. J.; Kinniburgh, D. G.; Dewit, J. C. M.; Vanriemsdijk, W. H.; Koopal, L. K., Analysis of Metal-Ion Binding by a Peat Humic-Acid Using a Simple Electrostatic Model. *Journal of Colloid and Interface Science* **1995,** *175*, (2), 448-460.

(7)   Hansen, E. H.; Ruzicka, J., Selectrode - Universal Ion Selective Electrode. 8. Solid-state lead (II) Selectrode in lead (II) buffers and potentiometric titrations. *Analytica Chimica Acta* **1974,** *72*, (2), 365-373.

(8)   Ruzicka, J.; Hansen, E. H., Selectrode TM - Universal Ion Selective Electrode. 4. Solid-state cadmium (II) Selectrode in EDTA titrations and cadmium buffers. *Analytica Chimica Acta* **1973,** *63*, (1), 115-128.

(9)   Swift, R. S., Part 3, Chemical Methods. In *Methods of Soils Analysis*, Sparks, D. L.; Bartel, J. M.; Bigham, J. M., Eds. Soil Science Society of America: Madison, 35, p 1011, 1996.

(10)   Qiang, T.; Xiao-quan, S.; Zhe-ming, N., Comparative characteristic studies on soil and commercial humic acids. *Fresenius' Journal of Analytical Chemistry* **1993,** *347*, (8), 330-336.

(11)   Chiou, C. T.; Kile, D. E.; Brinton, T. I.; Malcolm, R. L.; Leenheer, J. A.; Maccarthy, P., A comparison of water solubility enhancements of organic solutes by aquatic humic materials and commercial humic acids. *Environmental Science & Technology* **1987,** *21*, (12), 1231-1234.

(12)   Malcolm, R. L.; Maccarthy, P., Limitations in the use of commercial humic acids in water and soil research. *Environmental Science & Technology* **1986,** *20*, (9), 904-911.

(13)   Beckett, R.; Jue, Z.; Giddings, J. C., Determination of molecular-weight distributions of fulvic and humic acids using flow field-flow fractionation. *Environmental Science & Technology* **1987,** *21*, (3), 289-295.

(14)   Cornel, P. K.; Summers, R. S.; Roberts, P. V., Diffusion of humic-acid in dilute aqueous-solution. *Journal of Colloid and Interface Science* **1986,** *110*, (1), 149-164.

(15)   Summers, R. S.; Cornel, P. K.; Roberts, P. V., Molecular-size distribution and spectroscopic characterization of humic substances. *Science of the total environment* **1987,** *62*, 27-37.

(16)   Chin, Y. P.; Aiken, G.; Oloughlin, E., Molecular-weight, polydispersity and spectroscopic properties of aquatic humic subtances. *Environmental Science & Technology* **1994,** *28*, (11), 1853-1858.

(17)   Florence, T. M., Development of physico-chemical speciation procedures to investigate the toxicity of copper, lead, cadmium and zinc towards aquatic biota. *Analytica Chimica Acta* **1982,** *141*, (0), 73-94.

(18)   Beveridge, A.; Pickering, W. F., Influence of humate-solute interactions on aqueous heavy metal ion levels. *Water, Air, & Soil Pollution* **1980,** *14*, (1), 171-185.

(19)   Vermeer, A. W. Interaction between humic acid and hematite and their effects on metal ion speciation Agricultural University, Wageningen, 1996.

(20)   Companys, E. Speciation of heavy metals in macromolecular systems by electroanalytical techniques. Universitat de Lleida (Spain), 2003.

(21)   Kinniburgh, D. G.; van Riemsdijk, W. H.; Koopal, L. K.; Borkovec, M.; Benedetti, M. F.; Avena, M. J., Ion binding to natural organic matter: competition, heterogeneity, stoichiometry and thermodynamic consistency. *Colloids and Surfaces a-Physicochemical and Engineering Aspects* **1999,** *151*, (1-2), 147-166.

CHAPTER 4

RESULTS AND DISCUSSION

COMPETITION EFFECTS IN CATION BINDING TO HUMIC ACID

- Foreword -

The aim of this study is to obtain information on the lead and cadmium binding to purified commercial humic acid by acid – base titrations in presence of the target metal at fixed total concentration. The NICA isotherm has been used for the description of the binding.

Electrostatic interactions are not taken into account in this paper, so that conditional NICA parameters, referred to the actual ionic strength conditions were obtained.

The resulting Conditional Affinity Spectrum of the proton binding to the humic acid at constant total metal concentration (CAScTM) is developed and applied to the experimental results.

Material and Methods

Proton titrations in absence and in presence of fixed total concentration of lead or cadmium were performed at 25ºC with a solution initially containing 0.45 g.L^{-1} of purified Aldrich humic acid. The ionic strength of the solution is adjusted to 0.1 mol.L^{-1} by potassium nitrate. The free metal concentration is also monitored by an Ion Selective Electrode (ISE). Tree replicates of each titration were performed.

See chapter 3 for furthers details on the experiments.

The coupling of the NICA isotherm with a mass balance for the metal allows the description of the proton and metal binding as a function of pH and total metal concentration. The numerical inversion of the binding coverage data in these conditions yield the corresponding CAScTM.

Results and Discussion

NICA conditional (ionic strength of 0.1 mol.L^{-1}) parameters of proton and metals are fitted in absence and in presence of metal using either the glass electrode or both the glass electrode and metal ISE simultaneously. The differences between both sets of parameters are not significant. These results confirm that the indirect description of the metal – humic acid binding can be feasible from acid – base titrations. This methodology can be useful to study the

binding between humic or fulvic acid and metals for which ISE are not commercially available.

Finally, the interpretation of the competition effects due to the presence of cadmium and lead on the effective proton binding was carried out in terms of the CAScTM.

Competition effects in cation binding to humic acid: Conditional affinity spectra for fixed total metal concentration conditions

Abstract

Information on the Pb and Cd binding to a purified Aldrich humic acid (HA) is obtained from the influence of different fixed total metal concentrations on the acid–base titrations of this ligand. NICA (Non-Ideal Competitive Adsorption) isotherm has been used for a global quantitative description of the binding, which has then been interpreted by plotting the Conditional Affinity Spectra of the H+ binding at fixed total metal concentrations (CAScTM). This new physicochemical tool, here introduced, allows the interpretation of binding results in terms of distributions of proton binding energies. A large increase in the acidity of the phenolic sites as the total metal concentration increases, especially in presence of Pb, is revealed from the shift of the CAScTM towards lower affinities. The variance of the CAScTM distribution, which can be used as a direct measure of the heterogeneity, also shows a significant dependence on the total metal concentration. A discussion of the factors that influence the heterogeneity of the HA under the conditions of each experiment is provided, so that the smoothed pattern exhibited by the titration curves can be justified.

SUPPORTING INFORMATION

Competition effects in cation binding to Humic Acid. Conditional affinity spectra for fixed total metal concentration conditions
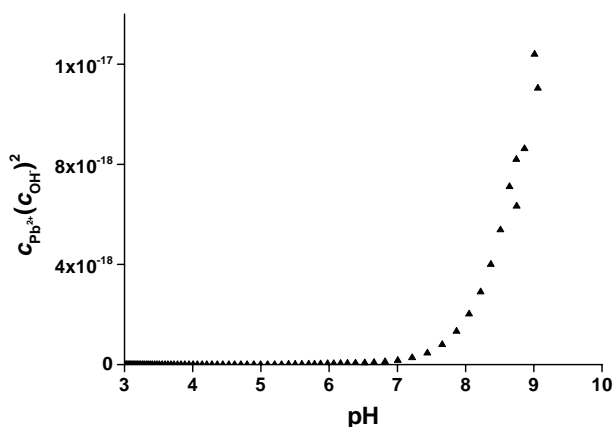
Figure SI-1. Values of the ionic concentration product $Q_{sp} = c_{Pb^{2+}} \left(c_{OH^-} \right)^2$ *vs.* pH throughout the proton titration of HA at the highest Pb concentration used in figure 2: $c_{T,Pb} = 10^{-3} \, \text{mol} \cdot \text{L}^{-1}$. The values of c_{H^+} and $c_{Pb^{2+}}$ have been recorded with the glass and the Pb-ISE respectively.

The observed change of $Q_{sp} = c_{Pb^{2+}} \left(c_{OH^-} \right)^2$ with pH, even at high pH values, indicates the absence of Pb precipitation (at least under equilibrium conditions) in the system.
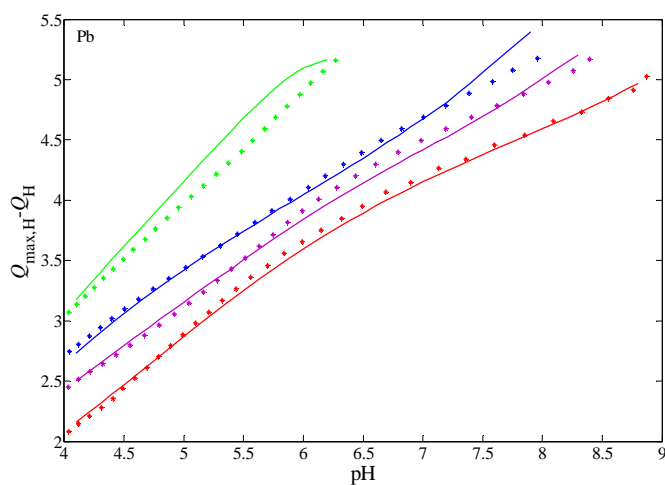
Figure SI-2. Concentration of non-protonated sites $Q_{max,H}$-Q_H (mol·kg^{-1}) as a function of pH in the presence of a fixed total lead concentration. Markers as in figure 2. Continuous lines: values calculated with the NICA parameters listed in table 2. Only one titration replicate of each metal concentration is shown for clarity reasons.
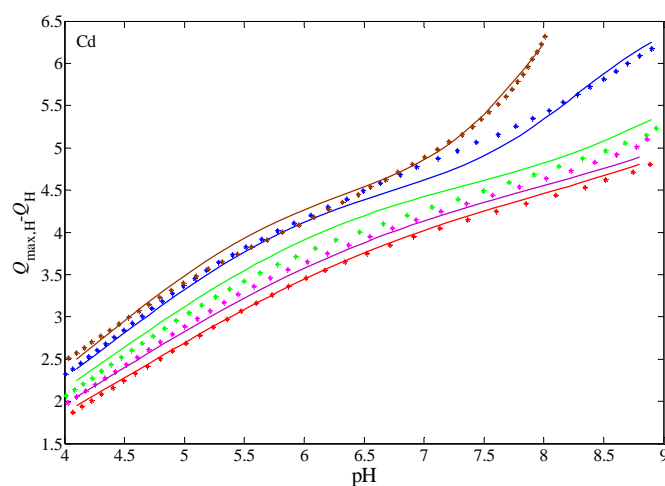
Figure SI-3. Concentration of non-protonated sites $Q_{max,H}$-Q_H (mol·kg^{-1}) as a function of pH in the presence of a fixed total cadmium concentration. Markers as in figure 3. Continuous lines: values calculated with the NICA parameters listed in table 2. Only one titration replicate of each metal concentration is shown for clarity reasons.

CHAPTER 5

RESULTS AND DISCUSSION

BINDING OF METAL IONS TO A GENERIC

FULVIC ACID IN NATURAL WATERS

- Foreword -

The competition effects due to the background ions on the binding of trace metals by a generic fulvic acid have been interpreted thought the *Conditional Affinity Spectrum* underlying the multicomponent NICA isotherm in conditions representative of a typical freshwater.

Theoretical Background

This work is a modelling study. The composition of a typical freshwater is taken from literature, it corresponds to filtered (0.2 μm) Arve River water were trace metals and fulvic acid (for simplicity, no humic acid was considered) were added at representative concentrations.

In order to take into account electrostatic interactions, the Donnan model was applied (see section 2.2.2.2). To estimate the Donnan concentrations, a speciation calculation at 25 ºC was carried out at fixed pH and ionic strength using a speciation modelling software, Visual Minteq.

By constraining the concentration of all competing cations to a fixed value (the Donnan concentration) except one (ion of interest), the competitive isotherm of the cation of interest becomes monocomponent and the corresponding affinity spectrum will be denoted as the *Conditional Affinity Spectrum* (CAS). The advantage of this constrain is that it allows to obtain the CAS by applying inversion formulas of a monocomponent isotherm. Therefore, with this procedure, an analytical expression for the CAS underlying NICA isotherm in multicomponent system can be obtained.

The average binding affinity of fulvic acid, as well as the distribution of fulvic sites occupied by the metals in freshwater conditions are reported for each ion.

Results and Discussion

The results allowed us to distinguish three groups of cations: one group of cations are preferentially bound to the phenolic sites of fulvic acid (contained aluminium, proton, lead, mercury and chrome), a second group where the cations show a greater affinity for the carboxylic sites (calcium, magnesium,

cadmium and iron (II)) and a third group where the phenolic and carboxylic distributions are overlapped (copper, zinc and iron (III)).

It is shown that the phenolic sites are almost completely occupied, whereas most of carboxylic sites remain free (92 %). The most important coverage is represented by the proton (78 % of the phenolic sites are protonated). In agreement with this observation, the competition effect is several orders of magnitude more intense in the phenolic sites than in the carboxylic ones. The competitive effect of the proton cation (in these conditions) is the most important, followed by aluminium and copper, whereas the competitive effect of major cations (such magnesium or calcium) is relatively small despite their high concentration.

Effective Affinity Distribution for the Binding of Metal Ions to a Generic Fulvic Acid in Natural Waters

Abstract

The effective distribution of affinities (*Conditional Affinity Spectrum*, CAS) seen by a metal ion binding to a humic substance under natural water conditions is derived and discussed within the NICA−Donnan model. Analytical expressions for the average affinity of these distributions in general multi-ion mixtures are reported here for the first time. These expressions enable a simple evaluation of the effect of all interfering cations on the affinity distribution of a given one. We illustrate this methodology by plotting the affinity spectra of a generic fulvic acid for 14 different cations in the presence of major inorganic ions and trace metals at pH and concentration values representative of a river water. The distribution of occupied sites and their average affinity at the typical freshwater conditions are also reported for each ion. The CAS allows us to distinguish three groups of cations: (a) Al, H, Pb, Hg, and Cr, which are preferentially bound to the phenolic sites of the fulvic ligand; (b) Ca, Mg, Cd, Fe(II), and Mn, which display a greater effective affinity for carboxylic sites, in contrast to what would be expected from their individual complexation parameters; and (c) Fe(III), Cu, Zn, and Ni, for which phenolic and carboxylic distributions are overlapped.

Effective Affinity Distribution for the Binding of Metal Ions to a Generic Fulvic Acid in Natural Waters

SUPPORTING INFORMATION

Section 1: Derivation of the CAS underlying the competitive bimodal NICA isotherm.

Section 2: Average of the CAS underlying the NICA isotherm.

Section 3: Additional plots of CAS in the test natural water sample at pH 7.

> 3.1. Additional plots of CAS in the test natural water at pH7
>
> 3.2. Cations for which a generic fulvic acid in freshwater exhibits a double peak CAS with low affinity phenolic sites
>
> 3.3. Cations for which a generic fulvic acid in freshwater exhibits a single peak CAS with phenolic and carboxylic distributions overlapped

Section 4: Comments on the Fe-fulvic binding parameters.

Results – Binding of metal ions to a generic fulvic acid in natural waters

<u>Section 1</u>: CAS underlying the competitive bimodal NICA isotherm

Let us consider the bimodal isotherm

$$\theta_i = \frac{Q_{\max i,1}\theta_{i,1} + Q_{\max i,2}\theta_{i,2}}{Q_{\max i,1} + Q_{\max i,2}} \tag{SI-1}$$

where

$$\theta_{i,j}\left(c_H, c_1, c_2, ..., c_n\right) = \frac{\left(\bar{k}_{i,j}c_i\right)^{n_{n,j}}}{\left(\bar{k}_{H,j}c_H\right)^{n_{H,j}} + \sum_{m=1}^{n}\left(\bar{k}_{m,j}c_m\right)^{n_{m,j}}}$$

$$\times \frac{\left(\left(\bar{k}_{H,j}c_H\right)^{n_{H,j}} + \sum_{m=1}^{n}\left(\bar{k}_{m,j}c_m\right)^{n_{m,j}}\right)^{p_j}}{1 + \left(\left(\bar{k}_{H,j}c_H\right)^{n_{H,j}} + \sum_{m=1}^{n}\left(\bar{k}_{m,j}c_m\right)^{n_{m,j}}\right)^{p_j}} \tag{SI-2}$$

The underlying affinity spectrum under the constrain $c_H, c_m = cnt \quad \forall m \neq i$; $m = 1, 2, ..., n$ can be calculated using the following inversion formula[1]

$$p\left(\log k_i'; c_H, c_{m\neq i} = cnt\right) = \frac{\ln(10)}{\pi}\left|\mathrm{Im}\left[\theta_i\left(c_H, c_{m\neq i} = cnt; c_i = -1/k_i'\right)\right]\right| \tag{SI-3}$$

This formula involves a linear operation, so it can be applied to each of the elementary distributions j independently. Finally, the overall spectrum is obtained by considering the adequate weighting factors. We introduce

$$F\left(c_i\right) = \left(\bar{k}_{H,j}c_H\right)^{n_{H,j}} + \sum_{m=1}^{n}\left(\bar{k}_{m,j}c_m\right)^{n_{m,j}} \tag{SI-4}$$

In this way, **equation SI-2** reads

$$\theta_{i,j} = \frac{\left(\bar{k}_{i,j}c_i\right)^{n_{i,j}}}{F\left(c_i\right)} \frac{\left(F\left(c_i\right)\right)^{p_j}}{1 + \left(F\left(c_i\right)\right)^{p_j}} \tag{SI-5}$$

In order to solve **equation SI-3**, we first compute

Results – Binding of metal ions to a generic fulvic acid in natural waters

$$F\left(-1/k_i'\right) = \left(\overline{k}_{H,j} c_H\right)^{n_{H,1}} + \sum_{m \neq i} \left(\overline{k}_{m,j} c_m\right)^{n_{m,j}} + \left(\overline{k}_{i,j} / k_i'\right)^{n_{i,j}} e^{\pi n_{i,j} i} =$$

$$= \left[\left(\overline{k}_{H,j} c_H\right)^{n_{H,1}} + \sum_{m \neq i} \left(\overline{k}_{m,j} c_m\right)^{n_{m,j}} + \left(\overline{k}_{i,j} / k_i'\right)^{n_{i,j}} \cos\left(\pi n_{i,j}\right)\right] + \quad \textbf{(SI-6)}$$

$$+ \left[\left(\overline{k}_{i,j} / k_i'\right)^{n_{i,j}} \sin\left(\pi n_{i,j}\right)\right] i = M_{i,j} e^{i\phi_{i,j}}$$

where the module $M_{i,j}$ and the argument $\phi_{i,j}$ are to be determined. Elementary complex algebra indicates

$$M_{i,j}\left(k_i'; c_H, c_{m \neq i}\right) = \left[\begin{cases} \left(\overline{k}_{H,j} c_H\right)^{n_{H,j}} + \sum_{m \neq i} \left(\overline{k}_{m,j} c_m\right)^{n_{m,j}} \\ + \left(\overline{k}_{i,j} / k_i'\right)^{n_{i,j}} \cos\left(\pi n_{i,j}\right) \end{cases}^2 \\ + \left\{\left(\overline{k}_{i,j} / k_i'\right)^{n_{i,j}} \sin\left(\pi n_{i,j}\right)\right\}^2 \right]^{1/2} \quad \textbf{(SI-7)}$$

and

$$\cos\left(\phi_{i,j}\right) = \frac{\left(\overline{k}_{H,j} c_H\right)^{n_{H,j}} + \sum_{m \neq i} \left(\overline{k}_{m,j} c_m\right)^{n_{m,j}} + \left(\overline{k}_{i,j} / k_i'\right)^{n_{i,j}} \cos\left(\pi n_{i,j}\right)}{M_{i,j}} \quad \textbf{(SI-8)}$$

The rest of the procedure is similar to that outlined in reference[2] (Supporting Information) with the definition of the module $M_{i,j}$ and the argument $\phi_{i,j}$ declared above. The final result is the analytical expression for the CAS of ion i in a complex mixture of protons and n metal ions that compete with each other for the binding sites of a humic substance described by the multicomponent bi-modal NICA isotherm:

$$p\left(\log k_i'; c_{\mathrm{H}}, c_{m \neq i} = \mathrm{cnt}\right) = \frac{\ln(10)}{\pi} \left(\frac{1}{\frac{n_{i,1}}{n_{\mathrm{H},1}} Q_{\max \mathrm{H},1} + \frac{n_{i,2}}{n_{\mathrm{H},2}} Q_{\max \mathrm{H},2}} \right) \times$$

$$\times \sum_{j=1}^{2} \left(\frac{n_{i,j}}{n_{\mathrm{H},j}} Q_{\max \mathrm{H},j} \frac{\left(\overline{k}_{i,j} / k_i'\right)^{n_{\mathrm{Pb},j}} M_{i,j}^{p_j-1}}{1 + M_{i,j}^{2p_j} + 2M_{i,j}^{p_j} \cos\left(p_j \phi_{i,j}\right)} \times \right. $$
$$\left. \times \left[\sin\left(\pi n_{i,j} - \left(1 - p_j\right)\phi_{i,j}\right) + M_{i,j}^{p_j} \sin\left(\pi n_{i,j} - \phi_{i,j}\right) \right] \right)$$

(SI-9)

This is the analytical expression used to evaluate the CAS of every component throughout the manuscript, **equation 6**.

<u>Section 2:</u> Average of the CAS underlying multicomponent NICA isotherm

For a general unimodal multicomponent isotherm, the coverage is a function of the concentrations of all the different species (protons and n different metal ions), i.e.: $\theta_i\left(c_{\mathrm{H}}, c_1, \ldots c_k, \ldots, c_n\right)$

All the combinations of two different ions must satisfy the thermodynamic consistency relationship, i.e.:

$$\left(\frac{\partial Q_{\mathrm{H}}}{\partial \log c_i}\right)_{\log c_{\mathrm{H}}, \log c_{m \neq i}} = \left(\frac{\partial Q_i}{\partial \log c_{\mathrm{H}}}\right)_{\log c_m}$$

$$\left(\frac{\partial Q_i}{\partial \log c_k}\right)_{\log c_{\mathrm{H}}, \log c_{m \neq k}} = \left(\frac{\partial Q_k}{\partial \log c_i}\right)_{\log c_{\mathrm{H}}, \log c_{m \neq i}}$$

(SI-10)

The same procedure that was developed in previous papers[2,3] for the case of a two-component NICA isotherm, can be generalized to the multicomponent case in a straightforward way. First we proceed with the three-component NICA isotherm (proton, H; and two metallic ions, 1 and 2). Taking the derivative of the consistency relationship

$$\left(\frac{\partial Q_2}{\partial \log c_1}\right)_{\log c_{\mathrm{H}}, \log c_2} = \left(\frac{\partial Q_1}{\partial \log c_2}\right)_{\log c_{\mathrm{H}}, \log c_1}$$

(SI-11)

with respect to log c_2, and then multiplying by log c_2 and integrating, we obtain

$$\frac{\partial}{\partial \log c_1}\left(\int_{-\infty}^{\infty} \log c_2 \frac{\partial Q_2}{\partial \log c_2} d \log c_2\right) = \int_{-\infty}^{\infty} \log c_2 \frac{\partial^2 Q_1}{\partial \left(\log c_2\right)^2} d \log c_2 \qquad \textbf{(SI-12)}$$

Recalling the definition of the binding capacity distribution

$$B^{(2)}\left(\log c_2\right) = \frac{\partial \theta_2}{\partial \log c_2} = \frac{1}{Q_{\max,2}}\left(\frac{\partial Q_2}{\partial \log c_2}\right) \qquad \textbf{(SI-13)}$$

and the relationship between the affinity spectrum average and the mean of the binding capacity distribution (equation 51 in reference [4]):

$$\left\langle \log k_2 \right\rangle = -\frac{1}{Q_{\max,2}} \int_{-\infty}^{\infty} \log c_2 \left(\frac{\partial Q_2}{\partial \log c_2}\right) d \log c_2 \qquad \textbf{(SI-14)}$$

the integral between brackets of the l.h.s. of **equation SI-12** can be easily evaluated, leading to

$$-Q_{\max,2}\left(\frac{\partial \left\langle \log k_2' \right\rangle}{\partial \log c_1}\right) = \int_{-\infty}^{\infty} \log c_2 \left(\frac{\partial^2 Q_1}{\partial \left(\log c_2\right)^2}\right) d \log c_2 \qquad \textbf{(SI-15)}$$

Where the prime over *k* indicates *conditional affinity constants* (i.e., under the constrain of constant concentration of the competing ions). Integration of the r.h.s. of **equation SI-15** by parts, leads to

$$-Q_{\max,2}\frac{\partial \left\langle \log k_2' \right\rangle}{\partial \log c_1} = 0 - \int_{-\infty}^{\infty} \frac{\partial Q_1}{\partial \log c_2} d \log c_2 = Q_1\left(c_H, c_1; c_2 = 0\right) \qquad \textbf{(SI-16)}$$

Integration of the preceding expression on the interval $(-\infty \,(c_1 = 0), \ \log c_1]$, yields

$$\left\langle \log k_2' \right\rangle_{c_H, c_1 = cnt} = \left\langle \log k_2' \right\rangle_{c_H = cnt; c_1 = 0} - \frac{Q_{\max,1}}{Q_{\max,2}} \int_{-\infty}^{\log c_1} \theta_1\left(c_H, c_1; c_2 = 0\right) d \log c_1 \qquad \textbf{(SI-17)}$$

The first term in the r.h.s. of this equation is the CAS average of ion 2 in the presence of protons only, which can be expressed as[3]:

$$\left\langle \log k_2^{'} \right\rangle_{c_H=cnt;c_1=0} = \left\langle \log k_2 \right\rangle_{c_H=c_1=0} - \frac{Q_{max,H}}{Q_{max,2}} \int\limits_{-\infty}^{\log c_H} \theta_H\left(c_H;c_1=c_2=0\right)d\log c_H \qquad \textbf{(SI-18)}$$

By combining **equations SI-17-18**, we obtain a general equation for the CAS average of ion 2 in a three-component system where the concentrations of the competing ions (H, 1) are kept constant:

$$\left\langle \log k_2^{'} \right\rangle_{c_H,c_1=cnt} = \left\langle \log k_2 \right\rangle_{c_H=c_1=0} - \frac{Q_{max,H}}{Q_{max,2}} \int\limits_{-\infty}^{\log c_H} \theta_H\left(c_H;c_1=c_2=0\right)d\log c_H -$$

$$-\frac{Q_{max,1}}{Q_{max,2}} \int\limits_{-\infty}^{\log c_1} \theta_1\left(c_H,c_1;c_2=0\right)d\log c_1 \qquad \textbf{(SI-19)}$$

Now the integral of the isotherms must be evaluated in each case. First, in absence of ions 1 and 2, the NICA isotherm of proton ions reads

$$\theta_H\left(c_H;c_1=c_2=0\right) = \frac{\left(\overline{k}_H c_H\right)^{n_H p}}{1+\left(\overline{k}_H c_H\right)^{n_H p}} \qquad \textbf{(SI-20)}$$

The integration of this expression yields

$$\int\limits_{-\infty}^{\log c_H} \theta_H\left(c_H;c_1=c_2=0\right)d\log c_H = \frac{1}{n_H p}\log\left(1+\left(\overline{k}_H c_H\right)^{n_H p}\right) \qquad \textbf{(SI-21)}$$

Second, in absence of ion 2 the two-component NICA isotherm applies

$$\theta_1\left(c_H,c_1;c_2=0\right) = \left(\overline{k}_1 c_1\right)^{n_1} \left[\frac{\left(\left(\overline{k}_H c_H\right)^{n_H}+\left(\overline{k}_1 c_1\right)^{n_1}\right)^{p-1}}{1+\left(\left(\overline{k}_H c_H\right)^{n_H}+\left(\overline{k}_1 c_1\right)^{n_1}\right)^{p}} \right] \qquad \textbf{(SI-22)}$$

which can be expressed as a derivative with respect to $\ln c_1$:

$$\frac{\partial \ln\left[1+\left(\left(\bar{k}_H c_H\right)^{n_H}+\left(\bar{k}_1 c_1\right)^{n_1}\right)^p\right]}{\partial \ln c_1}=$$

$$=n_1 p\left(\bar{k}_1 c_1\right)^{n_1}\left[\frac{\left(\left(\bar{k}_H c_H\right)^{n_H}+\left(\bar{k}_1 c_1\right)^{n_1}\right)^{p-1}}{1+\left(\left(\bar{k}_H c_H\right)^{n_H}+\left(\bar{k}_1 c_1\right)^{n_1}\right)^p}\right]=n_1 p\theta_1\left(c_H,c_1;c_2=0\right)$$

(SI-23)

Therefore, the second integral term in r.h.s. of **equation SI-19** yields

$$\int_{-\infty}^{\log c_1}\theta_1\left(c_H,c_1;c_2=0\right)d\log c_1=\frac{1}{n_1 p}\left\{\log\left[1+\left(\left(\bar{k}_H c_H\right)^{n_H}+\left(\bar{k}_1 c_1\right)^{n_1}\right)^p\right]-\right.$$

$$\left.-\log\left[1+\left(\bar{k}_H c_H\right)^{n_H p}\right]\right\}$$

(SI-24)

And, hence, **equation SI-19** becomes

$$\left\langle\log k_2'\right\rangle_{c_H,c_1=cnt}=\left\langle\log k_2\right\rangle_{c_H=c_1=0}-\frac{Q_{max,H}}{Q_{max,2}}\frac{1}{n_H p}\log\left(1+\left(\bar{k}_H c_H\right)^{n_H p}\right)$$

$$-\frac{Q_{max,1}}{Q_{max,2}}\frac{1}{n_1 p}\left\{\log\left[1+\left(\left(\bar{k}_H c_H\right)^{n_H}+\left(\bar{k}_1 c_1\right)^{n_1}\right)^p\right]-\log\left[1+\left(\bar{k}_H c_H\right)^{n_H p}\right]\right\}$$

(SI-25)

Finally, taking into account the thermodynamic consistency relationship (**equation SI-10**):

$$\frac{Q_{max,i}}{Q_{max,2}}=\frac{n_i}{n_2}\quad;\quad i=H,1$$

(SI-26)

the following analytical expression for the CAS average of metal ion 2 in a three-component NICA isotherm is obtained

$$\left\langle\log k_2'\right\rangle_{c_H,c_1=cnt}=\left\langle\log k_2\right\rangle_{c_H=c_1=0}-\frac{1}{n_2 p}\log\left[1+\left(\left(\bar{k}_H c_H\right)^{n_H}+\left(\bar{k}_1 c_1\right)^{n_1}\right)^p\right]$$

(SI-27)

It is straightforward to generalize this procedure to a multicomponent NICA isotherm for *n* metal ions, leading to

Results – Binding of metal ions to a generic fulvic acid in natural waters

$$\left\langle \log k_i^{'} \right\rangle_{c_H,c_{m\neq i}=cnt} = \left\langle \log k_i^{'} \right\rangle_{c_H:c_{m\neq i}=0} - \frac{Q_{max,H}}{Q_{max,i}} \int\limits_{-\infty}^{\log c_H} \theta_H \left(c_H;c_m=0\right) d\log c_H -$$

$$- \frac{Q_{max,1}}{Q_{max,i}} \int\limits_{-\infty}^{\log c_1} \theta_1 \left(c_H,c_1;c_2=...=c_n=0\right) d\log c_1 -$$

$$-...- \frac{Q_{max,i-1}}{Q_{max,i}} \int\limits_{-\infty}^{\log c_{i-1}} \theta_{i-1} \left(c_H,c_1,...,c_{i-1};c_i=...=c_n=0\right) d\log c_{i-1} - \qquad \textbf{(SI-28)}$$

$$- \frac{Q_{max,i+1}}{Q_{max,i}} \int\limits_{-\infty}^{\log c_{i+1}} \theta_{i+1} \left(c_H,c_1,...,c_{i-1},c_{i+1};c_i=c_{i+2}=...=c_n=0\right) d\log c_{i+1} -$$

$$-...- \frac{Q_{max,n}}{Q_{max,i}} \int\limits_{-\infty}^{\log c_n} \theta_n \left(c_H,c_{m\neq i};c_i=0\right) d\log c_n$$

The integrals corresponding to the different coverages can be easily evaluated

$$\int\limits_{-\infty}^{\log c_k} \theta_k \left(c_H,c_1,...,c_{i-1},c_{i+1},...,c_k;c_{k+1},...,c_n=0\right) d\log c_k =$$

$$= \frac{1}{n_k p} \left\{ \log \left[1 + \left(\left(\overline{k}_H c_H\right)^{n_H} + \left(\overline{k}_1 c_1\right)^{n_1} +...+ \left(\overline{k}_{i-1} c_{i-1}\right)^{n_{i-1}} + \left(\overline{k}_{i+1} c_{i+1}\right)^{n_{i+1}} +...+ \left(\overline{k}_k c_k\right)^{n_k} \right)^p \right] - \qquad \textbf{(SI-29)}$$

$$- \log \left[1 + \left(\left(\overline{k}_H c_H\right)^{n_H} + \left(\overline{k}_1 c_1\right)^{n_1} +...+ \left(\overline{k}_{i-1} c_{i-1}\right)^{n_{i-1}} + \left(\overline{k}_{i+1} c_{i+1}\right)^{n_{i+1}} +...+ \left(\overline{k}_{k-1} c_{k-1}\right)^{n_{k-1}} \right)^p \right] \right\}$$

Taking into account the thermodynamic consistency relationships SI-10 for the general multicomponent case

$$\frac{Q_{max,k}}{Q_{max,i}} = \frac{n_k}{n_i} \quad ; k = H,1,...,i-1,i+1,...,n \qquad \textbf{(SI-30)}$$

we obtain

$$\left\langle \log k_i^{'} \right\rangle_{c_H,c_{m\neq i}=cnt} = \left\langle \log k_i \right\rangle_{c_H,c_{m\neq i}=0} - \frac{1}{n_i p} \log \left[1 + \left(\left(\overline{k}_H c_H\right)^{n_H} + \sum_{m\neq i} \left(\overline{k}_m c_m\right)^{n_m} \right)^p \right] \qquad \textbf{(SI-31)}$$

Note that $\left\langle \log k_i \right\rangle_{c_H,c_{m\neq i}=0}$, i.e.: the average affinity in absence of any competing ion, corresponds to the tabulated intrinsic binding parameter $\log \overline{k}_i$ in NICA (**equation SI-2**). Finally, the bimodal version of NICA is considered, leading to the final formula:

$$\left\langle \log k_i' \right\rangle_{c_{\mathrm{H}}, c_{m \neq i} = \mathrm{cnt}} = \sum_{j=1}^{2} \left(\frac{\dfrac{n_{i,j}}{n_{\mathrm{H},j}} Q_{\mathrm{maxH},j}}{\dfrac{n_{i,1}}{n_{\mathrm{H},1}} Q_{\mathrm{maxH},1} + \dfrac{n_{i,2}}{n_{\mathrm{H},2}} Q_{\mathrm{maxH},2}} \right) \times$$

$$\times \left(\log \overline{k}_{i,j} - \frac{1}{n_{i,j} p_j} \log \left[1 + \left(\left(\overline{k}_{\mathrm{H},j} c_{\mathrm{H}} \right)^{n_{\mathrm{H},j}} + \sum_{m \neq i} \left(\overline{k}_{m,j} c_m \right)^{n_{m,j}} \right)^{p_j} \right] \right)$$

(SI-32)

which corresponds to **equation 9** in the manuscript.

<u>Section 3</u>: Additional plots of CAS in the test natural water at pH 7

3.1.- Cations for which the generic fulvic acid exhibits a double peak CAS with high affinity phenolic sites.
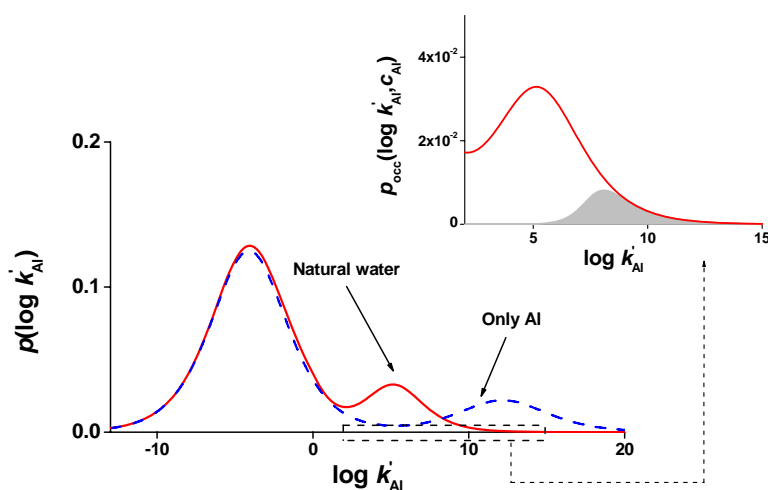
Figure S1. Dashed line: affinity spectrum of Al in absence of any other competing ion; solid line: CAS of Al in the natural water. The contour of the shaded area in the inset shows the density of fulvic sites occupied by Al at the conditions of the natural water
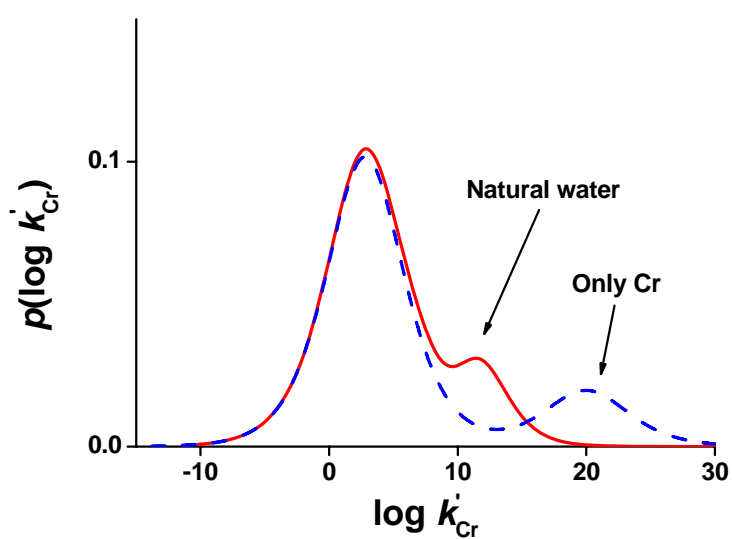
Figure S2. CAS of Cr. Meaning of the lines as in figure S1. There is no shaded area, since this cation is not present in the composition of the natural water given in table 1
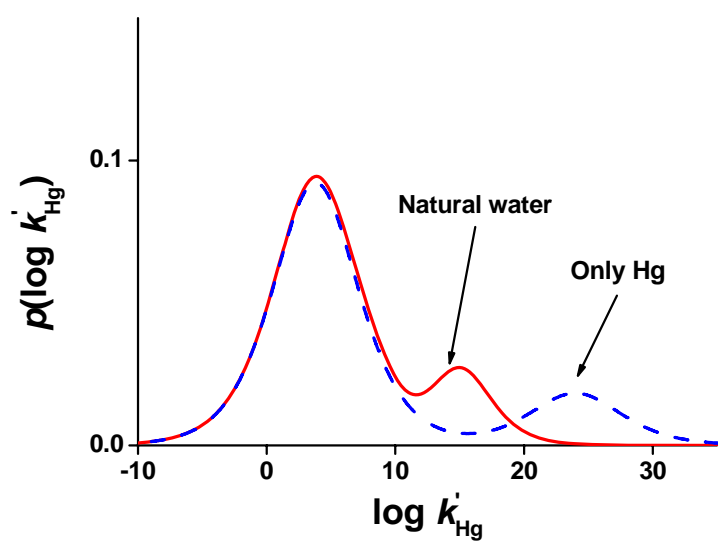
Figure S3. CAS of Hg. Meaning of the lines as in figure S1. There is no shaded area, since this cation is not present in the composition of the natural water given in table 1
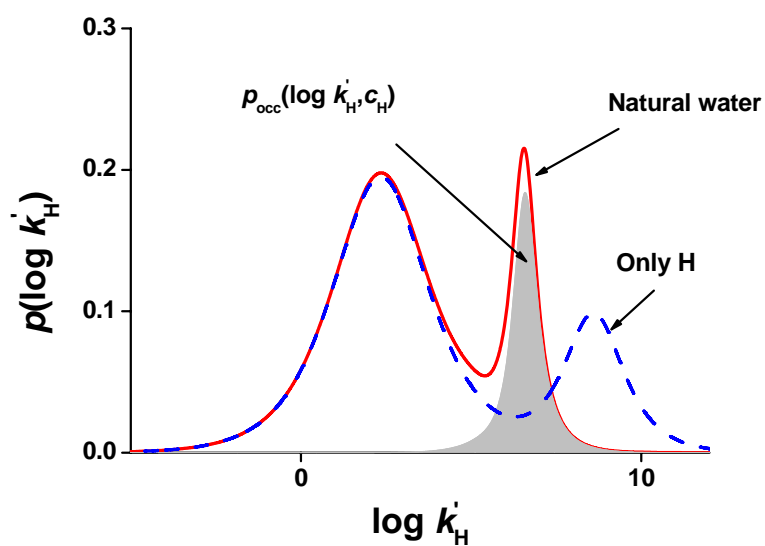
Figure S4. CAS of H. Meaning of the lines as in figure S1.

3.2.- Cations for which a generic fulvic acid in freshwater exhibits a double peak CAS with low affinity phenolic sites.
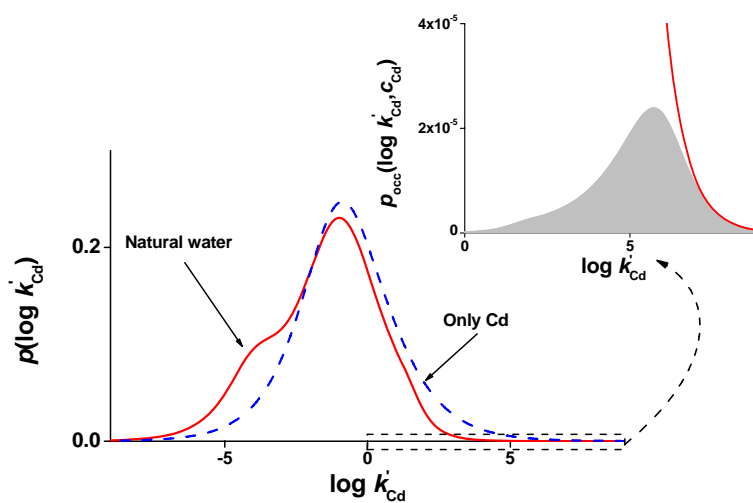
Figure S5. CAS of Cd. Meaning of the lines as in figure S1.
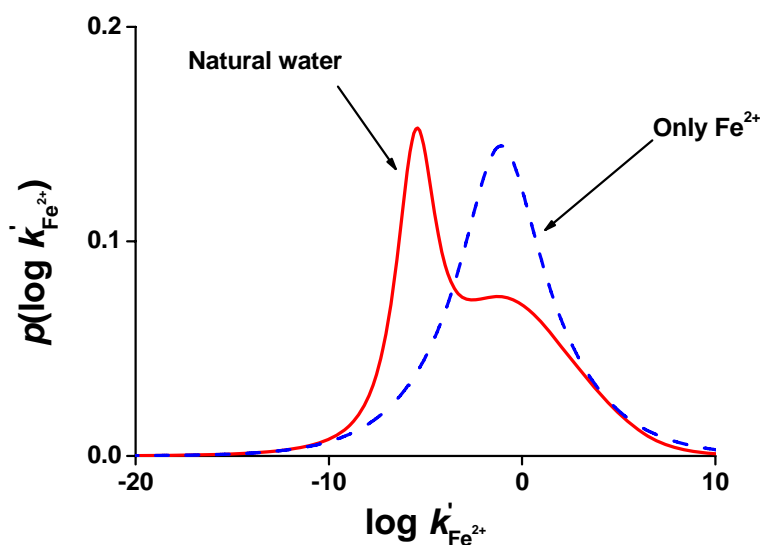
Figure S6. CAS of Fe(II). Meaning of the lines as in figure S1. There is no shaded area, since this cation is not present in the composition of the natural water given in table 1
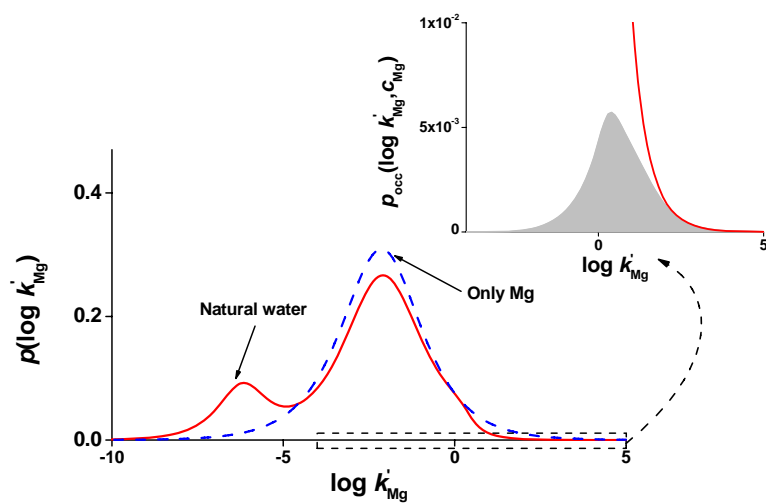
Figure S7. CAS of Mg. Meaning of the lines as in figure S1.
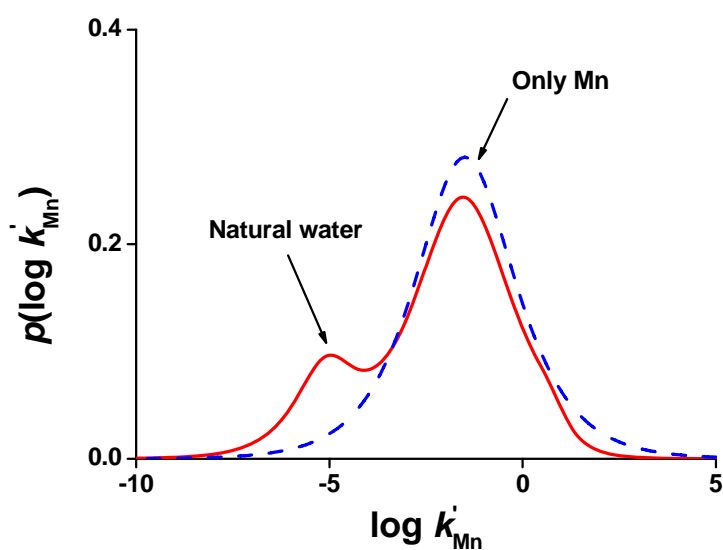
Figure S8. Case of Mn. Meaning of the lines as in figure S1. There is no shaded area, since this cation is not present in the composition of the natural water given in table 1

3.3.- Cations for which a generic fulvic acid in freshwater exhibits a single peak CAS with phenolic and carboxylic distributions overlapped.
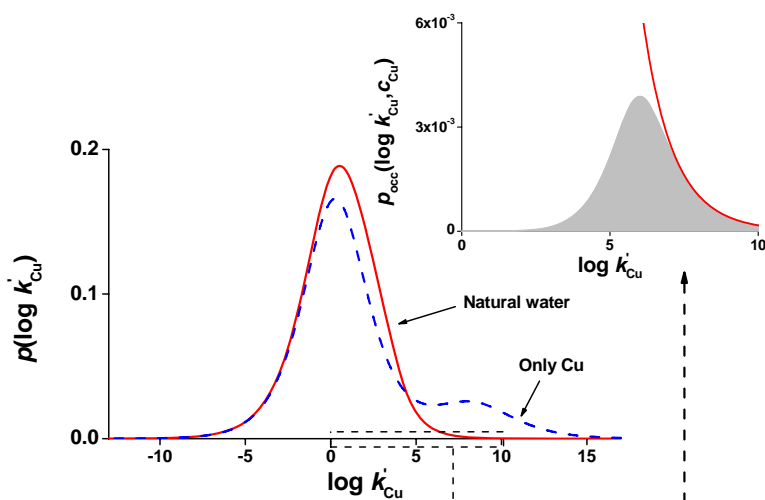
Figure S9. CAS of Cu. Meaning of the lines as in figure S1.

Results – Binding of metal ions to a generic fulvic acid in natural waters
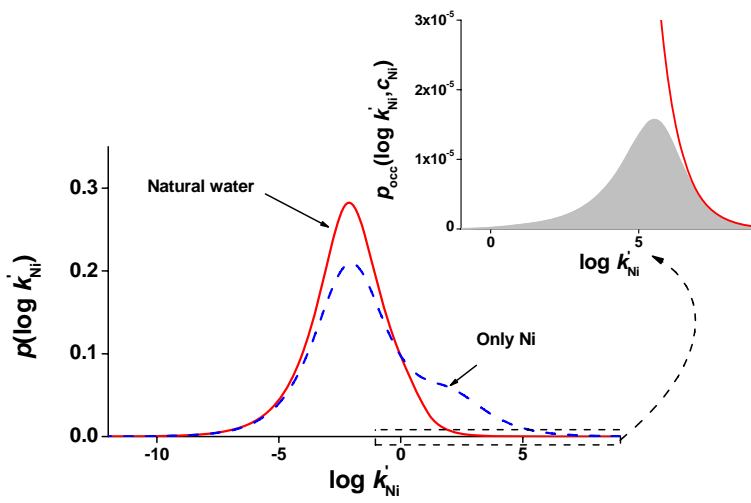
Figure S10. CAS of Ni. Meaning of the lines as in figure S1
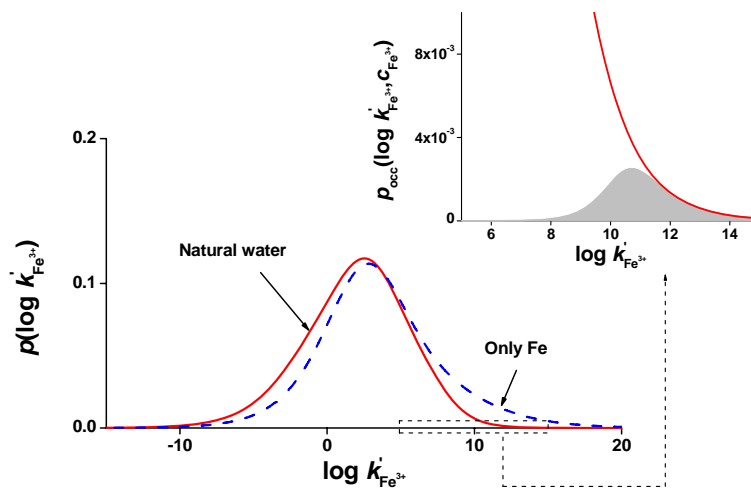
Figure S11. CAS of Fe(III). Meaning of the lines as in figure S1

Section 4: Comments on the Fe-fulvic binding parameters

Amongst the main inorganic ions typically present in natural waters, Fe(III) probably is the species for which the accuracy of the specific binding parameters with humic substances is currently more uncertain, due to the limited amount of available data [5-7]. To our knowledge, the most recent parameterization of the NICA-Donnan model for Fe complexation by dissolved organic matter was published by Hiemstra and van Riemsdijk [8]. These authors reported new binding parameters for the Fe-fulvic acid complexes (log $\bar{k}_{Fe,1} = 2.7$, log $\bar{k}_{Fe,2} = 8.3$, $n_{Fe,1} = 0.36$, $n_{Fe,2} = 0.23$) which have been used in the present work instead of the generic parameters originally suggested by Milne et al.[5] (i.e.: log $\bar{k}_{Fe,1} = 6.0$, log $\bar{k}_{Fe,2} = 36$, $n_{Fe,1} = 0.25$, $n_{Fe,2} = 0.19$). The latter were derived from incomplete data sets by means of empirical correlations found by comparison with the binding behaviour of other metal ions (see the original reference for further details). Hence, the parameters of Hiemstra et al. probably represent a more accurate description of the actual binding behaviour of fulvic acids with Fe(III). However, the experimental data used by Hiemstra and van Riemsdijk for parameterization (namely, solubility measurements of Fe-hydroxides in seawater[9]) correspond to samples containing marine (not freshwater) dissolved organic matter that was not isolated, purified and characterized according to standard fulvic acid extraction procedures. These seawater samples would probably contain, within their DOM, an unknown fraction of various organic substances that do not behave as active fulvic acid. Moreover, the actual acid-base and complexation behaviour of this DOM towards other metals was not experimentally tested. Consequently, the set of Fe-fulvic NICA parameters from Hiemstra and van Riemsdijk may still be somewhat inaccurate when applied to pure, freshwater fulvic acid.

Due to the huge difference between both sets of parameters, they imply very significant differences in the speciation results and, accordingly, in the calculated CAS of the fulvic ligand in freswater. It seems appropriate to us to include a selection of the results obtained using the "old" iron binding parameters originally published by Milne *et al.*, as an example of the critical influence that the current uncertainty about the iron binding behaviour of organic matter may have on model calculations. It also seems fair to mention that the old iron binding parameters have been previously used in the literature for the modelling of competitive metal ion binding (including the effect of Fe) to

humic substances in reasonably good agreement with experimental data [7,10,11], although the binding parameters of Fe(III) might not be relevant in these cases.

Using this binding parameter set in our calculations, it is found that the main competitive contribution from the background ions is due to Fe^{3+}, which binds strongly and preferentially to the phenolic sites (see figure S 12.)). We chose the CAS of H and Pb ions as the two cases where the influence of the set of Fe binding constants is more significant (Figures S 13 and S 14). As a conclusion, it is clear that iron binding to humic substances still requires more investigation.
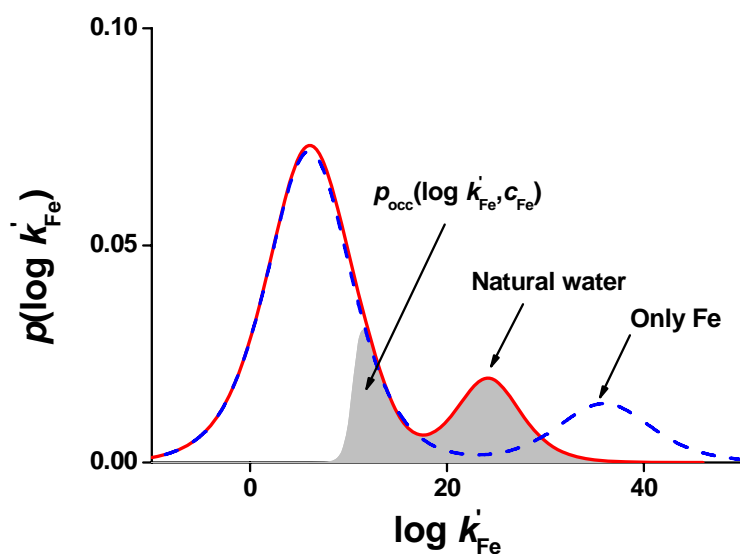
Figure S12. CAS of Fe(III) calculated using the Fe NICA binding parameters of Milne *et al*. Meaning of the lines as in figure S1. Notice the large amount of high affinity sites in the spectra, compared with figure S11 and the significant fraction of occupied sites (shaded area) at the iron concentration of the freshwater.
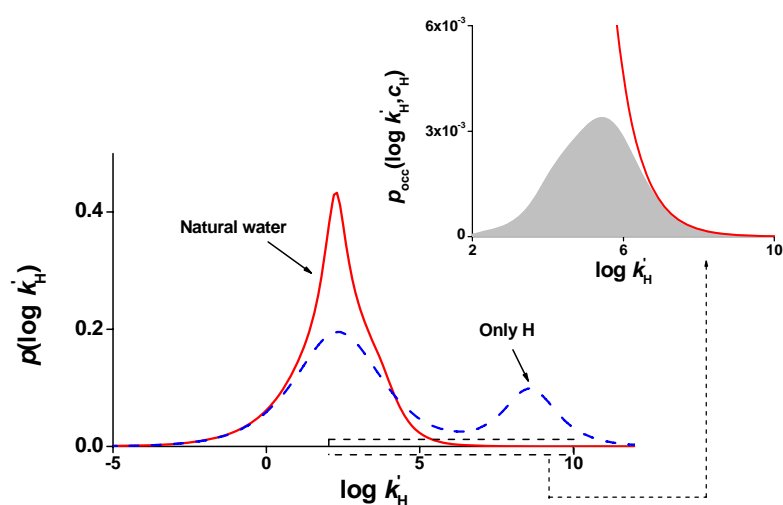
Figure S13. CAS of H calculated using the Fe NICA binding parameters of Milne *et al*. Notice the single peak shape of the CAS, compared with figure S4., and the little amount of fulvic sites occupied by protons (shaded area) in these conditions.
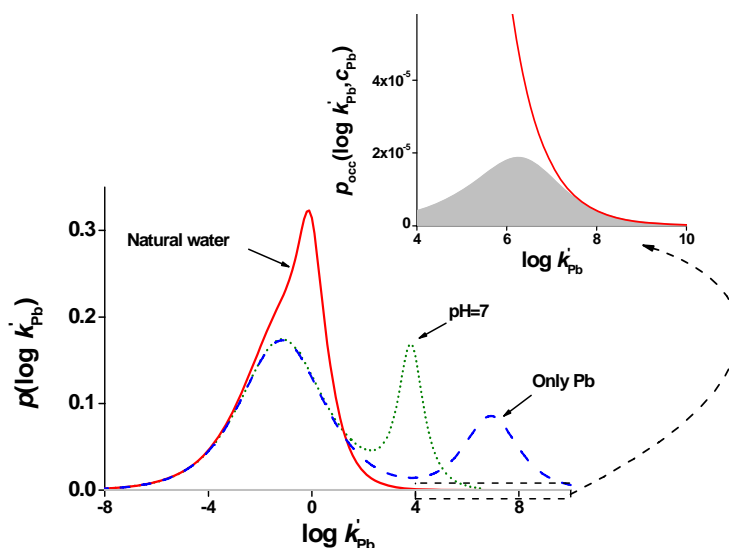
Figure S14. CAS of Pb calculated using the Fe NICA binding parameters of Milne *et al*. Dotted line: CAS at pH 7 in absence of other metal ions. Meaning of the rest of lines as in figure S1. Compare with figure 1 and notice the single peak shape of the CAS. In these conditions, the competition effect due to Fe is larger than that due to protons.

Literature cited

(1)   Garcés, J. L.; Mas, F.; Puy, J., Conditional equilibrium constants in multicomponent heterogeneous adsorption: The conditional affinity spectrum. *Journal of Chemical Physics* **2006,** *124*, 044710.

(2)   Puy, J.; Galceran, J.; Huidobro, C.; Companys, E.; Samper, N.; Garces, J. L.; Mas, F., Conditional Affinity Spectra of Pb2+-Humic Acid Complexation from Data Obtained with AGNES. *Environmental Science & Technology* **2008,** *42*, (24), 9289-9295.

(3)   Puy, J.; Huidobro, C.; David, C.; Rey-Castro, C.; Salvador, J.; Companys, E.; Garces, J. L.; Galceran, J.; Cecilia, J.; Mas, F., Conditional affinity spectra underlying NICA isotherm. *Colloids and Surfaces A: Physicochemical and Engineering Aspects* **2009,** *347*, (1-3), 156-166.

(4)   Garcés, J. L.; Mas, F.; Puy, J., Affinity distribution functions in multicomponent heterogeneous adsorption. Analytical inversion of isotherms to obtain affinity spectra. *Journal of Chemical Physics* **2004,** *120*, (19), 9266-9276.

(5)   Milne, C. J.; Kinniburgh, D. G.; van Riemsdijk, W. H.; Tipping, E., Generic NICA-Donnan model parameters for metal-ion binding by humic substances. *Environmental Science & Technology* **2003,** *37*, (5), 958-971.

(6)   Weber, T.; Allard, T.; Tipping, E.; Benedetti, M. F., Modeling iron binding to organic matter. *Environmental Science & Technology* **2006,** *40*, (24), 7488-7493.

(7)   Koopmans, G. F.; Schenkeveld, W. D. C.; Song, J.; Luo, Y. M.; Japenga, J.; Temminghoff, E. J. M., Influence of EDDS on metal speciation in soil extracts: Measurement and mechanistic multicomponent modeling. *Environmental Science & Technology* **2008,** *42*, 1123-1130.

(8)   Hiemstra, T.; van Riemsdijk, W. H., Biogeochemical speciation of Fe in ocean water. *Marine Chemistry* **2006,** *102*, (3-4), 181-197.

(9)   Liu, X. W.; Millero, F. J., The solubility of iron in seawater. *Marine Chemistry* **2002,** *77*, (1), 43-54.

(10)   Allard, T.; Menguy, N.; Salomon, J.; Calligaro, T.; Weber, T.; Calas, G.; Benedetti, M. F., Revealing forms of iron in river-borne material from major tropical rivers of the Amazon Basin (Brazil). *Geochimica Et Cosmochimica Acta* **2004,** *68*, (14), 3079-3094.

(11)   Ge, Y.; MacDonald, D.; Sauve, S.; Hendershot, W., Modeling of Cd and Pb speciation in soil solutions by WinHumicV and NICA-Donnan model. *Environmental Modelling & Software* **2005,** *20*, (3), 353-359.

Part II

CHAPTER 6

THEORETICAL BACKGROUND

COMPLEX LABILITY AND DIFFUSIVE GRADIENTS IN THIN FILMS TECHNIQUE

6.1 Ion activity models

As mentioned in the general introduction of this thesis, most biogeochemical and environmental processes are dynamic in nature, and their modeling requires the combination of hydrodynamic processes, diffusive transport and chemical kinetics.[1] However, the first simple models developed to describe bioavailability (e.g. FIAM and BLM) were based only on equilibrium concepts. The following sections review the main assumption and limitations of these models. Later on, section 6.2 will introduce the importance of the dynamic aspects on the bioavailability, e.g. through the lability concept.

6.1.1 Free Ion Activity Model (FIAM)

In the early 1980s, the FIAM[2-4] was developed to explain the good correlation between the concentration of the free metal cation present in solution and the observed biological effects.[5,6] The goal of the FIAM is to predict the bioavailabilty of a metal as a function of its speciation in water.

The FIAM supposes the existence of metal specific binding sites in the surface of the organism. One of the major hypotheses is that: the biological effect is proportional to the amount of sites occupied by the metal. This model describes the interactions between the metal and the organism (see **figure 6.1**) according to two successive steps.[7] First, the metal, either complexed or free, diffuses through the diffusive boundary layer to the cell and binds the active sites of the cell membrane following chemical equilibrium relationships. Second, uptake or "internalization" of the metal through the membrane occurs.[8,9] Diffusion is so fast that depletion of the free metal concentration at the membrane surface can be neglected.

Theoretical Background – Complex Lability and Diffusive Gradients in Thin films
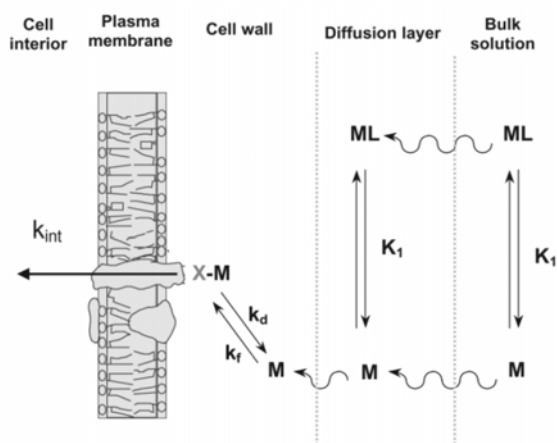
Figure 6.1. Conceptual model of metal – cell interactions. M represents the free metal ion, ML a metal complex in solution; K_1 is the equilibrium constant for the formation of ML; M-X is the membrane,surface metal complex; k_f and k_d are the rate constants for the formation and dissociation (respectively) of the surface complex;, k_{int} is the rate constant for "internalization" or transport of the metal across the biological membrane.[10]

The interaction of the metal with the cell surface, involving either the free metal (M) or a metal complex (ML) as a reactive species, can be represented in terms of formation of M-X-membrane surface complexes by the following reactions, where –X-membrane is a cellular ligand present at the cell surface:

- Solution equilibria:

$$M + L \xrightleftharpoons{K_1} ML \qquad\qquad (6.1)$$

$$K_1 = \frac{c_{ML}}{c_M \, c_L} \qquad\qquad (6.2)$$

- Surface reaction of M:

$$M + X\text{-membrane} \xrightleftharpoons{K_2} M\text{-X-membrane} \qquad\qquad (6.3)$$
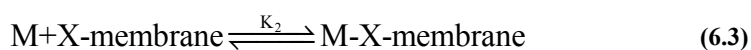
$$c_{M\text{-X-membrane}} = K_2 \, c_{X\text{-membrane}} \, c_M \qquad\qquad (6.4)$$

where K_1 and K_2 are conditional equilibrium constants, L is a ligand in solution, the charges of species are omitted for simplicity. **Equation 6.4** indicates that the biological response will vary directly as a function of c_M.

A number of key assumptions underlie the FIAM, some of them are obvious and others are rather subtler:

1. the plasma membrane is the primary site for metal interactions with living organisms

2. the interaction with the plasma membrane can be described as a surface complexation reaction, forming M-X-membrane complexes

3. metal transport in solution is considered faster than metal uptake (i.e. faster than the expression of the biological response) meaning that the limiting steep is the internalization of metal by the organism

4. the metal uptake by the organism is strictly dependent on the concentration of M-X-cell surface complex

5. the concentration of free sites $c_{X\text{-membrane}}$ remains virtually constant and variation in $c_{M\text{-X-membrane}}$ follow those of M in solution

6. the metal does not induce any changes in the nature of the plasma membrane

Since the development of the FIAM, limitations and exceptions to the model were rapidly reported (see, e.g., some reports of these exceptions in Cambell's review).[7]

6.1.2 Biotic Ligand Model (BLM)

The BLM is shown schematically in **figure 6.2.** While this model is based on the same conceptual basis as the FIAM, it moreover considers that major cations may also interact with the cell and influence the number of sites available for the trace metal to bind to the membrane (i.e. it takes into account the binding competition among cations at the surface membrane).

In fact, Zitko[11] identified competition of the hardness cations (Ca^{2+} and Mg^{2+}) with trace metal ions for binding at sites where the metals exert a toxic effect, as the mechanism by which hardness mitigates toxicity. Payle[12] shows that competition phenomena with H^+, Ca^{2+}, Mg^{2+} and Na^+ cations occur in the accumulation mechanisms on the fish gills. For the first time, Pagenkopf *et al.*[13]

in 1974 employed a chemical equilibrium model to explain how water chemistry affects the form of the metal that is present, and how this is related to the toxicity of the metal. Nearly 10 years after these initial investigations, the Gill Surface Interaction Model (GSIM) for trace metal toxicity to fish was proposed.[3] The GSIM framework accounted for the previously observed decreasing metal toxicity with increasing hardness by competition between the metal stressor and hardness cations for binding at the physiologically active gill sites. In their review of the main assumptions of the FIAM and GSIM, Di Toro et al.[14] propose more robust interpretation integrating the speciation of metal and the competitive effects of cations: the Biotic Ligand Model (illustrated in **figure 6.2**).
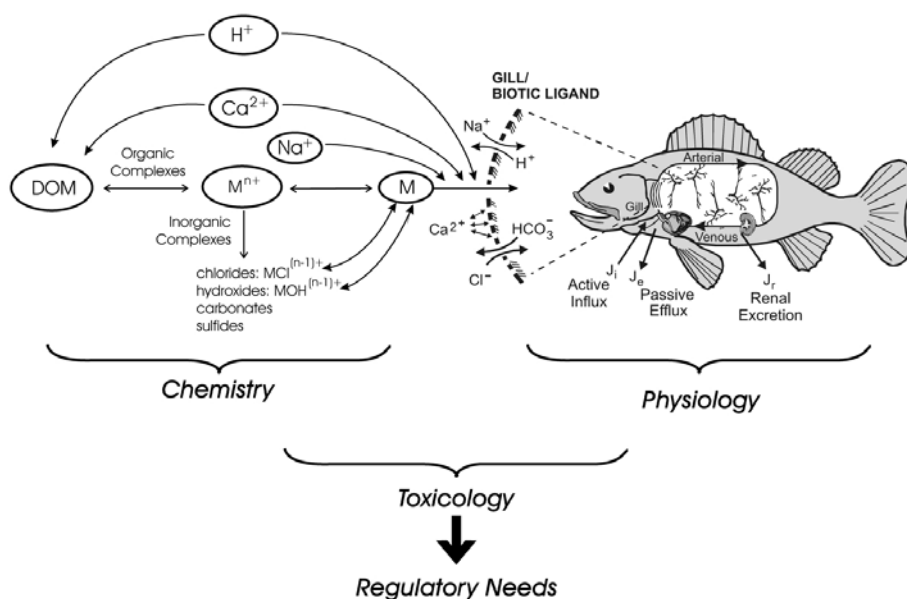
Figure 6.2. Schematic representation of the biotic model and the inter-relationship among chemistry, physiology and toxicology.[15]

According to the formalism of the BLM, the biological effect is proportional to the amount of specific sites occupied by the metal; since all species are considered at equilibrium, this amount is dependent on free metal present in solution and also on the concentration of competitive cations. Thermodynamic and conditional binding constants are used to calculate the concentration of metal species in the system and to take into account the major cation competition. The conceptual model can be considered in terms of two separate components **(figure 6.2)**. One component involves the solution chemistry in the

bulk water, which allows prediction of the concentration of the toxic free metal ion (M^{n+}; **figure 6.2**). A second component involves the binding of the toxic metal to the biotic ligand. The formulation and the assumptions of the BLM are very similar to the FIAM, but BLM, in addition, considers the effect of competing cations and competing ligands.[10,14-16]

6.1.3 Limitation of these models

The different assumptions at the basis of the BLM and the FIAM have been widely discussed, and limitations of the model were emphasized.[7,10,17,18] A critical point for ion activity models is the consideration of rate-limiting internalization. In fact, a main assumption of ion activity models is that the metal uptake is under thermodynamic control (i.e. that the internalization is slow compared to the transport of the metal from bulk solution to the cell membrane surface, see **figure 6.3. a)**), which has been rarely verified[10]. Comparisons of calculated metal diffusion rates with measured metal uptake rates, suggest that under certain conditions, the diffusion supply of the metal from the bulk solution may probe to be the rate-limiting step.[18-20] In this case, the internalization rate is relatively faster than the transport of the metal, which may shift the equibrium between species at interface surface organism-solution. A free metal concentration gradient is established, and complexes of metal may dissociate. In this case, the metal uptake by the organism is controlled by the dissociation kinetic of complexes and the diffusion of species in the medium (**figure 6.3 b)**). The limits of these models and the possibility of a diffusion as a dissociation limitation of the metal were treated theoretically in a study comparing the diffusion and the uptake fluxes under different conditions.[21] It was shown that, in case of an internalization limitation, the uptake is controlled by the diffusion (labile form) or by dissociation (partially labile or inert system) of complexes.

To mention just a few experimental examples, total silver concentration rather than free silver ion concentration was found to control silver uptake by *Chlamydamonas reinhardtii*, since this metal has a very fast uptake rate compared to the diffusion of metal to the cell.[22] Other study shows a similar conclusion: bioaccumulation of copper in periphyton was controlled by weakly complexed copper; in contrast, uptake of zinc was apparently controlled by free zinc concentration.[23] The uptake of cadmium by zebra mussel, *D. polymorpha*, in presence of humic acid was higher than expected on the basis of free cadmium[24]. Uptakes of cadmium by common carp, *Cyprinus carpio*, in presence of citrate, glycine and histidine were not solely a function of the free cadmium

concentration; in contrast, bioaccumulations of cadmium in presence of EDTA or NTA and bioaccumulation of zinc in presence of any of these ligands, were function of the free metal in solution.[25]

In summary, the amount of metal uptake by an organism can be determined by a concentration ranging between the free and the total metal concentration. This depends on different parameters: such as the properties of the metal complexes (e.g. their facility of dissociation, called lability) and relative rates of cellular uptake and diffusion of metal species. The followings sections are devoted to the definition and implication of the dynamical aspects of the metals complexes such as lability.
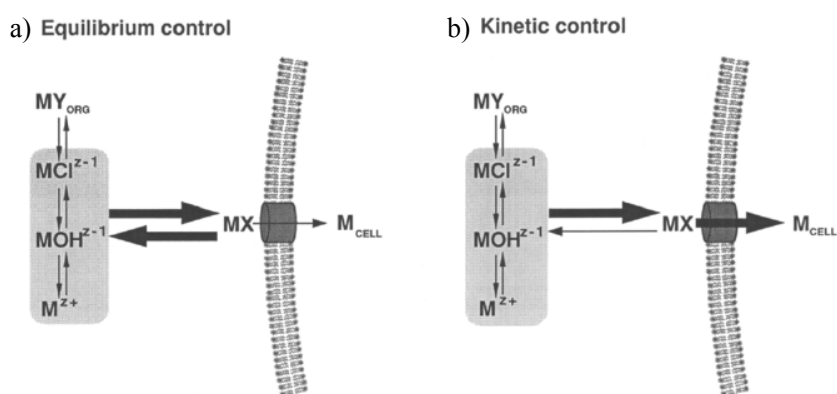
Figure 6.3. Two limiting cases for control of metal binding to transporters. (a) Equilibrium control as assumed in the free ion model. (b) Kinetic control. The width of the arrows for the formation and dissociation reactions of the MX complex and for the internalization step indicate the relative magnitude of the rates.[17]

6.2 Definition of lability of a metal complex

When the transport of the metal from bulk solution to the membrane surface is slow compared to the internalization of the metal through the membrane (**figure 6.3 b)**), the consumption of metal species at the membrane induces mass transport of metal species from the bulk to the surface active site. Thus, the understanding of dynamic bioavailability of metal species requires consideration of the overall flux towards the surface of the organism, as arising from the coupled diffusion and formation / dissociation involving the various metal species in the medium.

If the medium contains the metal in its free form (M), as well as in a complex form (ML), the question is to what extent and under which conditions the complex species ML may contribute to the uptake process via dissociation into free M. In a system where M is depleted at a consuming interface (e.g. a bioanalogical dynamic sensor or the plasma membrane of a organism), a gradient of metal concentration is developed in the diffusion layer (see **figure 6.4**) where concentrations of species are controlled by diffusion.
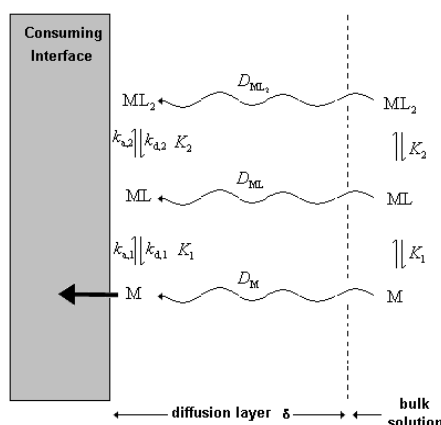
Figure 6.4. Schematic representation of reaction-diffusion processes of successive metal complexes ML$_n$, at a consuming interface. D_i = diffusion coefficient of species i. K_n, $k_{a,n}$, $k_{d,n}$ are respectively the equilibrium constant, formation and dissociation rate constants of ML$_n$.

The complex ML is defined as labile if the dissociation process reaches the equilibrium at all distances from the consuming interface (in the diffusion layer, see **figure 6.5a)**). In other words, if the kinetic dissociation rate of ML is faster than its diffusion, the kinetic limitations vanish and the system is controlled only by diffusion. The flux of metal "seen" by the sensor (or the microorganism) is related to the free and metal complex concentrations.

On the other hand, if the complex does not dissociate, the system is inert and the flux of metal is directly related to the free metal concentration (see **figure 6.5c)**). In this case, the kinetic dissociation of ML is slower than its diffusion, the system is controlled by kinetics and, therefore the complex is inert. The thermodynamic equilibrium relationship is not fulfilled throughout the diffusion layer.

Metal complexes presenting an intermediate behaviour between labile and inert are called partially labile complexes (see **figure 6.5b)**)

The diffusion layer thickness has an important role in the complex lability, since the maximum flux of diffusion is proportional to the concentration gradient in the diffusion layer, which decrease when the thickness of this layer increase. That is, the larger the diffusion layer thickness, the greater the time scale on which complex dissociation may occur.
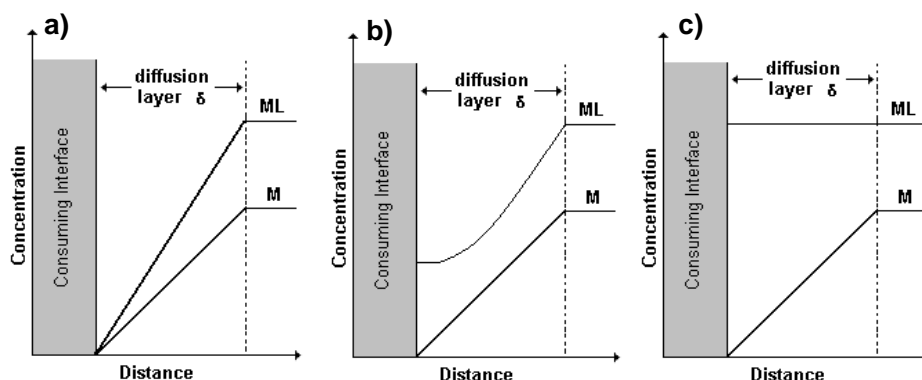
Figure 6.5. Schematic representation of the concentration gradients of M and ML in the diffusion layer, a) labile complex, b) partially labile complex and c) inert complex

6.3 Lability criterion and lability degree

The lability parameter L[26,27] (see **figure 6.6**) is used to describe the contribution of metal species to the overall flux towards a consuming interface based on the comparison of the maximum kinetic (dissociation) and diffusive (mass transport) fluxes. Two extreme conditions can be described:[28](i) Complex species do not have time to dissociate / associate in the diffusion layer due to the slowness of the kinetic process and will not contribute to the flux (static system). (ii) The rates of metal complex association / dissociation are high enough, so that the kinetic flux arising from dissociation of the complex into metal in the diffusion layer is greater than the diffusion-limited flux, therefore, the complex species dissociate / associate in the diffusion layer (dynamic system). In this case, the lability parameter L can be defined as the ratio between J_{kin} and J_{dif}. J_{kin} is the maximum complex contribution to the metal flux:

$$J_{kin} = k_d c_{ML}^* \mu \tag{6.5}$$

where c_{ML}^* is the complex concentration present in solution, k_d is the dissociation constant and μ is the classical definition of a reaction layer developed by Koutecky,[29]

$$\mu = \sqrt{\frac{D_M}{k_a c_L^*}} \tag{6.6}$$

where D_M represents the diffusion coefficient of the metal, c_L^* is the ligand concentration present in solution and k_a is the association constant.

J_{dif} is the maximum diffusive flux:

$$J_{dif} = D_{ML} \frac{c_{ML}^*}{\delta} \tag{6.7}$$

where D_{ML} represents the diffusion coefficient of the complex and δ is the diffusion layer.

The parameter L allows the identification of the rate limiting step. Two situations are possible (a) The kinetic flux (J_{kin}) is much larger than the diffusive one (J_{dif}), so that the total metal concentration will contribute to the flux (labile system $L \gg 1$). (b) The kinetic flux is lower than the diffusive one. In this case the measured signal will be influenced by kinetic characteristics (non labile complexes $L \ll 1$).
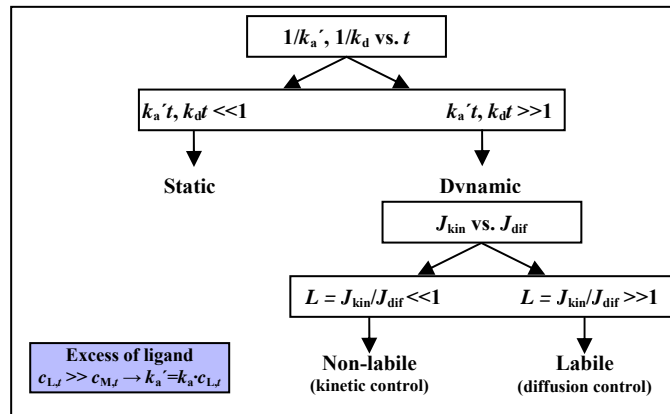
Figure 6.6. Lability parameter L. $c_{L,t}$ and $c_{M,t}$ are the ligand and metal concentrations, respectively, t is the time scale of the technique.

The lability criterion is an inequality, it cannot describe quantitatively the partially labile cases. Thus, in order to quantify the contribution of the complex, the lability degree, ξ, is defined as the fraction of the actual contribution with respect to the maximum contribution[30-33]:

$$\xi = \frac{J_M - J_{free}}{J_{labile} - J_{free}} \tag{6.8}$$

where, J_M is the metal flux arriving to the interface, J_{free} is the diffusional transport of the free M present in the system and J_{labile} is the metal flux arising to the system if all of the complexes are labile (i.e. $J_{labile} = J_{free} + J_{dif}$). If the complex is completely labile, the lability is equal to 1 and if the complex is inert, the lability degree is equal to 0. A partially labile complex has a lability degree between 0 and 1.

6.4 Amount of metal uptake by the organism

In order to summarize in a simple, visual way, the relationship between lability and bioavailability, the above explanations are regrouped in this section in the form of a scheme (**figure 6.7**).

When the metal transport in solution is considered faster than the cellular metal uptake, meaning that the limiting step is the internalization of the metal by the organism, the metal is not depleted at the membrane surface. In these conditions, the ion activity models (FIAM and BLM) can be applied and the biological effect is directly dependent on free metal present in solution.

If the internalization of metal by the cell is rapid compared to the transport of the metal from bulk solution to the cell surface, meaning that the internalization is not the limiting step, the metal is depleted at the cell interface. In this case, the ion activity models (FIAM and BLM) may not be applied and the amount of metal uptake by the organism depends on the facility of dissociation and diffusion of the metallic complexes present in solution. When the dissociation of the complexes is slower than its diffusion, the complexes are inert (their lability degree is 0) and the flux of metal received by the organism cell is directly related to the free metal concentration. When the dissociation of the complexes is faster than its diffusion, the complexes are labile (the lability degree of the complexes is 1) and the flux of metal "seen" by the organism cell is related to the total metal concentration (free metal plus metallic complexes). If the

dissociation rate of the complexes is in the same order as its diffusion, the complexes are partially labile (the lability degree of complexes is between 0 and 1) and the flux of metal received by the organism is between the fluxes in the two previous limiting cases.
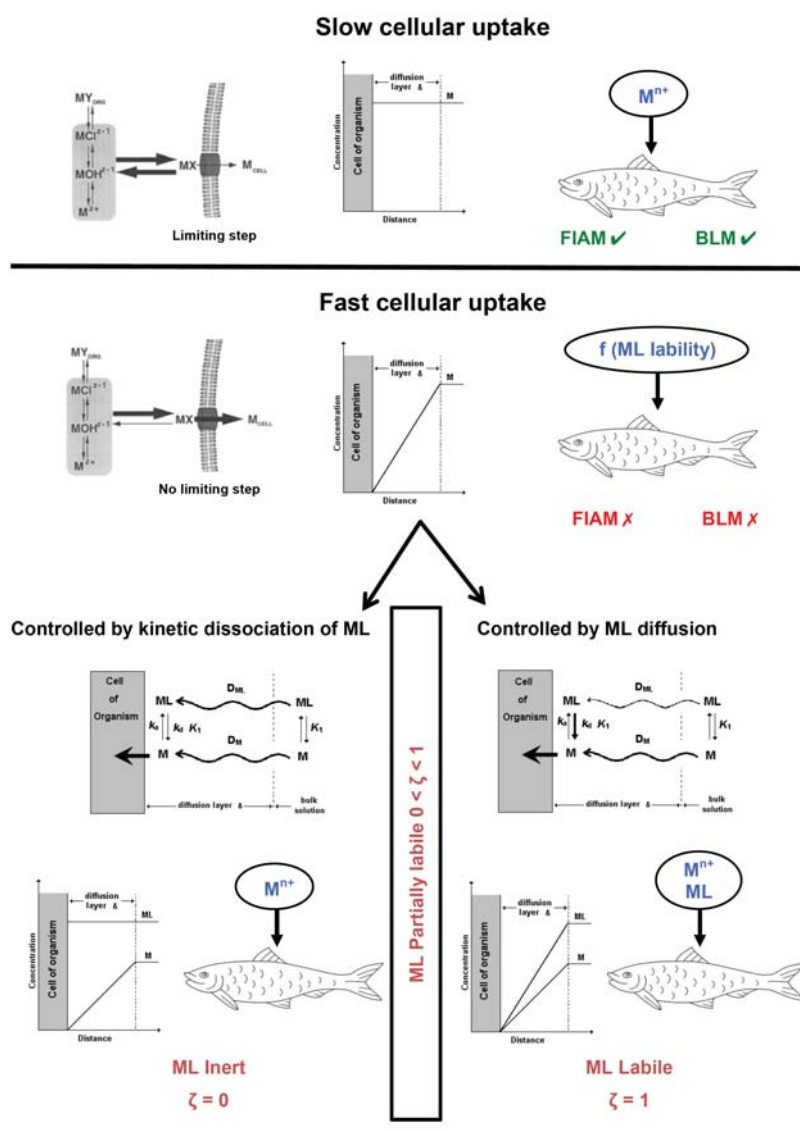
Figure 6.7. Amount of metal uptake by an organism depending on the cellular uptake rate and the properties of metallic complexes present in the system (see the text for explanation)

6.5 Dynamic sensors

A dynamic analytical sensor is composed by a binding metal layer, that can be of different types (for example, a mercury amalgam in voltammetry, a complexing solution in PLM, or a binding resin layer in DGT, see below). This binding layer generates a flux of metal, and therefore a gradient of metal concentration is developed in the surrounding layer (diffusive layer). The metal consumption by the binding material disturbs the distribution of metal species in the diffusion layer. Therefore, the amount of metal measured is not only due to the free metal but also to the metal originated by the dissociation of the existing metal complexes. The amount resulting from the complexes depends on the properties of the complexes themselves, but also on the characteristics of the sensors. The larger the thickness of the diffusion layer is, the more time the complex has to dissociate. As this time increases, so does the contribution of the metal complex to the overall metal flux received by the sensor.

A dynamic sensor is characterized by its (i) "response time", and its (ii) accumulation time, i.e., the time period over which pollutant species are accumulated in (loaded onto) the sensor prior to quantification. The signal resulting from the accumulation step represents an integration of all fluctuations in the test medium and thus provides an average value for this time period.

Depending on the mode of employment of sensors, they may work on either dynamic or equilibrium regimes (e.g. PLM). These techniques are briefly described below. All the techniques presented here are deployable *in situ,* which is a major advantage over sampling-based, sequential step "kinetic speciation schemes".[34]

6.5.1 Stripping voltammetry

Stripping voltammetry is a voltammetric technique that includes a preconcentration step. The instrumentation consists of a voltammetric analyser, a three-electrode cell (working, reference and counter electrodes) and a computer for the automation of the measurement and the data acquisition. Generally, the working electrode is a mercury electrode, of which two types are most commonly used: Handing Drop Mercury Electrode (HDME) and Thin Mercury Film Electrode (TMFE).[35] The advantage of HDME is it reliability, while TMFE offers increased sensitivity due to the concentration of metals into a smaller volume of mercury film. TMFE, however, is subject to interferences

due to surfactants collected on the electrode surface, while HDME is less affected by this problem, because a new drop is used for each assay.

A stripping experiment is composed of three important steps:

- Deposition or preconcentration

- Equilibration time

- Stripping

In the deposition step, the potential applied to the mercury electrode is usually kept constant at a value where metallic cations are reduced to metal during a determined time period and form a metal amalgam with the mercury electrode. Amalgamation allows to concentrate the metal in the mercury electrode (consequently, the deposition step is often called preconcentration or accumulation step). After the deposition, the stirring is stopped, and the system is allowed to reach equilibrium typically during $10 - 15$ s, which is called the equilibration time. The stripping step allows to quantify the accumulated metal, as the magnitude of the signal is proportional to the concentration of the analyte accumulated in the mercury electrode. Since the concentration of the analyte in the electrode is related to its concentration in solution, the stripping signal is therefore a function of the solution concentration.

From the early 1970's the voltammetric techniques based on preconcentration at the electrode have been widely applied to metal ion determination in environmental waters, because of their sensitivity, low detection limit (10^{-10} – 10^{-12} M), multi-element capacity and the absence of sample pretreatment.[35] These techniques can be used for metals that can be reduced at the mercury electrode, such as copper, lead, cadmium and zinc.

The consumption of the metal at the electrode produces a metal flux, which induces the formation of a diffusion layer where the metal-ligand equilibrium is disturbed. Many efforts have been devoted to model the data with the integration of this phenomenon and the contribution of the metal dissociated from the complex in the diffusion layer to the overall signal measured. However, the interpretation of titration curves in terms of complexation may be very difficult.[36]

Different stripping methods may be used to quantify the metal accumulated in the mercury. For instance, a scanning potential can be applied so that the metal present in form of amalgam in the mercury is oxidized back to cations in

solution while the current signal is measured. This method is called Anodic Stripping Voltammetry (ASV). ASV can be used for metals soluble in mercury (such as Pb, Cd, Cu, Zn[37]). Many other metals and other types of compounds can be determined by Adsorptive Cathodic Stripping Voltammetry (ACSV). Compared to ASV, it involves a preconcentration by adsorption at the electrode surface through the addition of a suitable compound. Detection limits comparable to those obtained in ASV can be achieved by ACSV.

Another stripping method, involving a constant oxidising current (or a constant flux of some chemical oxidant) as stripping step is the Stripping ChronoPotentiometry (SCP), which has also been widely used recently.[38-40] In this case, the analytical signal is the time required for the reoxidation, or transition time.[38] Whereas in most stripping techniques there is incomplete depletion of deposited metal from the electrode during the stripping step, in SCP full depletion is obtained when a low oxidizing current is applied. Thereby, depletive SCP is less susceptible than ASV to interference from adsorption of components on the working electrode surface.[39,41]

6.5.2 Permeation Liquid Membrane (PLM)

In this technique, a water-immiscible organic solvent, containing a carrier ligand, C (which is selective for the target metal, M) is embedded in a porous hydrophobic membrane sandwiched between two aqueous phases: the sample source solution on one side, and the receiving (strip or acceptor) solution on the other into which the target metal is trapped by a complexing agent (**figure 6.8**).[42]

The PLM principle has been widely used for industrial application (e.g. in food, pharmaceutical, clinical and environmental fields) and much less for analytical applications.[42] Nevertheless, this technique has powerful capabilities for analytical separation and preconcentration of trace metal ions in biological and environmental samples prior to their determination by sensitive instrumental methods such as atomic adsorption spectrometry, ICP-MS, ICP-OES, fluorimetry, etc.

In PLM, the species separation is based on liquid / liquid partition: $A^{n-} + M^{n+}_{aq} + C_{org} \rightleftharpoons AMC_{org}$ (where A^{n-} is a counterion). The flux of metal across the membrane is evaluated from the variation of the metal concentration in the strip solution as a function of time.[42] This flux depends on the thermodynamic stability constant of the carrier – metal complex, on the

diffusion across the membrane and on the thermodynamic and kinetic properties of both the source and the strip solutions. The flux, and thus the nature of the test species measured, can be varied by manipulation of these diffusion-controlling steps. If the diffusion in the source solution is rate limiting, free metal and metal dissociated from the complex are determined. It is said that the complex is labile. If diffusion across the membrane is governing the flux, then only the free metal is measured, and it is said that the complex is inert. The rate-controlling step can be tuned by varying the membrane thickness (diffusion layer of the membrane δ) and the carrier ligand concentration.[43-45] Since 1994, Buffle and co-workers have largely developed PLM using hollow fibre devices in a miniaturized version[46] with the aim to improve the preconcentration factor.

In addition to its dynamic flux mode, PLM can also be used to determine the free metal ion concentration after equilibrium is reached in the whole system, as in the Donnan Membrane Technique (DMT)[47].
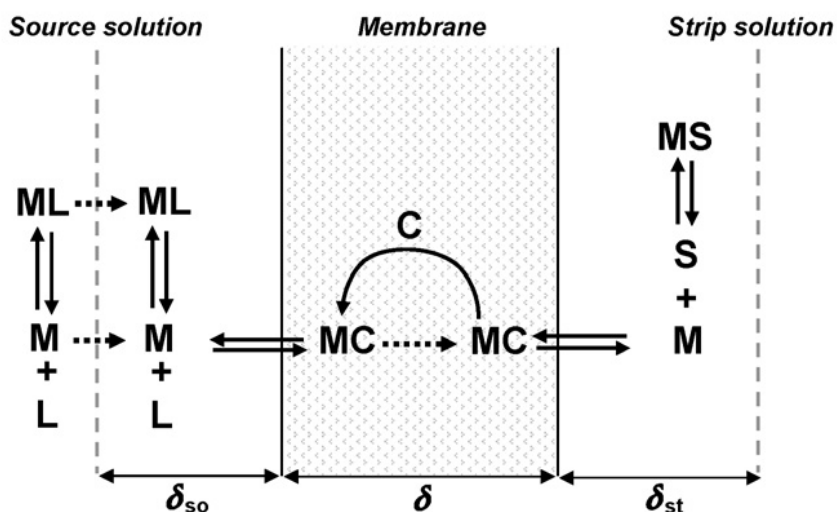
Figure 6.8. Schematic representation of the transfer of metal ion, M, through a PLM, in the presence of a ligand (L). C, carrier; S, complexant of the strip solution; δ$_{so}$, δ$_{st}$, diffusion layer thickness in the source and strip solutions; δ, diffusion layer of the membrane.[48]

6.5.3 Diffusive Gradients in Thin films (DGT)

In the 90's decade, Davison and Zhang[49,50] developed this technique that allows to measure an "effective" concentration higher than the free metal concentration since metal coming from complex dissociation is also accumulated in the DGT resin layer. A large number of scientific articles have been published reporting DGT applications and developments. The technique has been applied on almost every continent by researchers from all over the world. The DGT technique was developed for *in situ* measurement of labile trace metal in aquatic environments, and therefore is referred to as a dynamic speciation technique.[51] DGT sampling has been applied to waters (e.g. [49]), sediment (e.g. [52]) and soils (e.g. [53]).

In the early stage of DGT development the technique was first characterised for Ni, Zn, Mn, Fe, Cu and Cd measurement[49]. Later Garmo et al.[54] evaluated the Chelex for 55 elements and concluded it useful for measurement of the following 24: Pb, Zn, Co, Ni, Cu, Cd, Al, Mn, Ga, La, Ce, Pr, Nd, Sm, Eu, Gd, Tb, Dy, Ho, Er, Tm, Tb, Lu and Y. By modification on the binding layer the DGT has been further developed for other elements. For example, by exchange of the Chelex for synthetic ferrhydrite (an ion oxyhydroxide), the DGT was characterised for determination of labile anionic phosphate[55] and in later years to inorganic As.[56] Recently, full characterisation was reported for the measurement of As(V), V(V), Se(VI), Mo(VI), W(V) and Sb(V).[57,58] Futhermore, TEVA and Dowex anion exchange resins have been used for determination of Tc[59] and U[60], respectively, and thiol resin to determine labile Hg[61] and methyl-Hg[62] concentrations.

As an *in situ* separation technique, DGT has the advantage to minimise speciation changes during sampling and storage.[63] Further benefits are that the sampling device is simple to use and relatively inexpensive since the user does not need any costly equipment and the sample can be send to commercial laboratories to analysis.

6.5.3.1 Principles of the technique

The DGT is composed of three layers (see **figure 6.9**): 1) a binding-impregnated hydrogel layer (or resin layer, e.g. Chelex), 2) a hydrogel as a diffusion layer, and 3) a membrane filter. These three layers are mounted in a plastic sampling device with an opening exposed to the sampling medium.[49] The hydrogels consist of a hydrophilic network consisting of acrylamide-polymer chains,

linked with agarose cross-linkers. The diffusive gel allows the diffusion of the species. The membrane filter (pore size 0.45 μm) protects the hydrogel surface.

Analytes in the sampling medium diffuse through the membrane filter and hydrogel to finally accumulate in the binding layer. Thereby a concentration gradient is developed in the diffusion layer. The concentration gradient is maintained as long as the binding layer is not saturated. The flux, J, through the diffusive layer, can be described by Fick's first law of diffusion:

$$J = D\frac{dc}{dx}$$

(6.9)

where D is the diffusion coefficient, c is the concentration and x the distance (and dc/dx the concentration gradient).
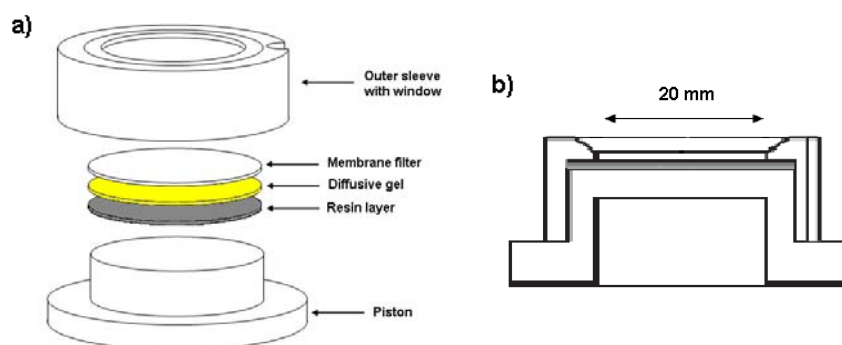
Figure 6.9. Scheme of a DGT device a) in 3D, b) in cross section

The DGT device is exposed to the target solution for a known time, t. After retrieval, the DGT is opened and the analytes are desorbed/eluted from the binding layer followed by determination using a suitable analytical technique. For the normal Chelex-DGT, nitric acid is recommended as eluent. Various concentrations and volumes have been tried resulting in different elution efficiencies, f_e, which has to be taken into account in the calculations of the number of moles of metal accumulated by the sensor, n:

$$n = \frac{c_e\left(V_e + V_r\right)}{f_e}$$

(6.10)

where c_e is the concentration of the analyte in the eluate, V_e is the volume of eluent and V_r, the volume of the binding layer hydrogel.

Knowing the accumulated moles and diffusion coefficient of the analyte, as well as the deployment time and temperature, the average concentration during the time of exposure can be calculated. DGT measurements generate time-weighted average concentrations during deployment time. Longer deployment times will improve the detection limit since greater analyte amounts will be accumulated.

In principle, the DGT technique is quite simple, but the detailed interpretation of the results of DGT-based measurements is associated with a range of uncertainties and questions that need further investigation, as will be discussed in the following chapters.

6.6 Complex lability in a DGT sensor

In solution, the metal is in equilibrium with the complexes. It is generally considered that all complexes may diffuse through the diffusive gel, but only metal species can be bound by the resin hydrogel layer.

6.6.1 Labile complexes

When the amount of metal accumulated by the DGT corresponds to the total metal concentration present in solution, the complex is "seen" as labile by the DGT sensor. This occurs when the rate of complex dissociation is faster than its diffusion through the hydrogel thickness. The complex is in equilibrium with the metal throughout the diffusive layer. During the diffusion through the diffusive layer, the complex has time to dissociate and it arrives at the resin as dissociated, so its concentration at the binding resin interface is zero ($c_{ML}^r = 0$), see **figure 6.10**, therefore, the lability degree of the complex, ξ, is equal to 1. This is the case of the majority of inorganic complexes (e.g. carbonate, hydroxide, chloride), and a few organic complexes, as citrate.[64,65]

6.6.2 Inert complexes

In this case, the amount of metal accumulated by the DGT corresponds to the free metal concentration present in solution. Opposite to the labile case, the complex is "seen" as inert by the DGT. This happens when the dissociation rate of complex is so slow that the complex does not have time to dissociate throughout its diffusion from bulk solution to the resin binding layer. The

equilibrium between complex and metal is not fu.lfilled throughout the diffusive layer. The complex diffuses through the diffusive layer and arrives at the resin in its undissociated form ($c_{ML}^{r} = c_{ML}^{*}$, where * labels the concentration value of species i at the bulk solution), see **figure 6.10**, therefore, the lability degree of complex, ξ, is equal to 0. It is the case of very stable complexes as EDTA complexes.[65,66]

6.6.3 Partially labile complexes

In this case, the amount of metal accumulated by the DGT is higher than the amount corresponding to the free metal and smaller than the amount corresponding to the total metal concentration. The complex is "seen" as partially labile by the DGT sensor, and it has an intermediate behaviour between the two above mentioned cases: the equilibrium between complex and free metal is fulfilled in part of the diffusive domain. The complex concentration at the resin surface is lower than its bulk concentration but nonzero ($0 < c_{ML}^{r} < c_{ML}^{*}$), see **figure 6.10**, therefore, the lability degree of complex, ξ, ranges between 0 and 1. The amount of metal accumulated by the DGT comes from the free metal and a part of complex that it is able to dissociate. This is the case of complexes with humic[66] and fulvic[67] acids.
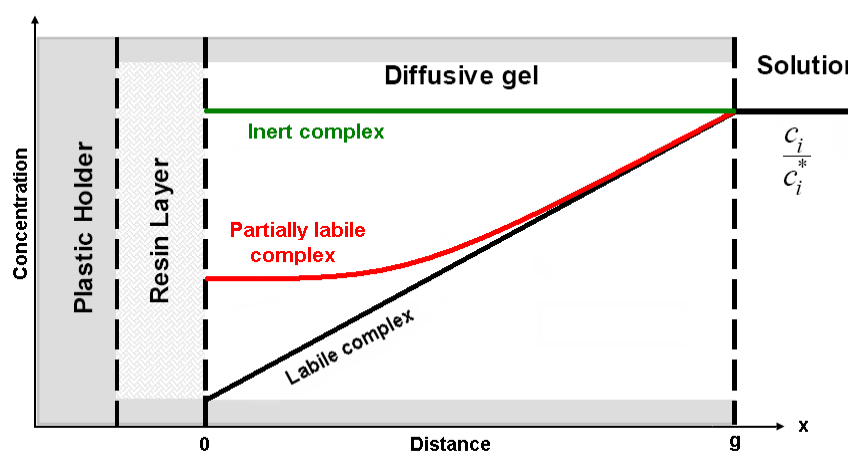
Figure 6.10. Representation of the concentration of labile, partially and inert complexed metal species in a DGT device and adjacent water during the deployment

6.7 Calculation of the lability degree of a complex from DGT measurements

The deployment of DGT in a solution of known composition, allows the calculation of the lability degree of a complex. Lets us consider, the complexation of a metal M with a ligand L according to the scheme:

$$M + L \underset{k_d}{\overset{k_a}{\rightleftharpoons}} ML \tag{6.11}$$

where k_a and k_d are, respectively, the association and dissociation kinetic constants, and the corresponding equilibrium constant is:

$$K = \frac{k_a}{k_d} = \frac{c_{ML}^*}{c_M^* \, c_L^*} \tag{6.12}$$

Balance equations for the different species at any point of the diffusive gel are given by the second Fick's law as[65,68,69]:

$$\begin{cases} \dfrac{\partial c_M}{\partial t} = D_M \dfrac{\partial^2 c_M}{\partial x^2} + k_d c_{ML} - k_a c_M c_L \\[2mm] \dfrac{\partial c_L}{\partial t} = D_L \dfrac{\partial^2 c_L}{\partial x^2} + k_d c_{ML} - k_a c_M c_L \\[2mm] \dfrac{\partial c_{ML}}{\partial t} = D_{ML} \dfrac{\partial^2 c_{ML}}{\partial x^2} - k_d c_{ML} + k_a c_M c_L \end{cases} \tag{6.13}$$

where D_M, D_L and D_{ML} are the diffusion coefficients in the diffusive gel layer of metal, ligand and complex respectively.

In steady state, the moles of metal accumulated by the DGT may be calculated as:

$$n = \left[\frac{D_M \, c_M^*}{g} + D_{ML} \left(\frac{c_{ML}^* - c_{ML}^r}{g} \right) \right] A \times t \tag{6.14}$$

where g is the thickness of the diffusion domain (see **figure 6.10**), A the area of the DGT window (see **figure 6.9**) and t, the deployment time.

Equation 6.14 can be written in terms of the lability degree as:

$$n = \left[\frac{D_{\mathrm{M}} \, c_{\mathrm{M}}^{*}}{g} + \xi \, \frac{D_{\mathrm{ML}} \, c_{\mathrm{ML}}^{*}}{g} \right] A \times t \tag{6.15}$$

From the above equation, knowing the concentration of the species in bulk solution and the diffusion coefficient of metal and complex in the diffusive gel, the lability degree of complex can be calculated. This value allows the calculation of the kinetic constants of the complex (k_{a} and k_{d}) through **equation 6.17** below.

6.8 Prediction of the lability degree of a complex in a DGT sensor

For a given complex, the calculation of the lability degree allows to know if the DGT sees the complex as labile, inert or partially labile. The lability degree depends on the value of the complex concentration at the resin surface. This problem is formally analogous to what can be formulated in a planar electrode. As a first approximation, the equations derived for planar electrodes can be used to DGT.

Considering that the ligand concentration present in the system is in excess with respect to the metal ($c_{\mathrm{L}} = c_{\mathrm{L}}^{*}$), the system of **equations 6.13** can be uncoupled and solved analytically. The concentration profiles may be calculated in the domain of diffusion solving the corresponding system. Following the usual boundary conditions of voltammetric electrodes, the penetration of the complex into the resin layer will not be allowed being the metal the only one species consumed at the resin surface[68]:

$$\text{For } x = r \quad \rightarrow \quad c_{\mathrm{M}} = 0 \quad \text{and} \quad \left(\frac{dc_{\mathrm{ML}}}{dz} \right)_{z=r} = 0$$

$$\text{For } x = g \quad \rightarrow \quad c_{\mathrm{M}} = c_{\mathrm{M}}^{*} \quad \text{and} \quad c_{\mathrm{ML}} = c_{\mathrm{ML}}^{*} \tag{6.16}$$

Under these conditions, the rigorous solution of the lability degree is[68]:

$$\xi = 1 - \frac{1 + \dfrac{D_{ML}}{D_M} K\, c_L^*}{\dfrac{D_{ML}}{D_M} K\, c_L^* + \dfrac{g}{m}\coth\left[\dfrac{g}{m}\right]} \tag{6.17}$$

where:

$$m = \sqrt{\frac{D_{ML} D_M}{D_M k_d + D_{ML} k_a c_L^*}} \tag{6.18}$$

A key point in the derivation of this equation is the assumption that the penetration of metal complexes in the resin layer can be considered as negligible. This assumption will be tested in chapter 8, and compared with experimental data. The results will allow us to derive more accurate expressions for the complex lability measured by DGT.

6.9 References

(1)   Thibodeaux, L. J., *Environmental Chemodynamics*. Wiley Interscience: New York, **1996**.

(2)   Morel, F. M. M., *Principles of Aquatic Chemistry*. Wiley Interscience: New York, **1983**.

(3)   Pagenkopf, G. K., Gill surface interaction-model for trace-metal toxicity to fishes - Role of complexation, pH, and water hardness. *Environmental Science & Technology* **1983,** *17*, (6), 342-347.

(4)   Sunda, W. G.; Huntsman, S. A., Effect of competitive interactions between manganese and copper on cellular manganese and growth in estuarine and oceanic species of the diatom thalassiosira. *Limnology and Oceanography* **1983,** *28*, (5), 924-934.

(5)   Allen, H. E.; Hall, R. H.; Brisbin, T. D., Metal speciation - effects on aquatic toxicity. *Environmental Science & Technology* **1980,** *14*, (4), 441-443.

(6)   Anderson, M. A.; Morel, F. M. M.; Guillard, R. R. L., Growth limitation of a coastal diatom by low zinc ion activity. *Nature* **1978,** *276*, (5683), 70-71.

(7)   Campbell, P. G. C., Interactions between Trace Metal and Aquatic Organisms : A Critique of the Free-ion Activity Model. In *Metals Speciation and Bioavailability in Aquatic Systems*, Tessier, A.; Turner, D. R., Eds. John Wiley & Sons: Chichester, 1995.

(8)   Tessier, A.; Turner, D. R., *Metal speciation and bioavailability in aquatic systems*. Wiley: Chichester, **1995**.

(9)   Wilkinson, K. J.; Slaveykova, V. I.; Hassler, C. S.; Rossier, C., Physicochemical mechanisms of trace metal bioaccumulation by microorganisms. *Chimia* **2002,** *56*, (12), 681-684.

(10)   Campbell, P. G. C.; Errécalde, O.; Hiriart-Baer, P.; Vigneault, B., Metal bioavailability to phytoplakton-applicability of the biotic ligand model. *Comparative Biochemistry and Physiology Part C* **2002,** *133*, (1-2), 189-206.

(11)   Zitko, V., Structure - Activity relations and toxicity of trace elements to aquatic biota. In *Toxicity to Biota of Metal Forms in Natural Water*, Andrew, R. W.; Hodson, P. V.; Konasewic, D. E., Eds. Internat. Joint Commission, Great Lakes Research Advisory Board: Widsor, 1976.

(12)   Playle, R. C., Modelling metal interactions at fish gills. *Science of the total environment* **1998,** *219*, (2-3), 147-163.

(13)   Pagenkopf, G. K.; Russo, R. C.; Thurston, R. V., Effect of complexation on toxicity of copper to fishes. *Journal of the Fisheries Research Board of Canada* **1974,** *31*, (4), 462-465.

(14)   Di Toro, D. M.; Allen, H. E.; Bergman, H. L.; Meyer, J. S.; Paquin, P. R.; Santore, R. C., Biotic ligand model of the acute toxicity of metals. 1. Technical basis. *Environmental Toxicology and Chemistry* **2001,** *20*, (10), 2383-2396.

(15)   Paquin, P. R.; Gorsuch, J. W.; Apte, S.; Batley, G. E.; Bowles, K. C.; Campbell, P. G. C.; Delos, C. G.; Di Toro, D. M.; Dwyer, R. L.; Galvez, F.; Gensemer, R. W.; Goss, G. G.; Hogstrand, C.; Janssen, C. R.; McGeer, J. C.; Naddy, R. B.; Playle, R. C.; Santore, R. C.; Schneider, U.; Stubblefield, W. A.; Wood, C. M.; Wu, K. B., The biotic ligand model: a historical overview. *Comparative Biochemistry and Physiology C-Toxicology & Pharmacology* **2002,** *133*, (1-2), 3-35.

(16)   Bell, R. A.; Ogden, N.; Kramer, J. R., The biotic ligand model and a cellular approach to class B metal aquatic toxicity. *Comparative Biochemistry and Physiology C-Toxicology & Pharmacology* **2002,** *133*, (1-2), 175-188.

(17)   Hudson, R. J. M., Which aqueous species control the rates of trace metal uptake by aquatic biota? Observations and predictions of non-equilibrium effects. *Science of the total environment* **1998,** *219*, (2-3), 95-115.

(18)   Buffle, J.; Zhang, Z.; Startchev, K., Metal flux and dynamic speciation at (Bio)interfaces. part 1: Critical evaluation and compilation of physicochemical parameters for complexes with simple Ligands and Fulvic/Humic substances. *Environmental Science & Technology* **2007,** *41*, (22), 7609-7620.

(19)   Hudson, R. J. M.; Morel, F. M. M., Iron transport in marine-phytoplankton - kinetics of cellular and medium coordination reactions. *Limnology and Oceanography* **1990,** *35*, (5), 1002-1020.

(20)   Tran, D.; Boudou, A.; Massabuau, J. C., How water oxygenation level influences cadmium accumulation pattern in the asiatic clam Corbicula fluminea: A laboratory and field study. *Environmental Toxicology and Chemistry* **2001,** *20*, (9), 2073-2080.

(21)   Van Leeuwen, H. P., Metal speciation dynamics and bioavailability: Inert and labile complexes. *Environmental Science & Technology* **1999,** *33*, (21), 3743-3748.

(22)   Fortin, C.; Campbell, P. G. C., Silver uptake by the green alga Chlamydomonas reinhardtii in relation to chemical speciation: Influence of chloride. *Environmental Toxicology and Chemistry* **2000,** *19*, (11), 2769-2778.

(23)   Meylan, S.; Behra, R.; Sigg, L., Influence of metal speciation in natural freshwater on bioaccumulation of copper and zinc in periphyton: A microcosm study. *Environmental Science & Technology* **2004,** *38*, (11), 3104-3111.

(24)   Voets, J.; Bervoets, L.; Blust, R., Cadmium bioavailability and accumulation in the presence of humic acid to the zebra mussel, Dreissena polymorpha. *Environmental Science & Technology* **2004,** *38*, (4), 1003-1008.

(25)   van Ginneken, L.; Chowdhury, M. J.; Blust, R., Bioavailability of cadmium and zinc to the common carp, Cyprinus carpio, in complexing environments: A test for the validity of the free ion activity model. *Environmental Toxicology and Chemistry* **1999,** *18*, (10), 2295-2304.

(26)   Van Leeuwen, H. P., Dynamic aspects of in situ speciation processes and techniques. In *In situ Monitoring of Aquatic Systems*, Buffle, J.; Horvai, G., Eds. Wiley: Chichester, Chapter 8, pp. 253-277, 2000.

(27)   Van Leeuwen, H. P., Voltammetric titrations involving metal-complexes - effect of kinetics and diffusion-coefficients. *Science of the total environment* **1987,** *60*, 45-55.

(28)   Mota, A. M.; Pinheiro, J. P.; Simoes Gonçalves, M. L., Electrochemical Methods for Speciation of Trace Elements in Marine Waters. Dynamic Aspects. *The Journal of Physical Chemistry A* **2011**.

(29)   Koutechy, J.; Brdicka, R., Fundamental equation for the electrolytic current when depending on the formation rate of the depolariser jointly with diffusion and its polarographic verification. *Collection Czechoslovak Chemical Communication* **1947,** *12*, 337-355.

(30)   Galceran, J.; Van Leeuwen, H. P., Dynamic of Biouptake Processes: the Role of Transport, Adsorption and Internalization. In *Physicochemical kinetics and*

transport at chemical-biological surface, Van Leeuwen, H. P.; Köster, W., Eds. Wiley: Chichester, UK, Chapter 4, 2004.

(31)   Galceran, J.; Puy, J.; Salvador, J.; Cecilia, J.; van Leeuwen, H. P., Voltammetric lability of metal complexes at spherical microelectrodes with various radii. *Journal of Electroanalytical Chemistry* **2001,** *505*, (1-2), 85-94.

(32)   Galceran, J.; Puy, J.; Salvador, J.; Cecilia, J.; Mas, F.; Garces, J. L., Lability and mobility effects on mixtures of ligands under steady-state conditions. *Physical chemistry chemical physics* **2003,** *5*, (22), 5091-5100.

(33)   Pinheiro, J. P.; Galceran, J.; Van Leeuwen, H. P., Metal speciation dynamics and bioavailability: Bulk depletion effects. *Environmental Science & Technology* **2004,** *38*, (8), 2397-2405.

(34)   Chakrabarti, C. L.; Lu, Y. J.; Cheng, J. G.; Back, M. H.; Schroeder, W. H., Studies on metal speciation in the natural-environment. *Analytica Chimica Acta* **1993,** *276*, (1), 47-64.

(35)   Achterberg, E. P.; Braungardt, C., Stripping voltammetry for the determination of trace metal speciation and in-situ measurements of trace metal distributions in marine waters. *Analytica Chimica Acta* **1999,** *400*, 381-397.

(36)   Florence, T. M., Trace element speciation by anodic stripping voltammetry. *Analyst* **1992,** *117*, (3).

(37)   Chin, Y. P.; Aiken, G.; Oloughlin, E., Molecular-weight, polydispersity, and spectroscopic properties of aquatic humic substances. *Environmental Science & Technology* **1994,** *28*, (11), 1853-1858.

(38)   Town, R. M.; van Leeuwen, H. P., Fundamental features of metal ion determination by stripping chronopotentiometry. *Journal of Electroanalytical Chemistry* **2001,** *509*, (1), 58-65.

(39)   Town, R. M.; van Leeuwen, H. P., Effects of adsorption in stripping chronopotentiometric metal speciation analysis. *Journal of Electroanalytical Chemistry* **2002,** *523*, (1-2), 1-15.

(40)   van Leeuwen, H. P.; Town, R. M., Stripping chronopotentiometry at scanned deposition potential (SSCP). Part 1. Fundamental features. *Journal of Electroanalytical Chemistry* **2002,** *536*, (1-2), 129-140.

(41)   Daniele, S.; Bragato, C.; Baldo, M. A.; Wang, J.; Lu, J. M., The use of a remote stripping sensor for the determination of copper and mercury in the Lagoon of Venice. *Analyst* **2000,** *125*, (4), 731-735.

(42)   Buffle, J.; Parthasarathy, N.; Djane, N. K.; Matthiasson, L., Permeation liquid membranes for field analysis and speciation of trace coumpounds in waters. In *In situ Monitoring of Aquatic Systems; Chemistry of Environmental Systems*,

Buffle, J.; Horvai, G., Eds. John Wiley & Sons: Chichester, UK, Chapter 10, Vol. 6, pp. 407-493, 2000.

(43)   Salaun, P.; Bujard, F.; Berdondini, L.; Koudelka-Hep, M.; Buffle, J., Integrated microanalytical system coupling permeation liquid membrane and voltammetry for trace metal speciation. Technical description and optimization. *Electroanalysis* **2004,** *16*, (10), 811-820.

(44)   Slaveykova, V. I.; Parthasarathy, N.; Buffle, J.; Wilkinson, K. J., Permeation liquid membrane as a tool for monitoring bioavailable Pb in natural waters. *Science of the total environment* **2004,** *328*, (1-3), 55-68.

(45)   Tomaszewski, L.; Buffle, J.; Galceran, J., Theoretical and analytical characterization of a flow-through permeation liquid membrane with controlled flux for metal speciation measurements. *Analytical Chemistry* **2003,** *75*, (4), 893-900.

(46)   Parthasarathy, N.; Pelletier, M.; Tercier-Waeber, M. L.; Buffle, J., On-line coupling of flow through voltammetric microcell to hollow fiber permeation liquid membrane device for subnanomolar trace metal speciation measurements. *Electroanalysis* **2001,** *13*, (16), 1305-1314.

(47)   Temminghoff, E. J. M.; Plette, A. C. C.; Van Eck, R.; Van Riemsdijk, W. H., Determination of the chemical speciation of trace metals in aqueous systems by the Wageningen Donnan Membrane Technique. *Analytica Chimica Acta* **2000,** *417*, (2), 149-157.

(48)   Pesavento, M.; Alberti, G.; Biesuz, R., Analytical methods for determination of free metal ion concentration, labile species fraction and metal complexation capacity of environmental waters: A review. *Analytica Chimica Acta* **2009,** *631*, (2), 129-141.

(49)   Zhang, H.; Davison, W., Performance characteristics of diffusion gradients in thin films for the in situ mesurement of trace metals in aqueous solution. *Analytical Chemistry* **1995,** *67*, (19), 3391-3400.

(50)   Davison, W.; Zhang, H., In-situ speciation measurements of trace components in natural-waters using thin-film gels. *Nature* **1994,** *367*, (6463), 546-548.

(51)   Van Leeuwen, H. P.; Town, R.; Buffle, J.; Cleven, R.; Davison, W.; Puy, J.; Van Riemsdijk, W.; Sigg, L., Dynamic speciation analysis and bioavailabilty of metals in aquatic systems. *Environmental Science & Technology* **2005,** *39*, (22), 8545-8556.

(52)   Zhang, H.; Davison, W.; Miller, S.; Tych, W., In-Situ High-Resolution Measurements of Fluxes of Ni, Cu, Fe, and Mn and Concentrations of Zn and Cd in Porewaters by Dgt. *Geochimica Et Cosmochimica Acta* **1995,** *59*, (20), 4181-4192.

(53)   Zhang, H.; Zhao, F. J.; Sun, B.; Davison, W.; McGrath, S. P., A new method to measure effective soil solution concentration predicts copper availability to plants. *Environmental Science & Technology* **2001,** *35*, (12), 2602-2607.

(54)   Garmo, O. A.; Royset, O.; Steinnes, E.; Flaten, T. P., Performance study of diffusive gradients in thin films for 55 elements. *Analytical Chemistry* **2003,** *75*, (14), 3573-3580.

(55)   Zhang, H.; Davison, W.; Gadi, R.; Kobayashi, T., In situ measurement of dissolved phosphorus in natural water using DGT. *Analytica Chimica Acta* **1998,** *370*, (1), 29-38.

(56)   Panther, J. G.; Stillwell, K. P.; Powell, K. J.; Downard, A. J., Development and application of the diffusive gradients in thin films technique for the measurement of total dissolved inorganic arsenic in waters. *Analytica Chimica Acta* **2008,** *622*, (1-2), 133-142.

(57)   Luo, J.; Zhang, H.; Santner, J.; Davison, W., Performance Characteristics of Diffusive Gradients in Thin Films Equipped with a Binding Gel Layer Containing Precipitated Ferrihydrite for Measuring Arsenic(V), Selenium(VI), Vanadium(V), and Antimony(V). *Analytical Chemistry* **2010,** *82*, (21), 8903-8909.

(58)   Osterlund, H.; Chlot, S.; Faarinen, M.; Widerlund, A.; Rodushkin, I.; Ingri, J.; Baxter, D. C., Simultaneous measurements of As, Mo, Sb, V and W using a ferrihydrite diffusive gradients in thin films (DGT) device. *Analytica Chimica Acta* **2010,** *682*, (1-2), 59-65.

(59)   French, M. A.; Zhang, H.; Pates, J. M.; Bryan, S. E.; Wilson, R. C., Development and performance of the diffusive gradients in thin-films technique for the measurement of Technetium-99 in seawater. *Analytical Chemistry* **2005,** *77*, (1), 135-139.

(60)   Li, W.; Li, C.; Zhao, J.; Cornett, R. J., Diffusive gradients in thin films technique for uranium measurements in river water. *Analytica Chimica Acta* **2007,** *592*, (1), 106-113.

(61)   Docekalova, H.; Divis, P., Application of diffusive gradient in thin films technique (DGT) to measurement of mercury in aquatic systems. *Talanta* **2005,** *65*, (5), 1174-1178.

(62)   Clarisse, O.; Hintelmann, H., Measurements of dissolved methylmercury in natural waters using diffusive gradients in thin film (DGT). *Journal of Environmental Monitoring* **2006,** *8*, (12), 1242-1247.

(63)   Lead, J. R.; Davison, W.; Hamilton-Taylor, J.; Buffle, J., Characterizing Colloidal Material in Natural Waters. *Aquatic Geochemistry* **1997,** *3*, (3), 213-232.

(64)   Gimpel, J.; Zhang, H.; Hutchinson, W.; Davison, W., Effect of solution composition, flow and deployment time on the measurement of trace metals by the

diffusive gradient in thin films technique. *Analytica Chimica Acta* **2001,** *448*, (1-2), 93-103.

(65)   Tusseau-Vuillemin, M. H.; Gilbin, R.; Taillefert, M., A dynamic numerical model to characterize labile metal complexes collected with diffusion gradient in thin films devices. *Environmental Science & Technology* **2003,** *37*, (8), 1645-1652.

(66)   Ferreira, D.; Tousset, N.; Ridame, C.; Tusseau-Vuillemin, M. H., More than inorganic copper is bioavailable to aquatic mosses at environmentally relevant concentrations. *Environmental Toxicology and Chemistry* **2008,** *27*, (10), 2108-2116.

(67)   Unsworth, E. R.; Zhang, H.; Davison, W., Use of diffusive gradients in thin films to measure cadmium speciation in solutions with synthetic and natural ligands: Comparison with model predictions. *Environmental Science & Technology* **2005,** *39*, (2), 624-630.

(68)   Salvador, J.; Puy, J.; Cecilia, J.; Galceran, J., Lability of complexes in steady-state finite planar diffusion. *Journal of Electroanalytical Chemistry* **2006,** *588*, (2), 303-313.

(69)   Lehto, N. J.; Davison, W.; Zhang, H.; Tych, W., An evaluation of DGT performance using a dynamic numerical model. *Environmental Science & Technology* **2006,** *40*, (20), 6368-6376.

CHAPTER 7

EXPERIMENTAL SECTION

DIFFUSIVE GRADIENTS IN THIN FILMS (DGT)

Different factors may affect precision and accuracy of DGT measurements. When the study is realized in laboratory, some of these factors (as the stirring, the temperature and pH variations during the deployment) can be controlled by an appropriate experimental design. To reduce the uncertainty in other factors, different experiments were carried out to determine with greater accuracy some parameters of DGT sensors, such as the volume of the resin gel, the thickness of the diffusion layer, the diffusion coefficient of the metal species, the elution factor and the diffusive boundary layer.

7.1 Experimental design

7.1.1 DGT sensors

The regular DGT deployment mouldings made of polyethylene (2 cm diameter window), the diffusive gels (regular type: agarose polyacrylamide gel) and Chelex gels were purchased from DGT Research Ldt. (Lancaster, UK, http://www.dgtresearch.com). Cellulose nitrate membrane filter were purchased from Whatman® (pore size 0.45 μm, thickness 0.125 mm). Chelex is a trade name of the iminodiacetate chelating resin produced by Bio-Rad.[1]

The mounting of the sensor, following the scheme presented in the previous section (see **figure 6.8**), was realized in our lab: the Chelex-gel of 0.4 mm thickness was placed on the piston surface with the resin beads facing upward, on top of the Chelex-gel, it was placed the diffusive gel (0.8 mm of thickness), followed by the filter membrane.

7.1.2 DGT exposure chamber

A cylindrical 5 L polyethylene bucket was used as the exposure chamber. A large volume of exposition solution was used to ensure that the depletion of metal was negligible during the deployment (see **figure 7.1**).

7.1.2.1 Stirring

The stirring is very important during DGT deployment. Reproducibility may be greatly compromised if the stirring is not the same for all the sensors. Indeed, differences between renewal of the solution on the surface of the DGT may change the thickness of the diffusive boundary layer from one sensor to another. To overcome this problem, it is important to use a circular exposure chamber for

the deployment of sensors with a centred homogeneous agitation. In our exposure chamber, the solution was stirred using an overhead stirrer.

7.1.2.2 pH measurement

The pH of solution was adjusted with nitric acid or sodium hydroxide to the desired pH. The pH was monitored during all the experiment and readjustment was made if it was necessary. Keeping a constant pH during all the experiment is very important, because small variations of pH can cause dramatic changes in the lability of complexes. In our exposure chamber, the pH was continuously monitored with a glass electrode connected to an Orion Research Ionanalyzer 720A potentiometer and to a computer by means of a homemade data acquisition program (courtesy of Dr. Calin David).

7.1.2.3 Temperature control

The diffusive coefficients and kinetic parameters are dependent on temperature. In order to avoid errors by temperature changes, the temperature was kept constant during each experiment, by placing the exposure chamber in a thermostat bath. All the experiments were performed at 25 ± 0.1 ºC.

Figure 7.1. DGT exposure chamber

7.1.3 DGT exposure experiments

A series of experiments were performed to determine the mass of cadmium accumulated at different times by DGT devices deployed in solutions containing cadmium (prepared from the solid nitrate salt, Merck, analytical grade) and also in presence of different concentrations of NTA (Fluka, analytical grade). Ultra-pure water (Milli-Q plus 185 System, Millipore) was employed in all the experiments.

The 5 L exposure chamber was filled with 2 L of solution containing $NaNO_3$ to adjust a constant ionic strength of 0.05 M and NTA (experiments in presence of ligands). The pH was then adjusted to the desired value. The cadmium was added in the chosen concentration, and the solution was left to stabilize overnight with continuous stirring.

7.1.4 Retrieval and analysis

During all experiments, aliquots of the exposure chamber solution were collected at regular intervals to check the total cadmium concentration. These aliquots were acidified to pH 1-2 with HNO_3. DGT sensors, once removed from the solution, were rinsed with ultrapure water and dismounted for removal of the resin gels, which were then eluted in 1 mL of concentrated nitric acid (34.5 %) for at least 24 h. Solution aliquots and eluates were analyzed by Inductively Plasma Optical Emission Spectroscopy (ICP-OES) (Activa-S, Horiba Scientific).

7.2 Basic tests of the DGT performance

7.2.1 Resin gel volume

Although the first papers published on DGT[2] considered the volume of the resin gel as negligible, this parameter (approximately 0.18 mL) is relatively not so small compared to the volume of nitric acid (1 mL) required for elution of the Chelex. So it is necessary to take it into account for the calculation of the mass accumulated by the DGT sensor. In the literature, authors report a value of 0.15 - 0.16 mL[3-5], but they do not give a detailed procedure for its experimental determination (or theoretical calculation), nor an error estimate of this value. Therefore experimental measurements to determine with precision the volume of Chelex gel and its respective error are necessary.

Seven DGT replicates were assembled, deployed in milli-Q water and then, after sensor dismounting, Chelex gels were weighted wet and dry (after a few hours in a drying oven). The results are given in **table 7.1** and the average value of (0.18 ± 0.04) mL was used in the subsequent calculations.

	Wet gel (g)	Dry gel (g)	Water volume (mL)	Water percentage
1	0.1582	0.0075	0.1507	95.3
2	0.1714	0.0084	0.1630	95.1
3	0.1755	0.0085	0.1670	95.2
4	0.2321	0.0133	0.2188	94.3
5	0.1289	0.0065	0.1224	95.0
6	0.2105	0.0099	0.2006	95.3
7	0.2275	0.0135	0.2140	94.1
Average	0.19	0.010	**0.18**	94.9
σ	0.04	0.003	**0.04**	0.5

Table 7.1. Results of resin gel weighting and the volume of water resulting.

7.2.2 Stirring rate

When DGT is immersed in water, there is a region in solution close to its surface where the transport of metal ions and complexes undergoes a rapid transition from advective to diffusive control. The thickness of this layer, known as the Diffusive Boundary Layer (DBL see **figure 7.2**), will be dependent on both the velocity of the flow and the sensor geometry, and will increase the diffusive path-length of cations before their fixation by the Chelex.
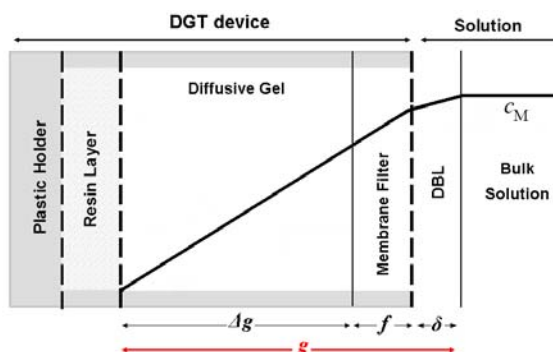
Figure 7.2. Schematic representation of the free concentration of metal species in a DGT device in contact with an aqueous solution. Diffusion coefficients in the diffusive gel and in the DBL (diffusion coefficient in water) are assumed to be different.

Under adequate stirring conditions, the renewal of the solution on the surface of the DGT is fast and the thickness of the DBL is independent of the flow[2,3], but this might not be the case in stirred solutions at low stirring speeds. In this case, several samplers with different thicknesses of diffusive gel must be deployed in order to determine the value of the DBL.

The conditions of adequate stirring speed were determined in order to have a DBL that does not depend on the flow. The experiments were performed in presence of 10^{-5} mol·L^{-1} Cd with three stirring rates. The results are given in **figure 7.3**, where the number of moles of cadmium accumulated was calculated with **equation 6.8** (see previous chapter), using a value of the elution factor equal to 1. The number of moles accumulated was independent of the stirring rate above 240 rpm. At 120 rpm, the renewal of the solution is not enough faster. A stirring rate of 240 rpm was chosen and applied in all the subsequent experiments.
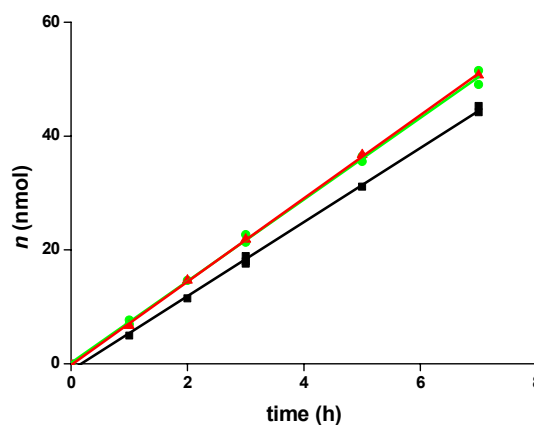
Figure 7.3. Number of amoles of metal accumulated by DGT in a system with 10^{-5} mol·L^{-1} Cd at different stirring rates. Markers: experimental measurements; lines: linear regressions. In black, stirring rate of 120 rpm, in green 240 rpm and in red 400 rpm.

7.2.3 Elution efficiency

Zhang and Davison[2] extracted the Chelex with 2 mol·L^{-1} nitric acid for six metals and have reported an elution efficiency for cadmium of 84 % with a 3 % standard deviation. Studies with 1 mol·L^{-1} nitric acid for the elution of the Chelex gel have reported similar values of elution efficiency.[6,7] Using

concentrated nitric acid would increase the elution efficiency and the results obtained by Garmo et al.[8] confirmed this hypothesis, as they report an elution efficient for cadmium of 99 % with a standard deviation of 1 %. In order to have high elution efficiency, Chelex gels are eluted by concentrated nitric acid (34.5 %). The efficiency of this elution method was checked by comparison with a complete digestion of Chelex gels in closed microwave bombs (≈ 170 ºC, HNO_3 69 % at elevated pressure).

The results (see **figure 7.4)** show that the complete digestion of Chelex gives the same number of moles accumulated by the DGT as the extraction of Chelex gels by concentrated nitric acid, which validates the 34.5 % HNO_3 elution method. An elution efficiency of 100 % is used in all subsequent calculations.
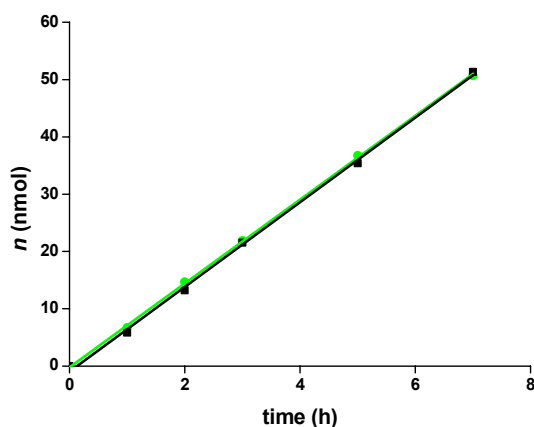
Figure 7.4. DGT accumulation in a system with 10^{-5} mol·L^{-1} Cd, measured by extraction of metal adsorbed by Chelex gels with concentrated nitric acid (34.5 %) in green, and with complete digestion in black. Markers: experimental measurements; lines: linear regressions.

7.2.4 Diffusion coefficient

A limit on the accuracy of the assayed concentration is imposed by uncertainty in the diffusion coefficient used in the calculations. For example, Alfaro-De la Torre *et al.*[6] determined that the diffusion coefficient of Cd in gel (D_{Cd}) was 10 % lower than that observed in water. Davison and Zhang[5] have measured the diffusion coefficient for most environmentally-significant trace metals and found that they were 0.85 times that of water (the value in pure water can be found elsewhere[9,10]). The differences among these values of D_{Cd} reported in

bibliography, can be ascribed to batch-to-batch variations in the agarose-derivative crosslinker.[11] This variability imposes a constraint on the accuracy that can probably be of the order of 10 %. Moreover, since diffusion coefficients are temperature dependent, it is essential to measure the temperature of the water in which the DGT is deployed. The value of the diffusion coefficient of cadmium at 25ºC used in this work is given by DGT Research Ltd.[5] as 6.09×10^{-10} $m^2 \cdot s^{-1}$.

7.2.5 Thickness of the Diffusive Boundary Layer

The DBL increases the diffusion domain in the sensor (see **figure 7.2**). In absence of any metal complexes, and when different diffusion coefficients are considered for the metal ion in water, gel and filter, the moles of metal accumulated by the sensor can be calculated from the Fick's law (see **equation 6.8**) as[6,12]:

$$n = c_{T,M} \left(\frac{D_M \, D_M^f \, D_M^w}{\Delta g \, D_M^f \, D_M^w + f \, D_M \, D_M^w + \delta \, D_M \, D_M^f \, D_M^w} \right) At \qquad (7.1)$$

where $c_{T,M}$ is the total concentration of metal, D_M, D_M^f, D_M^w are the diffusion coefficients of the metal ion in the diffusive gel, membrane filter and water, respectively, $\Delta g, f, \delta$ are the thicknesses of the diffusive gel, membrane filter and DBL, respectively, A is the area of the exposure window and t, the time of deployment.

Measurements have shown that the diffusion coefficient in the membrane filter is indistinguishable from that in the diffusion gel.[3,13] As shown in section 7.2.4, the diffusion coefficient in the diffusive gel diverges from that in water.

However, for the sake of simplicity, differences between diffusion coefficients in both media are neglected in this work, and an "effective" thickness of the diffusion domain, *g*, can be calculates by the simplification of **equation 7.1** as:

$$n = \frac{c_{T,M} D_M A}{g} t \qquad (7.2)$$

where g is the total thickness of the diffusion domain and D_M is the diffusion coefficient in the diffusive gel.

In order to determine the value of the DBL, three experiments in presence of cadmium at about 10^{-5} mol·L^{-1} have been conducted. **Figure 7.5** depicts the normalized Cd accumulation $n/c_{T,Cd}$ versus time. The normalized Cd accumulation is used as ordinate axis in order to include in the same figure the results obtained for different concentrations of cadmium. Using **equation 7.2** applied to $n/c_{T,Cd}$,

$$n/c_{T,Cd} = \frac{D_{Cd}A}{g}t$$

(7.3)

the slope of this plot can be used to fit the total thickness of the diffusion domain g. Using $D_{Cd} = 6.09 \times 10^{-10}$ m^2·s^{-1}, $A = 3.14 \times 10^{-4}$ m^2, the effective thickness of the diffusion layer is 1.13×10^{-3} m. The nominal diffusion domain of the DGT sensor $\Delta g + f$ is 9.25×10^{-4} m, the differences between these values provides a DBL thickness of 205 μm, which is similar to different reported values in well-stirred systems.[3,8,14]
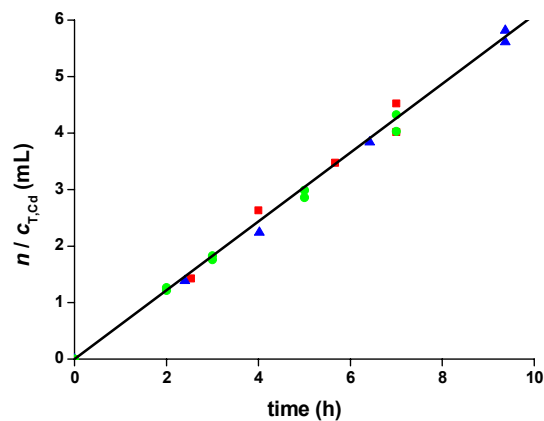
Figure 7.5. DGT accumulation in a system with Cd. Markers: experimental measurements with different Cd concentrations: 1.11×10^{-5} mol L^{-1} (▲), 1.06×10^{-5} mol L^{-1} (●) and 9.96×10^{-6} mol L^{-1} (■). Cd accumulated expected according to the equation (7.3) for a thickness of diffusion layer of $\Delta g = 1.13 \times 10^{-3}$ m . $D_{Cd} = 6.09 \times 10^{-10}$ m^2 s^{-1}

7.3 References

(1)   *Chelex 100 and Chelex 20 Chelating Exchange Resin Instruction Manual*. Bio-Rad Laboratories, **1993**.

(2)   Zhang, H.; Davison, W., Performance characteristics of diffusion gradients in thin films for the in situ mesurement of trace metals in aqueous solution. *Analytical Chemistry* **1995,** *67*, (19), 3391-3400.

(3)   Warnken, K. W.; Zhang, H.; Davison, W., Accuracy of the diffusive gradients in thin-films technique: Diffusive boundary layer and effective sampling area considerations. *Analytical Chemistry* **2006,** *78*, (11), 3780-3787.

(4)   Degryse, F.; Smolders, E.; Oliver, I.; Zhang, H., Relating soil solution Zn concentration to diffusive gradients in thin films measurements in contaminated soils. *Environmental Science & Technology* **2003,** *37*, (17), 3958-3965.

(5)   Davison, W.; Zhang, H. Technical Documentation - DGT for measurements in waters, soils ans sediments. http://www.dgtresearch.com

(6)   Alfaro-De la Torre, M. C.; Beaulieu, P. Y.; Tessier, A., In situ measurement of trace metals in lakewater using the dialysis and DGT techniques. *Analytica Chimica Acta* **2000,** *418*, (1), 53-68.

(7)   Warnken, K. W.; Zhang, H.; Davison, W., Performance characteristics of suspended particulate reagent-iminodiacetate as a binding agent for diffusive gradients in thin films. *Analytica Chimica Acta* **2004,** *508*, (1), 41-51.

(8)   Garmo, O. A.; Royset, O.; Steinnes, E.; Flaten, T. P., Performance study of diffusive gradients in thin films for 55 elements. *Analytical Chemistry* **2003,** *75*, (14), 3573-3580.

(9)   Li, Y. H.; Gregory, S., Diffusion of ions in sea-water and in deep-sea sediments. *Geochimica Et Cosmochimica Acta* **1974,** *38*, (5), 703-714.

(10)   Vanýsek, P., Ionic conductivity and diffusion at infinite dilution. In *Handbook of Chemistry and Physics 77th edition 1996-1997*, Lide, R. L., Ed. CRC Press: Boca Raton, New York, London, Tokyo, pp. 5.98-5.100, 1996.

(11)   Zhang, H.; Davison, W., Diffusional characteristics of hydrogels used in DGT and DET techniques. *Analytica Chimica Acta* **1999,** *398*, (2-3), 329-340.

(12)   Davison, W.; Fones, G.; Harper, M.; Teasdale, P.; Zhang, H., Dialysis, DET and DGT: in situ diffusional techniques for studying water, sediments and soils. In *In Situ Monitoring of Aquatic Systems: Chemical Analysis and Speciation*, Buffle, J.; Horvai, G., Eds. Wiley: New York, pp. 495-570, 2000.

(13)   Scally, S.; Davison, W.; Zhang, H., Diffusion coefficients of metals and metal complexes in hydrogels used in diffusive gradients in thin films. *Analytica Chimica Acta* **2006,** *558*, (1-2), 222-229.

(14)   Garmo, O. A.; Naqvi, K. R.; Royset, O.; Steinnes, E., Estimation of diffusive boundary layer thickness in studies involving diffusive gradients in thin films (DGT). *Analytical and Bioanalytical Chemistry* **2006,** *386*, (7-8), 2233-2237.

CHAPTER 8

RESULTS AND DISCUSSION

PENETRATION EFFECTS OF THE COMPLEXES IN THE DGT RESIN LAYER

- Foreword -

In the literature, the modelling of the DGT measurements had already taken into account the penetration of species into the resin layer. However, the effects of the resin layer thickness in the complex lability have not been highlighted to date. An analytical expression for the lability degree has been presented in section 6.8. This expression is derived assuming an analogy between the resin binding interface of DGT and the surface of a voltammetric electrode (where the penetration of the metal complexes does not occur).

Nevertheless, the experimental results obtained in this study for the complex Cd-NTA show a lability degree value greater than the predicted by this expression. Therefore, a model that takes into account the penetration of the species into the resin was developed. A good accuracy was obtained between the experimental and modelled results, which demonstrates the importance of the penetration of complexes in the lability measurement. The model simulations showed that a complex system is likely to appear more labile when measured by DGT (where the complexes penetrate into the resin binding layer) than when measured by other techniques where complexes are restricted to the diffusion layer. Therefore, it was shown that expressions reported for the lability of a complex in voltammetric sensors (where the complexes do not penetrate into the electrode) were, in general, not applicable to DGT, since the resin layer is characteristic a feature of DGT.

This development provides increased understanding of how the DGT measurement is affected by the complexities of solution speciation. One of the great advantages of the modelling approach is as an aid to conceptual appreciation, especially by the images it provides of temporal changes in the distribution of each species through the DGT devices.

The section 8.1 details the numerical model used to assess the impact of the resin layer on the lability complexes. The model predictions are then compared with experimental data for the Cd-NTA system.

This work is extended to provide approximate analytical expressions for the calculation of the metal flux, lability degree and concentration profiles in a DGT experiment (section 8.2). The results show the great dependence of the lability degree on the resin layer thickness. In a standard DGT arrangement (where the thickness of the diffusion layer is larger than the resin layer) a partially labile complex could increase its lability up to a fully labile behaviour, when the resin

layer thickness is increases, whereas an increase of the diffusion layer affects very little the lability degree.

Although, the accumulated mass can be successfully predicted for well defined metal-ligand systems (as shown in the following chapters), the measurement interpretation in truly unknown and very complicated systems, such as natural waters, is far more challenging.

8.1 KEY ROLE OF THE RESIN LAYER THICKNESS IN THE LABILITY OF COMPLEXES MEASURED BY DGT.

Key role of the Resin Layer Thickness in the Lability of Complexes Measured by DGT

Abstract

Analysis of the dynamic features of diffusion gradients in thin film devices (DGT) indicates that the penetration of complexes into the resin layer dramatically increases their lability. This should be taken into account when interpreting DGT measurements in terms of the dynamics of solution speciation. The experimental accumulation of Cd by DGT sensors in Cd-NTA systems confirmed these theoretical analyses. A computational code, which allows a rigorous digital simulation of the diffusion-reaction processes in the gel and resin layers, was used to model the results and to demonstrate the effect of the complex penetration into the resin layer on the lability degree. These findings suggest that DGT renders all complexes much more labile than if the resin-diffusive gel interface was considered as a perfect planar sink, explaining why DGT often measures a high proportion of the metal in a natural water. This information is relevant since some studies have stressed the importance of labile complexes as a source of bioaccumulated metal.

Key role of the resin layer thickness in the lability of complexes measured by DGT

SUPPORTING INFORMATION

Section 1: Numerical Simulation of a DGT sensor

    1.1. The model

    1.2. Dimensionless reformulation

    1.3. Discretization

    1.4. Solution procedure

Section 2: Concentration profiles in a DGT experiment

Section 3: Experimental Section

Section 4: Additional figures

Section 5: Formulation of the Cd-NTA speciation in a DGT sensor as a system with only one complex and ligand species

Section 6: Parameter values of all the figures of the manuscript

Section 1: Numerical Simulation of a DGT Sensor
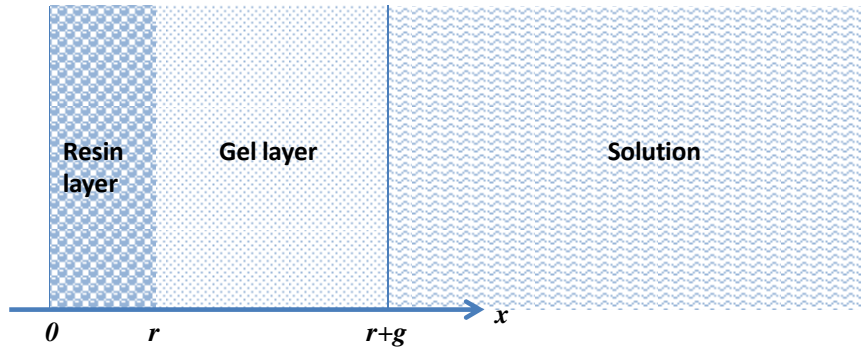
1.1.- The Model

Figure SI-1. Schematic representation of a DGT device.

The model formulation coincides with that of Lehto et al.[1] and Tusseau-Vuillemin et al.[2]

Let D_i and $D_{i,R}$ stand for the diffusion coefficients of species i in the diffusive gel or in the resin domain, respectively and let c_i stand for the concentration of species i at a given spatial position x and time t. Total concentrations are denoted as $c_{T,i}$.

The transport equations for the different species can be written as:

- For the metal in the gel layer and in the resin layer:

$$\frac{\partial c_M}{\partial t} = D_{M,R}\frac{\partial^2 c_M}{\partial x^2} - k_a c_M c_L + k_d c_{ML} - k_{a,R} c_M c_R + k_{d,R} c_{MR}, \quad \text{if} \quad 0 < x < r \qquad \textbf{(SI-1)}$$

$$\frac{\partial c_M}{\partial t} = D_M\frac{\partial^2 c_M}{\partial x^2} - k_a c_M c_L + k_d c_{ML}, \quad \text{if} \quad r < x < r + g \qquad \textbf{(SI-2)}$$

- For the ligand:

$$\frac{\partial c_L}{\partial t} = \left\{\begin{matrix} D_{L,R} \\ D_L \end{matrix}\right\} \frac{\partial^2 c_L}{\partial x^2} + k_a c_M c_L - k_d c_{ML}, \quad \text{if} \quad 0 < x < r + g \qquad \textbf{(SI-3)}$$

where the curly bracket indicates that $D_{L,R}$ applies when $0 < x < r$ and D_L applies when $r < x < r + g$

- For the complex (assuming the same diffusion coefficient for complex and ligand):

$$\frac{\partial c_{ML}}{\partial t} = \left\{ \begin{matrix} D_{L,R} \\ D_L \end{matrix} \right\} \frac{\partial^2 c_{ML}}{\partial x^2} + k_a c_M c_L - k_d c_{ML}, \quad \text{if} \quad 0 < x < r + g \qquad \textbf{(SI-4)}$$

- For the resin sites free (R) or occupied (MR):

$$\frac{\partial c_R}{\partial t} = -k_{a,R} c_M c_R + k_{d,R} c_{MR}, \quad \text{if} \quad 0 < x < r \qquad \textbf{(SI-5)}$$

$$\frac{\partial c_{MR}}{\partial t} = +k_{a,R} c_M c_R - k_{d,R} c_{MR}, \quad \text{if} \quad 0 < x < r \qquad \textbf{(SI-6)}$$

There are no resin sites in the gel domain: $c_R(x,t) = c_{MR}(x,t) = 0$ for $r < x < r + g$.

Initial conditions correspond to the absence of metal and ligand in the sensor:

$$c_M(x,0) = c_L(x,0) = c_{ML}(x,0) = 0, \quad \text{if} \quad 0 < x < r + g \qquad \textbf{(SI-7)}$$

$$c_{MR}(x,0) = 0 \quad \text{if} \quad 0 < x < r \qquad \textbf{(SI-8)}$$

$$c_R(x,0) = c_{T,R} \quad \text{if} \quad 0 < x < r \qquad \textbf{(SI-9)}$$

where $c_{T,R}$ denotes the total concentration of resin sites (free or occupied).

Boundary conditions at $x = r + g$ correspond to bulk concentrations:

$$c_M(r + g, t) = c_M^*, \quad c_L(r + g, t) = c_L^*, \quad c_{ML}(r + g, t) = c_{ML}^* \qquad \textbf{(SI-10)}$$

Boundary conditions at $x = r$:

at the gel-resin interface $c_M(x,t)$, $c_L(x,t)$, and $c_{ML}(x,t)$ and their fluxes must be continuous, that is

$$c_M(r^-, t) = c_M(r^+, t), \quad c_L(r^-, t) = c_L(r^+, t), \quad c_{ML}(r^-, t) = c_{ML}(r^+, t) \qquad \textbf{(SI-11)}$$

and

$$D_{M,R} \left. \frac{\partial c_M}{\partial x} \right|_{r^-} = D_M \left. \frac{\partial c_M}{\partial x} \right|_{r^+}, \quad D_{L,R} \left. \frac{\partial c_L}{\partial x} \right|_{r^-} = D_L \left. \frac{\partial c_L}{\partial x} \right|_{r^+}, \quad D_{L,R} \left. \frac{\partial c_{ML}}{\partial x} \right|_{r^-} = D_L \left. \frac{\partial c_{ML}}{\partial x} \right|_{r^+} \qquad \textbf{(SI-12)}$$

The continuity of the concentrations indicates that no Donnan effects are considered, so that charge effects of the resin are screened by the supporting electrolyte.

Boundary conditions at x = 0 stem from non-flux conditions:

$$\left.\frac{\partial c_M}{\partial x}\right|_{x=0} = \left.\frac{\partial c_L}{\partial x}\right|_{x=0} = \left.\frac{\partial c_{ML}}{\partial x}\right|_{x=0} = 0 \qquad \textbf{(SI-13)}$$

Equations (SI-1 - SI-6) with the initial conditions (**SI-7** to **SI-9**) and boundary value problem (**SI-10 - SI-13**) form a system of equations for $c_M(x,t)$, $c_L(x,t)$, $c_{ML}(x,t)$, $c_R(x,t)$ and $c_{MR}(x,t)$.

It could be useful to introduce the total ligand concentration, $c_{T,L}$. Adding **equations SI-3** and **SI-4**, the transport equation for $c_{T,L}$ becomes:

$$\frac{\partial c_{T,L}}{\partial t} = \left\{ \begin{array}{l} D_{L,R} \\ D_L \end{array} \right\} \frac{\partial^2 c_{T,L}}{\partial x^2}, \quad \text{if} \quad \left\{ \begin{array}{l} 0 < x < r \\ r < x < r+g \end{array} \right\} \qquad \textbf{(SI-14)}$$

with initial and boundary conditions given by:

$$c_{T,L}(x,0) = 0, \quad \left.\frac{\partial c_{T,L}}{\partial x}\right|_{x=0} = 0, \quad c_{T,L}(r+g,t) = c_{T,L}^* \qquad \textbf{(SI-15)}$$

And

$$c_{T,L}(r^-,t) = c_{T,L}(r^+,t), \quad D_{L,R}\left.\frac{\partial c_{T,L}}{\partial x}\right|_{r^-} = D_L\left.\frac{\partial c_{T,L}}{\partial x}\right|_{r^+} \qquad \textbf{(SI-16)}$$

Additionally, we can introduce the total resin concentration:

$$c_R(x,t) + c_{MR}(x,t) = c_{T,R} \qquad \textbf{(SI-17)}$$

The addition of **equations. SI-5** and **SI-6** indicates, as physically expected, that $c_{T,R}$ is time independent. Thus the finding of $c_M(x,t)$, $c_L(x,t)$, $c_{ML}(x,t)$, $c_R(x,t)$ and $c_{MR}(x,t)$ can be reduced to the finding of $c_M(x,t)$, $c_L(x,t)$, $c_{T,L}(x,t)$, and $c_R(x,t)$ in the domain $0 < x < r+g$.

1.2.- Dimensionless Reformulation

Let us reformulate the problem in terms of dimensionless functions and normalized variables.

Let z be the spatial normalized variable. Its relationship with x and with its derivatives is:

$$z = \frac{x}{\sqrt{D_\mathrm{M}}} \quad \rightarrow \quad \frac{\partial^2}{\partial z^2} = \frac{1}{D_\mathrm{M}} \frac{\partial^2}{\partial x^2} \tag{SI-18}$$

Then

$$r^* = \frac{r}{\sqrt{D_\mathrm{M}}}, \quad g^* = \frac{r+g}{\sqrt{D_\mathrm{M}}} \tag{SI-19}$$

The dimensionless diffusion coefficients:

$$d_i = \frac{D_i}{D_\mathrm{M}}, \quad i = \mathrm{M}, \mathrm{R}; \ \mathrm{L}; \ \mathrm{L}, \mathrm{R} \tag{SI-20}$$

The dimensionless concentrations:

$$q_\mathrm{M} = \frac{c_\mathrm{M}}{c_\mathrm{M}^*}, \quad q_\mathrm{L} = \frac{c_\mathrm{L}}{c_\mathrm{L}^*}, \quad q_\mathrm{TL} = \frac{c_\mathrm{T,L}}{c_\mathrm{T,L}^*}, \quad q_\mathrm{M} = \frac{c_\mathrm{R}}{c_\mathrm{T,R}^*} \tag{SI-21}$$

With these definitions, the transport equations become:

- For the dimensionless metal:

$$\frac{\partial q_\mathrm{M}}{\partial t} = d_\mathrm{M,R} \frac{\partial^2 q_\mathrm{M}}{\partial z^2} - k_\mathrm{a} c_\mathrm{L}^* q_\mathrm{M} q_\mathrm{L} + k_\mathrm{d} \left(\frac{c_\mathrm{T,L}^*}{c_\mathrm{M}^*} q_\mathrm{T,L} - \frac{c_\mathrm{L}^*}{c_\mathrm{M}^*} q_\mathrm{L} \right) - k_\mathrm{a,R} c_\mathrm{T,R}^* q_\mathrm{M} q_\mathrm{R} + \frac{k_\mathrm{d,R} c_\mathrm{T,R}^*}{c_\mathrm{M}^*} (1 - q_\mathrm{R}) \tag{SI-22}$$

for $0 < z < r^*$, and

$$\frac{\partial q_\mathrm{M}}{\partial t} = \frac{\partial^2 q_\mathrm{M}}{\partial z^2} - k_\mathrm{a} c_\mathrm{L}^* q_\mathrm{M} q_\mathrm{L} + k_\mathrm{d} \left(\frac{c_\mathrm{T,L}^*}{c_\mathrm{M}^*} q_\mathrm{T,L} - \frac{c_\mathrm{L}^*}{c_\mathrm{M}^*} q_\mathrm{L} \right), \quad \text{for } r^* < z < g^* \tag{SI-23}$$

with initial and boundary conditions:

$$q_{\mathrm{M}}(z,0) = 0, \quad \left.\frac{\partial q_{\mathrm{M}}}{\partial z}\right|_{z=0} = 0, \quad q_{\mathrm{M}}(g^*,t) = 1, \tag{SI-24}$$

$$q_{\mathrm{M}}(r^{*-},t) = q_{\mathrm{M}}(r^{*+},t), \quad d_{\mathrm{M,R}}\left.\frac{\partial q_M}{\partial z}\right|_{z=r^{*-}} = \left.\frac{\partial q_M}{\partial z}\right|_{z=r^{*+}}. \tag{SI-25}$$

- Equations for the dimensionless ligand:

$$\frac{\partial q_{\mathrm{L}}}{\partial t} = \left\{ \begin{matrix} d_{\mathrm{L,R}} \\ d_{\mathrm{L}} \end{matrix} \right\} \frac{\partial^2 q_{\mathrm{L}}}{\partial z^2} - k_{\mathrm{a}} c_{\mathrm{M}}^* q_{\mathrm{M}} q_{\mathrm{L}} + k_{\mathrm{d}}\left(\frac{c_{\mathrm{T,L}}^*}{c_{\mathrm{L}}^*} q_{\mathrm{T,L}} - q_{\mathrm{L}} \right) \tag{SI-26}$$

$$q_{\mathrm{L}}(z,0) = 0, \quad \left.\frac{\partial q_{\mathrm{L}}}{\partial z}\right|_{z=0} = 0, \quad q_{\mathrm{L}}(g^*,t) = 1 \tag{SI-27}$$

$$q_{\mathrm{L}}(r^{*-},t) = q_{\mathrm{L}}(r^{*+},t), \quad \frac{d_{\mathrm{L,R}}}{d_{\mathrm{L}}}\left.\frac{\partial q_L}{\partial z}\right|_{z=r^{*-}} = \left.\frac{\partial q_L}{\partial z}\right|_{z=r^{*+}} \tag{SI-28}$$

- Equations for the dimensionless total ligand:

$$\frac{\partial q_{\mathrm{T,L}}}{\partial t} = \left\{ \begin{matrix} d_{\mathrm{L,R}} \\ d_{\mathrm{L}} \end{matrix} \right\} \frac{\partial^2 q_{\mathrm{T,L}}}{\partial z^2} \tag{SI-29}$$

$$q_{\mathrm{T,L}}(z,0) = 0, \quad \left.\frac{\partial q_{\mathrm{T,L}}}{\partial z}\right|_{z=0} = 0, \quad q_{\mathrm{T,L}}(g^*,t) = 1 \tag{SI-30}$$

$$q_{\mathrm{T,L}}(r^{*-},t) = q_{\mathrm{T,L}}(r^{*+},t), \quad \frac{d_{\mathrm{L,R}}}{d_{\mathrm{L}}}\left.\frac{\partial q_{\mathrm{T,L}}}{\partial z}\right|_{z=r^{*-}} = \left.\frac{\partial q_{\mathrm{T,L}}}{\partial z}\right|_{z=r^{*+}} \tag{SI-31}$$

- Equation for the dimensionless free resin concentration:

$$\frac{\partial q_{\mathrm{R}}}{\partial t} = -k_{\mathrm{a,R}} c_{\mathrm{M}}^* q_{\mathrm{M}} q_{\mathrm{R}} + k_{\mathrm{d,R}}(1 - q_{\mathrm{R}}), \quad \text{if } 0 < z < r^*, \tag{SI-32}$$

with initial condition $q_{\mathrm{R}}(z,0) = 1$.

1.3.- Discretization
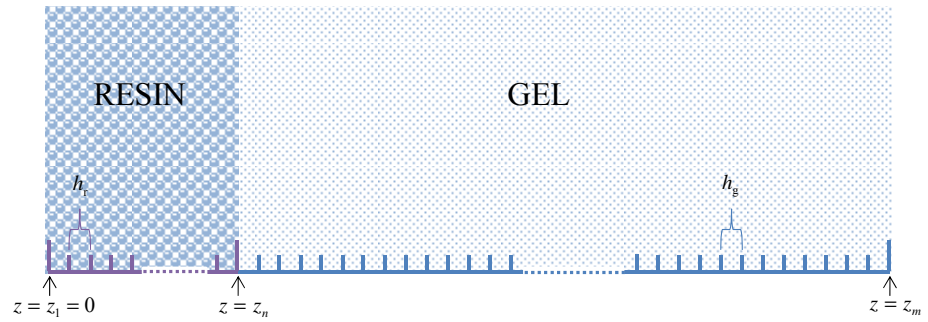
Figure SI-2. Schematic representation of spatial grid.

The resin layer domain will be divided into $n-1$ equal parts of length $h_r = \dfrac{r}{n-1}$. The gel domain will be divided into $m-1$ parts of length $h_g = \dfrac{g}{m-n-1}$ as shown in **figure SI-2**. The partial differential equations are discretized using spatial finite differences and a temporal Inverse-Euler scheme with constant Δt.

1.3.1- Resin sites concentration

The discretization of **equation SI-32** becomes:

$$q_R(z,t+\Delta t) - q_R(z,t) = -\Delta t k_{a,R} c_M^* q_M(z,t+\Delta t) q_R(z,t+\Delta t) + \Delta t k_{d,R}(1 - q_R(z,t+\Delta t)) \quad \textbf{(SI-33)}$$

which leads to:

$$q_R(z,t+\Delta t) = \frac{q_R(z,t) + \Delta t k_{d,R}}{1 + \Delta t k_{a,R} c_M^* q_M(z,t+\Delta t) + \Delta t k_{d,R}} \quad \textbf{(SI-34)}$$

1.3.2- Total ligand concentration

Although **equation SI-29** could be analytically solved, its computational cost is greater than the cost of its numerical solution. The discretized form of **equation SI-29** is:

$$q_{T,L}(z,t+\Delta t) - q_{T,L}(z,t) =$$

$$\begin{Bmatrix} \alpha_L \\ \alpha_{L,R} \end{Bmatrix} \left[q_{T,L}(z+h_i,t+\Delta t) - 2q_{TL}(z,t+\Delta t) + q_{T,L}(z-h_i,t+\Delta t) \right] \qquad \textbf{(SI-35)}$$

Where h_i is equal to h_r or hg depending on the domain, $\alpha_L = d_L \Delta t / h_g^2$ and $\alpha_{L,R} = d_{L,R} \Delta t / h_r^2$.

Equation SI-35 can be rewritten as:

$$-\begin{Bmatrix} \alpha_L \\ \alpha_{L,R} \end{Bmatrix} q_{T,L}(z-h_i,t+\Delta t) + \left(1 + 2\begin{Bmatrix} \alpha_L \\ \alpha_{L,R} \end{Bmatrix}\right) q_{T,L}(z,t+\Delta t) -$$

$$\begin{Bmatrix} \alpha_{L,R} \\ \alpha_L \end{Bmatrix} q_{T,L}(z+h_i,t+\Delta t) = q_{T,L}(z,t) \qquad \textbf{(SI-36)}$$

which enables the equation system for $q_{T,L}(z_i, t+\Delta t)$ to be built:

- For z_1, the equation for $q_{T,L}(z_1, t+\Delta t)$ is obtained from **equation SI-30**, corresponding to the null flux condition at the origin,

$$q_{T,L}(z_2, t+\Delta t) - q_{T,L}(z_1, t+\Delta t) = 0 \qquad \textbf{(SI-37)}$$

- For $j = 2$ to $n-1$, the equations are obtained from **SI-36** considering the resin layer domain:

$$-\alpha_{L,R} q_{T,L}(z_j - h_r, t+\Delta t) + (1 + 2\alpha_{L,R}) q_{T,L}(z_j, t+\Delta t)$$

$$-\alpha_{L,R} q_{T,L}(z_j + h_r, t+\Delta t) = q_{T,L}(z_j, t) \qquad \textbf{(SI-38)}$$

- At z_n, that is $z = r^*$, the equation is obtained from the boundary condition **SI-31**:

$$\frac{d_{\mathrm{L,R}}}{d_{\mathrm{L}}} \frac{q_{\mathrm{T,L}}(z_{\mathrm{n}},t+\Delta t) - q_{\mathrm{T,L}}(z_{\mathrm{n-1}},t+\Delta t)}{h_{\mathrm{r}}} = $$

$$\frac{q_{\mathrm{T,L}}(z_{\mathrm{n+1}},t+\Delta t) - q_{\mathrm{T,L}}(z_{\mathrm{n}},t+\Delta t)}{h_{\mathrm{g}}}$$

(SI-39)

which can be rewritten as

$$-\sigma q_{\mathrm{T,L}}(z_{\mathrm{n-1}},t+\Delta t) + (\sigma+1)q_{\mathrm{T,L}}(z_{\mathrm{n}},t+\Delta t) - q_{\mathrm{T,L}}(z_{\mathrm{n-1}},t+\Delta t) = 0$$

(SI-40)

where $\sigma = \dfrac{h_{\mathrm{g}} d_{\mathrm{LR}}}{h_{\mathrm{r}} d_{\mathrm{L}}}$

- For $j = n+1$ to $m-1$, we are in the gel domain and the equations for $q_{\mathrm{T,L}}(z_i, t+\Delta t)$ are obtained from **SI-36**:

$$-\alpha_{\mathrm{L}} q_{\mathrm{T,L}}(z_j - h_{\mathrm{g}}, t+\Delta t) + (1 + 2\alpha_{\mathrm{L}}) q_{\mathrm{T,L}}(z_j, t+\Delta t)$$
$$-\alpha_{\mathrm{L}} q_{\mathrm{T,L}}(z_j + h_{\mathrm{g}}, t+\Delta t) = q_{\mathrm{T,L}}(z_j, t)$$

(SI-41)

- Finally, for $z = g^*$ the equation is obtained from condition in **SI-30**:

$$q_{\mathrm{T,L}}(g^*, t+\Delta t) = 1$$

(SI-42)

1.3.3- Dimensionless ligand concentration

In the same way, the discretized form of **equation SI-26** is:

$$q_{\mathrm{L}}(z,t+\Delta t) - q_{\mathrm{L}}(z,t) = \begin{Bmatrix} \alpha_{\mathrm{L,R}} \\ \alpha_{\mathrm{L}} \end{Bmatrix}$$
$$[q_{\mathrm{L}}(z+h_i, t+\Delta t) - 2q_{\mathrm{L}}(z,t+\Delta t) + q_{\mathrm{L}}(z-h_i, t+\Delta t)]$$
$$-\Delta t k_{\mathrm{a}} c_{\mathrm{M}}^* q_{\mathrm{M}}(z,t+\Delta t) q_{\mathrm{L}}(z,t+\Delta t) + $$
$$\Delta t k_{\mathrm{d}} \frac{c_{\mathrm{T,L}}^*}{c_{\mathrm{L}}^*} q_{\mathrm{T,L}}(z,t+\Delta t) - \Delta t k_{\mathrm{d}} q_{\mathrm{L}}(z,t+\Delta t)$$

(SI-43)

or

$$-\begin{Bmatrix} \alpha_{L,R} \\ \alpha_L \end{Bmatrix} q_L(z-h_i, t+\Delta t) +$$

$$\left[1 + 2\begin{Bmatrix} \alpha_{L,R} \\ \alpha_L \end{Bmatrix} + \Delta t k_a c_M^* q_M(z, t+\Delta t) + \Delta t k_d \right]$$

$$q_L(z, t+\Delta t) - \begin{Bmatrix} \alpha_{L,R} \\ \alpha_L \end{Bmatrix} q_L(z+h_i, t+\Delta t)$$

$$= q_L(z,t) + \Delta t k_d \frac{c_{T,L}^*}{c_L^*} q_{T,L}(z, t+\Delta t)$$

(SI-44)

Particular equations for each $q_L(z_i, t+\Delta t)$ can be written.

- The first equation, for z_1 reads:

$$-\begin{Bmatrix} \alpha_{L,R} \\ \alpha_L \end{Bmatrix} q_L(z-h_i, t+\Delta t) +$$

$$\left[1 + 2\begin{Bmatrix} \alpha_{L,R} \\ \alpha_L \end{Bmatrix} + \Delta t k_a c_M^* q_M(z, t+\Delta t) + \Delta t k_d \right]$$

$$q_L(z, t+\Delta t) - \begin{Bmatrix} \alpha_{L,R} \\ \alpha_L \end{Bmatrix} q_L(z+h_i, t+\Delta t)$$

$$= q_L(z,t) + \Delta t k_d \frac{c_{T,L}^*}{c_L^*} q_{T,L}(z, t+\Delta t)$$

Particular equations for each $q_L(z_i, t+\Delta t)$ can be written.

- The first equation, for z_1 reads:

$$q_L(z_2, t+\Delta t) - q_L(z_1, t+\Delta t) = 0.$$

- From $j=2$ to $n-1$:

$$-\alpha_{\mathrm{L,R}}q_{\mathrm{L}}(z_j - h_{\mathrm{r}}, t + \Delta t)$$

$$+\left[1 + 2\alpha_{\mathrm{L,R}} + \Delta t k_{\mathrm{a}} c_{\mathrm{M}}^* q_{\mathrm{M}}(z_j, t + \Delta t) + \Delta t k_{\mathrm{d}}\right] q_{\mathrm{L}}(z_j, t + \Delta t)$$

$$-\alpha_{\mathrm{L,R}}q_{\mathrm{L}}(z_j + h_{\mathrm{r}}, t + \Delta t) = q_{\mathrm{L}}(z_j, t) + \Delta t k_{\mathrm{d}} \frac{c_{\mathrm{T,L}}^*}{c_{\mathrm{L}}^*} q_{\mathrm{T,L}}(z_j, t + \Delta t)$$

(SI-46)

- At $z = z_{\mathrm{n}} = r^*$:

$$\frac{d_{\mathrm{L,R}}}{d_{\mathrm{L}}} \frac{q_{\mathrm{L}}(z_{\mathrm{n}}, t + \Delta t) - q_{\mathrm{L}}(z_{\mathrm{n-1}}, t + \Delta t)}{h_{\mathrm{r}}} = \frac{q_{\mathrm{L}}(z_{\mathrm{n+1}}, t + \Delta t) - q_L(z_{\mathrm{n}}, t + \Delta t)}{h_{\mathrm{g}}}$$

(SI-47)

which rewrites as

$$-\sigma q_{\mathrm{L}}(z_{\mathrm{n-1}}, t + \Delta t) + (\sigma + 1)q_{\mathrm{L}}(z_{\mathrm{n}}, t + \Delta t) - q_{\mathrm{L}}(z_{\mathrm{n-1}}, t + \Delta t) = 0$$

(SI-48)

- For $j = n + 1$ to $m - 1$:

$$-\alpha_{\mathrm{L}} q_{\mathrm{L}}(z_j - h_{\mathrm{g}}, t + \Delta t) + \left[1 + 2\alpha_{\mathrm{L}} + \Delta t k_{\mathrm{a}} c_{\mathrm{M}}^* q_{\mathrm{M}}(z_j, t + \Delta t) + \Delta t k_{\mathrm{d}}\right]$$

$$q_{\mathrm{L}}(z_j, t + \Delta t) - \alpha_{\mathrm{L}} q_{\mathrm{L}}(z_j + h_{\mathrm{g}}, t + \Delta t) = q_{\mathrm{L}}(z_j, t) + \Delta t k_{\mathrm{d}} \frac{c_{\mathrm{T,L}}^*}{c_{\mathrm{L}}^*} q_{\mathrm{T,L}}(z_j, t + \Delta t)$$

(SI-49)

- At $z = z_{\mathrm{m}} = g^*$:

$$q_{\mathrm{L}}(z_{\mathrm{m}}, t + \Delta t) = 1$$

(SI-50)

1.3.4- Dimensionless metal concentration

Let us define $\alpha_{\mathrm{M}} = \frac{\Delta t}{\Delta x^2}$ and $\alpha_{\mathrm{M,R}} = d_{\mathrm{M,R}}\alpha_{\mathrm{M}}$.

Discretization of **equation SI-22** becomes:

$$q_M(z_j, t+\Delta t) - q_M(z_j, t) =$$

$$\alpha_{M,R} \left[q_M(z_j + h_r, t+\Delta t) - 2q_M(z_j, t+\Delta t) + q_M(z_j - h_r, t+\Delta t) \right]$$

$$-\Delta t k_a c_L^* q_M(z_j, t+\Delta t) q_L(z_j, t+\Delta t) + \Delta t k_d \frac{c_{T,L}^*}{c_M^*} q_{T,L}(z_j, t+\Delta t)$$

$$-\Delta t k_d \frac{c_L^*}{c_M^*} q_L(z_j, t+\Delta t) - \Delta t k_{a,R} c_{T,R}^* q_M(z_j, t+\Delta t) q_R(z_j, t+\Delta t)$$

$$+\Delta t k_{d,R} \frac{c_{T,R}^*}{c_M^*} \left[1 - q_R(z_j, t+\Delta t) \right]$$

$$(\text{SI-51})$$

and for **equation SI-23**:

$$q_M(z_j, t+\Delta t) - q_M(z_j, t) =$$

$$\alpha_M \left[q_M(z_j + h_g, t+\Delta t) - 2q_M(z_j, t+\Delta t) + q_M(z_j - h_g, t+\Delta t) \right]$$

$$-\Delta t k_a c_L^* q_M(z_j, t+\Delta t) q_L(z_j, t+\Delta t) + \Delta t k_d \frac{c_{T,L}^*}{c_M^*} q_{T,L}(z_j, t+\Delta t) \quad (\text{SI-52})$$

$$-\Delta t k_d \frac{c_L^*}{c_M^*} q_L(z_j, t+\Delta t)$$

The equations for each spatial node can be constructed with the same procedure as before.

- For z_1:

$$q_M(z_2, t+\Delta t) - q_M(z_1, t+\Delta t) = 0 \qquad (\text{SI-53})$$

- From $j=2$ to $n-1$:

$$-\alpha_{MR}q_M(z_j - h_r, t+\Delta t)+$$

$$\left[1+2\alpha_{MR}+\Delta t k_a c_L^* q_L(z_j, t+\Delta t)+\Delta t k_{a,R} c_{T,R}^* q_R(z_j, t+\Delta t)\right]$$

$$q_M(z_j, t+\Delta t)-\alpha_{M,R}q_M(z_j + h_r, t+\Delta t)$$

$$= q_M(z_j, t)+\Delta t k_d \frac{c_{TL}^*}{c_M^*}q_{T,L}(z_j, t+\Delta t)$$

$$-\Delta t k_d \frac{c_L^*}{c_M^*}q_L(z_j, t+\Delta t)+\Delta t k_{d,R}\frac{c_{T,R}^*}{c_M^*}\left[1-q_R(z_j, t+\Delta t)\right]$$

(SI-54)

- At $z = z_n = r^*$:

$$d_{M,R}\frac{q_M(z_n, t+\Delta t)-q_M(z_{n-1}, t+\Delta t)}{h_r}=\frac{q_M(z_{n+1}, t+\Delta t)-q_M(z_n, t+\Delta t)}{h_g}$$

(SI-55)

- From $j = n+1$ to $m-1$:

$$-\alpha_M q_M(z_j - h_g, t+\Delta t)+\left[1+2\alpha_M+\Delta t k_a c_L^* q_L(z_j, t+\Delta t)\right]q_M(z_j, t+\Delta t)$$

$$-\alpha_M q_M(z_j + h_g, t+\Delta t)=q_M(z_j, t)+\Delta t k_d \frac{c_{T,L}^*}{c_M^*}q_{T,L}(z_j, t+\Delta t)$$

$$-\Delta t k_d \frac{c_L^*}{c_M^*}q_L(z_j, t+\Delta t)$$

(SI-56)

- At $z = z_m = g^*$:

$$q_M(z_m, t+\Delta t)=1$$

(SI-57)

1.4.- Solution Procedure

The coupled system of non linear equations obtained in the previous section (**equations SI-34** to **SI-57**) will be solved separately for each species and time. The solution is obtained after iteration and convergence of the concentration of each species at each spatial position. This method allows a extremely huge

reduction of the computational time in comparison to the CPU time required for the direct solution of the non-linear system. Let us comment in more detail on the solution procedure.

The solution process begins by initializing the $m+n$ components of vectors $\vec{q}_{T,L}, \vec{q}_L, \vec{q}_M$ and $\vec{q}_R$ with the values reached at the previous time interval. The values of vectors $\vec{q}_{T,L}, \vec{q}_L, \vec{q}_M$ and $\vec{q}_R$ at $t+\Delta t$ are obtained iteratively. For $q_L(z_i, t+\Delta t)$, for example, the equations system **SI-45** - **SI-50** could be rewritten in a matrix from as,

$$
\begin{pmatrix}
-1 & 1 & & & & & \\
-\alpha_R & 1+2\alpha_R+\Delta t k_d c_M^* q_M(z_2,t+\Delta t)+\Delta t k_d & -\alpha_R & & & & \\
& & \ddots & \ddots & \ddots & & \\
& & -\alpha_R & 1+2\alpha_R+\Delta t k_d c_M^* q_M(z_i,t+\Delta t)+\Delta t k_d & -\alpha_R & & \\
& & & \ddots & \ddots & \ddots & \\
& & & -\sigma & \sigma+1 & 1 & \\
& & & & \ddots & \ddots & \ddots \\
& & & & -\alpha_R & 1+2\alpha_R+\Delta t k_d c_M^* q_M(z_j,t+\Delta t)+\Delta t k_d & -\alpha_R \\
& & & & & \ddots & \ddots \\
& & & & & & 1
\end{pmatrix}
\begin{pmatrix}
q_L(z_1,t+\Delta t) \\
q_L(z_2,t+\Delta t) \\
\vdots \\
q_L(z_i,t+\Delta t) \\
\vdots \\
q_L(z_n,t+\Delta t) \\
\vdots \\
q_L(z_j,t+\Delta t) \\
\vdots \\
q_L(z_m,t+\Delta t)
\end{pmatrix}
$$

$$
= \begin{pmatrix}
0 \\
q_L(z_2,t)+\Delta t k_d \dfrac{c_{TL}^*}{c_L^*} q_{TL}(z_2,t+\Delta t) \\
\vdots \\
q_L(z_i,t)+\Delta t k_d \dfrac{c_{TL}^*}{c_L^*} q_{TL}(z_i,t+\Delta t) \\
\vdots \\
0 \\
\vdots \\
q_L(z_j,t)+\Delta t k_d \dfrac{c_{TL}^*}{c_L^*} q_{TL}(z_j,t+\Delta t) \\
\vdots \\
1
\end{pmatrix}
$$

(SI-58)

This is a tridiagonal system for the unknowns $q_L(z_i, t+\Delta t)$ and it is solved iteratively through the TRIDAG.FOR subroutine.[3] Notice that this equation system for q_L, requires the values of $q_M(z_i, t+\Delta t)$ and $q_{T,L}(z_i, t+\Delta t)$ which are also unknowns. At iteration *j*, to uncouple $(q_M)_j$ and $(q_{T,L})_j$ from $(q_L)_j$, we use the values of both $(q_M(z_i, t+\Delta t))_{j-1}$ and $(q_{T,L}(z_i, t+\Delta t))_{j-1}$ obtained in the previous iteration (*j*-1) in the solution of $q_L(z_i, t+\Delta t)$ at some iteration *j*. This procedure is applied iteratively for each species until all the system converges to a solution for each time step. The time is then increased and the

first iteration for the next time starts initializing all the unknowns with the values obtained at the previous time.

Figure SI-3 shows schematically the algorithm used to solve the system
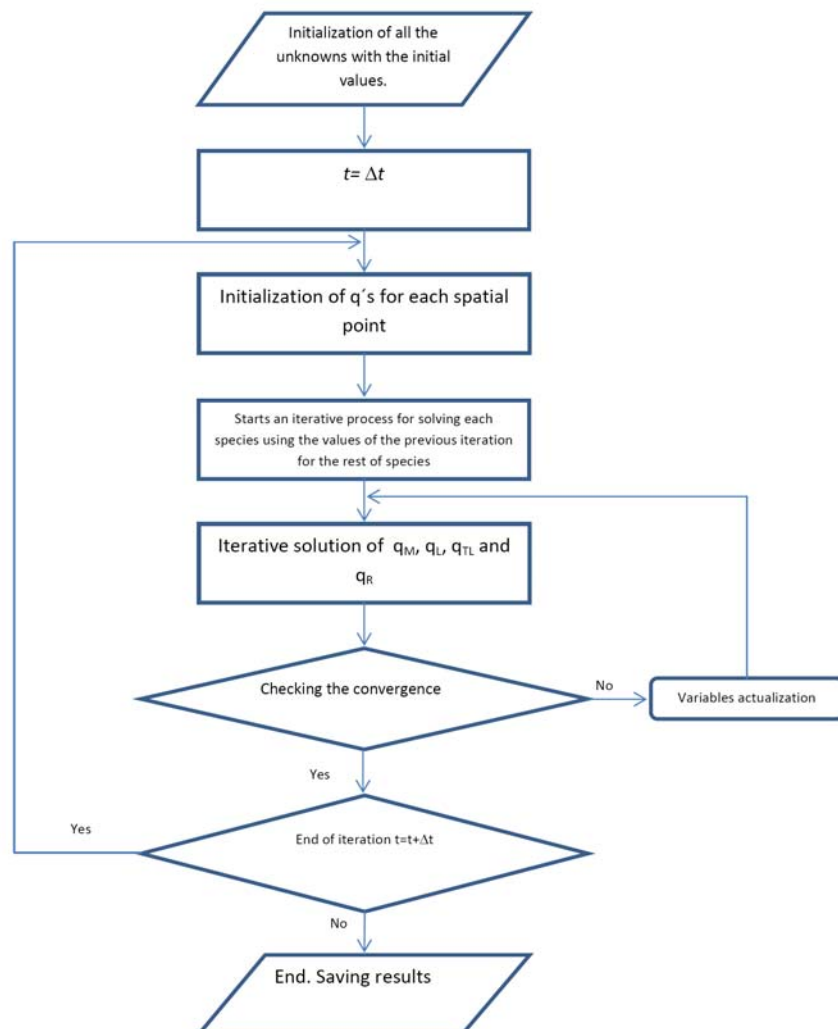
Figure SI-3 Flux diagram representing the algorithm used to solve the system

<u>Section 2:</u> Concentration profiles in a DGT experiment

Let us consider a DGT experiment using the numerical simulation described above. **Figure. SI-4** depicts the concentration profiles of metal and complex through the DGT layers and adjoining solution for different values of the kinetic complexation constants. With the parameters used in this figure, the metal concentration drops to almost zero at the resin interface due to the strong and fast resin binding. For low values of the dissociation rate constants (see panel a), the complex concentration profile is flat and equal to the complex concentration in solution, while the metal concentration profile is linear. This indicates the inert behaviour of the complex, which does not contribute to the flux received by DGT and the quasi-steady-state regime reached (the linear metal concentration profile indicates a time independent metal flux). On increasing the kinetic complexation constants (see panel b), the complex is depleted and its contribution to the metal flux through dissociation is apparent. Notice that the metal concentrations do not increase linearly with distance and their values at a given x are greater than those of the inert case, due to the complex dissociation contributing to a higher local metal concentration. A further increase of the kinetic constants leads to a more depleted complex concentration profile. Metal and complex concentration profiles increasingly coincide in the gel domain (see panel c). When both normalised profiles coincide, metal and complex are in local equilibrium, indicating that the complex is able to dissociate sufficiently rapidly to maintain equilibrium conditions with the metal. The thickness of the layer where both profiles diverge, can be related to the reaction layer. As expected, the thickness of the reaction layer decreases as the kinetic constants increase. Notice that at the interface between the resin and gel layers the slope of the complex concentration profile is not zero and the complex penetrates into the resin layer. The decrease in the complex concentration as the back plastic wall of the device is approached continues inside the resin, indicating that the dissociation process does not cease at the resin interface. A further increase of the kinetic constants (see panel d) leads to linear metal and complex concentration profiles superimposed throughout the entire gel domain. This corresponds to the labile situation where the dissociation of the complex is so fast that local equilibrium with the metal is reached at each relevant spatial and time position.

Results – Penetration effects of the complexes in the DGT resin layer
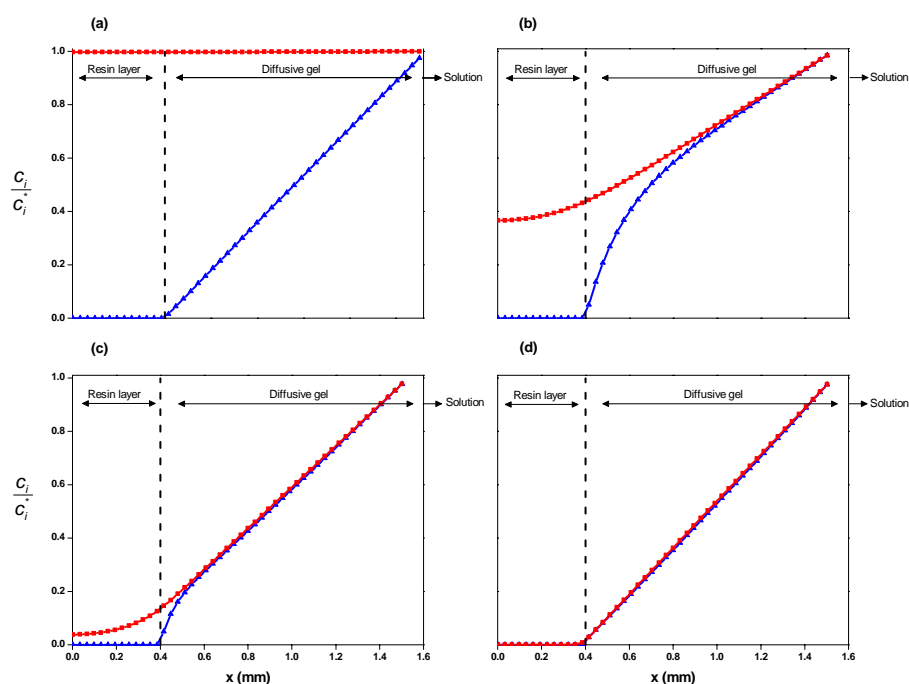
Figure SI-. Normalized concentration profiles of M (Blue line with ▲ markers) and ML (red line with ■ markers). Profiles are obtained by numerical simulation described in SI-1. Parameters: $r = 4 \times 10^{-4}$ m, $K = 10^2$ mol^{-1}·m^3·s^{-1}, panel a) $k_d = 10^{-6}$ s^{-1} panel b) $k_d = 10^{-3}$ s^{-1}, panel c) $k_d = 10^{-2}$ s^{-1} and panel d) $k_d = 10^{0}$ s^{-1}. The rest of parameters as in figure 1 of the manuscript.

<u>Section 3:</u> Experimental Section

- DGT sensors

All DGT sensors were purchased from DGT Research Ltd. (Lancaster, U.K.). Commercially available DGT deployment mouldings made of ABS polymer, based on a simple, tight-fitting piston design with a 2 cm diameter window, were used for all measurements. A 0.4 mm thick Chelex-gel was placed on the piston surface with the side packed with resin beads facing upward (i.e. in close contact with the diffusive layer). On the top of the Chelex-gel, a 0.8 mm thick diffusive agarose polyacrylamide gel and a cellulose nitrate membrane (Whatman, pore size 0.45 μm, thickness 0.125 mm) were placed. A more detailed description is found at DGT Research's homepage (http://www.dgtresearch.com).

- DGT Experiments

A series of experiments were performed to determine the mass of cadmium accumulated at different times by DGT devices deployed in solutions containing Cd (prepared from the solid nitrate product, Merck, analytical grade) at a concentration close to 10^{-2} mol·m^{-3} and NTA (Fluka, analytical grade) at concentrations of 0.249 and 1.8 mol·m^{-3} pH was adjusted by means of small additions of NaOH or HNO$_3$ to 7 or 7.5 before and during the deployment. Ionic strength of the solution was adjusted to 0.05 mol·L^{-1} with NaNO$_3$ (Merck, suprapur). Ultra-pure water (Mill-Q plus 185 System, Millipore) was employed in all the experiments.

- DGT Exposure Chamber

A 5L polyethylene bucket was used as the exposure chamber. 11 DGTs were fixed by press-stud. pH was monitored continuously with a glass electrode. A reference electrode Ag/AgCl/3 mol.L^{-1} KCl, with a 0.05 mol.L^{-1} NaNO$_3$ jacket was used. The exposure chamber was placed in a thermostated bath to keep the deployment solution at constant temperature of 25±0.1ºC. The solution was stirred during deployment using an overhead stirrer.

- Retrieval and analysis

For all experiments, aliquots of the solution were collected at regular intervals to check the total Cd concentration. DGT devices, once removed from solution, were rinsed with ultrapure water and opened for removal of the resin gels, which were then eluted in 1mL of concentrated nitric acid for at least 24h. The number of moles of metal in the form of non dissociated complex due to the complex penetration into the resin domain is negligible in comparison with those bound to the resin beads All solutions were analysed by inductively coupled plasma-optical emission spectroscopy (ICP-OES) (Activa-S, Horiba Scientific).

Section 4: Additional figures

Additional figures that verified the influence of the thickness of the DGT resin layer on the accumulated mass for the Cd-NTA system.

Conditional stability constants and kinetic parameters for the Cd NTA system at a given pH, ionic strength and total metal and total ligand concentration were estimated as reported in the manuscript. Values used in the numerical simulations for the kinetic association and dissociation constants of the metal to

the resin sites are $k_{a,R} = 10^{15}$ mol$^{-1} \cdot$m$^3 \cdot$s^{-1} and $k_{d,R} = 10^{-6} \cdot$s^{-1} while the total concentration of resin sites in the resin layer is $c_{T,R} = 50$ mol$^{-1} \cdot$m^3. These values are high enough to neglect saturation effects and to reach an almost null metal concentration at the resin interface.
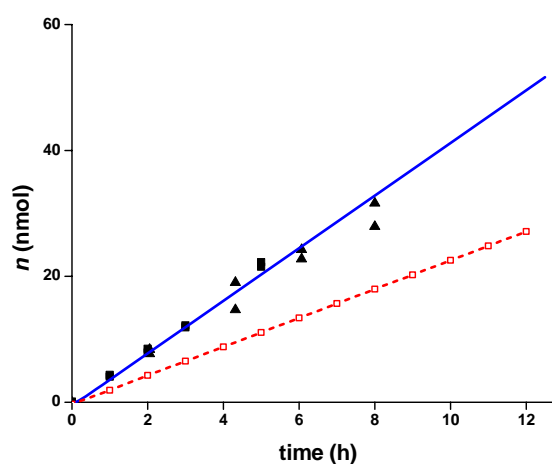
Figure SI-5. Moles of Cd accumulated by DGT in presence of NTA. Markers: experimental measurements, two deployments (■) and (▲). Blue continuous line: theoretical accumulation predicted by numerical simulation when penetration of the complex into the resin layer is considered ($r = 4 \times 10^{-4}$ m). Red dashed line with markers □: theoretical accumulation predicted by numerical simulation when penetration of the complex into the resin layer is not allowed (r = 0). Parameters: total NTA concentration $c_{T,NTA} = 0.249$ mol$\cdot$m^{-3}, total Cd concentration $c_{T,Cd} = 9.96 \times 10^{-3}$ mol$\cdot$m^{-3}, pH=7.03, I=0.05M, $k_a^{eff} = 8.77 \times 10^4$ m$^3 \cdot$mol$^{-1} \cdot$s^{-1} and $k_d = k_d^{eff} = k_a^{eff} / K_{CdNTA}^{eff} = 2.76$ s^{-1}. The rest of parameters as in figure 4 of the manuscript.
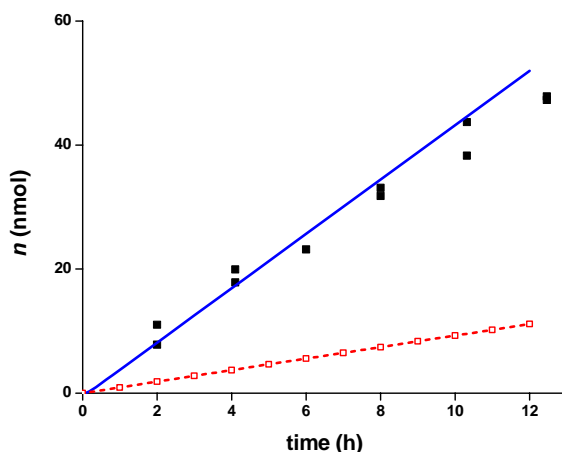
Figure SI-6. Moles of Cd accumulated by DGT in presence of NTA. Marker (■): experimental measurements. Blue continuous line: theoretical accumulation predicted by numerical simulation when penetration of the complex into the resin layer is considered ($r = 4\times10^{-4}$ m). Red line with markers □: theoretical accumulation predicted by numerical simulation when penetration of the complex into the resin layer is not allowed (r = 0). Parameters: total NTA concentration $c_{T,NTA} = 1.8$ mol·m^{-3}, total Cd concentration $c_{T,Cd} = 1.08\times10^{-2}$ mol·m^{-3}, pH=7.50,ionic strength 0.05M, $k_a^{eff} = 2.58\times10^5$ m^3·mol^{-1}·s^{-1} and $k_d = k_d^{eff} = k_a^{eff} / K_{CdNTA}^{eff} = 2.76$ s^{-1} . The rest of parameters as in figure 4 of the manuscript.

Section 5: Formulation of the Cd-NTA speciation in a DGT sensor as a system with only one complex and ligand species

NTA is involved in four acid-base equilibria. Among all these species only NTA^{3-} is known to interact with Cd to give the complex species CdNTA and Cd(NTA)$_2$. Thus only NTA^{3-} is the ligand in the Cd-NTA system. However, the concentration of NTA^{3-} is not only modified by the presence of Cd, but also by the pH of the system. The formulation of the Cd-NTA system as

$$ M + L \underset{k_{d,L}}{\overset{k_{a,L}}{\rightleftharpoons}} ML \qquad \textbf{(SI-59)} $$

with a fixed total ligand concentration, $c_{T,L}$, computed as $c_{T,L} = c_L + c_{M,L}$ is then not valid. It is the aim of this section of this supporting information to show

that the Cd-NTA system can be reformulated so that equations equivalent to the system represented with scheme **SI-60** can be applied.

Let us assume that

i) protonated and unprotonated NTA species have the same diffusion coefficient, D_L

ii) the kinetics of interconversion between the protonated/unprotonated NTA species is considered instantaneous (i.e. they are always at equilibrium), so that all the protonated and unprotonated species diffuse and react as one "single species".

A scheme of the processes in solution is:

$$
\begin{array}{c}
M + L \quad \underset{k_{d,L}}{\overset{k_{a,L}}{\rightleftharpoons}} \quad ML \\
+ \\
H \\
k_{d1,H} \uparrow\downarrow k_{a1,H} \\
HL \\
+ \\
H \\
k_{d2,H} \uparrow\downarrow k_{a2,H} \\
.... \\
H_4L
\end{array}
\tag{SI-60}
$$
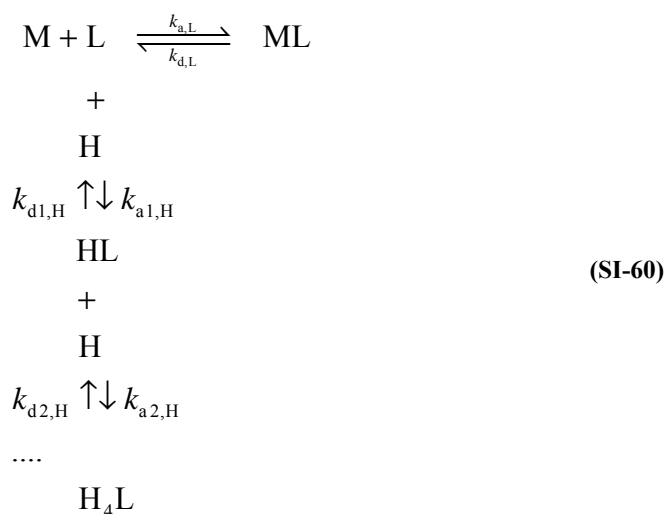
The transport problem can be stated as

$$
\frac{\partial c_M}{\partial t} = D_M \frac{\partial^2 c_M}{\partial x^2} + k_{d,L} c_{ML} - k_{a,L} c_M c_L
\tag{SI-61}
$$

$$
\frac{\partial c_{ML}}{\partial t} = D_L \frac{\partial^2 c_{ML}}{\partial x^2} - k_{d,L} c_{ML} + k_{a,L} c_M c_L
\tag{SI-62}
$$

$$\frac{\partial c_L}{\partial t} = D_L \frac{\partial^2 c_L}{\partial x^2} + k_{d,L} c_{M,L} - k_{a,L} c_M c_L + k_{d1,H} c_{HL} - k_{a1,H} c_H c_L \qquad \text{(SI-63)}$$

$$\frac{\partial c_{HL}}{\partial t} = D_L \frac{\partial^2 c_{HL}}{\partial x^2} + k_{d2,H} c_{H_2L} - k_{a2,H} c_H c_{HL} - k_{d1,H} c_{HL} + k_{a1,H} c_H c_L \qquad \text{(SI-64)}$$

…

$$\frac{\partial c_{H_4L}}{\partial t} = D_L \frac{\partial^2 c_{H_4L}}{\partial x^2} - k_{d4,H} c_{H_3L} + k_{a4,H} c_H c_{H_3L} \qquad \text{(SI-65)}$$

Adding the transport equations of all the protonated ligand forms (**equations SI-63 - SI-65**)

$$\frac{\partial c_{L,P}}{\partial t} = D_L \frac{\partial^2 c_{L,P}}{\partial x^2} + k_{d,L} c_{ML} - k_{a,L} c_M c_L \qquad \text{(SI-66)}$$

where $c_{L,P}$ stands for

$$c_{L,P} = c_L + c_{HL} + c_{H_2L} + c_{H_3L} + c_{H_4L} \qquad \text{(SI-67)}$$

Since protonation is instantaneous, acid-base equilibria relationship apply:

$$\beta_{i,H} = \frac{c_{H_iL}}{c_H^i \, c_L} \qquad \text{(SI-68)}$$

c_L can be rewritten as

$$c_L = \frac{c_{L,P}}{1 + \sum_{i=1}^{4} \beta_{i,H} c_H^i} \qquad \text{(SI-69)}$$

In terms of $c_{L,P}$, **equations SI-61**, **SI-62** and **SI-66** become

$$\frac{\partial c_M}{\partial t} = D_M \frac{\partial^2 c_M}{\partial x^2} + k_{d,L} c_{ML} - \frac{k_{a,L}}{1 + \sum_{i=1}^{4} \beta_{i,H} c_H^i} c_M c_{L,P} \tag{SI-70}$$

$$\frac{\partial c_{ML}}{\partial t} = D_L \frac{\partial^2 c_{ML}}{\partial x^2} - k_{d,L} c_{ML} + \frac{k_{a,L}}{1 + \sum_{i=1}^{4} \beta_{i,H} c_H^i} c_M c_{L,P} \tag{SI-71}$$

and

$$\frac{\partial c_{L,P}}{\partial t} = D_L \frac{\partial^2 c_{L,P}}{\partial x^2} + k_{d,L} c_{ML} - \frac{k_{a,L}}{1 + \sum_{i=1}^{4} \beta_{i,H} c_H^i} c_M c_{L,P} \tag{SI-72}$$

Equations. SI-70 - SI-72 are formally identical to a system with one ligand with concentration $c_{L,P}$, that is not involved in any protonation equilibria. The effective association and dissociation constants of this ligand with the metal are

$$k_d^{eff} = k_{d,L} \tag{SI-73}$$

and

$$k_a^{eff} = \frac{k_{a,L}}{1 + \sum_{i=1}^{4} \beta_{i,H} c_H^i} \tag{SI-74}$$

The effective stability constant of the metal complexation with this formal ligand $c_{L,P}$, of concentration given by **equation SI-67**, is

$$K^{eff} = \frac{k_a^{eff}}{k_d^{eff}} = \frac{K}{1 + \sum_{i=1}^{4} \beta_{i,H} c_H^i} \tag{SI-75}$$

Section 6: Parameter values in all the figures of the manuscript

Parameter		Fig. 1	Fig. 3	Fig. 3	Fig. 4	Units
Resin thickness	r			4×10^{-4}		m
Gel thickness	g	1.13×10^{-3}	1.13×10^{-3}		1.13×10^{-3}	m
Stability constant	K	10^{2}	10^{2}		10^{2}	mol^{-1}·m3
Association rate constant between M and L	k_{a}		10^{-1}		2.58×10^{5}	mol^{-1} m^{3} s^{-1}
Dissociation rate constant between M and L	k_{d}		10^{-3}		2.76	s^{-1}
Association rate constant between M and R	$k_{a,R}$	10^{15}	10^{15}	10^{15}	10^{15}	mol^{-1}·m^{3} s^{-1}
Dissociation rate constant between M and R	$k_{d,R}$	10^{-6}	10^{-6}	10^{-6}	10^{-6}	s^{-1}
Diffusion coefficient of M in resin and gel	D_{M} $D_{M,R}$	6.09×10^{-10}	6.09×10^{-10}	6.09×10^{-10}	6.09×10^{-10}	m^{2} s^{-1}
Diffusion coefficient of L in the resin and gel domains	D_{L} $D_{L,R}$	4.26×10^{-10} $D_{L,R}=D_{L}$	4.26×10^{-10} $D_{L,R}=D_{L}$		4.26×10^{-10} $D_{L,R}=D_{L}$	m^{2} s^{-1}
Diffusion coefficients of ML in resin and gel	D_{ML} $D_{ML,R}$	4.26×10^{-10} $D_{ML,R}=D_{ML}$	4.26×10^{-10} $D_{ML,R}=D_{ML}$		4.26×10^{-10} $D_{ML,R}=D_{ML}$	m^{2} s^{-1}
Total concentration of M	$c_{T,M}$	0.01	0.01		1.08×10^{-2}	mol m^{-3}
Total concentration of L	$c_{T,L}$	0.249	0.249		0.249	mol m^{-3}
Total concentration of R	$c_{T,R}$	50	50	50	50	mol m^{-3}
Ionic strength	I			0.05	0.05	M
pH					7.50	

Table SI-1

All simulations in this manuscript were calculated with a spatial grid of 2000 points and a time interval $\Delta t = 0.1$ s.

Literature cited

(1)   Lehto, N. J.; Davison, W.; Zhang, H.; Tych, W., An evaluation of DGT performance using a dynamic numerical model. *Environmental Science & Technology* **2006,** *40*, (20), 6368-6376.

(2)   Tusseau-Vuillemin, M. H.; Gilbin, R.; Taillefert, M., A dynamic numerical model to characterize labile metal complexes collected with diffusion gradient in thin films devices. *Environmental Science & Technology* **2003,** *37*, (8), 1645-1652.

(3)   Press, W. H.; Flannery, B. P.; Teukolsky, S. A.; Vetterling, W. T., *Numerical Recipes*. Cambridge University Press: Cambridge, **1986**.

8.2 Contribution of Partially Labile Complexes to the DGT Metal Flux

Contribution to the Partially Labile Complexes to the DGT Metal Flux

Abstract

Penetration of complexes into the resin layer can dramatically increase the contribution of complexes to the metal flux measured with a DGT (diffusive gradients in thin films) sensor, but equations to describe this phenomenon were not available. Here, simple approximate analytical expressions for the metal flux, the lability degree and the concentration profiles in a DGT experiment are reported. Together with the thickness of the reaction layer in the gel domain, the effective penetration distance into the resin layer that would be necessary for full dissociation of the complex (λ_{ML}) plays a key role in determining the metal flux. An increase in the resin-layer thickness (r) effectively increases the metal flux and the lability degree until $r \approx 3\lambda_{ML}$. For the usual DGT configuration, where the thickness of the gel layer exceeds that of the resin layer, the complex is labile if $r > (D_{ML}/k_d)^{1/2}$, where D_{ML} is the diffusion coefficient of the metal complex and k_d its dissociation rate constant. A general procedure for estimating the lability of any complex in a standard DGT configuration is provided.

Contribution of partially labile complexes to the DGT metal flux

SUPPORTING INFORMATION

Section 1: Steady state approximate analytical solution for the metal flux, lability degree and concentration profiles under typical DGT conditions in systems with dynamic complexes

Section 2: Additional figures and tables

Section 3: Metal Flux and Lability degree when the diffusion domain extends into the solution phase

Section 1: Steady state approximate analytical solution for the metal flux, lability degree and concentration profiles under typical DGT conditions in systems with dynamic complexes

1.1.- The Model

We make the following assumptions. i) There is fast and strong free metal ion binding by the resin, so that the free metal concentration inside the resin layer is negligible.

ii) Saturation effects of the resin are negligible, i.e. there is a large excess of resin sites (R) with respect to the metal bound (MR) throughout the deployment time of interest.

iii) Free metal (M) interacts with the ligand (L) to form a complex (ML) and there is an excess of ligand with respect to metal in solution, so that the free ligand concentration can be taken as constant regardless of ML formation.

iv) The complex can penetrate and diffuse within the resin layer, where its dissociation still applies. Thus, the complex inside the resin layer acts as a source of free metal that then becomes bound to the resin.

Under these conditions, the system reaches a quasi steady state in which any free metal, M, arriving in the resin layer being instantaneously bound to the resin and the complex arriving in the resin layer being consumed by dissociation, with the resulting free metal binding to the resin. We aim to find an analytical solution for the metal flux, lability degree and concentration profiles corresponding to this steady state. Limiting cases are those corresponding to a negligible dissociation (inert complex) or to a sufficiently rapid dissociation so that local equilibrium conditions apply everywhere (fully labile complex). In this last case, the complex fully dissociates at the resin-layer surface, in agreement with the metal concentration being effectively zero at this location. Another limiting case is that of the resin layer being so thin ($r=0$) that metal consumption effectively occurs at a surface.

1.2.- Diffusion-reaction conditions in the resin layer

With the above conditions, the diffusion equations for the resin layer explicitly reported in SI of Mongin et al.[1] can be greatly simplified.:

An effective zero concentration of metal in the resin layer.

$$c_{\mathrm{M}}(0 < x \le r) = 0 \tag{SI-1}$$

The diffusion of complex in the resin layer is described by

$$\frac{d^2 c_{\mathrm{ML}}}{dx^2} = \frac{k_{\mathrm{d}}}{D_{\mathrm{ML}}} c_{\mathrm{ML}} = \frac{c_{\mathrm{ML}}}{\lambda_{\mathrm{ML}}{}^2} \qquad 0 < x \le r \tag{SI-2}$$

with

$$\lambda_{\mathrm{ML}} = \sqrt{\frac{D_{\mathrm{ML}}}{k_{\mathrm{d}}}} = \sqrt{\varepsilon K'} \, \mu \tag{SI-3}$$

λ_{ML} has dimensions of a distance and can be seen as a "penetration parameter" related to the distance required for a complex diffusing into the resin layer to dissociate fully. See section 3.3 of the manuscript and section 1.7 of this SI, for a more detailed physical interpretation.

The general solution of **equation SI-2** can then be written as

$$c_{\mathrm{ML}}\left(x \le r\right) = A e^{\frac{x}{\lambda_{\mathrm{ML}}}} + B e^{-\frac{x}{\lambda_{\mathrm{ML}}}} \tag{SI-4}$$

where A and B are integration constants that have to fulfil the boundary value problem

$$\left(\frac{dc_{\mathrm{ML}}}{dx}\right)_{x=0} = 0 \tag{SI-5}$$

and

$$\left(\frac{dc_{\mathrm{ML}}}{dx}\right)_{x=r^-} = \left(\frac{dc_{\mathrm{ML}}}{dx}\right)_{x=r^+} \tag{SI-6}$$

which implicitly assumes a common complex diffusion coefficient both in the resin and gel layers.

The application of **equation SI-5** in **equation SI-4** leads to *A=B*, so that the solution can be rewritten as

$$c_{\mathrm{ML}}\left(x \le r\right) = c_{\mathrm{ML}}\left(x = 0\right) \cosh\left(\frac{x}{\lambda_{\mathrm{ML}}}\right) \tag{SI-7}$$

Labelling as c_{ML}^r, the complex concentration at the frontier between the resin and diffusion layer ($x=r$), gives

$$c_{ML}^r = c_{ML}(x=r) = c_{ML}(x=0)\cosh\left(\frac{r}{\lambda_{ML}}\right) \qquad \textbf{(SI-8)}$$

the complex concentration profile inside the resin layer becomes

$$c_{ML}(x \le r) = c_{ML}^r \frac{\cosh\left(\dfrac{x}{\lambda_{ML}}\right)}{\cosh\left(\dfrac{r}{\lambda_{ML}}\right)} \qquad \textbf{(SI-9)}$$

The application of **equation SI-7** requires knowledge of the flux of complex entering the resin layer, calculated from the resin side. From **equation SI-9**, it becomes

$$J_{ML} = D_{ML}\left(\frac{dc_{ML}}{dx}\right)_{x=r} = D_{ML}\frac{c_{ML}^r}{\lambda_{ML}}\tanh\left(\frac{r}{\lambda_{ML}}\right) = k_d c_{ML}^r \lambda_{ML}\tanh\left(\frac{r}{\lambda_{ML}}\right) \qquad \textbf{(SI-10)}$$

1.3.- Diffusion reaction conditions in the gel layer

In the gel layer, steady state conditions for M and ML apply

$$0 = D_M\frac{d^2 c_M}{dx^2} - k_a' c_M + k_d c_{ML} \qquad \textbf{(SI-11)}$$

$$0 = D_{ML}\frac{d^2 c_{ML}}{dx^2} + k_a' c_M - k_d c_{ML} \qquad \textbf{(SI-12)}$$

An equivalent system of equations to that given by **equations SI-11** and **SI-12** is

$$0 = \frac{d^2}{dx^2}\left(D_M c_M + D_{ML} c_{ML}\right) \qquad \textbf{(SI-13)}$$

$$0 = \frac{d^2}{dx^2}\left(c_{ML} - K' c_M\right) - \left(\frac{k_d}{D_{ML}} + \frac{k_a'}{D_M}\right)\left(c_{ML} - K' c_M\right) \qquad \textbf{(SI-14)}$$

which has the advantage of allowing the uncoupling of the system.

Equation SI-13 is just the addition of **equations SI-11** and **SI-12**. Its integration yields

$$D_{\mathrm{M}} c_{\mathrm{M}} + D_{\mathrm{ML}} c_{\mathrm{ML}} = D_{\mathrm{ML}} c_{\mathrm{ML}}^{r} + \frac{\left(D_{\mathrm{M}} c_{\mathrm{M}}^{*} + D_{\mathrm{ML}} c_{\mathrm{ML}}^{*} \right) - D_{\mathrm{ML}} c_{\mathrm{ML}}^{r}}{g} \left(x - r \right) \quad \textbf{(SI-15)}$$

Equation SI-14 constitutes a closed equation for

$$\phi = c_{\mathrm{ML}} - K' c_{\mathrm{M}} \tag{SI-16}$$

We introduce now a new parameter *m*, with dimensions of distance, which could be called a "disequilibration" parameter. It is related to the thickness of the gel layer where M and ML are not in equilibrium and can be seen as an extension of the reaction layer for this particular problem. See section 3.3 of the manuscript and below, in section 1.8 of this SI, for a more detailed physical interpretation.

$$\frac{1}{m^2} = \frac{k_{\mathrm{d}}}{D_{\mathrm{ML}}} + \frac{k_{\mathrm{a}}'}{D_{\mathrm{M}}} = \frac{1}{\lambda_{\mathrm{ML}}^2} + \frac{1}{\mu^2} = \frac{1}{\mu^2} \left(\frac{1 + \varepsilon K'}{\varepsilon K'} \right) \tag{SI-17}$$

where μ is the classical definition of reaction layer introduced by Koutecky in planar semi-infinite diffusion[2]:

$$\mu = \sqrt{\frac{D_{\mathrm{M}}}{k_{\mathrm{a}}'}} \tag{SI-18}$$

Thus, **equation SI-14** can be rewritten as

$$\frac{d^2}{dx^2} \phi = \frac{\phi}{m^2} \tag{SI-19}$$

whose general solution is

$$\phi = A \sinh \left(\frac{g + r - x}{m} \right) + B \cosh \left(\frac{g + r - x}{m} \right) \tag{SI-20}$$

where *A* and *B* are integration constants.

The boundary conditions are given by

$$\phi \left(x = g + r \right) = 0 \tag{SI-21}$$

$$\phi \left(x = r \right) = c_{\mathrm{ML}}^{r} \tag{SI-22}$$

which indicate that $B=0$ and $A = \dfrac{c_{ML}^r}{\sinh(g/m)}$, so that

$$\phi = c_{ML}^r \frac{\sinh\big((g+r-x)/m\big)}{\sinh(g/m)} \qquad \text{(SI-23)}$$

The derivative of ϕ in $x=r$

$$\left(\frac{d\phi}{dx}\right)_{x=r} = -\frac{c_{ML}^r}{m}\coth\left(\frac{g}{m}\right) = \left(\frac{dc_{ML}}{dx}\right)_{x=r} - K'\left(\frac{dc_M}{dx}\right)_{x=r} \qquad \text{(SI-24)}$$

and that of **equation SI-15**

$$D_M\left(\frac{dc_M}{dx}\right)_{x=r} + D_{ML}\left(\frac{dc_{ML}}{dx}\right)_{x=r} = \frac{\big(D_M c_M^* + D_{ML} c_{ML}^*\big) - D_{ML} c_{ML}^r}{g} \qquad \text{(SI-25)}$$

allows the flux of ML entering into the resin layer, calculated from the diffusive gel side, to be written as

$$J_{ML} = D_{ML}\left(\frac{dc_{ML}}{dx}\right)_{x=r} = \frac{-D_{ML}\,g\,c_{ML}^r\coth(g/m)/m + \varepsilon K'\big(D_M c_M^* + D_{ML} c_{ML}^* - D_{ML} c_{ML}^r\big)}{g\big(1+\varepsilon K'\big)} \qquad \text{(SI-26)}$$

The continuity of the flux requires the equality of J_{ML} calculated from **equation SI-26** and from **equation SI-10**, as stated in **equation SI-7**. The fulfilment of condition **SI-7** can then be used to isolate c_{ML}^r so that

$$c_{ML}^r = \frac{c_{ML}^*\big(1+\varepsilon K'\big)}{\varepsilon K' + \dfrac{g}{m}\coth\left(\dfrac{g}{m}\right) + \dfrac{g}{\lambda_{ML}}\big(1+\varepsilon K'\big)\tanh\dfrac{r}{\lambda_{ML}}} \qquad \text{(SI-27)}$$

1.4.- Metal flux

Under steady state conditions, the metal flux bound to the resin layer, *J*, is the total metal flux entering the resin layer both as free metal and complex,

$$J = D_M\left(\frac{dc_M}{dx}\right)_{x=r} + D_{ML}\left(\frac{dc_{ML}}{dx}\right)_{x=r} \qquad \text{(SI-28)}$$

and due to the linearity of the profile of $D_M c_M + D_{ML} c_{ML}$ in the gel layer (as given by **equation SI-15**),

$$J = D_{\mathrm{M}} \frac{c_{\mathrm{M}}^*}{g} + D_{\mathrm{ML}} \frac{c_{\mathrm{ML}}^* - c_{\mathrm{ML}}^r}{g} \qquad \textbf{(SI-29)}$$

which, using **equation SI-27**, becomes

$$J = D_{\mathrm{M}} \frac{c_{\mathrm{M}}^*}{g} + D_{\mathrm{ML}} \frac{c_{\mathrm{ML}}^*}{g} \left(1 - \frac{1 + \varepsilon K'}{\varepsilon K' + \dfrac{g}{m} \coth\left(\dfrac{g}{m}\right) + \dfrac{g}{\lambda_{\mathrm{ML}}} \left(1 + \varepsilon K'\right) \tanh \dfrac{r}{\lambda_{\mathrm{ML}}}} \right) \qquad \textbf{(SI-30)}$$

1.5.- Lability degree

For a labile case, full dissociation of the complex at the resin-gel interface is reached, $c_{\mathrm{ML}}^r = 0$ and according to **equation SI-25**, the metal flux bound to the resin becomes

$$J_{\mathrm{labile}} = \frac{D_{\mathrm{M}} c_{\mathrm{M}}^*}{g} + \frac{D_{\mathrm{ML}} c_{\mathrm{ML}}^*}{g} \qquad \textbf{(SI-31)}$$

In the opposite case, when the complex is inert, it does not contribute at all to the metal flux, $c_{\mathrm{ML}}^r = c_{\mathrm{ML}}^*$ and the metal flux bound to the resin is just due to the diffusion of the free metal present in the system

$$J_{\mathrm{free}} = J_{\mathrm{inert}} = \frac{D_{\mathrm{M}} c_{\mathrm{M}}^*}{g} \qquad \textbf{(SI-32)}$$

The lability degree, defined as

$$\xi = \frac{J - J_{\mathrm{free}}}{J_{\mathrm{labile}} - J_{\mathrm{free}}} \qquad \textbf{(SI-33)}$$

can, then, be written as

$$\xi = 1 - \frac{c_{\mathrm{ML}}^r}{c_{\mathrm{ML}}^*} \qquad \textbf{(SI-34)}$$

or

$$\xi = 1 - \frac{1 + \varepsilon K'}{\varepsilon K' + \dfrac{g}{m} \coth\left(\dfrac{g}{m}\right) + \dfrac{g}{\lambda_{\mathrm{ML}}} \left(1 + \varepsilon K'\right) \tanh \dfrac{r}{\lambda_{\mathrm{ML}}}} \qquad \textbf{(SI-35)}$$

or

$$\xi = 1 - \frac{1+\varepsilon K'}{\varepsilon K' + \dfrac{g\sqrt{1+\varepsilon K'}}{\mu\sqrt{\varepsilon K'}}\coth\left(\dfrac{g\sqrt{1+\varepsilon K'}}{\mu\sqrt{\varepsilon K'}}\right) + \dfrac{g\left(1+\varepsilon K'\right)}{\mu\sqrt{\varepsilon K'}}\tanh\dfrac{r}{\mu\sqrt{\varepsilon K'}}} \quad \textbf{(SI-36)}$$

Equation SI-36 allows recovery of $\xi = 1$ or $\xi = 0$ for the labile or inert limits by taking $\mu \to 0$ or $\mu \to \infty$, respectively.

The maximum ξ that can exhibit a complex in a DGT for a given $g \gg m$ will be obtained for a thick enough resin ($r \gg \mu\sqrt{\varepsilon K'}$) and is given by

$$\xi = 1 - \frac{1+\varepsilon K'}{\varepsilon K' + \dfrac{g\sqrt{1+\varepsilon K'}}{\mu\sqrt{\varepsilon K'}} + \dfrac{g\left(1+\varepsilon K'\right)}{\mu\sqrt{\varepsilon K'}}} \quad \textbf{(SI-37)}$$

In the other limit, $r \to 0$, ξ given by **SI-36** reverts to the case of ML not penetrating into the resin layer, equation 22 in Salvador et al.[3].

1.6.- Concentration profiles

As stated by **equations SI-1** and **SI-9**, in the resin layer $c_M(0 < x \le r) = 0$ and

$$c_{ML}(x \le r) = \frac{c^*_{ML}\left(1+\varepsilon K'\right)}{\varepsilon K' + \dfrac{g}{m}\coth\left(\dfrac{g}{m}\right) + \dfrac{g}{\lambda_{ML}}\left(1+\varepsilon K'\right)\tanh\dfrac{r}{\lambda_{ML}}} \times \frac{\cosh\left(\dfrac{x}{\lambda_{ML}}\right)}{\cosh\left(\dfrac{r}{\lambda_{ML}}\right)} \quad \textbf{(SI-38)}$$

where **equation SI-27** has been used.

In the gel layer, **equations SI-15** and **SI-23** can be combined to obtain c_M and c_{ML} so that

$$c_M(r < x \le r+g) = \frac{\left(c^*_M + \varepsilon c^*_{ML}\right) - \varepsilon c^r_{ML}}{g\left(1+\varepsilon K'\right)} - \frac{\varepsilon c^r_{ML}\sinh\left((g+r-x)/m\right)}{\left(1+\varepsilon K'\right)\sinh\left(g/m\right)} \quad \textbf{(SI-39)}$$

and

$$c_{ML}(r < x \le r+g) = \frac{K'\left(c^*_M + \varepsilon c^*_{ML}\right) - \varepsilon c^r_{ML}}{g\left(1+\varepsilon K'\right)} + \frac{\varepsilon c^r_{ML}\sinh\left((g+r-x)/m\right)}{\left(1+\varepsilon K'\right)\sinh\left(g/m\right)} \quad \textbf{(SI-40)}$$

with c_{ML}^r given by **equation SI-27**.

1.7.- Physical Meaning of the penetration parameter

The complex concentration profile inside the resin layer is given by equation **SI-9**.

The derivative of this profile at $x=r$ is then

$$\frac{dc_{\mathrm{ML}}(x=r)}{dx} = \frac{c_{\mathrm{ML}}^r}{\lambda_{\mathrm{ML}}}\tanh\left(\frac{r}{\lambda_{\mathrm{ML}}}\right) \tag{SI-41}$$

To find an effective distance of penetration of the complex into the resin layer, we can represent the complex profile inside the resin by a straight line that is a tangent to the complex concentration profile where it coincides at $x=r$. The equation for this straight line is

$$c_{\mathrm{ML}}(x) - c_{\mathrm{ML}}(x=r) = \frac{c_{\mathrm{ML}}^r}{\lambda_{\mathrm{ML}}}\tanh\left(\frac{r}{\lambda_{\mathrm{ML}}}\right)(x-r) \tag{SI-42}$$

The effective penetration for the complex can be found by just requiring that $c_{\mathrm{ML}}(x)$, as given by **equation SI-42**, is zero. With this condition, and recalling **SI-27** for $c_{\mathrm{ML}}(x=r)$, x becomes

$$x = r - \lambda_{\mathrm{ML}}\coth\left(\frac{r}{\lambda_{\mathrm{ML}}}\right) \tag{SI-43}$$

For $r \gg \lambda_{\mathrm{ML}}$, $\coth\left(\frac{r}{\lambda_{\mathrm{ML}}}\right) \approx 1$ and, then

$$x = r - \lambda_{\mathrm{ML}} \tag{SI-44}$$

so that, in this case, λ_{ML} is a quantification of the distance of penetration of the complex before falling to zero concentration by dissociation.

1.8.- Physical Meaning of the disequilibration parameter m

Inside the gel layer, moving towards decreasing x-values, the concentration profiles of both metal and complex decrease due to the consumption of the metal at the resin phase. At long distances from the resin layer, the dissociation of the complex is sufficiently fast to allow local equilibrium with the metal. However,

as the resin-layer is approached, there is a distance where dissociation is not fast enough to reach equilibrium with the metal. In this region, $\phi = c_{ML} - K'c_M$ starts to increase. Let us obtain the effective thickness of this reaction layer or disequilibration layer. This thickness will be obtained by assuming that ϕ is a straight line that passes trough $(x = r, \phi(x = r))$ and the "effective" thickness will be given by the distance necessary for ϕ to drop to zero.

The slope of this straight line is given by **equation SI-24**:

$$\left(\frac{d\phi}{dx}\right)_{x=r} = -\frac{c_{ML}^r}{m}\coth\left(\frac{g}{m}\right) \tag{SI-45}$$

so that the eqn. for the straight line is

$$\phi - \phi(x = r) = -\frac{c_{ML}^r}{m}\coth\left(\frac{g}{m}\right)(x - r) \tag{SI-46}$$

and, recalling that $\phi(x = r) = c_{ML}^r$ (see **equation SI-22**), the x-value that corresponds to $\phi = 0$ is

$$x = r + m\tanh\left(\frac{g}{m}\right) \tag{SI-47}$$

Thus the disequilibration layer in the gel domain has an effective thickness given by $m\tanh\left(\frac{g}{m}\right)$. When $g \gg m$, $\tanh\left(\frac{g}{m}\right) \approx 1$ and the effective thickness of the disequilibration layer is given by m.

1.9.- Condition for fully labile behaviour when εK'>>1

We now focus on the case of interest $\varepsilon K'>1$ $\left(\sqrt{\varepsilon K'} > 1\right)$ and $g > r$ (typical standard DGT sensor). In general, $\lambda_{ML} > m$ since $\lambda_{ML} = \sqrt{1 + \varepsilon K'}\,m$ (see **equation SI-3**). Then, if $r > \lambda_{ML}$, we have $g > r > \lambda_{ML} > m$, so that $g > m$. Also, when $\varepsilon K'>1$, $m \approx \mu$ as can be seen from **equation SI-17**.

Let us apply the condition $r > \lambda_{ML}$ to **equation SI-35**. If $r > \lambda_{ML}$ and $g > m$, $\tanh\left(\frac{r}{\lambda_{ML}}\right) \approx 1$ and $\coth\left(\frac{g}{m}\right) \approx 1$ so that **equation SI-35** becomes

$$\xi = 1 - \cfrac{1}{1 + \cfrac{1}{\varepsilon K^{'}}\cfrac{g}{m} + \cfrac{g}{\lambda_{ML}}} \tag{SI-48}$$

Recalling that $m \approx \mu$ and $\lambda_{ML} \approx \sqrt{\varepsilon K^{'}}\,\mu$ (see **equation SI-3**), **equation SI-48** becomes

$$\xi = 1 - \cfrac{1}{1 + \cfrac{g}{\lambda_{ML}}\left(\cfrac{1}{\sqrt{\varepsilon K^{'}}} + 1\right)} \approx 1 - \cfrac{1}{1 + \cfrac{g}{\lambda_{ML}}} \approx 1 - \cfrac{\lambda_{ML}}{g} \approx 1 \tag{SI-49}$$

whenever $\left(\sqrt{\varepsilon K^{'}} > 1\right)$ as assumed above.

Thus, the condition $r > \lambda_{ML}$ when $\left(\sqrt{\varepsilon K^{'}} > 1\right)$ and $g > r$ (typical standard DGT sensor).

1.10.- Accuracy of the analytical expressions for the metal flux and lability degree

Figures SI-1 and **SI-2** show an increase in both the flux received by the resin and the lability degree as the kinetic complexation constants increase. In both figures, analytical results of expressions **SI-30** and **SI-35** superimpose with the rigorous numerical results (computed with the code detailed in Mongin et al.[1]), indicating the accuracy of these approximate analytical expressions.

Figures SI-1 and **SI-2** also depict (see discontinuous line) the flux and the lability degree of a complex that is unable to penetrate into the resin layer while the surface of the resin layer acts as a perfect sink for the metal. These values have been computed with **equations SI-30** and **SI-35** using $r=0$, which coincide with equations 14 and 22 in Salvador et al.[3] that were developed for a planar voltammetric sensor and an electroinactive complex under diffusion limited conditions. As can be seen in the figures, **equations SI-30** and **SI-35** reproduce with good accuracy the numerical simulation results, indicating that the penetration of the complex into the resin layer increases both the metal flux and the lability degree of the complex. The analytical expressions **SI-30** and **SI-35** can, then, be used with good accuracy to predict the metal flux or the lability degree of a complex in a DGT sensor whenever the binding of the corresponding metal to the resin is fast enough for the metal concentration in the resin layer to be negligible.

<u>Section 2:</u> Additional figures and tables
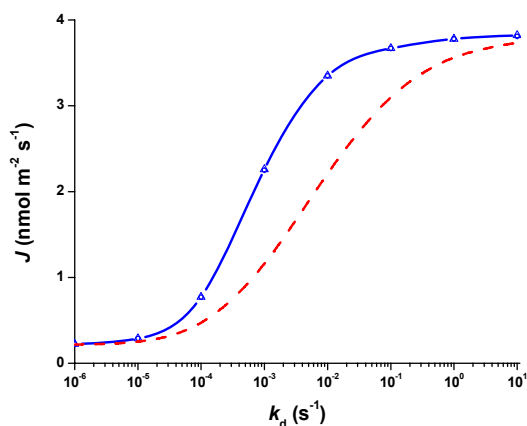
Figure SI-1. Metal flux received by the DGT sensor vs. the dissociation constant of the complex (k_d). Markers: values of J obtained by numerical simulation at 4 (□), 7 (Δ) and 15 (◊) hours (superimposed). Blue continuous line: Values obtained from the analytical expression given by equation SI-30. Red dashed line: Metal flux from equation SI-30 with $r=0$. Remaining parameters: $K=10^2$ m^3·mol^{-1}; g=1.13×10^{-3} m; $D_M=D_{M,R}=6.09\times10^{-10}$ m^2·s^{-1}; $D_L=D_{L,R}=4.26\times10^{-10}$ m^2·s^{-1}; $c_{T,M}=0.01$ mol·m^{-3}; $c_{T,M}=0.249$ mol·m^{-3};$k_{a,R}=10^{15}$ m^3 mol^{-1}·s^{-1}; $k_{d,R}=10^{-6}$ s^{-1} and $c_{T,R}=50$ mol·m^{-3}.
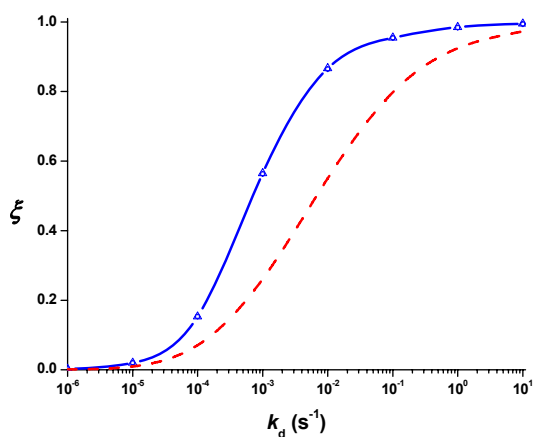
Figure SI-2. Lability degree of a complex in terms of k_d / s^{-1} (k_d). Markers: values of ξ obtained by numerical simulation at 4 (□), 7 (Δ) and 15 (◊) hours (superimposed). Blue continuous line: Values obtained from the analytical expression given by equation SI-35. Red dashed line: lability from equation SI-35 with $r=0$. Remaining parameters: $K=10^2$ m^3·mol^{-1}; g=1.13×10^{-3} m; $D_M=D_{M,R}=6.09\times10^{-10}$ m^2·s^{-1}; $D_L=D_{L,R}=4.26\times10^{-10}$ m^2·s^{-1}; $c_{T,M}=0.01$ mol·m^{-3}; $c_{T,M}=0.249$ mol·m^{-3};$k_{a,R}=10^{15}$ m^3 mol^{-1}·s^{-1}; $k_{d,R}=10^{-6}$ s^{-1} and $c_{T,R}=50$ mol·m^{-3}.

Results – Penetration effects of the complexes in the DGT resin layer
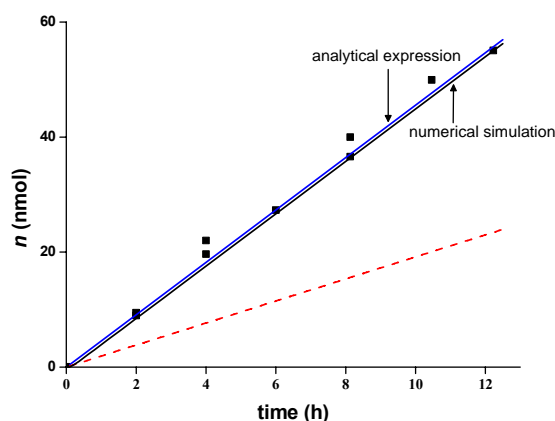
Figure SI-3. Moles of Cd accumulated in a DGT in presence of NTA for pH=7.5, total NTA concentration 0.249 mol·m^{-3} and total Cd concentration 1.08×10^{-2} mol·m^{-3}. Markers (■): experimental measurements. Black line: theoretical accumulation predicted from numerical simulation when there is penetration of the complex into the resin layer (r=4×10^{-4} m). Blue line: theoretical accumulation predicted from the approximate analytical expression SI-30 with r=4×10^{-4} m. Red line: theoretical accumulation predicted with SI-30 and r=0. Parameters: I=0.05M; k_a^{eff}=2.58×10^5 m^3·mol^{-1}·s^{-1}; $k_d = k_d^{eff} = k_a^{eff} / K_{CdNTA}^{eff} = 2.76 s^{-1}$; g=1.13×10^{-3} m; D_M=$D_{M,R}$=6.09×10^{-10} m^2·s^{-1}; D_L=$D_{L,R}$=4.26×10^{-10} m^2·s^{-1}; $k_{a,R}$=10^{15} m^3·mol^{-1}·s^{-1}; $k_{d,R}$=10^{-6} s^{-1} and $c_{T,R}$=50 mol·m^{-3}.

Figure SI-4. Moles of Cd accumulated in a DGT in presence of NTA for pH=7.5, total NTA concentration 1.8 mol·m^{-3} and total Cd concentration 1.08×10^{-2} mol·m^{-3}. Markers (■): experimental measurements. Black line: theoretical accumulation predicted from numerical simulation when there is penetration of the complex into the resin layer (r=4×10^{-4} m). Blue line: theoretical accumulation predicted from the approximate analytical expression SI-30 with r=4×10^{-4} m. Red line: theoretical accumulation predicted with SI-30 and r=0. Parameters: I=0.05M; k_a^{eff}=2.58×10^5 m^3·mol^{-1}·s^{-1}; $k_d = k_d^{eff} = k_a^{eff} / K_{CdNTA}^{eff} = 2.76 s^{-1}$; g=1.13×10^{-3}m; D_M=$D_{M,R}$=6.09×10^{-10}m^2·s^{-1}; D_L=$D_{L,R}$=4.26×10^{-10} m^2·s^{-1}; $k_{a,R}$=10^{15} m^3·mol^{-1}·s^{-1}; $k_{d,R}$=10^{-6} s^{-1} and $c_{T,R}$=50 mol·m^{-3}.

Figure SI-5. Dependence of the lability degree on the thickness of the resin layer. Markers: Blue triangles indicate values from numerical simulation as described in Mongin et al.[1] Blue continuous line depicts the values from the analytical expression SI-35. Red dashed line stands for ξ given by equation SI-35 with $r = 0$. Red dotted line stands for ξ from equation SI-35 with thickness of the gel domain given by g'=g + r and no penetration inside the resin. Parameters: total NTA concentration $c_{T,NTA}$=0.249 mol·m^{-3}; total Cd concentration $c_{T,Cd}$=9.96×10^{-3} mol m^{-3}; pH=7.03; ionic strength 0.05 M; T=25ºC; k_a^{eff}=8.77×10^4 m^3·mol^{-1}·s^{-1}; k_d=2.76×10^{-1} s^{-1}; g=1.13×10^{-3} m; D_M=6.09×10^{-10} m^2·s^{-1}; D_{ML}=4.26×10^{-10} m^2·s^{-1}; $k_{a,R}$=10^{15} m^3·mol^{-1}·s^{-1}; $k_{d,R}$=10^{-6} s^{-1} and $c_{T,R}$=50 mol·m^{-3}.
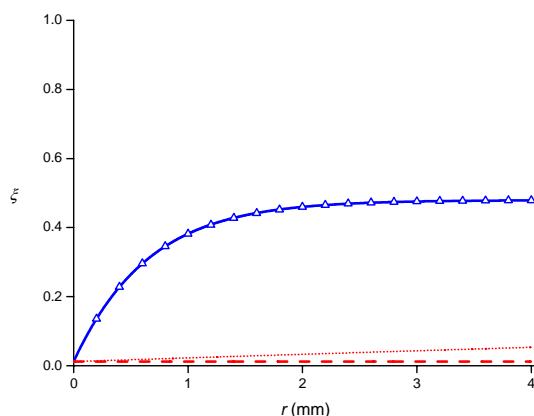
Figure SI- 6. Dependence of the lability degree on the thickness of the resin layer. Markers: Blue triangles indicate values from numerical simulation as described in Mongin et al.[1] Blue continuous line depicts the values from the analytical expression SI-35. Red dashed line stands for ξ given by Eqn SI-35 with r=0. Red dotted line stands for ξ from equation SI-35 with thickness of the gel domain given by g'=g + r and no penetration inside the resin. Parameters: total NTA concentration $c_{T,NTA}$=0.249 mol·m^{-3}; total Cd concentration $c_{T,Cd}$=9.96×10^{-3} mol m^{-3}; pH=7.03; ionic strength 0.05 M; T=25ºC; k_a^{eff}=8.77×10^4 m^3·mol^{-1}·s^{-1}; k_d=2.76×10^{-4} s^{-1}; g=1.13×10^{-3} m; D_M=6.09×10^{-10} m^2·s^{-1}; D_{ML}=4.26×10^{-10} m^2·s^{-1}; $k_{a,R}$=10^{15} m^3·mol^{-1}·s^{-1}; $k_{d,R}$=10^{-6} s^{-1} and $c_{T,R}$=50 mol·m^{-3}.

Results – Penetration effects of the complexes in the DGT resin layer

	[NTA]$_T$ mol/L	[Metal]$_T$ mol/L	pH	ξ
CdNTA	1.0×10^{-3}	1.00×10^{-7}	6	0.99
			9	0.98
	1.00×10^{-4}	1.00×10^{-7}	6	0.99
			9	0.99
	1.00×10^{-4}	1.00×10^{-8}	6	0.99
			9	0.99
	1.00×10^{-3}	1.00×10^{-8}	6	0.99
			9	0.98
CoNTA	1.00×10^{-3}	1.00×10^{-7}	6	0.82
			9	0.77
	1.00×10^{-4}	1.00×10^{-7}	6	0.83
			9	0.80
	1.00×10^{-4}	1.00×10^{-8}	6	0.83
			9	0.80
	1.00×10^{-3}	1.00×10^{-8}	6	0.82
			9	0.77
NiNTA	1.00×10^{-3}	1.00×10^{-7}	6	0.01
			9	0.00
	1.00×10^{-4}	1.00×10^{-7}	6	0.01
			9	0.01
	1.00×10^{-4}	1.00×10^{-8}	6	0.01
			9	0.01
	1.00×10^{-3}	1.00×10^{-8}	6	0.01
			9	0.01

Table S1. Theoretical lability degrees of Cd, Co and Ni complexes with NTA for different metal and NTA concentrations and pH values computed with equation SI-35. Metal diffusion coefficients in the gel layer have been taken from DGT Research Ltd., http://www.dgtresearch.com. Diffusion coefficients of complexes have been estimated as $0.7 \times D_M$. Speciation has been calculated with VMINTEQ using NIST 46.6. Kinetic parameters have been estimated using the Eigen mechanism. Formation of ML$_2$ and the influence of the protonation processes of the ligand have been considered when necessary.

Section 3: Metal Flux and Lability degree when the diffusion domain extends into the solution phase

3.1.- Metal flux received by the DGT sensor

Let us now consider the particular case in which diffusion proceeds not only inside the gel but also in a water diffusive boundary layer of thickness δ, i.e.

bulk conditions are restored beyond the gel phase at $x = r + g + \delta$. **Figure SI-7** schematizes the system considered.
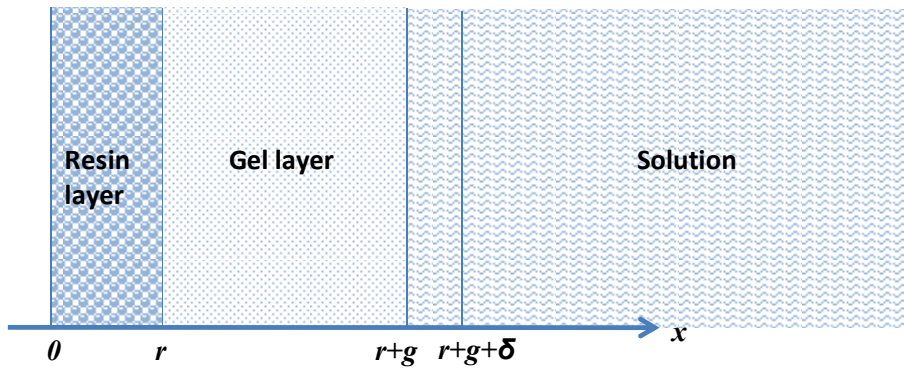
Figure SI-7. Schematic representation of a DGT device considering an additional water diffusive layer of thickness δ.

Let us represent the steady state concentrations at the gel/water interface as $c_i(x = r + g) = c_i^{r+g}$. At this interface, the concentrations of M and ML and their fluxes must be continuous:

$$c_M(g + r^-, t) = c_M(g + r^+, t), \qquad c_{ML}(g + r^-, t) = c_{ML}(g + r^+, t) \quad \text{(SI-50)}$$

$$D_M \left. \frac{\partial c_M}{\partial x} \right|_{g+r^-} = D_{M,W} \left. \frac{\partial c_M}{\partial x} \right|_{g+r^+}, \quad D_{ML} \left. \frac{\partial c_{ML}}{\partial x} \right|_{g+r^-} = D_{ML,W} \left. \frac{\partial c_{ML}}{\partial x} \right|_{g+r^+} \quad \text{(SI-51)}$$

The flux received by the DGT has been identified with

$$J = D_M \left. \frac{\partial c_M}{\partial x} \right|_r + D_{ML} \left. \frac{\partial c_{ML}}{\partial x} \right|_r \quad \text{(SI-52)}$$

Under steady state conditions this flux is common to all the planes of the DGT considered, so that

$$J = D_M \left. \frac{\partial c_M}{\partial x} \right|_r + D_{ML} \left. \frac{\partial c_{ML}}{\partial x} \right|_r = D_M \left. \frac{\partial c_M}{\partial x} \right|_{g+r^-} + D_{ML} \left. \frac{\partial c_{ML}}{\partial x} \right|_{g+r^-} = D_{M,W} \left. \frac{\partial c_M}{\partial x} \right|_{g+r^+} + D_{ML,W} \left. \frac{\partial c_{ML}}{\partial x} \right|_{g+r^+} \quad \text{(SI-53)}$$

where $D_{i,W}$ stands for the diffusion coefficient of species i in the water domain, and $\varepsilon_W = \dfrac{D_{ML,W}}{D_{M,W}}$

If we assume that equilibrium conditions are already reached at the gel-water interface,

$$c_{ML}^{r+g} = K' c_{M}^{r+g} \qquad \textbf{(SI-54)}$$

then the flux in the water phase (where there is equilibrium) can be computed as:

$$J = \frac{D_{M,W}(c_{M}^{*} - c_{M}^{r+g})(1 + \varepsilon_W K')}{\delta} \qquad \textbf{(SI-55)}$$

The flux in the gel phase can be computed by adapting the **equation SI-30** to the boundary conditions **SI-50** and **SI-51**. Thus

$$J = D_M \frac{c_M^{r+g}}{g} + D_{ML} \frac{c_{ML}^{r+g}}{g}\left(1 - \frac{1 + \varepsilon K'}{\varepsilon K' + \frac{g}{m}\coth\left(\frac{g}{m}\right) + \frac{g}{\lambda}\left(1 + \varepsilon K'\right)\tanh\frac{r}{\lambda}}\right) \qquad \textbf{(SI-56)}$$

or,

$$J = \frac{D_M(c_M^{*} - c_M^{r+g})(1 + \varepsilon K' \alpha)}{g} \qquad \textbf{(SI-57)}$$

where

$$\alpha = 1 - \frac{1 + \varepsilon K'}{\varepsilon K' + \frac{g}{m}\coth\left(\frac{g}{m}\right) + \frac{g}{\lambda}\left(1 + \varepsilon K'\right)\tanh\frac{r}{\lambda}} \qquad \textbf{(SI-58)}$$

By isolating the intermediate quantity c_M^{r+g} from **SI-55** and replacing it into the equality between **SI-55** and **SI-56**, after some algebra one finally obtains:

$$J = \frac{c_M^{*}}{\dfrac{\delta}{D_{M,W}(1 + \varepsilon_W K')} + \dfrac{g}{D_M(1 + \varepsilon K' \alpha)}} \qquad \textbf{(SI-59)}$$

3.2.- Lability degree

For a labile case, full dissociation of the complex at the resin-gel interface is reached, $c_{ML}^r = 0$ and expression **SI-31** for the fully labile flux in the gel phase, can be rewritten as

$$J = \frac{c_M^*}{\dfrac{\delta}{D_{M,W}(1+\varepsilon_W K')} + \dfrac{g}{D_M(1+\varepsilon K'\alpha)}}$$

(SI-60)

Where $c_{M,lab}^{r+g}$ and $c_{ML,lab}^{r+g}$ are the metal and complex values at gel-water interface, respectively.

This expression must be equal to the labile flux in the water phase

$$J_{labile} = \frac{D_M(c_M^* - c_{M,lab}^{r+g})(1+\varepsilon K')}{\delta}$$

(SI-61)

Isolating $c_{M,lab}^{r+g}$ from **SI-60**, we obtain for the fully labile flux:

$$J_{labile} = \frac{D_{M,W} D_M c_M^*(1+\varepsilon_W K')(1+\varepsilon K')}{\delta D_M(1+\varepsilon_W K') + g D_{M,W}(1+\varepsilon K'\alpha)}$$

(SI-62)

In the opposite case, when the complex is inert it does not contribute at all to the metal flux, $c_{ML}^r = c_M^{r+g} = c_{ML}^*$ and the metal flux bound to the resin is just due to the diffusion of the free metal present in the system

$$J_{free} = J_{inert} = \frac{D_M c_{M,free}^{r+g}}{g}$$

(SI-63)

Analogously to the last case, this flux must be equal to the inert flux in the water phase,

$$J_{free} = \frac{D_{M,W}(c_M^* - c_{M,free}^{r+g})}{\delta}$$

(SI-64)

As before, isolating the intermediate variable $c_{M,\text{free}}^{r+g}$ the inert flux can be write as

$$J_{\text{free}} = \frac{D_{M,W} D_M c_M^*}{\delta D_M + g D_{M,W}}$$

(SI-65)

The lability degree, defined as

$$\xi = \frac{J - J_{\text{free}}}{J_{\text{labile}} - J_{\text{free}}}$$

(SI-66)

can, then, be written as

$$\xi = \frac{\dfrac{(1+\varepsilon K'\alpha)(1+\varepsilon_W K')}{\delta D_M(1+\varepsilon K'\alpha) + g D_{M,W}(1+\varepsilon_W K')} - \dfrac{1}{\delta D_M + g D_{M,W}}}{\dfrac{(1+\varepsilon K')(1+\varepsilon_W K')}{\delta D_M(1+\varepsilon K') + g D_{M,W}(1+\varepsilon_W K')} - \dfrac{1}{\delta D_M + g D_{M,W}}}$$

(SI-67)

Literature cited

(1)   Mongin, S.; Uribe, R.; Puy, J.; Cecilia, J.; Galceran, J.; Zhang, H.; Davison, W., Key Role of the Resin Layer Thickness in the Lability of Complexes Measured by DGT. *Environmental Science & Technology* **2011,** *45*, (11), 4869-4875.

(2)   Heyrovský, J.; Kuta, J., *Principles of Polarography*. Academic Press: New York, **1966**.

(3)   Salvador, J.; Puy, J.; Cecilia, J.; Galceran, J., Lability of complexes in steady-state finite planar diffusion. *Journal of Electroanalytical Chemistry* **2006,** *588*, (2), 303-313.

CHAPTER 9

RESULTS AND DISCUSSION

TWO MODES OF OPERATION OF THE DGT SENSOR: KINETIC AND EQUILIBRIUM REGIMES

- Foreword -

One of the fundamental assumptions for the interpretation of the DGT data in terms of dynamic speciation, is the consideration of the resin layer as a *perfect sink* (a phase of unlimited binding capacity). This assumption is taken into account in the model used in the precedent section. However, the DGT experiments shown here for the Cd-NTA system at low pH or high ligand concentration show that the expected linear accumulation is disturbed, in contradiction with the perfect sink behaviour of the resin. For these cases, an equilibrium behaviour in the DGT sensor is suspected.

This work presents a rigorous analysis of the conditions were the perfect sink assumption is valid. In particular, the effects of pH (proton competition), deployment time and dissolved ligand concentration were studied. The results allowed us to determine the range where the metal binding to the Chelex sensor is well below equilibrium and, therefore, the operational conditions were DGT works as a purely dynamic sensor (where the metal accumulation in the devices is independent of the amount of resin). On the other hand, deployment conditions close to equilibrium allow the use of the DGT sensors to obtain information about the free metal concentration present in the sample.

Two modes of operation of the DGT sensor: kinetic and equilibrium regimes

Sandrine Mongin[a], Ramiro Uribe[a,b], Carlos Rey-Castro[a], Joan Cecília[c], Josep Galceran[a] and Jaume Puy[a]

[a]Departament de Química, Universitat de Lleida, Rovira Roure 191, 251698, Lleida, Spain

[b]Departamento de Física, Universidad del Tolima, Ibagué, Colombia

[c]Departament de Matemàtica, Universitat de Lleida, Rovira Roure 191, 251698, Lleida, Spain

ABSTRACT

The effects of two competition phenomena commonly present in solution on the metal accumulation by diffusive gradients in thin films devices (DGT) are studied in this work by a combined experimental / theoretical analysis. The first phenomenon is due to the presence of protons, which compete with the metal ions for the binding to the DGT resin sites at relatively low pH values. The second one is due to the presence of high affinity ligands in solution, which compete with the resin sites for the binding of the metal ions. A computation code, which allows a rigorous digital simulation of the diffusion-reaction processes and takes into account the metal-resin binding stoichiometry, was used to model the accumulation of metal in the sensors, and to demonstrate the effects of the proton and ligand competition on the binding of metal to the DGT resin. This model was tested against experimental data in the Cd-NTA system. The results show that the competitors can influence the metal accumulated in the DGT even at relatively short deployment times. In these cases, the metal-resin binding approaches equilibrium with the bulk metal concentration and the DGT behaviour deviates from a perfect sink. Therefore, the sensor departs from a purely dynamic behaviour and approaches an equilibrium behaviour, which could allow the assessment of the free metal concentration present in the medium.

1. INTRODUCTION

In a broad sense, the dynamic analytical techniques for the determination of labile complexes are based on a metal binding material that disturbs the distribution of the metal species in a solution layer adjacent to the sensor. Therefore, the amount of metal measured can be related to the fluxes of free metal and its labile species.[1] Voltammetry is widely applied as a dynamic technique, but techniques using a chelating resin for the binding of metals, have increased their use because of their simplicity.[2] Among these techniques, Diffusive Gradients in Thin films (DGT) is one of the most widespead.[3] The principle of this technique is that metals diffuse through a diffusion domain, with a well defined thickness, composed by a hydrogel and a membrane filter, to finally accumulate in the binding layer, consisting of a chelating resin (usually Chelex) suspended in a hydrogel. DGT is a powerful technique for *in-situ* measurement,[1,3] and it has successfully been applied to the measurement of trace metals[4], radionuclides[5,6] and phosphate[7], in fresh[8] and marine water[9], as well as a range of determinands in sediments[10] and soils[11].

The typical equation linking the concentration measured by the DGT to the concentration of the labile metal species present in the medium relies on several assumptions.[3] A major one being that the surface of the resin layer acts as a perfect planar sink, corresponding with the concept that the binding is irreversible, almost instantaneous and that the accumulated metal amount is much lower than the capacity of the resin. However, experimental studies have shown that the proportion of metal accumulated is influenced by the strength of the binding phase.[12,13] Lehto et al.[14] used numerical models of the DGT system to explore how the resin strength may have an impact on the metal accumulation. Moreover, experimental observations showed that the DGT does not work well at low pH.[3,15-17] In fact, at low pH, the major binding functional groups of the resin phase are predominantly in acidic forms.[12] Therefore, the proton competition can affect the apparent strength of the resin by reducing the capacity of the resin.

To our knowledge, no previous studies aiming to describe the metal accumulation by DGT sensors versus time in presence of competitors from a combined experimental / modelling perspective were published so far.

In this work, a model that takes into account the resin-binding stoichiometry is developed in order to study the effect of two competitors, proton and ligand, on the metal-resin binding. This model is checked against cadmium ion

experiments, given that the behaviour of cadmium in the DGT[3,15] and its complexation with Chelex resin[18-20] is well known. The competition of protons and cadmium for the resin sites is studied by the deployment of DGT devices in simple solutions at different pH values (in the absence of any organic ligands) and the competition effect of ligand is investigated with different concentrations of NTA (nitrilotriacetic acid).

2. NUMERICAL MODELLING

Let us consider the complexation of cadmium (focused metal in this study) with a ligand L according to the scheme:

$$Cd + L \underset{k_d}{\overset{k_a}{\rightleftharpoons}} CdL \tag{9.1}$$

With the equilibrium condition:

$$K = \frac{k_a}{k_d} = \frac{c_{CdL}^*}{c_{Cd}^* \, c_L^*} \tag{9.2}$$

where K, k_a and k_d are, respectively, the equilibrium, association and dissociation rate constants of the complexation process, whereas c_i^* labels the concentration of species i in the bulk solution. The charges of the different species are omitted for simplicity.

The model is similar to our previous model,[21] assuming the penetration of the species into the resin layer, where the free metal is bound by the resin sites after their diffusion through the membrane filter and diffusive gel. In addition, the stoichiometry of the resin binding and the metal-proton competition of the resin sites are considered by the adequate exchange equilibria (**9.3-9.4**) of the binding between Cd and resin sites.[18,20] In fact, previous study showed different patters for the binding of the metal ions to the Chelex resin groups (R). For copper and nickel, the mechanism involves only the formation of a MR complex.[20] Formation of MR and MR_2 complexes have been reported for iron, while for lead, the complexes PbR and PbHR are formed.[18,22] In the case of cadmium and zinc metal ions, both complexes, $M(HR)_2$ and MR_2 were identified.[18,20]

$$Cd + 2\,\overline{H_2R} \rightleftharpoons \overline{CdR_2} + 4\,H \tag{9.3}$$

$$\text{Cd} + 2\,\overline{\text{H}_2\text{R}} \rightleftharpoons \overline{\text{Cd}(\text{HR})_2} + 2\,\text{H} \qquad \textbf{(9.4)}$$
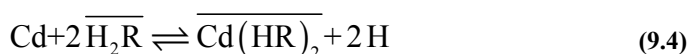
The overbar (here and everywhere in the text) represents species in solid phase. Protonation equilibria of the chelating sorbent[20] are given in the supporting information (SI.8 and SI.10).

Several assumptions are made in the model:

(i) Free metal ion, M, binds rapidly to the resin, so that the kinetics is not the limiting step and the binding reactions (**9.3** and **9.4**) are considered at equilibrium.

(ii) The complex ML can penetrate inside the resin gel, where its dissociation still proceeds, but binding of complex to the resin via ternary complexes is not considered.[23]

(iii) Resin sites are assumed to be evenly distributed in the resin domain and are immobile. Excluded volume of the resin beads is neglected.

(iv) The difference between diffusion coefficients of different species in the solution and the gel layer are considered negligible, therefore the membrane filter and boundary layer diffusion (DBL) thicknesses are accounted for by increasing the effective value of the diffusive gel layer thickness.[24]

(v) Null flux of all diffusive species is assumed at the side of the resin layer opposite to that contacting the diffusive gel.

(vi) At the interface between gel and resin layers, continuity of the concentrations and fluxes is assumed.

Initial conditions are defined by the equilibrium concentrations in the solution and concentrations of Cd, L and CdL are zero in the sensor. The numerical solution is achieved by using a finite differences method. Details of the mathematical formulation and numerical solution can be found in the Supporting Information (see SI, section 1).

In the previous model[21] different assumptions concerning the binding of metal by the resin were made: the resin was considered as a perfect sink, a 1:1 metal/resin ratio stoichiometry was assumed and the competition of proton and other cations in the metal binding was disregarded. These assumptions are valid when the number of free resin sites is high, whereas when the resin sites are almost fully occupied, the stoichiometry of metal-resin binding has a great importance. The refined model represents an improvement, by taking into

account the metal-proton competition, the eventually high occupation of the resin sites and the stoichiometry of the resin binding.

3. CHEMICAL EQUILIBRIUM IN THE CHELEX RESIN

The amount of metal bound to the resin at equilibrium in a determined condition can be calculated from the chemical model. In a simple solution where no ligands are present, this amount depends on the deployment solution conditions: metal concentration and pH. At a given pH, total cadmium concentration, and resin concentration, the chemical equilibrium speciation of the system Cd-resin can be calculated by solving the following equations:

- **equations 9.3**, **9.4** (corresponding to the cadmium-resin binding)

- **equations SI-8, SI-10,** (corresponding to the proton-resin equilibria)

- and the resin mass balance:

$$c_{\overline{\text{R, total}}} = c_{\overline{\text{R}}} + c_{\overline{\text{HR}}} + c_{\overline{\text{H}_2\text{R}}} + 2\,c_{\overline{\text{CdR}_2}} + 2\,c_{\overline{\text{Cd(HR)}_2}} \qquad \textbf{(9.5)}$$

The total amount of cadmium bound to the resin at equilibrium is given by the sum of the species $c_{\overline{\text{CdR}_2}}$ and $c_{\overline{\text{Cd(HR)}_2}}$. This amount (calculated per DGT device) is represented as a function of metal concentration for different pH in **figure 1**. For low proton concentrations (pH 8 or higher), the amount of cadmium is almost constant in the range of metal concentration due to the saturation of the resin sites. But at low pH values, the proton-metal competition is manifested, i.e.: an increase of metal concentration removes the protons bound to the resin, and the amount of cadmium bound at equilibrium is greatly dependent on the cadmium concentration. As will be discussed in Section 5.2, this effect may have significant consequences in DGT deployment experiments.
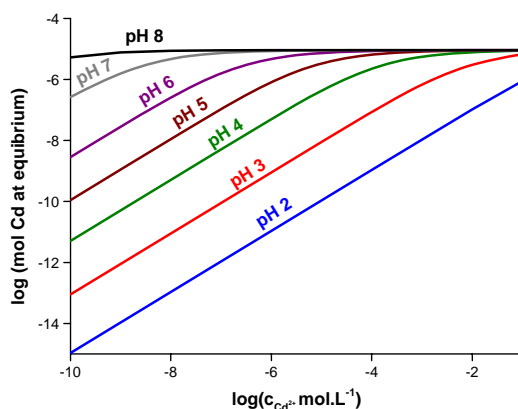
Figure 1. Amount of metal bound to the resin at equilibrium for different pH and cadmium concentrations calculated by the chemical equilibrium system [18,20] in absence of ligand L. Amount of resin sites per sensor: 18.4 μmols (see results section). The equilibrium binding constants are listed in table S2.

In a more complex solution, where a ligand is present, the following equations must be added to the previous system:

$$K = \frac{c_{ML}}{c_M c_L} \tag{9.6}$$

$$c_{Mtot} = c_M + c_{ML} \tag{9.7}$$

$$c_{Ltot} = c_L + c_{ML} \tag{9.8}$$

In these cases, there is an additional competition between the resin groups and the dissolved ligand L for the binding of Cd^{2+} ions. The effect of an increasing concentration of L causes a decrease in the free Cd^{2+} concentration, which leads to a decreasing amount of Cd bound to the resin, at a given pH and total cadmium concentration. The consequences of this effect for the metal accumulation in the DGT experiments will be analysed in Section 5.3.

4. EXPERIMENTAL PROCEDURE

4.1. DGT assembly, retrieval and analysis procedures

DGT holders (piston type, 2 cm diameter window) were purchased from DGT Research Ltd. as well as diffusive gel (0.8 mm thick) and Chelex resin gel (0.4

mm thick). A layer of resin gel was placed on the piston surface with the resin beads facing upward (i.e. in close contact with the diffusive layer). On the top of the Chelex-gel, a layer of diffusive gel and a cellulose nitrate membrane filter (Whatman, pore size 0.45 μm, 0.125 mm thick) were placed. The filter was used to separate the diffusive gel from the solution.

On retrieval, the DGT devices were rinsed with ultra-pure water (Milli-Q plus 185 System, Millipore) and disassembled for removal of the resin gels. Cadmium was eluted from retrieved resin membranes by immersing them in 1mL of concentrated nitric acid in micro-centrifuge PVC tubes for at least 24 h.

Following elution and appropriate dilution, the concentration of cadmium was analysed by ICP-OES (Activa-S, Horiba Scientific). The moles of cadmium accumulated by DGT were calculated from their concentration in the eluate.

4.2. DGT Exposure Chamber

A 5L polyethylene cylindrical bucket was used as the exposure chamber. 11 DGT sensors were fixed by press-studs. pH was monitored continuously during the deployment with a glass electrode. The exposure chamber was placed in a thermostated bath to keep the deployment solution at a constant temperature of 25 ± 0.1ºC. The solution was stirred using an overhead stirrer at 240 rpm. The ionic strength of the solution was adjusted to 0.05 mol·L^{-1} NaNO$_3$ and Milli-Q water was employed in all the experiments. During the deployment of the sensor, aliquots of exposition solution were collected and analysed by ICP-OES at regular intervals to check the total Cd concentration for each experiment.

4.3. Determination of the amount of binding sites in the DGT sensor

The sensors were exposed to a solution of 10^{-3} mol·L^{-1} Cd (prepared from Cd(NO$_3$)$_2$) for different time periods up to 50 h. The pH was adjusted to 8 using dilute NaOH before and during the deployment.

4.4. Exposure experiments in presence of cadmium

The DGTs were exposed to solutions of 10^{-3} mol·L^{-1} and 10^{-5} mol·L^{-1} Cd (prepared from Cd(NO$_3$)$_2$) and retrieved at different times. The pH was adjusted to the chosen value using diluted HNO$_3$ and NaOH.

4.5. Exposure experiments in presence of cadmium and NTA

The number of cadmium accumulated by DGT in presence of NTA at different times was determined in different experimental conditions. The devices were deployed in solutions containing cadmium at concentrations close to 10^{-5} mol·L^{-1} (prepared from Cd(NO$_3$)$_2$) and NTA at different concentrations (2.49 x 10^{-4} mol·L^{-1}, 1.8 x 10^{-3} mol·L^{-1} and 8 x 10^{-3} mol·L^{-1}). The pH was adjusted to the desired value by small additions of diluted HNO$_3$ and NaOH.

4.6. Numerical simulations

Several simulations were performed in presence of cadmium (absence of ligand) at different pH. The parameters used for these simulations are presented in **table S2**. The experimental conditions are the same as in Mongin et al.[21], therefore the effective thickness of the diffusion domain is considered identical, with a value of g=1.13 x 10^{-3} m. The diffusion coefficient of cadmium is given by DGT Research Ltd (http://www.dgtresearch.com), with a value of D_{Cd}=6.09×10^{-10} m^2·s^{-1} at 25ºC.

Simulations were also performed for cadmium and NTA at different metal, ligand concentrations and pH values. The numerical simulation model assumes a metal complexation scheme represented by **equation 9.1**, whereas the actual chemical model for Cd-NTA binding is more complicated. Therefore, the complexation between NTA and Cd was first reviewed in order to describe the Cd-NTA complexation as the simple binding scheme of **equation 9.1**.

This was carried out as following:

NTA interact with Cd to give the complex species CdNTA and Cd(NTA)$_2$,[25] according to the following reactions:

$$Cd + NTA \underset{}{\overset{K_1}{\rightleftharpoons}} CdNTA \tag{9.9}$$

$$CdNTA + NTA \underset{}{\overset{K_2}{\rightleftharpoons}} Cd(NTA)_2 \tag{9.10}$$
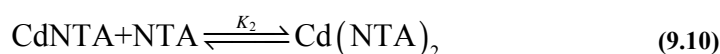
In addition, NTA is involved in four protonation processes, depending on the following exchange equilibria, therefore, its concentration not only modified by the presence of Cd, but also by the pH of the system.

$$NTA + H \underset{}{\overset{K_{H,1}}{\rightleftharpoons}} HNTA \tag{9.11}$$

$$\text{HNTA} + \text{H} \xrightleftharpoons{K_{\text{H},2}} \text{H}_2\text{NTA} \tag{9.12}$$

$$\text{H}_2\text{NTA} + \text{H} \xrightleftharpoons{K_{\text{H},3}} \text{H}_3\text{NTA} \tag{9.13}$$

$$\text{H}_3\text{NTA} + \text{H} \xrightleftharpoons{K_{\text{H},4}} \text{H}_4\text{NTA} \tag{9.14}$$

Assuming that,

i) protonated NTA, NTA and CdNTA species have the same diffusion coefficient

ii) protonation processes and formation of Cd(NTA)_2 complex are much faster than **process 9.9**, which is assumed to be the rate limiting step

then, the Cd-NTA can be reformulated as formally identical to a problem with only one ligand,[26,27] as **equation SI.43** (see Section 2 in the SI), with an effective ligand concentration, stability constant and kinetic constants given by:

$$c_{\text{NTA}}^{\text{eff}} = B \times c_{\text{NTA}^{3-}} \tag{9.15}$$

where $B = 1 + K_{\text{H},1}c_{\text{H}} + K_{\text{H},1}K_{\text{H},2}c_{\text{H}}^2 + K_{\text{H},1}K_{\text{H},2}K_{\text{H},3}c_{\text{H}}^3 + K_{\text{H},1}K_{\text{H},2}K_{\text{H},3}K_{\text{H},4}c_{\text{H}}^4$

$$K^{\text{eff}} = \frac{K_1\left(1 + \dfrac{K_2 c_{\text{NTA}}^{\text{eff}}}{B}\right)}{B} \tag{9.16}$$

$$k_{\text{a}}^{\text{eff}} = \frac{k_{\text{a},1}}{B} \tag{9.17}$$

$$k_{\text{d}}^{\text{eff}} = \frac{k_{\text{a}}^{\text{eff}}}{K^{\text{eff}}} \tag{9.18}$$

With these definitions, the effective ligand concentration is the sum of all protonated NTA species. An effective diffusion coefficient can be calculated by the following equation:

$$D_{\text{NTA}}^{\text{eff}} = \frac{D_{\text{CdNTA}} + D_{\text{CdNTA}_2} \dfrac{K_2 c_{\text{NTA}}^{\text{eff}}}{B}}{1 + \dfrac{K_2 c_{\text{NTA}}^{\text{eff}}}{B}} \tag{9.19}$$

In previous studies, the diffusion coefficient of CdNTA has been reported to be 0.7 times that of the free metal,[21,28] so this value was used in the simulation. It is considered that the ML$_2$ complex has the same diffusion behaviour, thus the diffusion coefficient of CdNTA$_2$ was also considered 0.7 times that of the CdNTA complex.

The association kinetic constant for CdNTA is estimated from the Eigen mechanism.[27,29] According to Eigen's ideas, the association kinetic constant is given by the product of the stability constant for the outer sphere complex, K_{CdNTA}^{os}, times the kinetic constant for the release of a water molecule from the inner hydration sphere of metal, k_w.[30] With $K_{CdNTA}^{os} = 1.65 \times 10^2$ L·mol^{-1} (for an ionic strength of 0.05 M) and $k_w = 3 \times 10^8$ s^{-1}, k_{a_CdNTA} is estimated to be 4.96×10^{10} L·mol^{-1}·s^{-1}.

The effective parameters used in the simulations are reported in **table S3** for the different simulated conditions.

In summary, all the values of the model parameters were taken (or derived) from bibliography, or obtained from independent experimental measurements (such as the maximum resin binding capacity). Therefore, no fitting of the simulation model was necessary to describe the experimental Cd accumulation data shown in the Results Section.

5. RESULTS AND DISCUSSION

5.1. Amount of binding sites in the DGT sensor

The maximum amount of metal that the DGT sensor can accumulate is an essential parameter for the modelling of the sensor performance. Also, when a DGT measurement is carried out, it is necessary to ensure that the metal accumulation in the sensors is well below this maximum capacity, to ensure accurate results. The situation where the sensor has achieved this maximum capacity, and all the resin sites are occupied by metal, is called *saturation*. The precise determination of this value for a given cation is, therefore, very important. In fact, the binding capacity of the resin might vary in function of the nature of the cations, as in the case of natural ligands.[31]

In order to determine the value of saturation for a given metal (in this case, Cd), it is important not to have competition effects from other cations, such as protons (see **figure 1**). For example, at pH=8, the proton concentration is sufficiently low to avoid competition when a high cadmium concentration (10^{-3}

mol·L^{-1}) is employed, so a rapid saturation of the resin sites is then expected. The achievement of saturation can be experimentally determined by a simple experiment where several sensors are deployed in this Cd solution, and retrieved at different times. In this particular case, after 50 h the resin is completely saturated and cannot accumulate more cadmium (see **figure S1** in SI), leading to a maximum binding of 9.2 μmols per DGT sensor. From this result, and assuming the binding stoichiometry between Cd ions and resin groups described in the chemical model (**equations 9.3** and **9.4**[18,20]), an amount of resin sites of 18.4 μmols (per sensor) is obtained. This yields a concentration of sites in the resin layer of 0.147 mol·L^{-1}.

5.2. Impact of pH on the DGT accumulation.

Black line in **figure 2** shows the Cd accumulated in the chelating resins of the DGT devices, calculated with the numerical model described in the precedent section. The parameters used for the numerical simulation are reported in **table S2**. The results are given for two different cadmium concentrations in the deployment solution: 2.7x10^{-8} mol·L^{-1}, **figure 2a)**, and 10^{-5} mol·L^{-1}, **figure 2b)**, both at pH 4. This value of pH was chosen in order to put clearly into manifest the influence of the proton competition effect on the metal accumulation.

Figure 2b) also shows experimental accumulation data obtained in the same conditions. The good agreement between experimental and simulated accumulations supports the accuracy of the present simulation model, which takes into account the effects of proton competition and stoichiometry on the metal binding.

At this pH, both the experimental and simulation results show a typical saturation-type behaviour: for short deployment times, a quasi-linear accumulation is observed, whereas at intermediate times there is a decrease of the slope and for long enough times a constant accumulation is finally achieved.

The maximum amount of cadmium that the DGT can accumulate is reached when the chemical equilibrium in the Chelex resin layer with the bulk metal concentration is achieved. The calculation of the equilibrium cadmium concentration is explained in Section 3. The calculated value is multiplied by the volume of the Chelex hydrogel to obtain the maximum accumulation for each condition, which is depicted by a red dashed line in **figure 2**. It is straightforward to demonstrate that an increase in the metal concentration increases the maximum amount that the DGT sensor can accumulate at this pH,

due to removal of bound protons by the metal ions. This effect can be observed from the comparison of the red dashed lines in **figure 2a)** and **2b)**.

On the other hand, the number of moles accumulated if the sensor is represented as a perfect planar sink is depicted by the blue line in **figure 2**, which was calculated by the simple diffusion equation,[3] based on Fick's first law:

$$m = \frac{D_{Cd}\, c_{Cd}^{*}\, A}{g} t \qquad\qquad (9.20)$$

where D_{Cd} is the diffusion coefficient of cadmium in the gel, g is the diffusive layer thickness, c_{Cd}^{*} is the bulk concentration of cadmium in the deployment solution, A is the exposed gel area, and t is the time of deployment.

The underlying assumption in this equation is that the concentration profile of free metal inside the diffusive gel, at steady state, follows a perfect straight line from $c_M = c_M^{*}$ (at the sensor / solution interface) to $c_M = 0$ (at the resin surface). **Equation 9.20** predicts an indefinite linear accumulation with time, in contrast with the asymptotic behaviour observed in experiments and simulations. These asymptotic results indicate that the DGT sensors have difficulty to work as a perfect sink at low pH values. In fact, the departure from perfect sink behaviour is represented in the inset of **figure 2**, which shows the metal concentration profiles inside the DGT sensor (calculated by the numerical simulation model) as a function of the deployment time. As can be noticed, the metal concentration inside the resin layer increases relatively fast with time due to the progressive occupation of the resin sites over time as the deployment proceeds. Consequently, the concentration gradient decreases, and the profiles flatten out with time as equilibrium between the chelating resin and the bulk metal is approached.

The departure from linear accumulation in DGT at low pH has previously reported in bibliography (see e.g., Gimpel et al.[15] and Zhang and Davison[3]). These authors consider the limit for accurate DGT measurements to be above pH 5.

Figure 2 clearly shows that, the difference between the standard DGT-expected accumulation (**equation 9.20**) and the actual accumulation in the sensors increases noticeably as the deployment time increases. Therefore, the consideration of the DGT as a perfect sink in these conditions (i.e., the use of **equation 9.20** to retrieve the metal concentration of the medium from the resin

elution concentration) leads to an underestimation of the metal concentration present in the medium, and this underestimation increases over the deployment time.
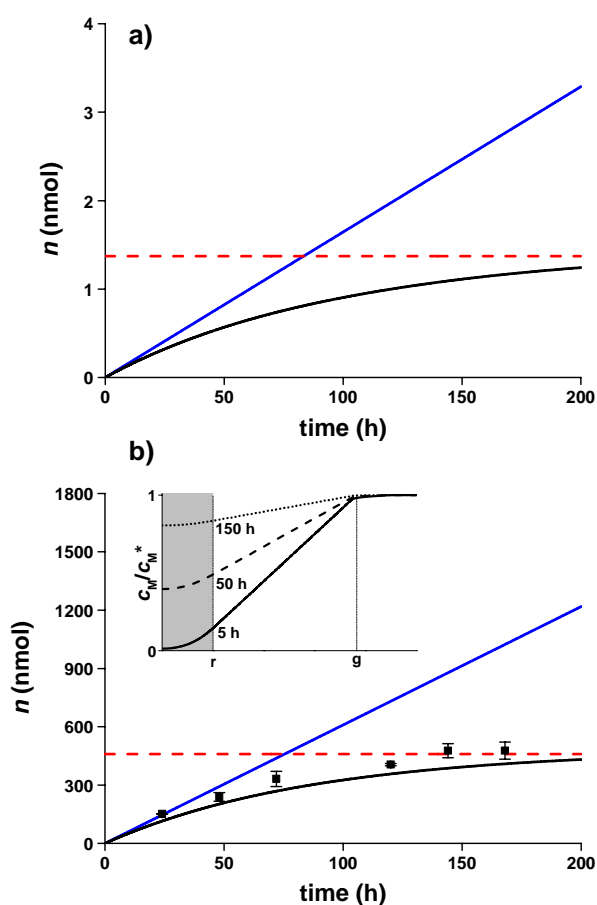
Figure 2. Moles of Cd accumulated by DGT at pH 4 in the presence of two Cd concentrations: a) 2.7×10^{-8} mol·L^{-1}; b) 10^{-5} mol·L^{-1}, the inset represents the metal concentration profiles for different deployment times: 5 h, 50 h and 150 h (numerical simulation). Black line: theoretical accumulation predicted by numerical simulation. Blue line: predicted accumulation if the DGT is considered as a perfect sink (equation 9.20). Red dashed line: maximum moles that the DGT can accumulate (calculated from the chemical binding model of the resin sites). Markers: experimental measurements. See table S2 for the parameters. Note the change in scale of the vertical axis of both figures.

To illustrate the accuracy of DGT at different pH values, the ratio n_{DGT}/n (Cd moles accumulated by DGT divided by the moles calculated by **equation 9.20**) was plotted against pH in **figure 3**. This ratio represents the quotient between the metal concentration in solution measured by DGT and the actual concentration in the immersion solution (obtained by direct measurement, in the case of experimental data). The results are given for different concentrations of cadmium (2.8×10^{-8} mol·L^{-1} (**figure 3a)**), 10^{-5} mol·L^{-1} (**figure 3b)**) and 10^{-3} mol·L^{-1} (**figure 3c)**) and for different deployment times. Simulation results are represented by continuous lines, whereas experimental measurements (from this work and from literature: Zhang and Davison[3]) are depicted as markers.

From **figure 3**, it can be concluded that simulation results are in good agreement with the experimental data for the different concentrations and deployment times. This agreement supports, once again, the accuracy of the chemical model in the description of the effects of pH and metal concentration.

At low pH, the observed accumulation lies below the value expected from the perfect sink behaviour. In these conditions, the proton concentration is high, causing a strong competition with the metal for the binding sites of the resin. Therefore, the free metal concentration at the resin sites is not zero, but it increases up to c_{M}^{*} as time processes. In this situation, the resin sites are in equilibrium with the bulk metal and the maximum amount of cadmium that the DGT can accumulate in this medium conditions (pH and total metal concentration) is reached causing a saturation behaviour. This phenomenon is observed in **figure 2**: the accumulated cadmium reaches equilibrium with the bulk Cd concentration (the black line approaches asymptotically the red dashed line). At this point, the DGT ceases to work as a dynamic technique and "becomes" an equilibrium sensor.

As the pH increases, the proton occupation decreases and the Cd accumulation approaches the value determined by **equation 9.20**, as long as the metal concentration and deployment time are not high enough to completely saturate the resin (**figure 3c**).

Results – Two modes of operation of the DGT sensor: kinetic and equilibrium regimes
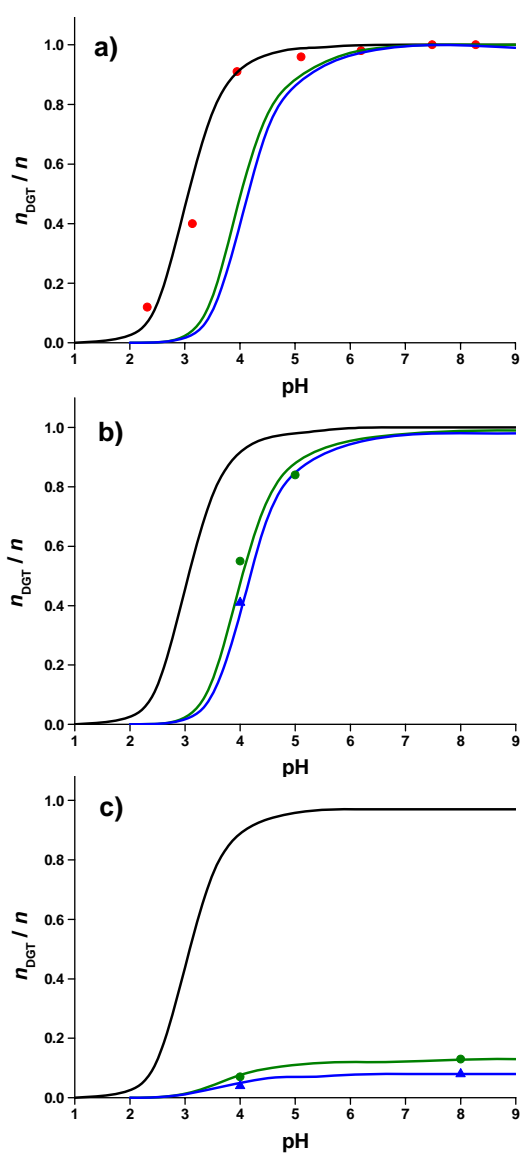
Figure 3. Effect of pH and deployment time on DGT measurements assessed by the ratio n_{DGT}/n in presence of different Cd concentrations: 2.7×10^{-8} mol·L^{-1} (figure 2a)), 10^{-5} mol·L^{-1} (figure 2b)) and 10^{-3} mol·L^{-1} (figure 2c)). Lines: theoretical accumulations predicted by numerical simulation for different times, 2 hours (black line), 5 days (green line) and 8 days (blue line). Markers: experimental measurements at 2 hours from Zhang and Davison[3] (red symbols), and experimental data from this work (blue and green symbols for 5 and 8 days, respectively). See table S2 for the parameters.

For 2h of deployment, the ratio n_{DGT}/n reaches a value of 1 above pH 5, which indicates a perfect sink behaviour, in accordance with literature (Gimpel et al.[15] and Zhang and Davison [3]). This is observed independently of the metal concentration (compare the black line in **figures 3 a-c)**. At higher deployment times, the adequate pH range for the measurements is shifted to higher values. For instance, at a deployment time of 5 days (or 8 days), the DGT measurements approach the perfect sink value above pH 6, but only at relatively low metal concentrations, i.e., less than 10^{-5} mol·L^{-1} (**figure 3a)** and **3b))**. In fact, reaching the equilibrium depends on the time of deployment: for short contact times, the sensor works as a perfect sink, while for long exposures, the accumulation approaches equilibrium and the sensor departs from the dynamic (kinetic) regime.

However, when the metal concentration is very high (10^{-3} mol·L^{-1}, **figure** 3**c)**), the resin saturation is reached after only 15 hours and, therefore the ratio n_{DGT}/n is very low after 5 days (ca. 0.1), whatever the pH. From an environmental point of view, such a high concentration of cadmium is probably not relevant (except in industrial wastewaters and mine tailings[16,17]). Nevertheless, in many aqueous media (e.g. seawater, soil solutions, etc.), other cations (such as Ca, Mg, etc.) are present at comparatively high concentrations. The competition effects due to these major cations may hinder the accumulation of trace metals by the chelating resin, which should be tested under these particular conditions. Several examples from bibliography have already pointed out the relevance of these effects (see e.g., Conesa *et al.*[17] or Degryse *et al.*[32] which showed how measurement of Zn was affected by competitive binding of calcium).

5.3. Impact of the ligand concentration on the DGT accumulation.

The same pattern of **figure 2** is represented in **figure 4** for the case of Cd-NTA complexes, i.e. modelling of accumulated Cd (black line), maximum accumulation (calculated by the chemical equilibrium model, red dashed line) and number of moles accumulated in a perfect sink behaviour (depicted in blue line). In the last case, **equation 9.20** must be modified to account for the concentration of cadmium complexes (assumed labile) and their diffusion coefficients, as follows:

$$m = \frac{D_{Cd}\, c^{*}_{Cd} + D_{CdNTA}\, c^{*}_{CdNTA} + D_{CdNTA_2}\, c^{*}_{CdNTA_2}}{g} At \qquad \textbf{(9.21)}$$

where D_{CdNTA}=$0.7 \times D_{Cd}$[28] and D_{CdNTA_2} =$0.7 \times D_{CdNTA}$.

From the speciation of cadmium in the medium, the accumulated mass in the sensor can be calculated by **equation 9.21**, for the situation where the resin behaves as a perfect planar sink.

The results are given for three NTA concentrations in the deployment solution: $2x10^{-5}$ mol·L^{-1} (**figure 4a)**) $1.8x10^{-3}$ mol·L^{-1} (**figure 4b)**) and $8x10^{-3}$ mol·L^{-1} (**figure 4c)**), all of them at pH 6 and a total cadmium concentration of 10^{-5} mol·L^{-1}. As can be observed, the simulation model reproduces with a good accuracy the experimental data in the three conditions. For the two highest NTA concentrations (**figures 4b)** and **c)**), the results show a saturation-type behaviour after a few deployment hours (8 hours for the higher concentration of NTA), whereas at the lowest NTA concentration (**figure 4a)**), the accumulation is linear. The value of accumulation at equilibrium (red dashed line) decreases as the concentration of NTA increases, indicating that the ligand competes with the resin for the binding of metal. It can be observed that, for a given total Cd concentration, an increase in the ligand concentration leads to an increase in the curvature of accumulation (i.e.: departure from perfect sink behaviour). As commented above (see **figure 1** and Theoretical Section), the presence of ligand leads to a decrease in free metal concentration which, in turn, leads to a lower equilibrium value of metal bound to the resin at a given pH.
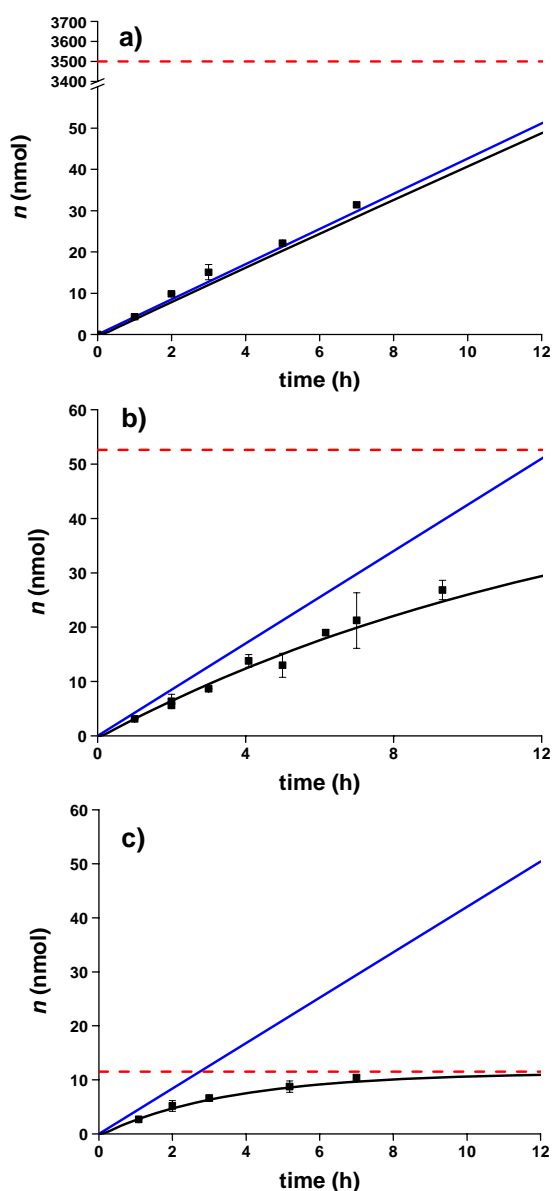
Figure 4. Moles of cadmium accumulated by DGT sensors at pH 6 in presence of a total Cd concentration of 10^{-5} mol·L^{-1} and three NTA concentrations: a) $2x10^{-5}$ mol·L^{-1} b) $1.8x10^{-3}$ mol·L^{-1}; c) $8x10^{-3}$ mol·L^{-1}. Black line: theoretical accumulation predicted by numerical simulation. Blue line: predicted accumulation if the DGT is considered as a perfect sink (equation 9.21). Red dashed line: maximum Cd moles that the DGT sensors can accumulate in these conditions. Markers: experimental measurements. See table S3 for the model parameters.

To illustrate the simultaneous influence of the ligand concentration and the pH in the DGT accumulation, the ratio n_{DGT}/n is plotted in **figure 5a)** for a cadmium concentration of 10^{-5} mol·L^{-1}. The colour / pattern of the graphic shows the value of the ratio as a function of both pH and NTA concentration. The orange circles show the experimental measurements of the ratio n_{DGT}/n (represented as the filling colour/pattern of each symbol). The agreement between experimental data and modelling results is acceptable, which validates the chemical model used in this work also in presence of ligand.

A perfect sink behaviour is fulfilled when the ratio n_{DGT}/n is higher than 0.95 (black area in **figure 5)**. Therefore, a dynamic behaviour of the technique is obtained for pH values greater than 5 and NTA concentrations lower than 10^{-5} mol·L^{-1}, after 10 h deployment. If the ligand concentration is lower than 10^{-6} mol·L^{-1}, the ligand has no effect on the DGT accumulation, therefore, the results are the same as in absence of any ligand, i.e.: only the pH affects the accumulation. Accumulation at higher pH (pH>8) deviates from perfect sink behaviour at ligand concentrations higher than 10^{-3} mol·L^{-1}.

A decrease in the metal concentration (2.7 x 10^{-8} mol·L^{-1}, **figure 5b)**) leads to almost identical results as the higher total cadmium concentration (10^{-5} mol·L^{-1}, **figure 5a)**). The reason of this very little dependence on the total metal concentration can be rationalised as follows: for a given ligand concentration and pH, a decrease in the total metal concentration leads, obviously, to a decrease in the free metal concentration, which (as shown in **figure 1**) leads to a decrease in the maximum amount of metal bound at equilibrium. At the same time, also the accumulation rate decreases (i.e., the slope of **equation 9.21**). In the end, both effects tend to compensate each other, and the ratio n_{DGT}/n remains almost unaltered. However, when the metal concentration is very high, the complete saturation of resin sites may be reached so that the sensor cannot accumulate any more metal (e.g., case of **figure 3c)**).

a)

b)
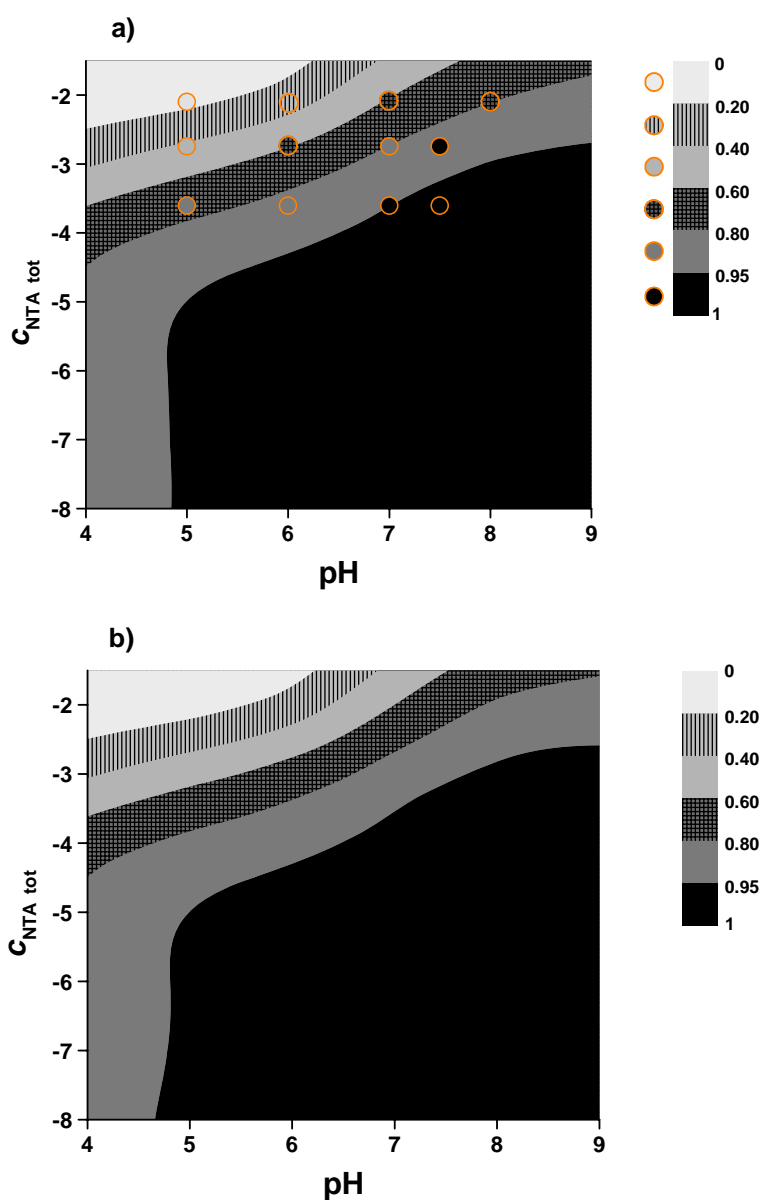
Figure 5. Effect of pH and NTA concentrations on DGT measurements assessed by the ratio n_{DGT}/n in immersion solutions of different total cadmium concentrations: 10^{-5} mol.L^{-1}(figure 5a)) and 2.7×10^{-8} mol.L^{-1} (figure 5b)) after 10 hours of deployment. Colour / pattern (see legend) shows the theoretical ratio predicted by numerical simulation. Orange circles: experimental measurements. See table S3 for the parameters.

For longer deployment times, the adequate pH and ligand concentration ranges for a kinetic operation of DGT are shifted. For instance, at a deployment time of 8 days (**figure 6**), the DGT measurements approach the perfect sink value only above pH 6, depending also on the NTA concentration. E.g.: pH≥6 for NTA concentrations lower than 10^{-6} mol·L^{-1}, pH≥7 for NTA concentrations lower than 10^{-5} mol·L^{-1}, pH above 8 for NTA concentrations lower than 10^{-4} mol·L^{-1}, etc.

The kinetic operation regime of the DGT technique depends not only on pH and ligand concentrations, but also on the stability of the metal complex. In presence of weak complexes, the influence of the resin equilibrium on the metal accumulation starts to be noticeable at higher ligand concentrations (i.e., the black region of **figures 5** and **6** is shifted upwards). In natural aqueous systems, the presence of fulvic (FA) and humic acids (HA) can form rather strong metal complexes. In these cases, the accurate range of the technique might be shifted to lower ligand concentrations. A deeper study of FA and HA systems would be necessary to have a more precise insight of the behaviour of DGT sensors in natural waters.
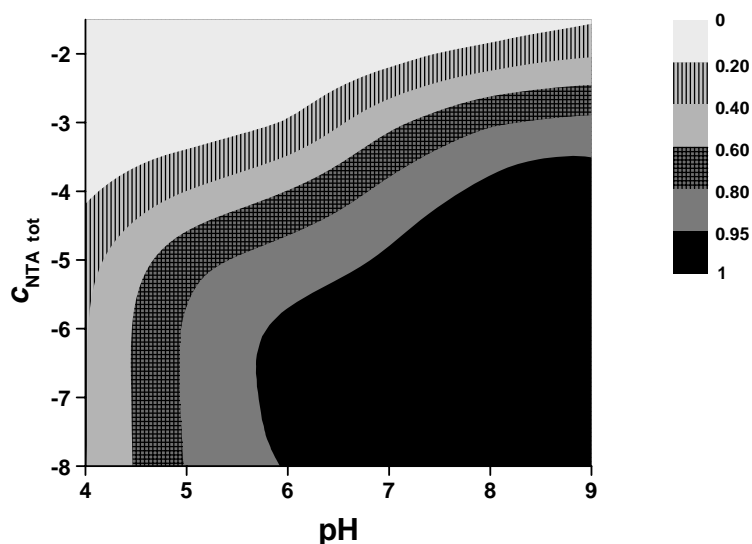
Figure 6. Effect of pH and NTA concentrations on DGT measurements assessed by the ratio n_{DGT}/n after 8 days of deployment. Colour / pattern (see legend) shows the theoretical ratio predicted by numerical simulation. See table S3 for the parameters.

When the equilibrium is reached by the binding resin of the DGT sensor, it ceases to work as a dynamic sensor, but the technique could still be useful to determine the free metal concentration present in the medium. For this purpose, the amount of cadmium eluted from the resin after DGT deployment in equilibrium conditions, can be taken as the value of $c_{\overline{CdR_2}} + c_{\overline{Cd(HR)_2}}$ in

equation 9.5. Then, by knowing the pH of the sample, and solving the set of equations described above (see the description of the equilibrium chemical model for the resin, in the Theoretical Section), the value of c_{Cd} can be obtained. Equivalently, the value of c_{Cd} can be calculated from the total cadmium accumulation, by interpolating its value in **figure 1** on the line corresponding to the pH value of the sample.

This "equilibrium mode of operation" in DGT resembles the technique named as "gellyfish" described in literature.[33] In fact, the gellyfish sensors are designed in a similar way as DGT: a polyacrylamide gel wafer embedded with a known quantity of iminodiacetate resin. This technique was developped in order to measure the free metal concentration, but *in situ* measurements were not reported up to date. The advantage of DGT device as an equilibrium sensor is that it is commercially available.

In order to verify if the DGT sensor works as a dynamic or equilibrium technique in real sample conditions, we propose a simultaneous deployment of two different sensors: one with twice the resin mass of the other. Three different cases can occur (see **figure 7**):

- If both sensors accumulated the same moles of metal, DGT works in the dynamic regime, and the perfect sink equation can be applied, so that the metal concentration determined corresponds to the labile fraction.

- If the DGT sensor with twice the mass of resin accumulated twice the amount of metal than the other one, the DGT sensors reached equilibrium, and the free metal concentration present in the medium can be determined by application of the chemical equilibrium model in the resin.

- In an intermediate case, the working mode of the sensor can not be determined precisely.
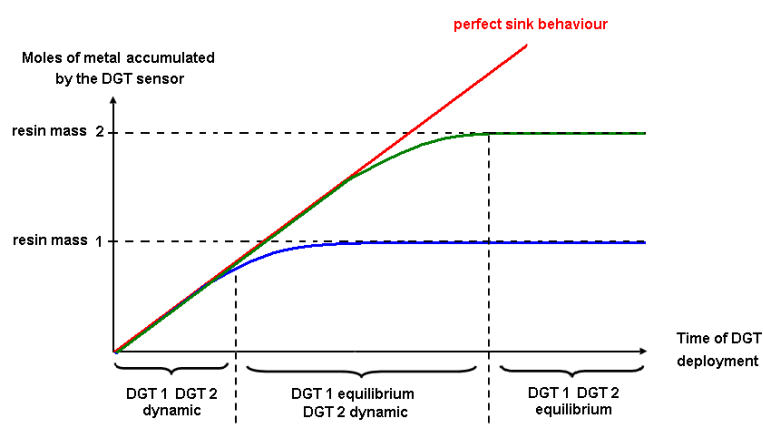
Figure 7. Behaviour of two different DGT sensors: DGT 2 having twice the mass of Chelex than DGT 1.

CONCLUSIONS

The results show the influence of two competitors (proton and ligand) present in the deployment solution on the metal accumulation by the DGT sensor. This study shows that the binding equilibrium of the resin can be reached at relatively low deployment times, depending on the conditions (pH, ligand concentration, stability constant of the complexes). In these equilibrium conditions, the interpretation of DGT measurements as the result of a dynamic behaviour leads to underestimation of the actual metal concentration in the system.

The results indicate that the dynamic behaviour of the DGT sensor, in presence of cadmium only, is fulfilled when the deployment time does not exceed 10 hours at pH 5. At higher pH, the deployment time can be longer, e.g.: 8 days at pH 7. The presence of a metal ligand leads to more strict deployment conditions for a purely dynamic operation of the DGT. E.g., in presence of 10^{-4} mol·L^{-1} of NTA, the dynamic behaviour is fulfilled at pH 7 if the deployment is less than 10 hours and at pH 8 if the deployment is less than 8 days. Moreover, the strength of the metal complexes plays a role, so an equilibrium behaviour of the sensor could presumably arise at lower concentrations, as the complex stability constant increases.

It can be concluded that the use of the DGT sensor as a kinetic method for labile metal determination should be carried out at conditions that ensure an amount of metal binding in the resin at least one order of magnitude below the expected

equilibrium value. On the other hand, a new working operation regime of the DGT sensor can be used for the determination of free metal concentration when the binding resin reaches the equilibrium with the bulk solution.

ACKNOWLEDGMENT

REFERENCES

(1)   Sigg, L.; Black, F.; Buffle, J.; Cao, J.; Cleven, R.; Davison, W.; Galceran, J.; Gunkel, P.; Kalis, E.; Kistler, D.; Martin, M.; Noel, S.; Nur, Y.; Odzak, N.; Puy, J.; Van Riemsdijk, W.; Temminghoff, E.; Tercier-Waeber, M. L.; Toepperwien, S.; Town, R. M.; Unsworth, E.; Warnken, K. W.; Weng, L. P.; Xue, H. B.; Zhang, H., Comparison of analytical techniques for dynamic trace metal speciation in natural freshwaters. *Environmental Science & Technology* **2006,** *40*, (6), 1934-1941.

(2)   Pesavento, M.; Alberti, G.; Biesuz, R., Analytical methods for determination of free metal ion concentration, labile species fraction and metal complexation capacity of environmental waters: A review. *Analytica Chimica Acta* **2009,** *631*, (2), 129-141.

(3)   Zhang, H.; Davison, W., Performance characteristics of diffusion gradients in thin films for the in situ mesurement of trace metals in aqueous solution. *Analytical Chemistry* **1995,** *67*, (19), 3391-3400.

(4)   Davison, W.; Zhang, H., In situ speciation measurement of trace components in natural waters using thin-film gels. *Nature* **1994,** *367*, (6463), 546-548.

(5)   Chang, L. Y.; Davison, W.; Zhang, H.; Kelly, M., Performance characteristics for the measurement of Cs and Sr by diffusive gradients in thin films (DGT). *Analytica Chimica Acta* **1998,** *368*, (3), 243-253.

(6)   Garmo, O. A.; Lehto, N. J.; Zhang, H.; Davison, W.; Royset, O.; Steinnes, E., Dynamic aspects of DGT as demonstrated by experiments with lanthanide complexes of a multidentate ligand. *Environmental Science & Technology* **2006,** *40*, (15), 4754-4760.

(7)   Zhang, H.; Davison, W.; Gadi, R.; Kobayashi, T., In situ measurement of dissolved phosphorus in natural water using DGT. *Analytica Chimica Acta* **1998,** *370*, (1), 29-38.

(8)   Alfaro-De la Torre, M. C.; Beaulieu, P. Y.; Tessier, A., In situ measurement of trace metals in lakewater using the dialysis and DGT techniques. *Analytica Chimica Acta* **2000,** *418*, (1), 53-68.

(9)   Larner, B. L.; Seen, A. J.; Snape, I., Evaluation of diffusive gradients. in thin film (DGT) samplers for measuring contaminants in the Antarctic marine environment. *Chemosphere* **2006,** *65*, (5), 811-820.

(10)   Tankere-Muller, S.; Zhang, H.; Davison, W.; Finke, N.; Larsen, O.; Stahl, H.; Glud, R. N., Fine scale remobilisation of Fe, Mn, Co, Ni, Cu and Cd in contaminated marine sediment. *Marine Chemistry* **2007,** *106*, 192-207.

(11)   Degryse, F.; Smolders, E.; Zhang, H.; Davison, W., Predicting availability of mineral elements to plants with the DGT technique: a review of experimental data and interpretation by modelling. *Environmental Chemistry* **2009,** *6*, (3), 198-218.

(12)   Li, W. J.; Zhao, H. J.; Teasdale, P. R.; John, R.; Wang, F. Y., Metal speciation measurement by diffusive gradients in thin films technique with different binding phases. *Analytica Chimica Acta* **2005,** *533*, (2), 193-202.

(13)   Docekalova, H.; Divis, P., Application of diffusive gradient in thin films technique (DGT) to measurement of mercury in aquatic systems. *Talanta* **2005,** *65*, (5), 1174-1178.

(14)   Lehto, N. J.; Davison, W.; Zhang, H.; Tych, W., An evaluation of DGT performance using a dynamic numerical model. *Environmental Science & Technology* **2006,** *40*, (20), 6368-6376.

(15)   Gimpel, J.; Zhang, H.; Hutchinson, W.; Davison, W., Effect of solution composition, flow and deployment time on the measurement of trace metals by the diffusive gradient in thin films technique. *Analytica Chimica Acta* **2001,** *448*, (1-2), 93-103.

(16)   Sondergaard, J., In situ measurements of labile Al and Mn in acid mine drainage using diffusive gradients in thin films. *Analytical Chemistry* **2007,** *79*, (16), 6419-6423.

(17)   Conesa, H. M.; Schulin, R.; Nowack, B., Suitability of using diffusive gradients in thin films (DGT) to study metal bioavailability in mine tailings:

possibilities and constraints. *Environmental Science and Pollution Research* **2010,** *17*, (3), 657-664.

(18)   Alberti, G.; Biesuz, R., Empore (TM) membrane vs. Chelex 100: Thermodynamic and kinetic studies on metals sorption. *Reactive & functional polymers* **2011,** *71*, (5), 588-598.

(19)   Pesavento, M.; Biesuz, R., Simultaneous determination of total and free metal ion concentration in solution by sorption on iminodiacetate resin. *Analytical Chemistry* **1995,** *67*, (19), 3558-3563.

(20)   Pesavento, M.; Biesuz, R.; Gallorini, M.; Profumo, A., Sorption mechanism of trace amounts of divalent metal ions on a chelating resin containing iminodiacetate groups. *Analytical Chemistry* **1993,** *65*, (18), 2522-2527.

(21)   Mongin, S.; Uribe, R.; Puy, J.; Cecilia, J.; Galceran, J.; Zhang, H.; Davison, W., Key Role of the Resin Layer Thickness in the Lability of Complexes Measured by DGT. *Environmental Science & Technology* **2011,** *45*, (11), 4869-4875.

(22)   Biesuz, R.; Alberti, G.; Pesavento, M., Sorption of lead(II) on two chelating resins: From the exchange coefficient to the intrinsic complexation constant. *Journal of Solution Chemistry* **2008,** *37*, (4), 527-541.

(23)   Chakrabarti, C. L.; Lu, Y. J.; Gregoire, D. C.; Back, M. H.; Schroeder, W. H., Kinetic-studies of metal speciation using chelex cation-exchange resin - application to cadmium, copper, and lead speciation in river water and snow. *Environmental Science & Technology* **1994,** *28*, (11), 1957-1967.

(24)   Uribe, R.; Mongin, S.; Puy, J.; Cecilia, J.; Galceran, J.; Zhang, H.; Davison, W., Contribution of Partially Labile Complexes to the DGT Metal Flux. *Environmental Science & Technology* **2011,** *45*, (12), 5317-5322.

(25)   Diaz Cruz, J. M.; Sanchis, J.; Chekmeneva, E.; Arino, C.; Esteban, M., Non-linear multivariate curve resolution analysis of voltammetric pH titrations. *Analyst* **2010,** *135*, (7), 1653-1662.

(26)   Puy, J.; Cecilia, J.; Galceran, J.; Town, R. M.; van Leeuwen, H. P., Voltammetric lability of multiligand complexes: the case of ML2. *Journal of Electroanalytical Chemistry* **2004,** *571*, (2), 121-132.

(27)   Van Leeuwen, H. P.; Town, R.; Buffle, J., Impact of ligand protonation on eigen-type metal complexation kinetics in aqueous systems. *Journal of Physical Chemistry A* **2007,** *111*, (11), 2115-2121.

(28)   Unsworth, E. R.; Zhang, H.; Davison, W., Use of diffusive gradients in thin films to measure cadmium speciation in solutions with synthetic and natural ligands: Comparison with model predictions. *Environmental Science & Technology* **2005,** *39*, (2), 624-630.

(29)   van Leeuwen, H. P.; Town, R. M., Stripping chronopotentiometry at scanned deposition potential (SSCP). Part 4. The kinetic current regime. *Journal of Electroanalytical Chemistry* **2004,** *561*, (1-2), 67-74.

(30)   Buffle, J.; Zhang, Z.; Startchev, K., Metal flux and dynamic speciation at (Bio)interfaces. part 1: Critical evaluation and compilation of physicochemical parameters for complexes with simple Ligands and Fulvic/Humic substances. *Environmental Science & Technology* **2007,** *41*, (22), 7609-7620.

(31)   Milne, C. J.; Kinniburgh, D. G.; Van Riemsdijk, W. H.; Tipping, E., Generic NICA-Donnan model parameters for metal-ion binding by humic substances. *Environmental Science & Technology* **2003,** *37*, (5), 958-971.

(32)   Degryse, F.; Smolders, E.; Oliver, I.; Zhang, H., Relating soil solution Zn concentration to diffusive gradients in thin films measurements in contaminated soils. *Environmental Science & Technology* **2003,** *37*, (17), 3958-3965.

(33)   Senn, D. B.; Griscom, S. B.; Lewis, C. G.; Galvin, J. P.; Chang, M. W.; Shine, J. P., Equilibrium-based sampler for determining Cu2+ concentrations in aquatic ecosystems. *Environmental Science & Technology* **2004,** *38*, (12), 3381-3386.

Two modes of operation of the DGT sensor: kinetic and equilibrium regimes

SUPPORTING INFORMATION

Section 1: Numerical Simulation of a DGT sensor

Section 2: Formulation of the Cd-NTA speciation in a DGT sensor as a system with only one complex and ligand species

Section 3: Additional figure.

Section 4: Simulation parameters of the figures of the manuscript.

<u>Section 1</u>. Numerical Simulation of a DGT sensor
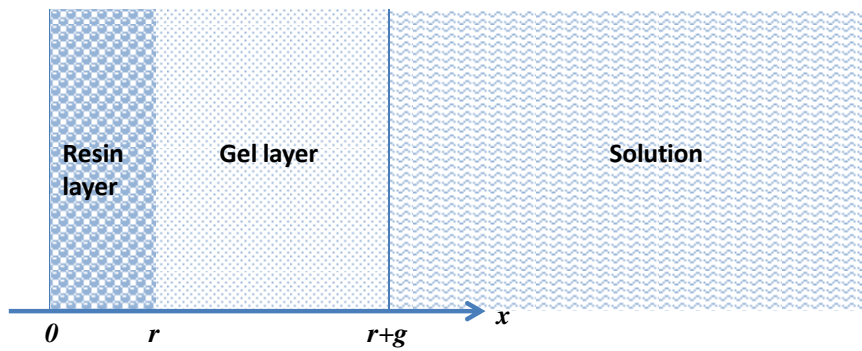
Figure S1. Schematic representation of a DGT device

The model is based on Mongin et al. 2011[1] and coincides with that of Lehto et al. 2006[2] and Tusseau-Vuillemin et al. 2003.[3]

The following reactions are considered:

- The complexation of Cd with a ligand L:

$$Cd + L \underset{k_d}{\overset{k_a}{\rightleftharpoons}} CdL \tag{SI.1}$$

$$K = \frac{k_a}{k_d} = \frac{c_{CdL}}{c_{Cd} c_L} \tag{SI.2}$$

- The cadmium ions bind to the resin sites:[4,5]

$$Cd + 2\,\overline{H_2R} \underset{k_{d,1}}{\overset{k_{a,1}}{\rightleftharpoons}} \overline{CdR_2} + 4\,H \tag{SI.3}$$
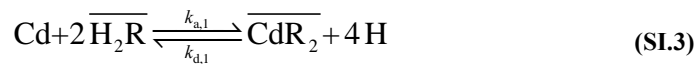
$$\beta_{120ex} = \frac{k_{a,1}}{k_{d,1}} = \frac{c_{\overline{CdR_2}} \left(c_H\right)^4}{\left(c_{\overline{H_2R}}\right)^2 c_{Cd}} \tag{SI.4}$$

$$Cd + 2\,\overline{H_2R} \underset{k_{d,2}}{\overset{k_{a,2}}{\rightleftharpoons}} \overline{Cd\left(HR\right)_2} + 2\,H \tag{SI.5}$$
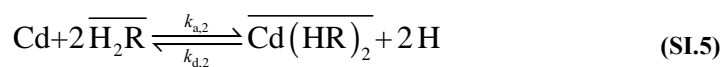
$$\beta_{122ex} = \frac{k_{a,2}}{k_{d,2}} = \frac{c_{\overline{Cd(HR)_2}} \left(c_H\right)^2}{\left(c_{\overline{H_2R}}\right)^2 c_{Cd}} \tag{SI.6}$$

where β_{120ex} and β_{122ex} label the equilibrium exchange coefficients of the Chelex. The exchange coefficients depend on the concentration of counter ion in solution and in resin phase, whereas the intrinsic complexation constants (β_{1iiin}), allow the characterization of the sorption equilibria independently of the composition of the solution. According to the Gibbs-Donnan model,[6] the exchange coefficient may be calculated from the intrinsic complexation constant for any given conditions by the relationship:

$$\beta_{1iiex} = \beta_{1iiin} \frac{\gamma_{Cd}}{\gamma_H^q \cdot \gamma_C^{(2-q)}} \cdot \frac{\left(c_{\overline{C}}\right)^{(2-q)}}{\left(c_C\right)^{(2-q)}} \tag{9.7}$$

where q is the number of protons released, γ_j indicates the activity coefficient of the species j, and C is the counterion, which is assumed monovalent for simplicity.

- Protonation of the chelating sorbent:[5]

$$\overline{R} + H \rightleftharpoons \overline{HR} \tag{SI.8}$$

$$K_{1ex}^H = \frac{k_{a,3}}{k_{d,3}} = \frac{c_{\overline{HR}}}{c_{\overline{R}} \, c_H} \tag{SI.9}$$

$$\overline{HR} + H \rightleftharpoons \overline{H_2R} \tag{SI.10}$$

$$K_{2ex}^H = \frac{k_{a,4}}{k_{d,4}} = \frac{c_{\overline{H_2R}}}{c_{\overline{HR}} \, c_H} \tag{SI.11}$$

The protonation coefficients ($K_{1\,ex}^H$ and $K_{2\,ex}^H$) are defined by analogy with the metal exchange coefficient, so their values depend on the counter ion concentration and the pH.

Numerical values of the intrinsic complexation and protonation constants are given in **table S1**.

$\log K_{H,1in}$	$\log K_{H,2in}$	$\log \beta_{120in}$	$\log \beta_{122in}$
3.2[a]	8.9[a]	-11.2[b]	-3.2[a]

Table S1 : Intrinsic protonation and Cd(II) complexation constants of the Chelex sites, [a]From data reported in references [4,7], [b]from data reported in references[4,5,8]

- The resin mass balance:

$$c_{\overline{R,\text{total}}} = c_{\overline{R}} + c_{\overline{HR}} + c_{\overline{H_2R}} + 2\,c_{\overline{MR_2}} + 2\,c_{\overline{M(HR)_2}} \tag{SI.12}$$

Let D_i and $D_{i,R}$ stand for the diffusion coefficients of species i in the diffusive gel or in the resin domain, respectively and let c_i stand for the concentration of species i at a given spatial position x and time t. Total concentrations are denoted as $c_{i,\text{total}}$.

Then, the transport equations for the different species can be written as:

$$\frac{\partial c_M}{\partial t} = D_{M,R}\frac{\partial^2 c_M}{\partial x^2} - k_a c_M c_L + k_d c_{ML} - k_{a,1} c_M c_{\overline{H_2R}}^2 + k_{d,1} c_{\overline{MR_2}} c_H^4 -$$
$$k_{a,2} c_M c_{\overline{H_2R}}^2 + k_{d,2} c_{\overline{M(RH)_2}} c_H^2, \quad \text{if} \quad 0 < x < r \tag{SI.13}$$

$$\frac{\partial c_M}{\partial t} = D_M\frac{\partial^2 c_M}{\partial x^2} - k_a c_M c_L + k_d c_{ML}, \quad \text{if} \quad r < x < r + g \tag{SI.14}$$

$$\frac{\partial c_{\overline{MR_2}}}{\partial t} = k_{a,1} c_M c_{\overline{H_2R}}^2 - k_{d,1} c_{\overline{MR_2}} c_H^4, \quad \text{if} \quad 0 < x < r \tag{SI.15}$$

$$\frac{\partial c_{\overline{M(RH)_2}}}{\partial t} = k_{a,2} c_M c_{\overline{H_2R}}^2 - k_{d,2} c_{\overline{M(RH)_2}} c_H^2, \quad \text{if} \quad 0 < x < r \tag{SI.16}$$

$$\frac{\partial c_{\overline{RH_2}}}{\partial t} = 2[-k_{a,1} c_M c_{\overline{H_2R}}^2 + k_{d,1} c_{\overline{MR_2}} c_H^4 - k_{a,2} c_M c_{\overline{H_2R}}^2 + k_{d,2} c_{\overline{M(RH)_2}} c_H^2] +$$
$$k_{a,4} c_{\overline{HR}} c_H - k_{d,4} c_{\overline{M(RH)_2}}, \quad \text{if} \quad 0 < x < r \tag{SI.17}$$

$$\frac{\partial c_{\overline{HR}}}{\partial t} = k_{a,3} c_{\overline{R}} c_H - k_{d,3} c_{\overline{HR}} - k_{a,4} c_{\overline{HR}} c_H + k_{d,4} c_{\overline{H_2R}}, \quad \text{if} \quad 0 < x < r \tag{SI.18}$$

$$\frac{\partial c_{\overline{R}}}{\partial t} = -k_{a,3} c_{\overline{R}} c_H + k_{d,3} c_{\overline{HR}}, \quad \text{if} \quad 0 < x < r \tag{SI.19}$$

$$\frac{\partial c_L}{\partial t} = D_{L,R}\frac{\partial^2 c_L}{\partial x^2} + k_a c_M c_L - k_d c_{ML}, \quad \text{if} \quad 0 < x < r \tag{SI.20}$$

$$\frac{\partial c_{\mathrm{L}}}{\partial t} = D_{\mathrm{L}} \frac{\partial^2 c_{\mathrm{L}}}{\partial x^2} + k_{\mathrm{a}} c_{\mathrm{M}} c_{\mathrm{L}} - k_{\mathrm{d}} c_{\mathrm{ML}}, \quad \text{if} \quad r < x < r+g \tag{SI.21}$$

$$\frac{\partial c_{\mathrm{ML}}}{\partial t} = D_{\mathrm{ML,R}} \frac{\partial^2 c_{\mathrm{ML}}}{\partial x^2} + k_{\mathrm{a}} c_{\mathrm{M}} c_{\mathrm{L}} - k_{\mathrm{d}} c_{\mathrm{ML}}, \quad \text{if} \quad 0 < x < r \tag{SI.22}$$

$$\frac{\partial c_{\mathrm{ML}}}{\partial t} = D_{\mathrm{ML}} \frac{\partial^2 c_{\mathrm{ML}}}{\partial x^2} + k_{\mathrm{a}} c_{\mathrm{M}} c_{\mathrm{L}} - k_{\mathrm{d}} c_{\mathrm{ML}}, \quad \text{if} \quad r < x < r+g \tag{SI.23}$$

A new formal species, $c_{\overline{\mathrm{FR}}}$, is introduced as the total free resin concentration:

$$c_{\overline{\mathrm{FR}}} = c_{\overline{\mathrm{R}}} + c_{\overline{\mathrm{HR}}} + c_{\overline{\mathrm{H_2R}}} \tag{SI.24}$$

Using the equilibria **equations SI.9** and **SI.11**,

$$c_{\overline{\mathrm{H_2R}}} = \alpha c_{\overline{\mathrm{FR}}}, \quad \text{with} \quad \alpha = \frac{1}{(1 + \dfrac{1}{K_{2ex}^{H} c_{\mathrm{H}}} + \dfrac{1}{K_{1ex}^{H} K_{2ex}^{H} c_{\mathrm{H}}^2})} \tag{SI.25}$$

Then, the system **SI.13** - **SI.23** can be rewritten as:

$$\frac{\partial c_{\mathrm{M}}}{\partial t} = D_{\mathrm{M,R}} \frac{\partial^2 c_{\mathrm{M}}}{\partial x^2} - k_{\mathrm{a}} c_{\mathrm{M}} c_{\mathrm{L}} + k_{\mathrm{d}} c_{\mathrm{ML}} - k_{\mathrm{a,1}} c_{\mathrm{M}} \alpha^2 c_{\overline{\mathrm{FR}}}^2 + k_{\mathrm{d,1}} c_{\overline{\mathrm{MR_2}}} c_{\mathrm{H}}^4 - $$
$$k_{\mathrm{a,2}} c_{\mathrm{M}} \alpha^2 c_{\overline{\mathrm{FR}}}^2 + k_{\mathrm{d,2}} c_{\overline{\mathrm{M(RH)_2}}} c_{\mathrm{H}}^2, \quad \text{if} \quad 0 < x < r \tag{SI.26}$$

$$\frac{\partial c_{\mathrm{M}}}{\partial t} = D_{\mathrm{M}} \frac{\partial^2 c_{\mathrm{M}}}{\partial x^2} - k_{\mathrm{a}} c_{\mathrm{M}} c_{\mathrm{L}} + k_{\mathrm{d}} c_{\mathrm{ML}} \quad \text{if} \quad r < x < r+g \tag{SI.27}$$

$$\frac{\partial c_{\overline{\mathrm{MR_2}}}}{\partial t} = k_{\mathrm{a,1}} c_{\mathrm{M}} \alpha^2 c_{\overline{\mathrm{FR}}}^2 - k_{\mathrm{d,1}} c_{\overline{\mathrm{MR_2}}} c_{\mathrm{H}}^4, \quad \text{if} \quad 0 < x < r \tag{SI.28}$$

$$\frac{\partial c_{\overline{\mathrm{M(RH)_2}}}}{\partial t} = k_{\mathrm{a,2}} c_{\mathrm{M}} \alpha^2 c_{\overline{\mathrm{FR}}}^2 - k_{\mathrm{d,1}} c_{\overline{\mathrm{M(RH)_2}}} c_{\mathrm{H}}^2, \quad \text{if} \quad 0 < x < r \tag{SI.29}$$

$$\frac{\partial c_{\overline{\mathrm{FR}}}}{\partial t} = 2[-k_{\mathrm{a,1}} c_{\mathrm{M}} \alpha^2 c_{\overline{\mathrm{FR}}}^2 + k_{\mathrm{d,1}} c_{\overline{\mathrm{MR_2}}} c_{\mathrm{H}}^4 - k_{\mathrm{a,2}} c_{\mathrm{M}} \alpha^2 c_{\overline{\mathrm{FR}}}^2 + k_{\mathrm{d,2}} c_{\overline{\mathrm{M(RH)_2}}} c_{\mathrm{H}}^2],$$
$$\text{if} \quad 0 < x < r \tag{SI.30}$$

$$\frac{\partial c_{\mathrm{L}}}{\partial t} = D_{\mathrm{L,R}} \frac{\partial^2 c_{\mathrm{L}}}{\partial x^2} + k_{\mathrm{a}} c_{\mathrm{M}} c_{\mathrm{L}} - k_{\mathrm{d}} c_{\mathrm{ML}}, \quad \text{if} \quad 0 < x < r \tag{SI.31}$$

$$\frac{\partial c_{\mathrm{L}}}{\partial t} = D_{\mathrm{L}}\frac{\partial^2 c_{\mathrm{L}}}{\partial x^2} + k_{\mathrm{a}} c_{\mathrm{M}} c_{\mathrm{L}} - k_{\mathrm{d}} c_{\mathrm{ML}}, \quad \text{if} \quad r < x < r+g \tag{SI.32}$$

$$\frac{\partial c_{\mathrm{ML}}}{\partial t} = D_{\mathrm{ML,R}}\frac{\partial^2 c_{\mathrm{ML}}}{\partial x^2} + k_{\mathrm{a}} c_{\mathrm{M}} c_{\mathrm{L}} - k_{\mathrm{d}} c_{\mathrm{ML}}, \quad \text{if} \quad 0 < x < r \tag{SI.33}$$

$$\frac{\partial c_{\mathrm{ML}}}{\partial t} = D_{\mathrm{ML}}\frac{\partial^2 c_{\mathrm{ML}}}{\partial x^2} + k_{\mathrm{a}} c_{\mathrm{M}} c_{\mathrm{L}} - k_{\mathrm{d}} c_{\mathrm{ML}}, \quad \text{if} \quad r < x < r+g \tag{SI.34}$$

It is important to note that even the equations contain kinetic terms, locally equilibrium is achieved in all time between resin and free metal.

No resin sites are present in the diffusive gel: $c_{\mathrm{R}}(x,t) = c_{\mathrm{MR}}(x,t) = 0$ for $r < x < r+g$

Initial conditions correspond to the absence of metal and ligand in the sensor:

$$c_{\mathrm{M}}(x,0) = c_{\mathrm{L}}(x,0) = c_{\mathrm{ML}}(x,0) = 0, \quad \text{if} \quad 0 < x < r+g \tag{SI.35}$$

$$c_{\mathrm{MR}}(x,0) = 0 \quad \text{if} \quad 0 < x < r \tag{SI.36}$$

$$c_{\mathrm{R}}(x,0) = c_{\mathrm{R,total}} \quad \text{if} \quad 0 < x < r \tag{SI.37}$$

Boundary conditions at $x = r+g$ correspond to bulk concentrations:

$$c_{\mathrm{M}}(r+g,t) = c_{\mathrm{M}}^*, \quad c_{\mathrm{L}}(r+g,t) = c_{\mathrm{L}}^*, \quad c_{\mathrm{ML}}(r+g,t) = c_{\mathrm{ML}}^* \tag{SI.38}$$

Boundary conditions at $x = r$:

at the gel-resin interface $c_{\mathrm{M}}(x,t)$, $c_{\mathrm{L}}(x,t)$, and $c_{\mathrm{ML}}(x,t)$ and their fluxes must be continuous, that is:

$$c_{\mathrm{M}}(r^-,t) = c_{\mathrm{M}}(r^+,t), \quad c_{\mathrm{L}}(r^-,t) = c_{\mathrm{L}}(r^+,t), \quad c_{\mathrm{ML}}(r^-,t) = c_{\mathrm{ML}}(r^+,t) \tag{SI.39}$$

and:

$$D_{\mathrm{M,R}}\frac{\partial c_{\mathrm{M}}}{\partial x}\bigg|_{r^-} = D_{\mathrm{M}}\frac{\partial c_{\mathrm{M}}}{\partial x}\bigg|_{r^+}, \quad D_{\mathrm{L,R}}\frac{\partial c_{\mathrm{L}}}{\partial x}\bigg|_{r^-} = D_{\mathrm{L}}\frac{\partial c_{\mathrm{L}}}{\partial x}\bigg|_{r^+}, \quad D_{\mathrm{L,R}}\frac{\partial c_{\mathrm{ML}}}{\partial x}\bigg|_{r^-} = D_{\mathrm{L}}\frac{\partial c_{\mathrm{ML}}}{\partial x}\bigg|_{r^+} \tag{SI.40}$$

The continuity of the concentrations indicates that no Donnan effects are considered, so that charge effects of the resin are screened by the supporting electrolyte.

Boundary conditions at $x = 0$ stem from non-flux conditions:

$$\left.\frac{\partial c_{\mathrm{M}}}{\partial x}\right|_{x=0} = \left.\frac{\partial c_{\mathrm{L}}}{\partial x}\right|_{x=0} = \left.\frac{\partial c_{\mathrm{ML}}}{\partial x}\right|_{x=0} = 0 \tag{SI.41}$$

Thus, we have a system of equations for:

$$c_{\mathrm{M}}(x,t), \quad c_{\mathrm{L}}(x,t), \quad c_{\mathrm{ML}}(x,t), \quad c_{\mathrm{FR}}(x,t), \quad c_{\mathrm{M(RH)_2}}(x,t) \quad \text{and} \quad c_{\mathrm{MR_2}}(x,t) \tag{SI.42}$$

To solve this system we use the same procedure used in Mongin *et al.*[1]

Section 2. Formulation of the Cd-NTA speciation in a DGT sensor as a system with only one complex and ligand species

A scheme of the processes in solution is:

$$\begin{array}{c}
\mathrm{M + L} \quad \underset{k_{\mathrm{d,1}}}{\overset{k_{\mathrm{a,1}}}{\rightleftharpoons}} \quad \mathrm{ML} + \mathrm{L} \underset{k_{\mathrm{d,2}}}{\overset{k_{\mathrm{a,2}}}{\rightleftharpoons}} \quad \mathrm{ML_2} \\
+ \\
\mathrm{H} \\
k_{\mathrm{d\_H,1}} \uparrow\downarrow k_{\mathrm{a\_H,1}} \\
\mathrm{HL} \\
+ \\
\mathrm{H} \\
k_{\mathrm{d\_H,2}} \uparrow\downarrow k_{\mathrm{a\_H,2}} \\
.... \\
\mathrm{H_4L}
\end{array} \tag{SI.43}$$
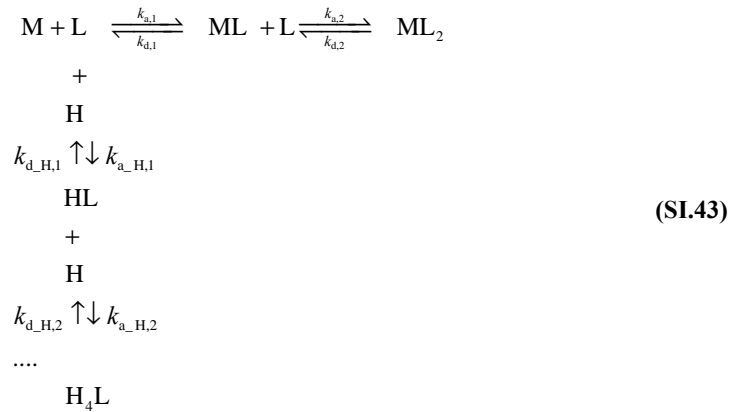
The transport problem of the processes in solution can be stated as:

$$\frac{\partial c_{\mathrm{M}}}{\partial t} = D_{\mathrm{M}} \frac{\partial^2 c_{\mathrm{M}}}{\partial x^2} + k_{\mathrm{d,1}} c_{\mathrm{ML}} - k_{\mathrm{a,1}} c_{\mathrm{M}} c_{\mathrm{L}} \tag{SI.44}$$

$$\frac{\partial c_{\mathrm{ML}}}{\partial t} = D_{\mathrm{ML}} \frac{\partial^2 c_{\mathrm{ML}}}{\partial x^2} - k_{\mathrm{d,1}} c_{\mathrm{ML}} + k_{\mathrm{a,1}} c_{\mathrm{M}} c_{\mathrm{L}} + k_{\mathrm{d,2}} c_{\mathrm{ML_2}} - k_{\mathrm{a,2}} c_{\mathrm{ML}} c_{\mathrm{L}} \tag{SI.45}$$

$$\frac{\partial c_{\mathrm{ML_2}}}{\partial t} = D_{\mathrm{ML_2}} \frac{\partial^2 c_{\mathrm{ML}}}{\partial x^2} - k_{\mathrm{d,2}} c_{\mathrm{ML_2}} + k_{\mathrm{a,2}} c_{\mathrm{ML}} c_{\mathrm{L}} \tag{SI.46}$$

$$\frac{\partial c_{\text{L}}}{\partial t} = D_{\text{L}} \frac{\partial^2 c_{\text{L}}}{\partial x^2} + k_{\text{d,1}} c_{\text{M,L}} - k_{\text{a,1}} c_{\text{M}} c_{\text{L}} + k_{\text{d\_H,1}} c_{\text{HL}} - k_{\text{a\_H,1}} c_{\text{H}} c_{\text{L}} \qquad \textbf{(SI.47)}$$

$$\frac{\partial c_{\text{HL}}}{\partial t} = D_{\text{HL}} \frac{\partial^2 c_{\text{HL}}}{\partial x^2} + k_{\text{d\_H,2}} c_{\text{H}_2\text{L}} - k_{\text{a\_H,2}} c_{\text{H}} c_{\text{HL}} - k_{\text{d\_H,1}} c_{\text{HL}} + k_{\text{a\_H,1}} c_{\text{H}} c_{\text{L}} \qquad \textbf{(SI.48)}$$

…

$$\frac{\partial c_{\text{H}_4\text{L}}}{\partial t} = D_{\text{H}_4\text{L}} \frac{\partial^2 c_{\text{H}_4\text{L}}}{\partial x^2} - k_{\text{d\_H,4}} c_{\text{H}_3\text{L}} + k_{\text{a\_H,1}} c_{\text{H}} c_{\text{H}_3\text{L}} \qquad \textbf{(SI.49)}$$

Adding the transport equations of the binding complexes forms (**SI.45** and **SI.46**):

$$\frac{\partial c_{\text{ML}_{\text{tot}}}}{\partial t} = \frac{\partial c_{\text{ML}} + \partial c_{\text{ML}_2}}{\partial t} = \frac{\partial^2 \left(D_{\text{ML}} c_{\text{ML}} + D_{\text{ML}_2} c_{\text{ML}_2} \right)}{\partial x^2} - k_{\text{d,1}} c_{\text{ML}} + k_{\text{a,1}} c_{\text{M}} c_{\text{L}} \qquad \textbf{(SI.50)}$$

Since the formation of ML_2 is instantaneous, equilibria relationship are applied:

$$c_{\text{ML}_{\text{tot}}} = c_{\text{ML}} \left(1 + K_2 c_{\text{L}} \right) \quad \Rightarrow \quad c_{\text{ML}} = \frac{1}{1 + K_2 c_{\text{L}}} c_{\text{M}\,bound} \qquad \textbf{(SI.51)}$$

$$c_{\text{ML}_{\text{tot}}} = c_{\text{ML}_2} \left(1 + \frac{1}{K_2 c_{\text{L}}} \right) \quad \Rightarrow \quad c_{\text{ML}_2} = \frac{K_2 c_{\text{L}}}{1 + K_2 c_{\text{L}}} c_{\text{M}\,bound} \qquad \textbf{(SI.52)}$$

The transport **equation SI.50** can be rewritten as:

$$\frac{\partial c_{\text{ML}_{\text{tot}}}}{\partial t} = \left(D_{\text{ML}} \frac{1}{1 + K_2 c_{\text{L}}} + D_{\text{ML}_2} \frac{K_2 c_{\text{L}}}{1 + K_2 c_{\text{L}}} \right) \frac{\partial^2 c_{\text{ML}_{\text{tot}}}}{\partial x^2} - \frac{k_{\text{d,1}}}{1 + K_2 c_{\text{L}}} c_{\text{ML}_{\text{tot}}} + k_{\text{a,1}} c_{\text{M}} c_{\text{L}} \qquad \textbf{(SI.53)}$$

Adding an effective concentration of ligand corresponding at of all the protonated ligand forms:

$$c_{\text{L}}^{\text{eff}} = c_{\text{L}} + c_{\text{HL}} + c_{\text{H}_2\text{L}} + c_{\text{H}_3\text{L}} + c_{\text{H}_4\text{L}} \qquad \textbf{(SI.54)}$$

Considering that protonated and NTA^{3-} have the same diffusion coefficient D_{L}, transport equation for the effective ligand concentration become (**equations SI.47 - SI.49**):

Results – Two modes of operation of the DGT sensor: kinetic and equilibrium regimes

$$\frac{\partial c_L^{eff}}{\partial t} = D_L \frac{\partial^2 c_L^{eff}}{\partial x^2} + k_{d,1} c_{ML} - k_{a,1} c_M c_L \qquad \textbf{(SI.55)}$$

Since protonation is instantaneous, acid-base equilibria relationship apply:

$$K_{H,i} = \frac{c_{H_i L}}{c_H^i\, c_{H_{(i-1)} L}} \qquad \textbf{(SI.56)}$$

c_L can be rewritten as

$$c_L = \frac{c_L^{eff}}{B} \qquad \textbf{(SI.57)}$$

where $B = 1 + K_{H,1} c_H + K_{H,1} K_{H,2} c_H^2 + K_{H,1} K_{H,2} K_{H,3} c_H^3 + K_{H,1} K_{H,2} K_{H,3} K_{H,4} c_H^4$

In terms of c_L^{eff} and $c_{M\,bound}$, **equations SI.44, SI.53** and **SI.55** become:

$$\frac{\partial c_M}{\partial t} = D_M \frac{\partial^2 c_M}{\partial x^2} + \frac{k_{d,1}}{1 + \dfrac{K_2 c_L^{eff}}{B}} c_{ML_{tot}} - \frac{k_{a,1}}{B} c_M c_L^{eff} \qquad \textbf{(SI.58)}$$

$$\frac{\partial c_{ML_{tot}}}{\partial t} = \left(\frac{D_{ML} + D_{ML_2} \dfrac{K_2 c_L^{eff}}{B}}{1 + \dfrac{K_2 c_L^{eff}}{B}} \right) \frac{\partial^2 c_{ML_{tot}}}{\partial x^2} - \frac{k_{d,1}}{1 + \dfrac{K_2 c_L^{eff}}{B}} c_{ML_{tot}} + \frac{k_{a,1}}{B} c_M c_L^{eff} \qquad \textbf{(SI.59)}$$

and

$$\frac{\partial c_L^{eff}}{\partial t} = D_L \frac{\partial^2 c_L^{eff}}{\partial x^2} + \frac{k_{d,1}}{1 + \dfrac{K_2 c_L^{eff}}{B}} c_{ML_{tot}} - \frac{k_{a,1}}{B} c_M c_L^{eff} \qquad \textbf{(SI.60)}$$

Equations SI.58-SI.60 are formally identical to a system with one ligand with concentration c_L^{eff}, that is not involved in any protonation and formation of ML_2 equilibria. The effective association and dissociation constants of this ligand with the metal are:

$$k_a^{eff} = \frac{k_{a,1}}{B} \qquad \textbf{(SI.61)}$$

$$k_{\mathrm{d}}^{\mathrm{eff}} = \frac{k_{\mathrm{d},1}}{1 + \dfrac{K_2 c_{\mathrm{L}}^{\mathrm{eff}}}{B}}$$

(SI.62)

The effective stability constant of the metal complexation with this formal ligand $c_{\mathrm{L}}^{\mathrm{eff}}$ is:

$$K^{\mathrm{eff}} = \frac{k_{\mathrm{a}}^{\mathrm{eff}}}{k_{\mathrm{d}}^{\mathrm{eff}}} = \frac{K_1 \left(1 + \dfrac{K_2 c_{\mathrm{L}}^{\mathrm{eff}}}{B} \right)}{B}$$

(SI.63)

The effective diffusion coefficient of the bound species is given by:

$$D_{\mathrm{NTA}}^{\mathrm{eff}} = \frac{D_{\mathrm{CdNTA}} + D_{\mathrm{CdNTA_2}} \dfrac{K_2 c_{\mathrm{NTA}}^{\mathrm{eff}}}{B}}{1 + \dfrac{K_2 c_{\mathrm{NTA}}^{\mathrm{eff}}}{B}}$$

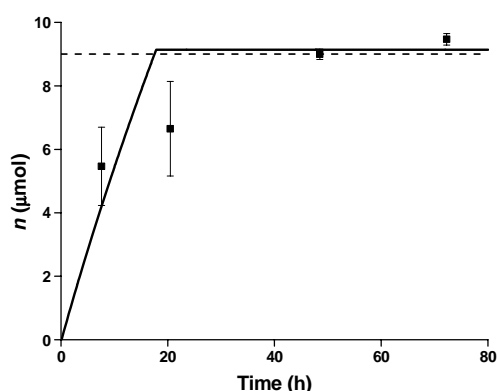**(SI.64)**

Section 3. Additional figure

Figure S2. Moles of cadmuim accumulated by DGT at pH 8 in presence of 10^{-3} mol·L^{-1} Cd. Line: theoretical accumulation predicted by numerical simulation. Dash line: saturation literature value from SI of Levy et al.[9] Markers: experimental measurement. See table S2 for the parameters. The maximum accumulation is 9.2 µmols which leads to a total amount of resin of 18 µmols per sensor DGT.

Section 4. Simulation parameters of the figures of the manuscript

pH	$\beta_{120ex}\left(m^3 \cdot mol^{-1}\right)^2$	β_{122ex}	$K^H_{1ex}\left(m^3 \cdot mol^{-1}\right)$	$K^H_{2ex}\left(m^3 \cdot mol^{-1}\right)$
2	1.33×10^{-6}	4.26×10^{-4}	1.41×10^6	2.82
3	2.05×10^{-7}	4.26×10^{-4}	3.63×10^6	7.24
4	2.82×10^{-8}	4.26×10^{-4}	9.77×10^6	1.95×10^1
5	6.47×10^{-9}	4.26×10^{-4}	2.04×10^7	4.07×10^1
6	3.64×10^{-9}	4.26×10^{-4}	2.69×10^7	5.37×10^1
7	3.31×10^{-9}	4.26×10^{-4}	2.82×10^7	5.62×10^1
8	3.26×10^{-9}	4.26×10^{-4}	2.88×10^7	5.75×10^1
9	3.07×10^{-9}	4.26×10^{-4}	2.95×10^7	5.89×10^1

Table S2. Simulation parameters in presence of cadmium only at ionic strength of 0.05 M. Simulations are realized for different cadmium concentrations: 2.7x10^{-8} mol·L^{-1}, 10^{-5} mol·L^{-1} and 10^{-3} mol·L^{-1}. Other parameters: diffusion layer thickness: g=1.13x10^{-3} m, resin layer thickness: r=4x10^{-4} m, Cd diffusion coefficient: D_{Cd}=6.09x10^{-10} m·s^{-1}, resin site concentration: $c_{T,R}$=0.147 mol·L^{-1}, T=25ºC, I=0.05 M.

Results – Two modes of operation of the DGT sensor: kinetic and equilibrium regimes

pH	$\log(c_{T\perp})(\log(\text{mol·L}^{-1}))$	$k_a^{\text{eff}}(\text{m}^3\cdot\text{mol}^{-1}\cdot\text{s}^{-1})$	$k_d^{\text{eff}}(\text{s}^{-1})$	$D_{\text{NTA}}^{\text{eff}}(\text{m}^2\cdot\text{s}^{-1})$
4	**-8**	7.89×10^1	2.76	4.26×10^{-10}
	-7	7.89×10^1	2.76	4.26×10^{-10}
	-6	7.89×10^1	2.76	4.26×10^{-10}
	-5	7.89×10^1	2.76	4.26×10^{-10}
	-4	7.89×10^1	2.76	4.26×10^{-10}
	-3	7.89×10^1	2.76	4.26×10^{-10}
	-2	7.89×10^1	2.76	4.26×10^{-10}
5	**-8**	8.18×10^2	2.76	4.26×10^{-10}
	-7	8.18×10^2	2.76	4.26×10^{-10}
	-6	8.18×10^2	2.76	4.26×10^{-10}
	-5	8.18×10^2	2.76	4.26×10^{-10}
	-4	8.18×10^2	2.76	4.26×10^{-10}
	-3	8.18×10^2	2.76	4.26×10^{-10}
	-2	8.18×10^2	2.75	4.25×10^{-10}
6	**-8**	8.21×10^3	2.76	4.26×10^{-10}
	-7	8.21×10^3	2.76	4.26×10^{-10}
	-6	8.21×10^3	2.76	4.26×10^{-10}
	-5	8.21×10^3	2.76	4.26×10^{-10}
	-4	8.21×10^3	2.76	4.26×10^{-10}
	-3	8.21×10^3	2.75	4.25×10^{-10}
	-2	8.21×10^3	2.60	4.19×10^{-10}
7	**-8**	8.20×10^4	2.76	4.26×10^{-10}
	-7	8.20×10^4	2.76	4.26×10^{-10}
	-6	8.20×10^4	2.76	4.26×10^{-10}
	-5	8.20×10^4	2.76	4.26×10^{-10}
	-4	8.20×10^4	2.75	4.25×10^{-10}
	-3	8.20×10^4	2.60	4.19×10^{-10}
	-2	8.20×10^4	1.69	3.77×10^{-10}
8	**-8**	8.08×10^5	2.76	4.26×10^{-10}
	-7	8.08×10^5	2.76	4.26×10^{-10}
	-6	8.08×10^5	2.76	4.26×10^{-10}
	-5	8.08×10^5	2.75	4.26×10^{-10}
	-4	8.08×10^5	2.60	4.19×10^{-10}
	-3	8.08×10^5	1.70	3.77×10^{-10}
	-2	8.08×10^5	0.382	3.16×10^{-10}
9	**-8**	7.04×10^6	2.76	4.26×10^{-10}
	-7	7.04×10^6	2.76	4.26×10^{-10}
	-6	7.04×10^6	2.75	4.26×10^{-10}
	-5	7.04×10^6	2.62	4.20×10^{-10}
	-4	7.04×10^6	1.79	3.81×10^{-10}
	-3	7.04×10^6	4.29×10^{-1}	3.18×10^{-10}
	-2	7.04×10^6	4.99×10^{-2}	3.01×10^{-10}

Table S3. Simulation parameters in presence of cadmium and NTA at ionic strength of 0.05 M. Simulations are realized for different cadmium concentrations: 2.7×10^{-8} mol·L^{-1}, 10^{-5} mol·L^{-1}. The resin parameters are given in the table S2. Other parameters: diffusion layer thickness: $g=1.13\times10^{-3}$ m, resin layer thickness: $r=4\times10^{-4}$ m, Cd diffusion coefficient: $D_{\text{Cd}}=6.09\times10^{-10}$ m·s^{-1}, complex diffusion coefficient: $D_{\text{CdNTA}}=0.7\times$ $D_{\text{Cd}}=4.26\times10^{-10}$ m·s^{-1}, resin site concentration: $c_{\text{T,R}}=0.147$ mol·L^{-1}, $T=25^{\circ}$C, $I=0.05$ M, $K_1=10^{11.28}$ L·mol^{-1} (value fitted from experimental titration data, $K_2=10^{4.07}$ L·mol^{-1} (NIST 46.6 database)

Literature cited

(1)   Mongin, S.; Uribe, R.; Puy, J.; Cecilia, J.; Galceran, J.; Zhang, H.; Davison, W., Key Role of the Resin Layer Thickness in the Lability of Complexes Measured by DGT. *Environmental Science & Technology* **2011,** *45*, (11), 4869-4875.

(2)   Lehto, N. J.; Davison, W.; Zhang, H.; Tych, W., An evaluation of DGT performance using a dynamic numerical model. *Environmental Science & Technology* **2006,** *40*, (20), 6368-6376.

(3)   Tusseau-Vuillemin, M. H.; Gilbin, R.; Taillefert, M., A dynamic numerical model to characterize labile metal complexes collected with diffusion gradient in thin films devices. *Environmental Science & Technology* **2003,** *37*, (8), 1645-1652.

(4)   Alberti, G.; Biesuz, R., Empore (TM) membrane vs. Chelex 100: Thermodynamic and kinetic studies on metals sorption. *Reactive & functional polymers* **2011,** *71*, (5), 588-598.

(5)   Pesavento, M.; Biesuz, R.; Gallorini, M.; Profumo, A., Sorption mechanism of trace amounts of divalent metal ions on a chelating resin containing iminodiacetate groups. *Analytical Chemistry* **1993,** *65*, (18), 2522-2527.

(6)   Pesavento, M.; Biesuz, R.; Alberti, G.; Dalla Riva, F., Evaluation of the sorption of metal ions on a complexing resin from different solutions based on the Gibbs-Donnan model. *Reactive & functional polymers* **2001,** *46*, (3), 233-246.

(7)   Alberti, G.; Guiso, M. G.; Biesuz, R., Usage of Empore (TM) membrane in alcoholic media for copper(II) distribution studies. *Talanta* **2009,** *79*, (3), 603-612.

(8)   Pesavento, M.; Biesuz, R., Simultaneous determination of total and free metal ion concentration in solution by sorption on iminodiacetate resin. *Analytical Chemistry* **1995,** *67*, (19), 3558-3563.

(9)   Levy, J. L.; Zhang, H.; Davison, W.; Puy, J.; Galceran, J., Assessment of trace metal binding kinetics in the resin phase of diffusive gradients in thin films. *Analytica Chimica Acta* **2012,** *717*, 143-150.

Part III

CHAPTER 10

GENERAL DISCUSION

The (bio)availability of a species determines its nutritive or ecotoxicity properties. It was seen that the (bio)availability depends on the species distribution over different physico-chemical forms, called speciation. When the internalization by the organism is the limiting step (in comparison with the transport of species, see **figure 6.3 a**)), the free-ion activity governs the (bio)availability of the species in the medium. In this assumption is based the Free Ion Activity Model (FIAM) and the Biotic Ligand Model (BLM). The first part of this manuscript is devoted to the speciation of metal ions in presence of humic substances (humic and fulvic acids).

In natural water and soil, organic matter is composed by a great proportion of humic substances that play an important role in the trace metal complexation phenomena. Due to the complexity of these species (**figure 2.2** shows a hypothetical structure of humic acid), they must be considered as macromolecular ligands where different sites for the complexation are present. The affinity of humic substances for a given metal ion decreases with increasing concentration of the metal, which can be explained considering the macromolecule as an ensemble of binding sites of different affinities.

In this ensemble, the sites with a stronger affinity are occupied first (i.e., at lower metal concentrations) whereas, the weaker sites will only be occupied at higher metal concentrations. The representation of the fraction of sites as a function of its binding equilibrium constant is called the Affinity Spectrum (AS). For instance, **figure 10.1** shows the AS of a fulvic acid for lead, as obtained from the generic NICA isotherm used in chapter 5. The distribution depicted in **figure 10.1** is a bimodal Sips distribution. The first peak is usually associated with the "carboxylic" type of sites, whereas the second peak is related to the "phenolic" distribution.

An additional problem in the study of cation binding to macromolecules is the competition among different cations. A variety of different inorganic species co-exist in natural systems. Therefore, they can compete with each other for the same complexation site of the humic substance. Even in the simplest case of the complexation of only one metal ion, the competition with protons is always present. Therefore, the affinity of a binding site for a cation depends on the concentration of other cations. However, we can describe apparent or effective affinity that a ligand displays toward a given metal in conditions where the free concentration of the competitor ions is kept constant. The resulting distribution

is called the Conditional Affinity Spectrum (CAS), and it is a generalisation of conditional constant concept in the analytical chemistry.
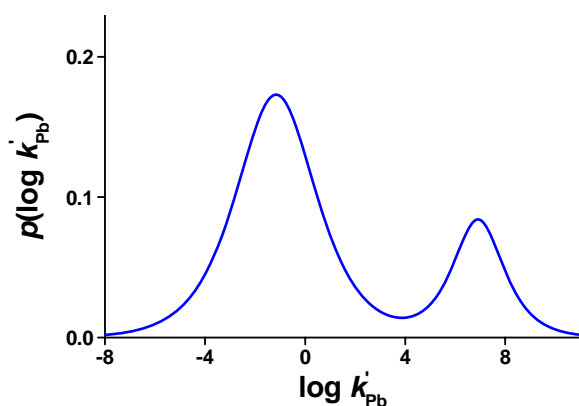

Figure 10.1. Affinity spectrum of lead binding by a generic fulvic acid. Generic NICA parameter are used for the calculation.[1]

Figure 10.2 represents the comparison between the affinity spectrum of fulvic acid for Pb in absence of any other ion (blue line), compared with the effective affinity in the presence of pH 7 (CAS, red line). The shift of the CAS toward lower affinity reflects a significant competition effect. However, only the phenolic distribution narrowed and shifted noticeable indicating that only these sites are occupied by the protons and the sites with high affinity for the protons also display a high affinity for Pb.
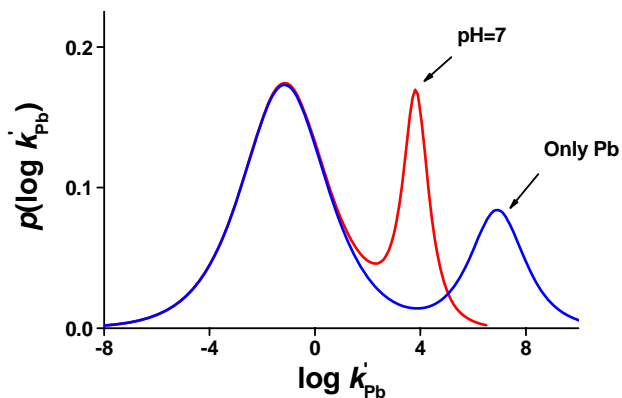

Figure 10.2. Effect of the competitive proton on the effective Pb binding affinity of a generic fulvic acid. Blue line: affinity spectrum in absence of competing ions; red line: CAS at pH 7. NICA parameter are used for the calculation.[1]

General discussion

The occupied site can be represented in the CAS. **Figure 10.3** shows the distribution of occupied site of the fulvic acid by proton at pH 7.
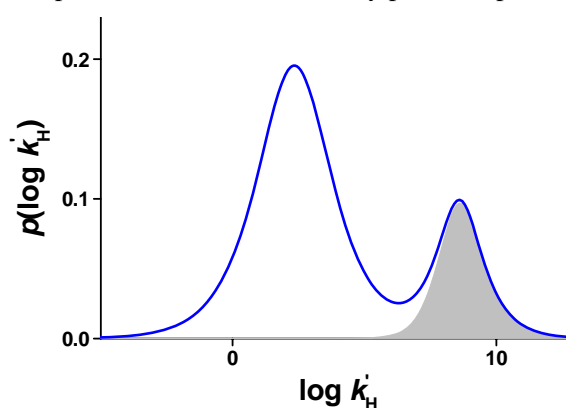

Figure 10.3. CAS of proton binding to the generic fulvic acid. The shaded area shows the density of occupied sites by H$^+$ at pH 7

This methodoly has been applied to draw the occupied fraction by one cation for a typical freshwater composition, these results are given in chapter x5

CAScTM, presented in chapter 4 is a generalisation of the CAS that represents the affinity spectrum of proton for a fixed total metal concentration. This physicochemical tool have great interest for titrations in laboratory, because it allows to obtain information on the metal binding to humic or fulvic acid by acid-base titration in presence of the target metal at fixed total concentration. This methodology can be very useful for metals whose ISE are not commercially available.

As mentioned above, the (bio)availability is governed by the free-ion activity when the transport is sufficiently fast in solution (see **figure 6.3 a**)). However, different studies suggest that under certain conditions, the diffusion supply of the metal from the bulk solution may prove to be the rate-limiting step.[2-4] In this case, the internalization rate is relatively faster than the transport of the metal, which may shift the equilibrium between species at the interface organism-solution. A free metal concentration gradient is established, and complexes of metal may dissociate. Therefore, the metal uptake by the organism is controlled by the dissociation kinetics of complexes and the diffusion of species in the medium (see **figure 6.3 b**)). The amount of metal uptake is thereby controlled by a concentration between the free metal concentration and the total metal concentration, depending on the ability of the metal complexes to dissociate.

General discussion

The amount of metal uptake by an organism depends on the effective flux of that metal reaches the organism. In order to estimate this flux, different type of dynamic analytical techniques were developed. In these techniques, the sensors are composed by a metal binding layer (representing an analogy with the organism), that generates a flux of metal. One of these techniques is the Diffusive Gradients in Thin films (DGT, see **figure 6.8**) developed in the 90's by Davison and Zhang.[5,6] The use of this technique is widespread nowadays, and it has been applied by researchers from all over the world. In fact, it has the advantages of being deployed *in situ*, it provides multi-element measurement, the sampling device is simple to use, relatively inexpensive, and the sample can be send to commercial laboratories to analysis. However, interpretations of the results obtained by the sensor are complicate and few studies deal with theoretical analyses of the data. Moreover, the number of published works aiming to the study of simple, synthetic is still low. The second part of this manuscript is devoted to interpretation of measurements obtained by DGT in synthetic solutions containing Cd-NTA complexes. The nitrilotriacetic acid was chosen, as it is a simple and well characterized ligand. The first contribution of this work (chapter 8) was to demonstrate the importance of the penetration of complexes in the lability measurement, by comparison of experimental results with a numerical simulation model. Section 8.1 details the numerical model used to assess the impact of the resin layer on the lability complexes. This work is extended to provide approximate analytical expressions for the calculation of the metal flux, lability degree and concentration profiles in a DGT experiment (section 8.2).

The results show the great dependence of the lability degree on the resin layer thickness. In a standard DGT arrangement (where the thickness of the diffusion layer is larger than the resin layer) a partially labile complex could increase its lability up to a fully labile behaviour, when the resin layer thickness is increased, whereas an increase of the diffusion layer affects very little the lability degree (see figure 3 of section 8.2).

It was shown that a complex is likely to appear more labile when measured by DGT (where the complexes penetrate into the resin binding layer) than when measured by other techniques where complexes are restricted to the diffusion layer. Therefore, it was demonstrated that the expressions reported for the lability of a complex in voltammetric sensors (where the complexes do not penetrate into the electrode) are, in general, not applicable to DGT, since the resin layer is a characteristic feature of DGT. In fact, for complexes that are

partially labile to the DGT measurement, their dissociation inside the resin domain is the main source of metal accumulation.

Although, the accumulated mass can be successfully predicted for well defined metal-ligand systems (as shown in the previous chapters), the measurement interpretation in truly unknown and very complicated systems, such as natural waters, is far more challenging.

Another contribution of this work (chapter 9) was the determination of the range of conditions where the DGT works as a dynamic technique, and what happens when the measurement conditions depart from this range. The results show that proton competition can affect the technique by a reduction of the amount free sites of the binding resin present in the sensor. On the other hand, the presence of ligands also have an influence, since they decrease the concentration of free metal and, in turn, the amount of metal bound to the DGT resin at equilibrium. Both effect, can induce the regime of equilibrium in the sensor to be reached relatively rapidly and the DGT cease to work as a dynamic sensor (see **figure 10.4**). The results allowed us to determine the range where the metal binding to the Chelex sensor is well below equilibrium and, therefore, the operational conditions were DGT works as a purely dynamic sensor (where the metal accumulation in the devices is independent of the amount of resin). Moreover, a perspective of a "new" application of the DGT technique avises: deployment conditions close to equilibrium allow to obtain information about the free metal concentration present in the sample.
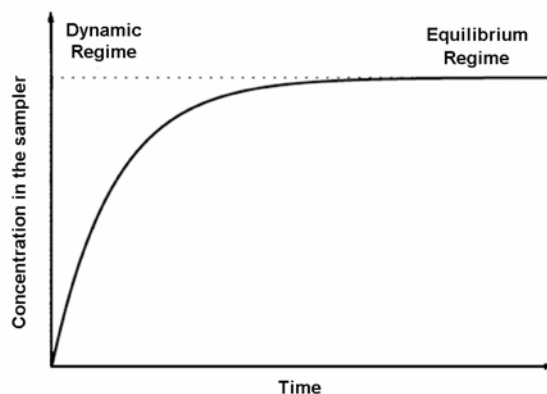

Figure 10.4. The passive sampling devices operate in two main regimes (kinetic and equilibrium).

References

(1)   Milne, C. J.; Kinniburgh, D. G.; Van Riemsdijk, W. H.; Tipping, E., Generic NICA-Donnan model parameters for metal-ion binding by humic substances. *Environmental Science & Technology* **2003,** *37*, (5), 958-971.

(2)   Hudson, R. J. M.; Morel, F. M. M., Iron transport in marine-phytoplankton - kinetics of cellular and medium coordination reactions. *Limnology and Oceanography* **1990,** *35*, (5), 1002-1020.

(3)   Tran, D.; Boudou, A.; Massabuau, J. C., How water oxygenation level influences cadmium accumulation pattern in the asiatic clam Corbicula fluminea: A laboratory and field study. *Environmental Toxicology and Chemistry* **2001,** *20*, (9), 2073-2080.

(4)   Buffle, J.; Zhang, Z.; Startchev, K., Metal flux and dynamic speciation at (Bio)interfaces. part 1: Critical evaluation and compilation of physicochemical parameters for complexes with simple Ligands and Fulvic/Humic substances. *Environmental Science & Technology* **2007,** *41*, (22), 7609-7620.

(5)   Zhang, H.; Davison, W., Performance characteristics of diffusion gradients in thin films for the in situ mesurement of trace metals in aqueous solution. *Analytical Chemistry* **1995,** *67*, (19), 3391-3400.

(6)   Davison, W.; Zhang, H., In-situ speciation measurements of trace components in natural-waters using thin-film gels. *Nature* **1994,** *367*, (6463), 546-548.

CHAPTER 11

CONCLUSIONS

Conclusions

This work presents some novel experimental results and theoretical modelling about the equilibrium and dynamic trace metal speciation in selected synthetic systems such as Pb and Cd with humic acid and NTA, using potentiometric techniques (equilibrium) and Diffusive Gradients in Thin films (DGT). Also, it was shown how the models can be extrapolated to estimate the binding behaviour of trace metals in natural systems (such as fulvic acid in a freshwater). The main conclusions of this work can be summarized as follows:

1.- The equilibrium binding between metal ions (Pb^{2+}, Cd^{2+}) and humic acid was studied in an indirect way through proton titrations at varying fixed total metal concentrations. From these data, the specific binding parameters of the NICA isotherm for both metal and proton ions with humic acid were fitted. The results demonstrate the feasibility of using the glass electrode as an indirect probe for the quantitative description of the metal binding.

2.- In order to interpret these binding results, a theoretical tool was developed: the Conditional Affinity Spectrum of the proton at fixed Total Metal concentration (CAScTM). The proton CAScTM distributions were calculated for the H^+-humic-Cd^{2+} and H^+-humic-Pb^{2+} systems using the previous data. The results yielded information about: a) the conditional affinity "seen" by the proton for each total metal concentration, b) the effective heterogeneity of the H^+-humic binding at different conditions, c) the distribution of occupied proton sites at a given metal concentration and pH.

3.- Natural waters represent complex multi-ion systems where major and minor cations are present at relatively large concentrations compared with trace metals. The simultaneous binding of the different competing metal ions at equilibrium can be described and modelled using multicomponent isotherms such as NICA. In this work, it was shown how the competition effects of these ions toward the effective binding of a trace metal can be achieved using the concept of Conditional Affinity Spectrum (CAS) applied to the NICA isotherm.

4.- Analytical expressions for the CAS of a model ligand and its average effective affinity toward a trace metal were derived for multicomponent systems with protons and *n* metal ions at a constant concentration, based on the NICA isotherm.

5.- The resulting expressions were applied to a generic fulvic acid dissolved in a representative freshwater using generic binding and electrostatic parameters from bibliography. This allowed the prediction of the apparent equilibrium binding affinities of fulvic acid toward a number of trace metals in environmental conditions, as well as the distribution of sites occupied by these metals. Also, the relative contribution of carboxylic and phenolic type groups was analysed in each case.

6.- The advantage of the dynamic speciation techniques (such as DGT) over the equilibrium methods (such as ion selective electrode potentiometry) is that they provide information about the kinetic contribution of the metal complexes to the overall metal flux received by a sensor. On the other hand, the interpretation of the experimental data obtained through DGT is often more complex. Some of the difficulties in the interpretation of the DGT results were dealt with in the present work, as summarized in the following paragraphs.

7.- The assumption that the free metal concentration is zero at the surface of the DGT binding resin layer does not reproduce the experimental results obtained in a synthetic model system (Cd-NTA). By making this assumption, the system should have been "seen" by the sensor as partially labile, while in the experimental measurements the DGT sensors "see" a completely labile system.

8.- Thereby, expressions for the lability degree deduced in the context of voltammetric techniques are, in general, inapplicable to the DGT measurement, as they neglect the complex penetration into the resin layer.

9.- A numerical model and simple analytical expressions for the metal flux, the lability degree and the concentration profiles in the DGT sensor that include the penetration of complexes were developed. The experimental results for the Cd-NTA system were accurately predicted by both the numerical model and the simple analytical expressions.

10.- The lability of complexes depends on the determination technique, it is not an intrinsic parameter. According to these findings, DGT can be expected to measure a greater proportion of the metal in a natural system than the conventional electrochemical methods.

11.- The lability of a complex measured by the standart DGT sensor (where the thickness of the diffusion layer exceeds that of the resin layer) only depends on the diffusion coefficient of the metal complex and its dissociation rate constant.

12.- The influence of two competitors (protons and ligand) on the metal mass accumulated by the DGT sensor was studied. This work shows that the DGT technique can operate in two different modes: dynamic and equilibrium.

13.- When the DGT works in the dynamic mode (its normal operation mode), the technique is able to measure the labile species. This work presented a rigorous analysis of the conditions were this dynamic mode is valid. In particular, the effects of pH (proton competition), deployment time and dissolved ligand concentration were studied. The results allowed us to determine the range where the metal binding to the Chelex sensor is well below equilibrium and, therefore, the operational conditions were DGT works as a purely dynamic sensor.

14.- When the DGT works as an equilibrium sensor, the resin is in equilibrium with the metal species present in the sample and the technique is able to measure the free metal concentration.

Este trabajo presenta nuevos resultados experimentales y modelos teóricos sobre el equilibrio y la especiación dinámica de metales traza en determinados sistemas sintéticos, como Pb y Cd con ácidos húmicos y NTA, mediante el uso de técnicas potenciométricas (equilibrio) y *Diffusive Gradients in Thin films* (DGT). Además, se muestra cómo estos modelos pueden ser extrapolados para estimar el enlace de metales traza en sistemas naturales (como el ácido fúlvico en agua dulce). Las principales conclusiones de este trabajo se pueden resumir en los siguientes apartados:

1.- El equilibrio de enlace entre los iones metálicos (Pb^{2+}, Cd^{2+}) y el ácido húmico se ha estudiado de forma indirecta a través de valoraciones ácido-base a diferentes concentraciones totales fijas de metales. A partir de los datos obtenidos, se han calculados los parámetros específicos de enlace entre el metal y el protón con el ácido húmico mediante ajuste a la isoterma de NICA. Los resultados demuestran la factibilidad del uso del electrodo de vidrio como sonda indirecta para la descripción cuantitativa de la complejación metálica.

2.- Para la interpretación de estos resultados de complejación se ha desarrollado una herramienta teórica: el espectro condicional de afinidad del protón a una concentración total fija de metal (CAScTM). Se han calculado los espectros CAScTM de protón para los sistemas H^+-húmico-Cd^{2+} y H^+-húmico-Pb^{2+} usando los datos anteriores. Los resultados arrojaron información sobre: a) la afinidad condicional "vista" por el protón a cada concentración total de metal, b) la heterogeneidad efectiva del enlace H^+-húmico para diferentes condiciones, c) la distribución de los sitios ocupados por el protón, a una concentración de metal y un pH fijos.

3.- Las aguas naturales son sistemas complejos que contienen múltiples iones y donde los cationes mayoritarios y minoritarios están presentes en concentraciones relativamente grandes comparadas con las de los metales traza. El enlace simultáneo de los diferentes iones metálicos competidores en equilibrio puede ser descritos y modelizado usando isotermas multi-componentes como la de NICA. En este trabajo, se ha desarollado el concepto de espectro de afinidad condicional (*Condicional Affinity Spectrum*, CAS) aplicado a la isoterma de NICA, para demostrar cómo los efectos competitivos de estos iones afectan al enlace de los metales traza.

4.- Se dedujeron expresiones analíticas para el CAS de un ligando modelo y su afinidad efectiva media por un metal traza en sistema multi-componentes compuestos por protones y *n* iones metálicos a concentración constante, basadas en la isoterma NICA.

5.- Las expresiones resultantes se han aplicado a un ácido fúlvico modelo disuelto en un agua dulce representativa, usando parámetros genéricos de enlace y parámetros electrostáticos presentes en la bibliografía. Esto ha permitido predecir las afinidades aparentes de enlace entre el ácido fúlvico y los metales traza en condiciones ambientales, así como la distribución de los sitios ocupados por estos metales. Además, se ha analizado en cada caso la contribución relativa de los grupos de tipo carboxílico y fenólico.

6.- La ventaja de las técnicas de especiación dinámicas (como DGT) en comparación con los métodos de equilibrio (como el electrodo selectivo de iones) es que proporcionan información sobre la contribución cinética de los complejos metálicos al flujo neto de metal recibido por el sensor. Pero, por otro lado, la interpretación de los datos experimentales obtenidos a través de la técnica DGT es, en general, más compleja. Algunas de las dificultades en la interpretación de los resultados de la DGT se han tratado en el presente trabajo, tal como se resume en los siguientes párrafos.

7.- La suposición de que la concentración de metal libre es cero en la superficie de la Chelex (resina complejante) en los sensores DGT, no reproduce los resultados experimentales obtenidos en un sistema sintético modelo (Cd-NTA). Haciendo esta suposición, el sistema debería haber sido "visto" como parcialmente lábil por el sensor, mientras que en las medidas experimentales los sensores DGT "ven" un sistema totalmente lábil.

8.- Por lo tanto, las expresiones para el grado labilidad deducidas en el contexto de las técnicas de voltametría son, en general, inaplicables a la medición por la técnica DGT, ya que no contemplan la penetración de los complejos en la capa de resina.

9.- Por este motivo, se ha desarrollado un modelo numérico y expresiones analíticas simples para simular el flujo de metal, el grado labilidad y los

perfiles de concentración en el sensor que tienen en cuenta la penetración de las distintas especies en la capa de resina. Los resultados experimentales para el sistema de Cd-NTA se han reproducido con precisión, tanto por el modelo numérico como por las expresiones analíticas simples.

10.- La labilidad de los complejos depende de la técnica de determinación, no es un parámetro intrínseco. De acuerdo con estas conclusiones, se puede esperar que se determine una proporción de metal mayor con la técnica DGT que con los métodos electroquímicos convencionales.

11.- La labilidad de un complejo medido por el sensor estándar DGT (donde el espesor de la capa de difusión es mayor al de la capa de resina) sólo depende del coeficiente de difusión del complejo metálico y su velocidad de disociación.

12.- Se ha estudiado la influencia de dos competidores (protones y ligando) sobre la masa de metal acumulado por el sensor DGT. Este trabajo muestra que la técnica DGT puede funcionar en dos modos diferentes: dinámico y equilibrio.

13.- Cuando el DGT trabaja en el modo dinámico (su modo de funcionamiento normal), la técnica es capaz de dar información sobre la especiación dinámica. Este trabajo presenta un análisis riguroso de las condiciones en las que es valido este modo de funcionamiento. En particular, se han estudiado los efectos del pH (competencia de protones), el tiempo de contacto y la concentración de ligando disuelto. Los resultados nos han permitido determinar el rango donde el metal enlazado a la Chelex está muy por debajo del valor de equilibrio y, por tanto, las condiciones operativas donde el DGT funciona como un sensor puramente dinámico.

14.- Cuando la DGT funciona como un sensor de equilibrio, la resina está en equilibrio con las especies metálicas presentes en la muestra y la técnica es capaz de medir la concentración de metal libre.